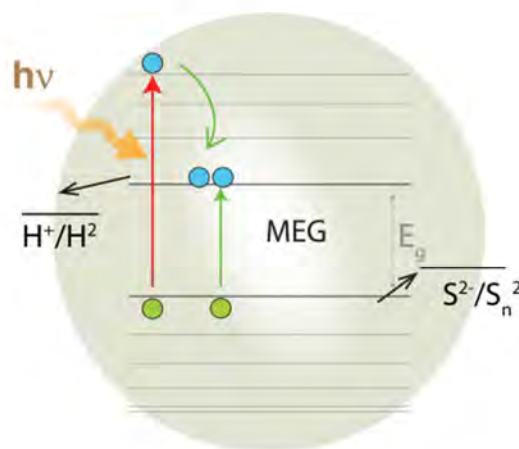
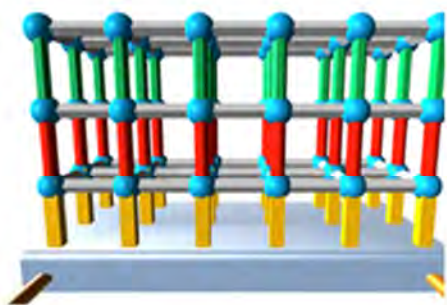
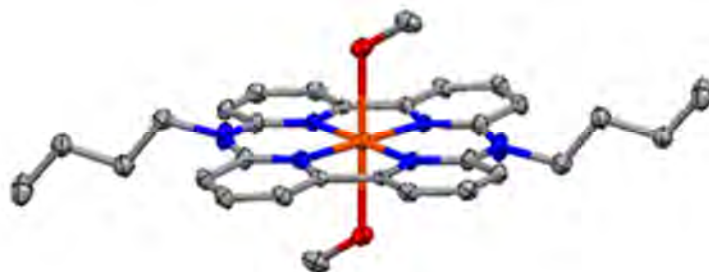


Proceedings of the  
**Thirty-Ninth  
 DOE Solar Photochemistry  
 P. I. Meeting**



**Marriott Washingtonian Center  
 Gaithersburg, Maryland June 5 - June 8, 2017**



*Sponsored by:*

**Chemical Sciences, Geosciences, and Biosciences Division  
 U.S. Department of Energy**



# Program and Abstracts

## Solar Photochemistry P.I. Meeting

Marriott Washingtonian Center  
Gaithersburg, Maryland  
June 5-8, 2017

Chemical Sciences, Geosciences, and Biosciences Division  
Office of Basic Energy Sciences  
Office of Science  
U.S. Department of Energy

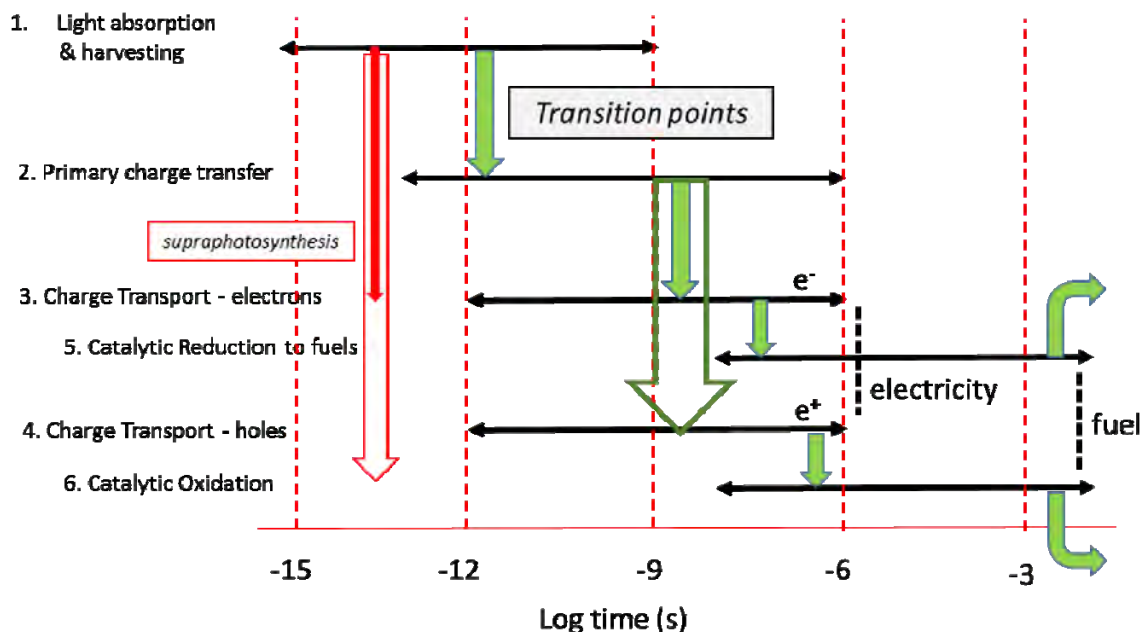
Cover Graphics:

The cover figures are drawn from the abstracts of this meeting. One represents the structure of a novel Fe chromophore (McCusker et al., p. 22). Another depicts a MOF structure for panchromatic light harvesting (Hupp et al., p. 153). A third shows a scheme for MEG production of H<sub>2</sub> (Turner et al. p. 182). At the bottom is the crystal structure of a molecular Co(III) proton reduction catalyst (Mulfort et al. p. 167.)

## Transitions in Solar Photoconversion

There are six principal functions in the classic view of solar photoconversion where one seeks to emulate solar energy transduction in the natural photosynthetic system. These are listed in the figure below. They begin with light absorption and harvesting to create an excited state. Subsequently, this excited state undergoes the primary charge separation and the two separate functions of hole and electron transport begin. At this point, the separated charges can be harvested as electricity, but if one seeks the production of fuels, the two additional functions of oxidative and reductive catalysis must be executed.

### Time Scale of Events in Classic Solar Photoconversion



These steps span a range of time scales which are depicted in the figure, stretching from attoseconds to seconds. Light harvesting can be as short as the attoseconds for absorption of a photon and can involve coherent interactions among chromophores. Fast energy transfer can also involve a Dexter mechanism and slower, Forster pathways can stretch out to a nanosecond time frame for delivery of the excited state to the point of charge separation. For the case of dye sensitized semiconductors the charge separation can happen within tens of femtoseconds, in contrast to the picoseconds required in Photosystem II. In solution, the triplet states of ruthenium complexes have a microsecond available for photoredox reactions. Once the charge transfer does occur, the fate of the hole state and the electron runs in different directions. Even in conductive inorganic solids their mobility is different and is usually much higher than their mobility in organic media. Although these two charges may travel at different rates, eventually they must reach a physical location where they are captured to produce electricity or to initiate the catalysis of an energy rich molecule. The former process waits only for the charges to arrive at the contacts, but the latter proceeds on the time scale of bond breaking and making in molecules and can stretch into the millisecond range. In any case, the oxidative and reductive catalysis reactions are decoupled and do not necessarily happen at the same rate. An example is found in the oxygen

evolving complex in the photosynthetic reaction center where the reaction occurs in milliseconds, which is much shorter than the seconds required for the rubisco enzyme to receive the photo-produced reducing power to fix CO<sub>2</sub>.

Of particular interest are the transition points between these six functions of this scheme – where the system moves from one step to the next. One can identify a number of these transitions. In PSII, for example, it is the place where the exciton harvested by the antenna complex is localized at the site of the primary donor. Subsequent to charge transfer at this site, it is the time where holes are transferred to the oxygen evolving complex. And here is another critical transition, from charge carriers to energy rich molecules, where multiple charges are held ready through a complex chemistry of protons and electrons until their number suffices to produce the desired molecule. In a transition in sensitized nanocrystalline semiconductor systems for electricity generation, charge separation occurs on the scale of tens of femtoseconds and transport of the electron in the substrate electrode is through a hopping process to the collection point.

These transitions require a designed physical structure where the flow of energy and matter is controlled so that photons, charges, protons, and atoms move along a desired pathway. This is Grand Challenge research as BES defines it, research that can have a significance even beyond the mission of the research in solar photoconversion. To be sure, there is Grand Challenge Research within each of the six functions, but in Solar Photochemistry, these transition points are the essential and enabling elements that allow a system to be assembled.

Going forward, the greatest weight in research investments will be made in support of the study of these enabling transition steps in solar photoconversion. Of special interest will also be the next generation of concepts, those which avoid the classic photosynthetic model of transitioning stepwise one function at a time, but rather go *supraphotosynthesis* in making transitions of more than one step at a time. Can excitons be coupled directly to a plasmonic redox mechanism for production of fuels? Can a coherent electron transfer structure be assembled that absorbs light and delivers an electron directly to an electrode for use as electricity? One comes to this conclusion about the selection of future investments quite simply. In looking backwards from a possible product concept to identify the essential fundamental research that must be addressed, one knows with certainty that these enabling transitions are among them.

If this task of understanding and assembling transitions were simple, or even just plain hard, then it would already be done by now. It is a stiff challenge, one yet to be met, one that will exercise the expertise and creativity of each one of us in this room, as individuals and as groups, both now and into the future.

Mark T. Spitler

May 2017





## FOREWORD

The 39th Department of Energy Solar Photochemistry P.I. Meeting, sponsored by the Chemical Sciences, Geosciences, and Biosciences Division of the Office of Basic Energy Sciences, is being held June 5-8, 2017 at the Washingtonian Marriott in Gaithersburg, Maryland. These proceedings include the meeting agenda, abstracts of the formal presentations and posters of the conference, and an address list for the participants.

This Conference is the annual meeting of the grantees who perform research in solar photochemical energy conversion with the support of the Chemical Sciences, Geosciences, and Biosciences Division. This gathering is intended to enable the exchange of new ideas and research concepts between attendees and to further the collaboration and cooperation required for progress in such a difficult field.

We have two guest speakers this year, each bringing a special viewpoint with their research on problems central to the interests of Solar Photochemistry. Professor Mohammed El Naggat of the University of Southern California will open the meeting with a presentation on his research sponsored by the Physical Biosciences Program of the BES Photochemistry and Biochemistry Team. His work illustrates the function of a unique charge transport scheme in nature where electrons are shuttled along an extracellular chain of multi-heme cytochromes. Professor Kelly Gaffney, Associate Laboratory Director for the Stanford Synchrotron Radiation Lightsource, will begin the second day with a discussion on how ultrafast X-ray studies can be used to analyze the dynamics of the excited state of Fe complexes.

We must thank all of the researchers whose enthusiasm, energy, and dedication to scientific inquiry have enabled these advances in solar photoconversion and made this meeting possible. We would also like to express our appreciation to Diane Marceau of the Division of Chemical Sciences, Geosciences, and Biosciences, and Connie Lansdon of the Oak Ridge Institute of Science and Education for their assistance with the coordination of the logistics of this meeting.

Mark T. Spitler  
Chris Fecko  
Chemical Sciences, Geosciences,  
and Biosciences Division  
Office of Basic Energy Sciences

| <b>Solar Photochemistry P.I. Meeting Overview</b> |                          |                              |                          |                             |             |
|---|--------------------------|------------------------------|--------------------------|-----------------------------|-------------|
| <b>Time</b>                                       | <b>Monday, June 5</b>    | <b>Tuesday, June 6</b>       | <b>Wednesday, June 7</b> | <b>Thursday, June 8</b>     | <b>Time</b> |
| 7:30 AM   |                          | <b>BREAKFAST</b>             | <b>BREAKFAST</b>         | <b>BREAKFAST</b>            | 7:30 AM     |
| 7:45 AM   |                          | 7:15 - 8:15                  | 7:15 - 8:15              | 7:15 - 8:30                 | 7:45 AM     |
| 8:00 AM   |                          |                              |                          |                             | 8:00 AM     |
| 8:15 AM   |                          | <b>Opening Remarks</b>       |                          |                             | 8:15 AM     |
| 8:30 AM   |                          |                              | <b>Session VI</b>        | <b>Session X</b>            | 8:30 AM     |
| 8:45 AM   |                          |                              |                          |                             | 8:45 AM     |
| 9:00 AM   |                          | <b>Session III</b>           | <b>Small Molecule</b>    | <b>Spectral</b>             | 9:00 AM     |
| 9:15 AM   |                          | <b>INVITED SPEAKER</b>       | <b>Activation I</b>      | <b>Sensitization</b>        | 9:15 AM     |
| 9:30 AM   |                          | <b>First Row</b>             |                          |                             | 9:30 AM     |
| 9:45 AM   |                          | <b>Chromophores</b>          | <b>BREAK</b>             |                             | 9:45 AM     |
| 10:00 AM  |                          |                              | 9:45-10:15               | <b>BREAK</b>                | 10:00 AM    |
| 10:15 AM  |                          | <b>BREAK</b>                 |                          | 10:00 - 10:30               | 10:15 AM    |
| 10:30 AM  |                          | 10:15 - 10:45                |                          |                             | 10:30 AM    |
| 10:45 AM  |                          |                              | <b>Session VII</b>       | <b>Session XI</b>           | 10:45 AM    |
| 11:00 AM  |                          | <b>Session IV</b>            |                          | <b>Natural</b>              | 11:00 AM    |
| 11:15 AM  |                          | <b>Photoelectrochemical</b>  | <b>Small Molecule</b>    | <b>Chromophores</b>         | 11:15 AM    |
| 11:30 AM  |                          | <b>Nanostructures</b>        | <b>Activation II</b>     |                             | 11:30 AM    |
| 11:45 AM  |                          |                              |                          | <b>DOE Closing Comments</b> | 11:45 AM    |
| 12:00 PM  |                          |                              |                          |                             | 12:00 PM    |
| 12:15 PM  |                          |                              | <b>WORKING LUNCH</b>     |                             | 12:15 PM    |
| 12:30 PM  |                          | <b>WORKING LUNCH</b>         | 12:00 - 1:00             |                             | 12:30 PM    |
| 12:45 PM  |                          | 12:15 - 1:15                 |                          |                             | 12:45 PM    |
| 1:00 PM   |                          |                              |                          |                             | 1:00 PM     |
| 1:15 PM   |                          |                              |                          |                             | 1:15 PM     |
| 1:30 PM   |                          |                              |                          |                             | 1:30 PM     |
| 1:45 PM   |                          | <b>Individual Time</b>       | <b>Session VIII</b>      |                             | 1:45 PM     |
| 2:00 PM   |                          | 1:15 - 4:00                  |                          |                             | 2:00 PM     |
| 2:15 PM   |                          |                              | <b>Models in</b>         |                             | 2:15 PM     |
| 2:30 PM   |                          |                              | <b>Electron transfer</b> |                             | 2:30 PM     |
| 2:45 PM   |                          |                              |                          |                             | 2:45 PM     |
| 3:00 PM   |                          |                              |                          |                             | 3:00 PM     |
| 3:15 PM   | <b>Registration</b>      |                              |                          |                             | 3:15 PM     |
| 3:30 PM   | 3:00 - 6:00 PM           |                              |                          |                             | 3:30 PM     |
| 3:45 PM   |                          |                              | <b>Individual Time</b>   |                             | 3:45 PM     |
| 4:00 PM   |                          |                              | 3:00-4:30                |                             | 4:00 PM     |
| 4:15 PM   |                          | <b>Session V</b>             |                          |                             | 4:15 PM     |
| 4:30 PM   |                          |                              |                          |                             | 4:30 PM     |
| 4:45 PM   | <b>Session I</b>         | <b>Photons and Electrons</b> | <b>Session IX</b>        |                             | 4:45 PM     |
| 5:00 PM   | <b>Opening Session</b>   | <b>Designed Interactions</b> | <b>Novel</b>             |                             | 5:00 PM     |
| 5:15 PM   |                          |                              | <b>Semiconductors</b>    |                             | 5:15 PM     |
| 5:30 PM   | <b>INVITED SPEAKER</b>   |                              |                          |                             | 5:30 PM     |
| 5:45 PM   |                          |                              |                          |                             | 5:45 PM     |
| 6:00 PM   |                          |                              |                          |                             | 6:00 PM     |
| 6:15 PM   |                          | <b>DINNER</b>                |                          |                             | 6:15 PM     |
| 6:30 PM   | <b>WORKING DINNER</b>    | 6:00 - 7:30                  | <b>WORKING DINNER</b>    |                             | 6:30 PM     |
| 6:45 PM   | 6:00 - 7:30              | (on the town)                | 6:00 - 7:30              |                             | 6:45 PM     |
| 7:00 PM   |                          |                              |                          |                             | 7:00 PM     |
| 7:15 PM   |                          |                              |                          |                             | 7:15 PM     |
| 7:30 PM   |                          |                              |                          |                             | 7:30 PM     |
| 7:45 PM   | <b>Session II</b>        |                              |                          |                             | 7:45 PM     |
| 8:00 PM   |                          | <b>POSTERS</b>               | <b>POSTERS</b>           |                             | 8:00 PM     |
| 8:15 PM   | <b>Photoconversion</b>   | odd numbers                  | even numbers             |                             | 8:15 PM     |
| 8:30 PM   | <b>Systems</b>           |                              |                          |                             | 8:30 PM     |
| 8:45 PM   |                          |                              |                          |                             | 8:45 PM     |
| 9:00 PM   |                          |                              |                          |                             | 9:00 PM     |
| 9:15 PM   | <b>No-Host Reception</b> |                              |                          |                             | 9:15 PM     |
| 9:30 PM   | 9:00 - 10:00             | 7:30 - 10:00                 | 7:30 - 10:00             |                             | 9:30 PM     |
| 9:45 PM   |                          |                              |                          |                             | 9:45 PM     |

# *Table of Contents*



# TABLE OF CONTENTS

|                |     |
|----------------|-----|
| Foreword.....  | iii |
| Overview ..... | iv  |
| Program .....  | xv  |

## Abstracts of Oral Presentations

### Session I – Opening Session

|   |   |
|---|---|
| Hotwired Life: Extracellular Electron Transport Across the Biotic-Abiotic Interface<br>M.Y. El-Naggar, University of Southern California..... | 1 |
|---|---|

### Session II – Photoconversion Systems

|  |   |
|--|---|
| Manipulating the Manifold of Charge Transfer Reactions through Redox Shuttle and<br>Photoanode Designs for Next-Generation Dye Sensitized Solar Cells<br>Josh Baillargeon, Dhritabrata Mandal, Yuling Xie, and<br>Thomas W. Hamann, Michigan State University..... | 7 |
|--|---|

|  |    |
|--|----|
| Functionalizing Oxide Surfaces with Molecular Assemblies<br>—Applications in Energy Conversion<br>Bing Shan, Animesh Nayak, Degao Wang, Raja U. Mathiyazhagan, and<br>Thomas J. Meyer, University of North Carolina..... | 10 |
|--|----|

|   |    |
|---|----|
| Electron/hole Selectivity in Organic Semiconductor Contacts for Solar Energy<br>Conversion Chris D. Weber, D. Westley Miller, Colin Bradley, Kira Egelhofer, and<br>Mark C. Lonergan, University of Oregon..... | 13 |
|---|----|

### Session III –First Row Chromophores

|  |    |
|--|----|
| Towards Control of Electronic Excited State Phenomena in 3d Metal Complexes:<br>Ultrafast X-ray Laser Studies of Chemical Dynamics<br>Kelly J. Gaffney<br>SLAC, Stanford University..... | 19 |
|--|----|

|   |    |
|---|----|
| Redefining the Photophysics of Fe(II)-Based Chromophores<br>James K. McCusker, Michigan State University..... | 21 |
|---|----|

## **Session IV – Photoelectrochemical Nanostructures**

|  |    |
|--|----|
| Sensitization of Oxide Single Crystals with Quantum Confined Semiconductors<br>Lenore Kubie, Kevin Watkins, Mark Spitler, Jeff Blackburn, William Rice, Henry<br>Wladkowski, Laurie A. King, Meghan E. Kern, Subash Kattel, Qian Yang and<br><b>Bruce Parkinson</b> , University of Wyoming..... | 27 |
| Spatial and Temporal Imaging of Multi-Scale Interfacial Charge Transport in Two-<br>Dimensional Heterostructures<br>Long Yuan, Tong Zhu, Ti Wang, Shibin Deng, and <b>Libai Huang</b> , Purdue University....  | 32 |
| The Role of Surface Motifs in Group VI Dichalcogenide Photoelectrodes and Two-<br>Dimensional Materials as Protective Layers<br>Fan Yang, Jesús Velázquez, Jimmy John, Joshua D. Wiensch, Ellen X. Yan<br>and <b>Nathan S. Lewis</b> California Institute of Technology.....                     | 34 |

## **Session V – Photons and Electrons – Designed Interactions**

|  |    |
|--|----|
| Design and Photophysics of Next Generation Cu(I) MLCT Excited States and<br>Photochemical Upconversion in Water<br>Catherine E. McCusker, Sofia Garakyaraghi, Petr Koutnik, Karim El Roz,<br>and <b>Felix N. Castellano</b> , North Carolina State University..... | 39 |
| Direct Observation of Charge Transfer and Quintet State Intermediates in Singlet Fission<br><b>Michael Wasielewski</b> , Northwestern University.....  | 43 |
| Organic, Nanoscale, and Self-Assembled Structures Relevant to Solar Energy Conversion<br><b>Michael J. Therien</b> , Duke University.....  | 51 |
| Carrier Delocalization and Long-lived Charges in Doped Conjugated Polymers<br>Michael Ortiz, Natalie Pace, Jessica Ramirez, Jaehong Park, Wei Zhang, Obadiah Reid,<br>and <b>Garry Rumbles</b> , National Renewable Energy Laboratory.....                         | 55 |

## **Session VI – Small Molecule Activation I**

|  |    |
|--|----|
| Catalytic Reduction of Nitrogen to Ammonia with Molybdenum Catalysts<br>Lasantha A. Wickramasinghe, Takaya Ogawa,<br>and <b>Richard R. Schrock</b> , Massachusetts Institute of Technology.....          | 63 |
| Molecular Photoelectrocatalysts for Hydrogen Evolution<br>Matthew B. Chambers, Catherine L. Pitman, Daniel A. Kurtz<br>and <b>Alexander J.M. Miller</b> , University of North Carolina, Chapel Hill..... | 65 |

|   |    |
|---|----|
| Design of Efficient Molecular Electrocatalysts for Water and Carbon Dioxide Reduction Using Predictive Models of Thermodynamic Properties<br>Charlene Tsay, Bianca M. Ceballos, Zachary Thammavongsy, Juliet F. Khosrowabadi Kotyk, Samantha Ruelas, Drew Cunningham, Brooke Livesay, Ivy M. Kha, and <b>Jenny Yang</b> University of California, Irvine..... | 68 |
|---|----|

## **Session VII – Small Molecule Activation II**

|   |    |
|---|----|
| C-H Bond Formation with CO <sub>2</sub> : Insights for Designing Selective (Electro)catalysts<br>Atefeh Taheri, Natalia D. Loewen, and <b>Louise A. Berben</b><br>University of California, Davis.....  | 73 |
| Artificial Photosynthesis for Fuel Generation in Solution and at Interfaces<br>Javier. J. Concepcion, Mehmed Z. Ertem, David C. Grills, Gerald F. Manbeck, James T. Muckerman, Dmitry E. Polyansky,<br>and <b>Etsuko Fujita</b> Brookhaven National Laboratory..... | 75 |
| Exploiting Templating to Engineer Acid Stability for OER Catalysts<br><b>Daniel Nocera</b> Harvard University.....  | 83 |

## **Session VIII – Models in Electron Transfer**

|   |    |
|---|----|
| Proton-Coupled Electron Transfer Processes Underpinning the Electrocatalytic Generation of Hydrogen<br>Noémie Elgrishi, Banu Kandemir, Katherine J. Lee, Brian D. McCarthy, and Eric S. Rountree and <b>Jillian L. Dempsey</b> University of North Carolina, Chapel Hill..... | 89 |
| Plasmon Induced Interfacial Charge Transfer Transition: A New Mechanism for Efficient Hot Electron Transfer<br><b>Tianquan Lian</b> , Emory University.....   | 92 |
| Temperature and solvent polarizability in electron-transfer reactions<br>M. M. Waskasi, M. D. Newton,<br>and <b>D. V. Matyushov</b> , Arizona State University.....   | 95 |

## **Session IX – Novel Semiconducting Solids**

|   |     |
|---|-----|
| Silica Nanolayers with Embedded Molecular Wires for Closing the Cycle of CO <sub>2</sub> Photoreduction by H <sub>2</sub> O under Membrane Separation<br><b>Heinz Frei</b> , Lawrence Berkeley National Laboratory.....               | 99  |
| Intriguing Excited State Behavior of Ternary Semiconductor and Hybrid Perovskite Nanostructures<br>Jacob B. Hoffman, Danilo H. Jara, Seog J. Yoon, Subila Balakrishna<br>and <b>Prashant V. Kamat</b> , University of Notre Dame..... | 103 |

|   |     |
|---|-----|
| Structurally-Correlated Charge Carrier Dynamics in Disordered Semiconductors<br>Eric S. Massaro, Andy H. Hill, Casey L. Kennedy<br>and <b>Eric M. Grumstrup</b> , Montana State University..... | 108 |
|---|-----|

**Session X –Spectral Sensitization**

|  |     |
|--|-----|
| Development of p-GaP Photocathodes for Dye-Sensitization and Ultramicroelectrode<br>Platforms for the Measurement of Heterogeneous Charge-Transfer Kinetics<br>Elizabeth Brown, Sudarat Lee, Sofiya Hlynchuk, Molly MacInnes, Mitchell Lancaster,<br>Saurabh Acharya, and <b>Stephen Maldonado</b> , University of Michigan..... | 113 |
|--|-----|

|   |     |
|---|-----|
| Electron Transfer Dynamics in Efficient Molecular Solar Cells<br>Brian DiMarco, Tim Barr, William Ward and <b>Gerald J. Meyer</b><br>University of North Carolina, Chapel Hill..... | 116 |
|---|-----|

|  |     |
|--|-----|
| Electronic and Vibrational Coherence in Heterogeneous Electron Transfer<br>Baxter Abraham, Jesus Nieto-Pescador, Jolie Blake, Hao Fan, Elena Galoppini<br>and <b>Lars Gundlach</b> University of Delaware..... | 120 |
|--|-----|

**Session XI –Natural Chromophores**

|  |     |
|--|-----|
| Two Dimensional Electronic-Vibrational Spectroscopy<br>N.H.C. Lewis, T.A.A. Oliver, N. Gruenke<br>and <b>G.R. Fleming</b> , Lawrence Berkeley National Laboratory..... | 125 |
|--|-----|

|  |     |
|--|-----|
| Fundamental Studies of the Vibrational, Electronic, and Photophysical Properties of<br>Tetrapyrrolic Architectures<br><b>David F. Bocian, Dewey Holten, Christine Kirmaier, and Jonathan S. Lindsey</b><br>University of California, Riverside, Washington University, and North Carolina State<br>University..... | 128 |
|--|-----|

## Poster Abstracts (by poster number)

1. Molecular and Structural Probes of Defect States in Quantum Dots for Solar Photoconversion  
Christopher Grieco, Grayson Doucette, Kyle T. Munson, John B. Asbury.....135
2. Optoelectronic and Charge Injection Traits of Dyes for Photoelectrochemical Applications  
Adam J. Matula, Svante Hedström, Shin Hee Lee, Jianbing Jiang, Robert. H. Crabtree, Gary W. Brudvig, Victor S. Batista.....136
3. Time-resolved Optical Studies of Perovskite Polycrystalline Films, Single Crystals, Quantum Dots and their Surfaces  
Matthew C. Beard, Kai Zhu, Jao van de Lagemaat, Elisa M. Miller, Joseph M. Luther, Ye Yang.....137
4. Controlling the Endohedral and Exohedral Environment of SWCNTs for Improved Energy Harvesting and Transport  
Jeff Blackburn, Rachelle Ihly, Dylan Arias, Stein van Bezou, Sofie Cambré, Wim Wenseleers, Andrew Ferguson, Justin Johnson.....138
5. Charge Transfer Processes in Catalyzed Photoelectrodes for Solar Water Splitting  
Shannon W. Boettcher, Jingjing Qui, Michael Nellist, Forrest Laskowski.....139
6. Modular Nanoscale and Biomimetic Systems for Photocatalytic Hydrogen Generation  
Kara L. Bren, Richard Eisenberg, Todd D. Krauss.....140
7. Light-Driven Water Oxidation using a High-Potential Porphyrin Photosensitizer and a Molecular Iridium Catalyst  
Kelly L. Materna, Jianbing Jiang, Kevin P. Regan, Charles A. Schmittenmaer, Robert H. Crabtree and Gary W. Brudvig.....141
8. Ultrafast Excited State Relaxation and Vibrational Wave-packet Motions in Pt Dimer Complexes  
L. X. Chen, P. Kim, S. E. Brown-Xu, M. S. Kelley, A. Chacraborty, X. Li, F. N. Castellano, G. C. Schatz.....142
9. Photoelectrochemical Properties of Nanostructured Cu-based Photoelectrodes Prepared from Copper Hydroxy Double Salt Precursor Films  
Allison C. Cardiel, Margaret A Lumley, Kyoung-Shin Choi.....143
10. Fast Single-site Molecular Water Oxidation Catalysts: One Site is Still Enough  
David W. Shaffer, Yan Xie, Gerald F. Manbeck, David J. Szalda, and Javier J. Concepcion.....144
11. Time-Resolved Study of Luminescent Molecular Crystals with Anomously Short Br...Br Contacts  
Philip Coppens, Krishnayan Basuroy, Sounak Sarkar, Gage Bateman, and Jason Benedict.....145

|     |   |     |
|-----|---|-----|
| 12. | Iridium on Steroids: Covalently Binding Catalytic Centers to Metal-Oxide Surfaces with Rigid, Polycyclic, Aliphatic Molecular Linkers<br>Aaron J. Bloomfield, Subhajyoti Chaudhuri, Svante Hedström, Victor S. Batista, <u>Robert H. Crabtree</u> ..... | 146 |
| 13. | Multimetallic Systems for the Photocatalytic Production of Fuels from Abundant Sources<br><u>Claudia Turro</u> and <u>Kim R. Dunbar</u> .....   | 147 |
| 14. | Computational Investigation of Photoinduced Proton Coupled Electron Transfer from Phenols to Polypyridine Ruthenium Complexes<br><u>Mehmed Z. Ertem</u> , Dmitry E. Polyansky, Sergei V. Lyamar.....  | 148 |
| 15. | Bridge Design for Photoactive Molecules at Semiconductor Interfaces<br>Hao Fan, Ryan Harmer, Sylvie Rangan, Baxter Abraham, Jesus Nieto-Pescador, Lars Gundlach, <u>Robert A. Bartynski</u> and <u>Elena Galoppini</u> .....                            | 149 |
| 16. | Femtosecond Energy Transport Properties with Spatial Resolution Measured in an Organic Solar Cell Film<br>Oleg Varnavski and <u>Theodore Goodson III</u> .....  | 150 |
| 17. | Kinetic and Mechanistic Investigations of CO <sub>2</sub> Reduction Catalysts<br><u>David C. Grills</u> , Mehmed Z. Ertem, Etsuko Fujita, James T. Muckerman, Dmitry E. Polyansky.....  | 151 |
| 18. | Integrated Synthetic, Computational, Spectroelectrochemical Study of Polyoxometalate Water Oxidation Catalyst-Based Photoanodes<br><u>Craig L. Hill</u> , <u>Tianquan Lian</u> , <u>Djamaladdin G. Musaev</u> .....                                     | 152 |
| 19. | Light Harvesting, Antenna Behavior, and Directional Charge Transport in Metal-Organic Frameworks<br>Subhadip Goswami, Aaron Peters, Omar K. Farha, <u>Joseph T. Hupp</u> .....  | 153 |
| 20. | Transient Grating Spectroscopy for Measuring Transport of Charges and Excitons in Polycrystalline Thin Films<br><u>Justin C. Johnson</u> , Dylan H. Arias, David T. Moore, Jao van de Lagemaat.....   | 154 |
| 21. | Weak Carrier Interactions in Lead-Sulfide Quantum Dots<br>Dmitry Baranov, Jisu Ryu, Samuel D. Park, <u>David M. Jonas</u> .....   | 155 |
| 22. | Establishing the Role of the Electrode Surface in Solar-Driven Pyridine-Catalyzed CO <sub>2</sub> Reduction<br>Zhu Chen, Coleman X. Kronawitter, <u>Bruce E. Koel</u> .....   | 156 |
| 23. | Photophysics of Charged Excitons in Single-Walled Carbon Nanotubes<br>Zhentao Hou, Amanda R. Amori, Nicole M. B. Cogan, <u>Todd D. Krauss</u> .....   | 157 |
| 24. | Dynamics of the Injection and Transport of Holes and Electrons in DNA<br><u>Frederick D. Lewis</u> .....  | 158 |

|     |   |     |
|-----|---|-----|
| 25. | Exploring the Synergy between Semiconductor Surfaces and Molecular Catalysts for Efficient Solar CO <sub>2</sub> Reduction<br>Sebastian Pantovich, Ethan Jarvis, Peipei Huang, Christine Caputo, <u>Gonghu Li</u> .....   | 159 |
| 26. | Nanostructured Solar Fuel Systems<br>Pengtao Xu, Nicholas S. McCool, Yuguang C. Li, Zhifei Yan, Christopher Gray, Yixin Hu, Sylvia Bintrim-Yang, Kamryn Curry, AJ Rothenberger, <u>Thomas E. Mallouk</u> , John R. Swierk, Coleen T. Nemes, and Charles A. Schmuttenmaer, Ian D. Sharp.....   | 160 |
| 27. | Singlet Fission: Optimization of Chromophore Packing<br>Eric Buchanan, Zdenek Havlas, <u>Josef Michl</u> .....  | 161 |
| 26. | Controlling the Energetics and Stability of Metallic 2D MoS <sub>2</sub> with Surface Modifiers<br>Eric E. Benson, Samuel A. Schuman, Sanjini U. Nanayakkara, Suzanne Ferrere, Jeffery L. Blackburn, <u>Elisa M. Miller</u> .....   | 162 |
| 29. | Redox Potentials Without Electrolyte and Ion Pairing<br>Matthew J. Bird, Tomokazu Iyoda, Nicholas Bonura, Jin Bakalis, Abram Ledbetter, <u>John R. Miller</u> .....   | 163 |
| 30. | Concerted One-Electron Two-Proton Transfer Processes in Models Inspired by the Tyr-His Couple of Photosystem II<br>Mioy T. Huynh, S. Jimena Mora, Matias Villalba, Marely E. Tejada-Ferrari, Paul A. Liddell, Anne-Lucie Teillout, Charles W. Machan, Clifford P. Kubiak, <u>Devens Gust</u> , <u>Thomas A. Moore</u> , Sharon Hammes-Schiffer, <u>Ana L. Moore</u> ..... | 164 |
| 31. | Enhanced Catalysis through Metal Organic Framework Incorporation – MOFs for Water Oxidation and Carbon Dioxide Reduction<br>S.Y. Lin, J. Zhu, P. Usov, S.R. Ahrenholtz, <u>A.J. Morris</u> .....  | 165 |
| 32. | Interconversion of Formic Acid and Carbon Dioxide by Proton-Responsive, Half-Sandwich Cp*Ir(III) Complexes: A Computational Mechanistic Investigation<br>M.Z. Ertem, Y. Himeda, E. Fujita, <u>J.T. Muckerman</u> .....  | 166 |
| 33. | Design of Molecular Modules for Artificial Photosynthesis<br><u>Karen L. Mulfort</u> , Lars Kohler, Dugan Hayes, Lin X. Chen, Oleg G. Poluektov, David M. Tiede.....  | 167 |
| 34. | Tuning Semiconductor Photoelectrode Energetics by Molecular Surface Modification<br>Logan E. Garner, K. Xerxes Steirer, James L. Young, Nicholas C. Anderson, Elisa M. Miller, Jonathan S. Tinkham, Todd G. Deutsch, Alan Sellinger, John A. Turner, <u>Nathan R. Neale</u> .....   | 168 |
| 35. | Enhanced Multiple Exciton Generation (MEG) in PbS/CdS Janus-like Heterostructure Nanocrystals<br>Daniel Kroupa, G. Pach, B. Chernomordik, <u>A.J. Nozik</u> , M.C. Beard.....   | 169 |
| 36. | Surface Photovoltage Spectroscopy Observes Built-in Voltage, Space Charge Layer Width and Effective Band Gap in CdSe Quantum Dot Films<br>Jing Zhao, Benjamin A. Nail, Michael A. Holmes, <u>Frank E. Osterloh</u> .....  | 170 |

|     |  |     |
|-----|--|-----|
| 37. | Earth Abundant Transition Metal Catalysts for Photochemical Hydrogen Production: A Combined Study using Multi-Frequency EPR and DFT Calculations<br><u>Oleg G. Poluektov</u> , Jens Niklas, Karen L. Mulfort, Lisa M. Utschig, David M. Tiede, Kristy L. Mardis.....   | 171 |
| 38. | The Role of Hydrogen Bonding in Proton-Coupled Electron Transfer: Reactions between Photoexcited Metal Complexes and Phenol Donors<br><u>Dmitry E. Polyansky</u> , Mehmed Z. Ertem, Sergei V. Lyamar.....  | 172 |
| 39. | Time-Domain Atomistic Modeling of Photo-Excitation Dynamics in Hybrid Nanoscale Systems for Solar Energy Harvesting<br><u>Oleg Prezhdo</u> .....   | 173 |
| 40. | Chemo-Structural Composition and Photovoltaic Efficiency of CH <sub>3</sub> NH <sub>3</sub> PbI <sub>3</sub> Perovskite affected by external factors<br><u>Sylwia Ptasinska</u> .....  | 174 |
| 41. | Transformations of Ru Complexes under Catalytic Condition of Water Oxidation<br><u>Yulia Pushkar</u> , Yuliana Smirnova, Darren Erdman.....  | 175 |
| 42. | Carrier Dynamics in Metals Oxides for Water-Splitting Dye-Sensitized Photoelectrochemical Cells<br>John R. Swierk, Kevin P. Regan, Jens Neu, Jianbing Jiang, Gary W. Brudvig, <u>Charles A. Schmuttenmaer</u> .....  | 176 |
| 43. | What does Coherence Mean in Electron Transfer Reactions? The betaine-30 Example. Shahnawaz Rafiq and <u>Gregory D. Scholes</u> .....   | 177 |
| 44. | Interfacial Charge Transfer Pathways and Photocarrier Dynamics in Heterostructured Nanocomposite Photoanodes<br>Lucas H. Hess, Jason K. Cooper, <u>Ian D. Sharp</u> .....  | 178 |
| 45. | Chromophores for Efficient Photoinduced Charge Generation<br><u>Stephen Bradforth</u> , <u>Mark Thompson</u> , Jessica Golden, Laura Estergreen, and Peter Djurovich.....  | 179 |
| 46. | Evidence for Oxidative Decay of a Ru-Bound Ligand during Catalyzed Water Oxidation Husain Kagalwala, Lianpeng Tong, Lars Kohler, <u>Randolph P. Thummel</u> .....  | 180 |
| 47. | Resolving Sites for Solar-Driven Catalysis in Amorphous Oxide and Molecular Water Oxidation Catalysts Using In-situ X-ray Techniques<br><u>David M. Tiede</u> , Gihan Kwon, Alex B. F. Martinson, Hoyoung Jang, Jun-Sik Lee, Karen L. Mulfort, Lisa M. Utschig, Oleg G. Poluektov, Lin X. Chen.....  | 181 |
| 48. | Studies in Photoelectrochemical Processes in Interfacial Catalysis and MEG<br>Jing Gu, Yong Yan, Ryan W. Crisp, Jeffery A. Aguiar, Boris D. Chernomordik, Gregory Pach, Suzanne Ferrere, K. Xerxes Steirer, Chuanxiao Xiao, James L. Young, Andrew Norman, Mowafak Al-Jassim, Ashley R. Marshall, Nathan R. Neale, Matthew C. Beard, <u>John A. Turner</u> ..... | 182 |

|     |  |     |
|-----|--|-----|
| 49. | A Semiconductor-to-Metal Transition in Rutile TiO <sub>2</sub> is Induced by Tensile Strain and Improves Electrochemical Activity<br>Eric E. Benson, Elisa M. Miller, Sanjini U. Nanayakkara, Drazenka Svedruzic, Suzanne Ferrere, Nathan R. Neale, <u>Jao van de Lagemaat</u> , Brian A. Gregg..... | 183 |
| 50. | Developing a Molecular Toolbox for Efficient Singlet Fission<br><u>Xiaoyang Zhu</u> and <u>Colin Nuckolls</u> .....  | 184 |
| 51. | Studies of Electrocatalysts for Water Oxidation<br>Bryan R. Wygant, Oluwaniyi Mabayoje, <u>C. Buddie Mullins</u> , and Allen J. Bard.....  | 185 |
| 52. | Metal-Tipped and Electrochemically Wired Semiconductor Nanocrystals: Modular Constructs for Directed Charge Transfer<br><u>Neal R. Armstrong</u> , Jeffry Pyun, S. Scott Saavedra.....   | 186 |
| 53. | Coherent Coupling of Electronic and Phononic Resonances<br>M. Kirschner, C.M, Le Thiec, C. Chapman, X.M. Lin, G.C. Schatz, L.X. Chen, and <u>R.D. Schaller</u> .....   | 187 |
|     | <b>LIST OF PARTICIPANTS</b> .....  | 189 |
|     | <b>AUTHOR INDEX</b> .....  | 199 |



# *Program*



**39<sup>th</sup> DOE SOLAR PHOTOCHEMISTRY  
P.I. MEETING**

**June 5-8, 2017**

**Washingtonian Marriott  
Gaithersburg, MD**

**PROGRAM**

**Monday, June 5**

3:00 – 6:00 p.m.      Registration

**Monday Afternoon, June 5**

**SESSION I**

**Opening Session**

Mark T. Spitler, Chair

4:45 p.m.      Opening Remarks  
                    **Mark Spitler**, Department of Energy

5:00 p.m.      **Opening Lecture.**  
                    Hotwired Life: Extracellular Electron Transport Across the Biotic-Abiotic  
                    Interface  
                    **M.Y. El-Naggar**, University of Southern California

6:00 p.m.      Working Dinner

**Monday Evening, June 5**

**SESSION II**

**Photoconversion Systems**

John Turner, Chair

7:30 p.m.      Manipulating the Manifold of Charge Transfer Reactions through Redox Shuttle  
                    and Photoanode Designs for Next-Generation Dye Sensitized Solar Cells  
                    **Thomas W. Hamann**, Michigan State University

- 8:00 p.m. Functionalizing Oxide Surfaces with Molecular Assemblies  
—Applications in Energy Conversion  
**Thomas J. Meyer**, University of North Carolina, Chapel Hill
- 8:30 p.m. Electron/Hole Selectivity in Organic Semiconductor Contacts for Solar Energy Conversion  
**Mark C. Lonergan**, University of Oregon
- 9:00 p.m. No-Host Reception

### **Tuesday Morning, June 6**

- 7:15 a.m. Continental Breakfast

#### **SESSION III** **First Row Chromophores** Mark T. Spitler, Chair

- 8:15 a.m. Opening Remarks  
**Bruce Garrett and Mark Spitler**, Department of Energy
- 8:45 a.m. Towards Control of Electronic Excited State Phenomena in 3d Metal Complexes:  
Ultrafast X-ray Laser Studies of Chemical Dynamics  
**Kelly J. Gaffney**, SLAC, Stanford University
- 9:45 a.m. Redefining the Photophysics of Fe(II)-Based Chromophores  
**James K. McCusker**, Michigan State University
- 10:15 a.m. Break

#### **SESSION IV** **Photoelectrochemical Nanostructures** Nathan Neale, Chair

- 10:45 a.m. Sensitization of Oxide Single Crystals with Quantum Confined Semiconductors  
**Bruce Parkinson**, University of Wyoming
- 11:15 a.m. Spatial and Temporal Imaging of Multi-Scale Interfacial Charge Transport in  
Two-Dimensional Heterostructures  
**Libai Huang**, Purdue University
- 11:45 a.m. The Role of Surface Motifs in Group VI Dichalcogenide Photoelectrodes and  
Two-Dimensional Materials as Protective Layers  
**Nathan S. Lewis**, California Institute of Technology

12:15 p.m. Working Lunch

**Tuesday Afternoon, June 6**

**SESSION V**  
**Photons and Electrons – Designed Interactions**  
Karen Mulfort, Chair

- 4:00 p.m. Design and Photophysics of Next Generation Cu(I) MLCT Excited States and Photochemical Upconversion in Water  
**Felix N. Castellano**, North Carolina State University
- 4:30 p.m. Direct Observation of Charge Transfer and Quintet State Intermediates in Singlet Fission  
**Michael Wasielewski**, Northwestern University
- 5:00 p.m. Organic, Nanoscale, and Self-Assembled Structures Relevant to Solar Energy Conversion  
**Michael J. Therien**, Duke University
- 5:30 p.m. Carrier Delocalization and Long-lived Charges in Doped Conjugated Polymers  
**Garry Rumbles**, National Renewable Energy Laboratory

**Tuesday Evening, June 6**

- 6:00 – 7:30 p.m. Dinner (on the Town)
- 7:30 p.m. Posters (Odd numbers)

**Wednesday Morning, June 7**

7:15 a.m. Continental Breakfast

**SESSION VI**  
**Small Molecule Activation I**  
Javier Concepcion, Chair

- 8:15 a.m. Catalytic Reduction of Nitrogen to Ammonia with Molybdenum Catalysts  
**Richard R. Schrock**, Massachusetts Institute of Technology

- 8:45 a.m. Molecular Photoelectrocatalysts for Hydrogen Evolution  
**Alexander J.M. Miller**, University of North Carolina, Chapel Hill
- 9:15 a.m. Design of Efficient Molecular Electrocatalysts for Water and Carbon Dioxide Reduction Using Predictive Models of Thermodynamic Properties  
**Jenny Yang**, University of California, Irvine
- 9:45– 10:15 a.m. Break

**SESSION VII**  
**Small Molecule Activation II**  
David Grills, Chair

- 10:15 a.m. C-H Bond Formation with CO<sub>2</sub>: Insights for Designing Selective (Electro)catalysts  
**Louise A. Berben**, University of California, Davis
- 10:45 a.m. Artificial Photosynthesis for Fuel Generation in Solution and at Interfaces  
**Etsuko Fujita**, Brookhaven National Laboratory
- 11:15 a.m. - Exploiting Templating to Engineer Acid Stability for OER Catalysts  
11:45 a.m. **Daniel Nocera**, Harvard University
- 12:00 p.m. Lunch

**Wednesday Afternoon, June 7**

**Session VIII**  
**Models in Electron Transfer**  
Joseph Hupp, Chair

- 1:30 p.m. Proton-Coupled Electron Transfer Processes Underpinning the Electrocatalytic Generation of Hydrogen  
**Jillian L. Dempsey**, University of North Carolina, Chapel Hill
- 2:00 p.m. Plasmon Induced Interfacial Charge Transfer Transition: A New Mechanism for Efficient Hot Electron Transfer  
**Tianquan Lian**, Emory University
- 2:30 p.m. - Temperature and Solvent Polarizability in Electron-Transfer Reactions  
3:00 p.m. **D. V. Matyushov**, Arizona State University

**Session IX**  
**Novel Semiconducting Solids**  
Frank Osterloh, Chair

- 4:30 p.m. Silica Nanolayers with Embedded Molecular Wires for Closing the Cycle of CO<sub>2</sub> Photoreduction by H<sub>2</sub>O under Membrane Separation  
**Heinz Frei**, Lawrence Berkeley National Laboratory
- 5:00 p.m. Intriguing Excited State Behavior of Ternary Semiconductor and Hybrid Perovskite Nanostructures  
**Prashant V. Kamat**, Notre Dame Radiation Laboratory
- 5:30 p.m. Structurally-Correlated Charge Carrier Dynamics in Disordered Semiconductors  
**Erik M. Grumstrup**, Montana State University

**Wednesday Evening, June 7**

- 6:00 p.m. Working Dinner
- 7:30 p.m. Posters (Even numbers)

**Thursday Morning, June 8**

- 7:15 a.m. Continental Breakfast

**Session X**  
**Spectral Sensitization**  
Xiaoyang Zhu, Chair

- 8:30 a.m. Development of p-GaP Photocathodes for Dye-Sensitization and Ultramicroelectrode Platforms for the Measurement of Heterogeneous Charge-Transfer Kinetics  
**Stephen Maldonado**, University of Michigan
- 9:00 a.m. Electron Transfer Dynamics in Efficient Molecular Solar Cells  
**Gerald J. Meyer**, University of North Carolina, Chapel Hill
- 9:30 a.m. Electronic and Vibrational Coherence in Heterogeneous Electron Transfer  
**Lars Gundlach**, University of Delaware

10:00 a.m. – 10:30 a.m. Break

**Session XI**  
**Natural Chromophores**  
Kara Bren, Chair

10:30 a.m. Two-Dimensional Electronic-Vibrational Spectroscopy  
**G.R. Fleming**, Lawrence Berkeley National Laboratory

11:00 a.m. Fundamental Studies of the Vibrational, Electronic, and Photophysical Properties of Tetrapyrrolic Architectures, **David F. Bocian, Dewey Holten, Christine Kirmaier, and Jonathan S. Lindsey**, University of California, Riverside, Washington University, and North Carolina State University

11:45 a.m. Closing Remarks  
**Mark Spitler**, U.S. Department of Energy

*Session I*

*Opening Session*



## Hotwired Life: Extracellular Electron Transport Across the Biotic-Abiotic Interface

M.Y. El-Naggar<sup>1,2,3</sup>, S. Pirbadian<sup>1</sup>, H.S. Byun<sup>1</sup>, S. Xu<sup>1</sup>, Y. Jangir<sup>1</sup>, B.J. Gross<sup>1</sup>, A.R. Rowe<sup>1,4</sup>, G. Chong<sup>2</sup>, S.E. Barchinger<sup>5</sup>, J.H. Golbeck<sup>5</sup>, A. Nakano<sup>1,6</sup>, P. Subramanian<sup>7</sup>, G.J. Jensen<sup>7</sup>

<sup>1</sup>Department of Physics and Astronomy, University of Southern California, <sup>2</sup>Department of Biological Sciences, University of Southern California, <sup>3</sup>Department of Chemistry, University of Southern California, <sup>4</sup>Department of Earth Sciences, University of Southern California, <sup>5</sup>Department of Biochemistry and Molecular Biology, The Pennsylvania State University, <sup>6</sup>Collaboratory for Advanced Computing and Simulations, University of Southern California, <sup>7</sup>Howard Hughes Medical Institute, California Institute of Technology

Electron Transfer (ET) is the stuff of life. The stepwise movement of electrons within and between molecules dictates all biological energy conversion strategies, including respiration and photosynthesis. With such a universal role across all domains of life, the fundamentals of ET and its precise impact on bioenergetics have received considerable attention, and the broad mechanisms allowing ET over small length scales in biomolecules are now well appreciated.

In what has become an established pattern, however, our planet's oldest and most versatile organisms are now pushing the limits of our knowledge. During the last few years our understanding of biological ET has been challenged by studies of the biophysical and structural basis of ultra-long-distance (over micrometer length scales) and fast extracellular electron transport (EET) through the extended redox systems of environmental bacteria. These remarkable organisms have evolved direct charge transfer mechanisms to solid surfaces outside the cells, allowing them to use abundant redox-active minerals as electron acceptors for respiration (Fig. 1), instead of oxygen or other soluble oxidants that would normally diffuse inside cells. Microbes that perform EET are major players in global elemental cycles, with important consequences for climate change and bioremediation of toxic compounds and heavy metals. And by performing electron transfer to or from electrodes, such microbes can be used as biocatalysts for converting the energy stored in diverse chemical fuels to electricity, or vice versa, in renewable energy technologies.

*But how can an organism transfer electrons to a surface micrometers away from the cell? What molecules mediate this transport? And, from a physics standpoint, what are the relevant length, time, and energy scales? Here we will focus on biophysical measurements, electron transfer simulations, and tomographic studies of the extracellular electron transport (EET) machinery of the dissimilatory metal-reducing bacterium *Shewanella oneidensis* MR-1. Focusing*

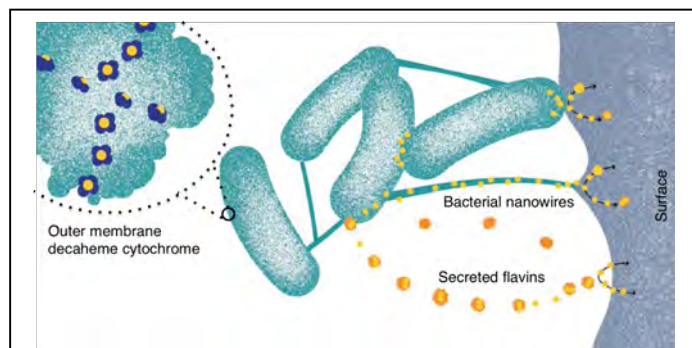


**Fig. 1.** Proposed mechanisms of extracellular electron transport (EET) by *Shewanella oneidensis* MR-1. Electrons are routed from the inner membrane to extracellular acceptors through a network of periplasmic and outer membrane multi-heme cytochromes that extend to the cellular surface and along micrometer-long extensions known as ‘bacterial nanowires’. Endogenously secreted flavins accelerate EET by functioning either as soluble diffusing shuttles or cytochrome-bound cofactors.

on the multiheme cytochrome conduits that allow direct EET by *S. oneidensis* MR-1, we show how the rates gleaned from single molecule conductance measurements (scanning tunneling microscopy and spectroscopy) and kinetic Monte Carlo simulations can explain single cell respiration rates measured using an integrated platform that combines optical trapping and on-chip electrochemistry (Fig. 2). To shed light on how endogenous flavins accelerate EET from *S. oneidensis* MR-1, we report live cell electrochemical measurements that reveal both flavin-dependent and flavin-independent EET pathways, while allowing us to disentangle the previously proposed EET contributions of both diffusible and cytochrome-bound flavins. Our results indicate that endogenous flavins accelerate EET from *Shewanella* to high surface area electrodes primarily as cytochrome-bound cofactors, rather than free soluble shuttles, thereby supporting one of the two debated models of flavin-enhanced EET. We also examine the reversibility of *Shewanella*'s electron transport conduits; while optimized for interaction with anodes, we show that cathodic electrons can enter the electron transport chain of *S. oneidensis* MR-1 when oxygen is used as the terminal electron acceptor.

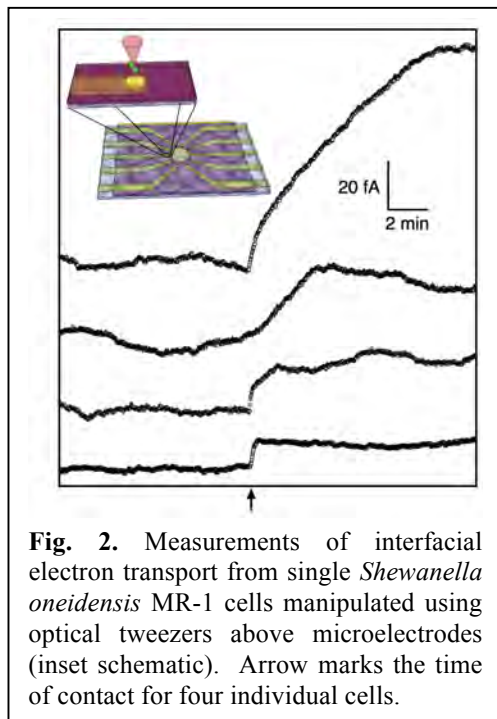


**Fig. 2.** Measurements of interfacial electron transport from single *Shewanella oneidensis* MR-1 cells manipulated using optical tweezers above microelectrodes (inset schematic). Arrow marks the time of contact for four individual cells.

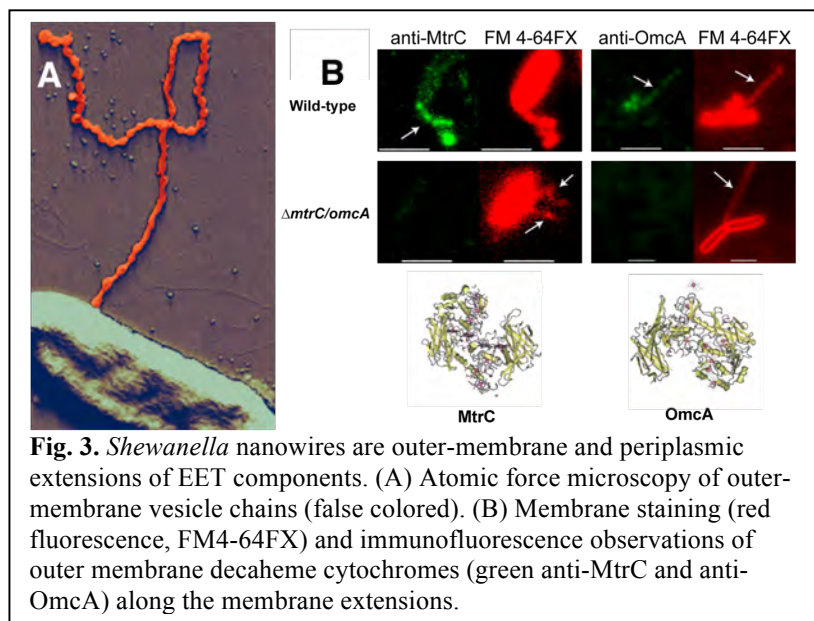


**Fig. 3.** *Shewanella* nanowires are outer-membrane and periplasmic extensions of EET components. (A) Atomic force microscopy of outer-membrane vesicle chains (false colored). (B) Membrane staining (red fluorescence, FM4-64FX) and immunofluorescence observations of outer membrane decaheme cytochromes (green anti-MtrC and anti-OmcA) along the membrane extensions.

In addition, we describe our current understanding of how *Shewanella* organizes heme networks along the filamentous membrane tubes known as ‘bacterial nanowires’ (Fig. 3). Until recently, studies of these micrometer-scale structures were limited to nanoelectrode measurements performed under non-native conditions. Here, using correlative redox-dependent labeling, electron cryo-tomography and *in vivo* fluorescent microscopy, we are gaining new insight into the native localization patterns of orientation of these multiheme

cytochrome conduits along nanowires as well as the morphology and formation mechanism of these structures. These experimental developments are being coupled into large-scale Divide-Conquer-Recombine kinetic Monte Carlo high performance computations of transport in structures ranging from nanowires to full microbial biofilms.

## References

1. S. Pirbadian and M.Y. El-Naggar. *Multistep Hopping and Extracellular Charge Transfer in Microbial Redox Chains*, Physical Chemistry Chemical Physics, 14, 13802-13808, 2012.
2. S. Pirbadian, S. E. Barchinger, K.M. Leung, H.S. Byun, Y. Jangir, R.A. Bouhenni, S.B. Reed, M.F. Romine, D.A. Saffarini, L. Shi, Y.A. Gorby, J. H. Golbeck, M.Y. El-Naggar. *Shewanella oneidensis MR-1 nanowires are outer membrane and periplasmic extensions of the extracellular electron transport components*, PNAS, 111, 12883-12888, 2014.
3. H.S. Byun, S. Pirbadian, A. Nakano, L. Shi, M.Y. El-Naggar. *Kinetic Monte Carlo simulations and molecular conductance measurements of the bacterial decaheme cytochrome MtrF*, ChemElectroChem, 1, 1932-1939, 2014.
4. B.J. Gross and M.Y. El-Naggar. *A combined electrochemical and optical trapping platform for measuring single cell respiration rates at electrode interfaces*, Review of Scientific Instruments, 86, 064301, 2015.
5. M.D. Yates, J. Golden, J. Roy, S.M. Strycharz-Glaven, S. Tsoi, J. Erickson, M.Y. El-Naggar, S. Calabrese Barton and L. Tender, *Thermally activated long range electron transport in living biofilms*, Physical Chemistry Chemical Physics, 17, 32564-32570, 2015.
6. S. Xu, Y. Jangir, M.Y. El-Naggar. *Disentangling the roles of free and cytochrome-bound flavins in extracellular electron transport from Shewanella oneidensis MR-1*, Electrochimica Acta, 198, 49-55, 2016.
7. A.R. Rowe, P. Rajeev, A. Jain, S. Pirbadian, A. Okamoto, J.A. Gralnick, M.Y. El-Naggar, K.H. Nealson, *Tracking electron uptake from a cathode into Shewanella cells: implications for generating maintenance energy from solid substrates*, preprint posted on bioRxiv, doi: 10.1101/116475, 2017.
8. P. Subramanian, S. Pirbadian, M.Y. El-Naggar, G.J. Jensen, *The ultrastructure of Shewanella oneidensis MR-1 nanowires revealed by electron cryo-tomography*, preprint posted on bioRxiv, doi: 10.1101/103242, 2017.



## *Session II*

### *Photoconversion Systems*



# Manipulating the Manifold of Charge Transfer Reactions through Redox Shuttle and Photoanode Designs for Next-Generation Dye Sensitized Solar Cells

Josh Baillargeon, Dhritabrata Mandal, Yuling Xie, Thomas W. Hamann

Department of Chemistry  
Michigan State University  
East Lansing, MI 48824

Dye-sensitized solar cells (DSSCs) hold promise as a disruptive technology for solar energy conversion as they have the potential to break the cost-efficiency paradigm that limits current generation photovoltaics in addition to serving as an ideal platform for solar fuels generation. The excellent performance of the most efficient DSSCs rely on balancing the kinetics of several electron-transfer processes involving multiple components: 1) electron *injection* into the photoanode from the photo-excited dye before it relaxes to its ground state 2) reduction of the oxidized dye by a redox shuttle (*regeneration*) before it is reduced by an electron in the photoanode (*recombination*) 3) electron transfer (*interception*) from the photoanode to the oxidized form of the redox shuttle which controls charge collection and the maximum photovoltage. While the best existing research cells have achieved an impressive 13 % solar-to-electricity power conversion efficiencies through optimizing these kinetic processes, they still fall short of their potential of > 20 % primarily due to the energy lost in each electron-transfer step. In the first part of this talk I will outline the bottlenecks of current DSSCs and introduced our multi-component approach to understanding and improving the performance controlling processes.

The second part of this talk will describe our efforts to manipulate the self-exchange kinetics of one-electron outersphere cobalt complexes and understand the effect on the charge transfer processes when employed as redox shuttles. For example, we compared regeneration and recombination in DSSCs with a high spin cobalt (II) redox shuttle,  $[\text{Co}(\text{bpy})_3]^{3+/2+}$ , where bpy is 2,2'-bipyridine, and a low spin cobalt (II) redox couple,  $[\text{Co}(\text{ttcn})_2]^{3+/2+}$ , where ttcn is trithiacyclononane. A detailed analysis of the measured incident photon to current efficiencies showed that the electron diffusion length,  $L_n$ , is  $3.3 \mu\text{m}$  for  $[\text{Co}(\text{bpy})_3]^{3+/2+}$ , but only  $1.3 \mu\text{m}$  for  $[\text{Co}(\text{ttcn})_2]^{3+/2+}$ , due to faster recombination. The dye regeneration efficiency,  $\eta_{\text{reg}}$ , was found to be only 0.55 for  $[\text{Co}(\text{bpy})_3]^{3+/2+}$ , but is quantitative for  $[\text{Co}(\text{ttcn})_2]^{3+/2+}$ . These results demonstrate the fine kinetic balancing act needed to design new redox shuttles. In order to overcome the poor dye regeneration with  $[\text{Co}(\text{bpy})_3]^{2+}$ , we synthesized a Co(IV/III) redox shuttle, cobalt tris(2-(p-tolyl)pyridine),  $[\text{Co}(\text{ptpy})_3]^{+/0}$ , which we determined has an incredibly fast self-exchange rate constant of  $(9.2 \pm 3.9) \times 10^8 \text{ M}^{-1}\text{s}^{-1}$ , making it an ideal candidate for dye regeneration. To avoid fast recombination and solubility limitations, a tandem

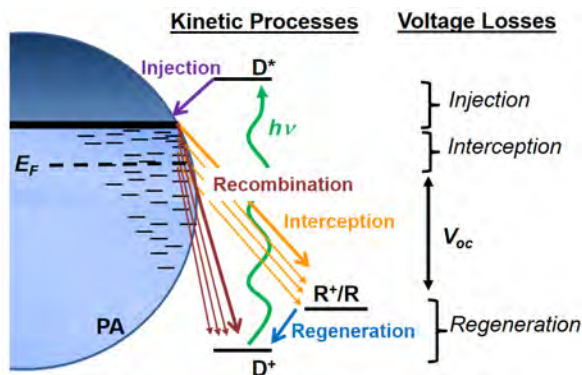


**Figure 1.** Energy diagram under illumination ( $h\nu$ ) showing electron-transfer processes of interest: electron *injection* into the photoanode (PA) by the photoexcited dye ( $D^*$ ), dye *regeneration* by the redox shuttle ( $R$ ), *recombination* to the oxidized dye ( $D^+$ ) and electron *interception* by the oxidized form of the redox shuttle ( $R^+$ ). Also shown are the voltage losses associated with each reaction.

**Table 1.** Potentials and self-exchange electron-transfer rate constants for redox shuttles investigated. Also shown are fit results of  $\eta_{reg}$  for DSSCs employing  $[\text{Co}(\text{bpy})_3]^{3+/2+}$  and  $[\text{Co}(\text{ttn})_2]^{3+/2+}$  redox shuttles, the driving forces of regeneration,  $-\Delta G^0_{reg}$ , and electron diffusion length,  $L_n$ .

| Redox Couple                        | $E^0$ (mV vs. Fc) | $k_{R+/R}$ ( $\text{M}^{-1} \text{s}^{-1}$ ) | $\eta_{reg}$    | $-\Delta G^0_{reg}$ (eV) | $L_n$ ( $\mu\text{m}$ ) |
|-------------------------------------|-------------------|--|-----------------|--------------------------|-------------------------|
| $[\text{Co}(\text{bpy})_3]^{3+/2+}$ | $-51 \pm 2$       | $0.27 \pm 0.06$                              | $0.54 \pm 0.03$ | 0.506                    | $3.25 \pm 0.16$         |
| $[\text{Co}(\text{ttn})_2]^{3+/2+}$ | $3 \pm 3$         | $(9.1 \pm 0.7) \times 10^3$                  | $1.00 \pm 0.05$ | 0.452                    | $1.30 \pm 0.05$         |

electrolyte containing  $[\text{Co}(\text{ppy})_3]^{+0}$  and  $[\text{Co}(\text{bpy})_3]^{3+/2+}$  was utilized. An improved short circuit current density is achieved for DSSCs employing the tandem electrolyte, compared to electrolytes containing only  $[\text{Co}(\text{bpy})_3]^{3+/2+}$ , consistent with superior dye regeneration expected based on predictions using Marcus Theory. Finally, future directions that we are pursuing in the design and study of next generation redox couples to decrease the voltage loss without sacrificing kinetics will be discussed. Preliminary results of  $\text{Co}(\text{PY5Me}_2)(\text{CN})$  will be presented, where the spin state

is controlled by introduction of the strong field  $\text{CN}^-$  ligand to increase the dye regeneration kinetics, as well as pushing the redox potential to a more negative value to decrease recombination.

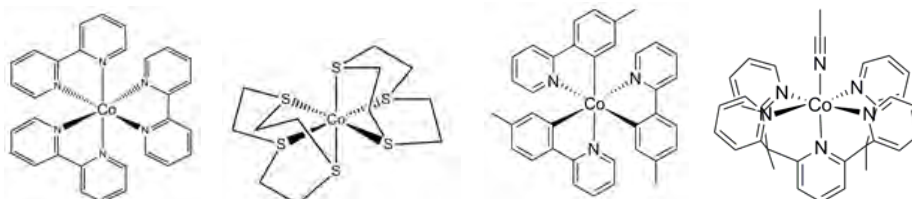


**Figure 2.** Structures of the cobalt complexes discussed in this presentation as redox shuttles in DSSCs, from left to right:  $\text{Co}(\text{bpy})_3$ ,  $\text{Co}(\text{ttn})_2$ ,  $\text{Co}(\text{ppy})$  and  $\text{Co}(\text{PY5Me}_2)(\text{CN})$

The third part of this talk will describe our efforts at understanding the energetics and recombination pathways of mesoscopic photoanodes. The photoanode plays a critical role as the electron donor in interception, therefore it is vital to develop a more detailed understanding of interception as a function of semiconductor property. For example, we previously showed that interception to positive, low reorganization energy redox shuttles occurs primarily via surface states with  $\text{TiO}_2$  photoanodes which prohibits the exploiting inverted region interception, but the role of surface states has not been determined for alternative systems. Recent efforts at using spectroelectrochemical and electrochemical measurements to determine the energetics of mesoscopic electrodes will be described. In addition, initial results at making mesoporous perovskite metal oxides, such as  $\text{SrTiO}_3$ , which may offer a high degree of property tenability, will also be presented. Finally, the implications for identifying new redox shuttle and photoanode combinations in advancing DSSCs will be discussed.

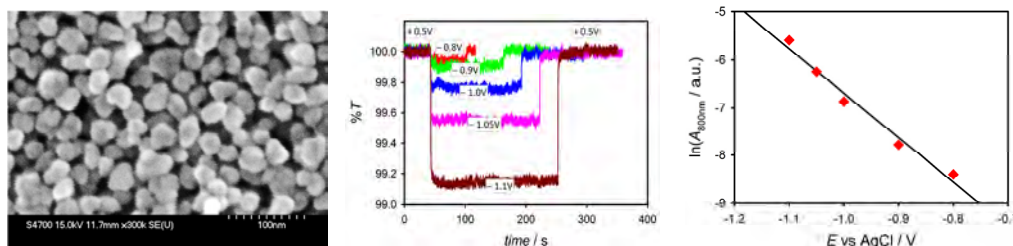


**Figure 3.** Left to right: SEM image of mesoporous  $\text{SrTiO}_3$  photoanodes, plots of transmittance ( $\%T$ ) at 800 nm measured as a function of applied potential, and the corresponding exponential absorbance change attributed to free conduction band electrons.

## DOE Sponsored Publications 2014-2017

1. Baillargeon, J., Xie, Y., Hamann, T.W.; “Bifurcation of Regeneration and Recombination in Dye-Sensitized Solar Cells via Electronic Manipulation of Tandem Cobalt Redox Shuttles” *ACS Applied Materials & Interfaces* **2017** DOI: 10.1021/acsami.7b01626
2. Mandal, D., Hamann, T.W.; “Charge distribution in nanostructured TiO<sub>2</sub> photoanodes determined by quantitative analysis of the band edge unpinning” *ACS Applied Materials & Interfaces* **2016**, 8 (1), 419–424
3. Xie, Y., Baillargeon, J., Hamann, T.W.; “Regeneration and Recombination Reactions in Dye Sensitized Solar Cells Employing Cobalt Redox Shuttles” *Journal of Physical Chemistry C.*, **2015**, 119 (50), 28155–28166
4. Mandal, D., Hamann, T.W.; “Energetics of Nanoparticle Semiconductor Electrodes Determined by Spectroelectrochemical Measurements of Free Electrons.” *Physical Chemistry Chemical Physics* **2015**, 17, 11156–11160
5. Soman, S., Xie, Y., Hamann, T.W.; “Cyclometalated sensitizers for DSSCs employing cobalt redox shuttles” *Polyhedron*, **2014**, 82, 139 – 147

## Functionalizing Oxide Surfaces with Molecular Assemblies —Applications in Energy Conversion

Bing Shan, Animesh Nayak, Degao Wang, Raja U. Mathiyazhagan, Thomas J. Meyer

Department of Chemistry  
University of North Carolina at Chapel Hill  
Chapel Hill, NC, 27514

In devices at the heart of energy conversion - fuels to electricity, solar energy to fuels - electrodes and their surfaces play outsized roles. At these surfaces, molecules are interconverted and electrons transferred into or out of the energy conversion device. It is, therefore, no surprise that device performance is dictated in large part by the properties of the surface and that manipulation of the interface at the surface is a key to improving performance. In our applications, we use molecular dyes as light absorbers, redox mediators for enhancing charge-separation, and catalysts for carrying out chemical reactions on the surfaces of oxide electrodes. We have explored ways to prepare combinations of redox mediators, light absorbers and catalysts directly on oxide surfaces. Direct surface synthesis is desirable for its simplicity and with the success, as a way to scale up for device purposes in the future. In addition to synthesis, existing capabilities for characterizing molecular surfaces have been applied, including spectroscopic, electrochemical, and rapid pulsed laser measurements, to explore the effect of chemical changes on surface properties.

For dye-sensitized photoelectrodes, interfacial dynamics can be modulated by varying the structures of surface-attached molecular assemblies. We have successfully applied a self-assembly approach based on zirconium-phosphonate bridging as a synthetic basis for preparing dye-sensitized molecular p/n junctions on electrode surfaces. In assemblies for energy conversion, a surface-attached redox mediator is added between a ruthenium polypyridyl or porphyrin dye on p- or n-type semiconductors or degenerately doped conductive oxide electrodes. In a donor-dye assembly with surface attachment on p-type nickel oxide, or degenerately doped indium tin oxide, the yield of generating reductive equivalents at the external assembly is enhanced by at least a factor of four and the recombination kinetics are significantly slowed due to the long distance of back electron transfer. The right design of the electron mediator, whose redox potentials align well with those of the excited state and the valence band edge of the p-type semiconductor, dictates the efficiencies of initial light-induced redox-separation and subsequent back electron transfer with the inner electrode.

In a photocathode with surface attached donor-dyes on NiO, the reduced dye formed after light excitation and intra-assembly quenching is spatially separated from the oxidized NiO surface, greatly decreasing the recombination rate and prolonging the lifetime of the reduced dye. The efficiency of hole injection, the kinetics of interfacial back electron transfer, and the quantum yield for redox-separated states were investigated with nanosecond transient absorption spectroscopy. The results of those experiments provided clear evidence for decreased recombination and long lifetimes for the reduced dye (milliseconds), even under open circuit conditions. The long-lived redox-separated states can improve the efficiency of the photocathode in dye-sensitized photoelectrosynthetic applications by providing persistent reductive equivalents

to water/CO<sub>2</sub> reduction catalysts. Detailed analyses of the underlying electron transfer steps show that the overall efficiency of the cell is limited by hole injection and charge recombination. Compared with the highly doped ITO photocathodes with the same assembly, the NiO photocathode shows higher photoconversion efficiencies for generating reductive equivalents and longer lifetimes for surface-bound redox-separated states due to inhibited back electron transfer.

We also examined the photo-induced electron transfer dynamics of ALD-prepared assemblies based on the configuration -RuP<sub>2</sub><sup>2+</sup>-ALD MO<sub>2</sub>-hole acceptor, with nanosecond transient absorption measurements for comparing solution-processed electrode assemblies. Analysis of the kinetics of back electron transfer from the reduced donor to the electrode, reveals that the ALD metal oxide bridging layer plays an important role in retarding the intra-assembly back electron transfer. Fitting of the decay traces for DA<sup>+</sup>, once it forms in the laser flash, with a monophasic stretched exponential model gave lifetimes for the interfacial redox separated state, *nano*ITO(e<sup>-</sup>)-RuP<sub>2</sub><sup>2+</sup>-MO<sub>2</sub>-DA<sup>+</sup>. Based on the fitting results, average lifetimes for back electron transfer vary depending on the ALD metal oxide bridging layer in the series:  $\tau(\text{ZrO}_2) < \tau(\text{Zr}^{\text{IV}}) < \tau(\text{TiO}_2) < \tau(\text{SnO}_2)$ . Compared with related bridges, SnO<sub>2</sub> assembled photoanode gave the slowest recombination rates with a lifetime of ~0.34 s. The extended lifetime and varying dynamic behavior of the ALD assembled structures emphasizes the advantages of the ALD strategy in tuning interfacial recombination kinetics, highlighting a key point in the assembly strategy. With systematic variations in the ALD bridge layer, it was possible to significantly improve the internal electronic properties of the assemblies, in this case, with variations in the lifetimes of the interfacial redox separated states that vary by a factor of ~10.

Additionally, we have explored an alternate strategy with the assembly synthesized directly on oxide surfaces to avoid the limitations inherent in the synthesis of pre-formed assemblies. In an initial series of experiments with surface-attached phosphonate-derivatized pyridyl/bipyridyl ligands on mesoporous ITO in *cis*-[Ru(bpy)<sub>2</sub>(OH<sub>2</sub>)<sub>2</sub>]<sup>2+</sup> or *cis*-[Ru(bpy)<sub>2</sub>Cl<sub>2</sub>] solutions show that the substitution of both aquo and chloro ligands by surface-attached bipyridine is uphill and requires extensive heating to drive the coordination reaction, due to the strained coordination geometry at the surface attached Ru(bpy)<sub>2</sub> center. In an alternate method, surface attached *cis*-[Ru(4,4'-(H<sub>2</sub>O<sub>3</sub>P)<sub>2</sub>bpy)<sub>2</sub>Cl<sub>2</sub>] or *cis*-[Ru(4,4'-(H<sub>2</sub>O<sub>3</sub>P)<sub>2</sub>bpy)<sub>2</sub>(OH<sub>2</sub>)<sub>2</sub>]<sup>2+</sup> are added as the assembly precursor in bipyridyl solutions. With its two relatively labile aqua ligands, the di-aqua complex is an ideal surface precursor for forming assemblies by ligand substitution. By having the *cis*-[Ru(4,4'-(H<sub>2</sub>O<sub>3</sub>P)<sub>2</sub>bpy)<sub>2</sub>(OH<sub>2</sub>)<sub>2</sub>]<sup>2+</sup> attached to *nano*ITO electrode immersed in ethanol/water /2,2'-bipyridine solution, surface-assembled *nano*ITO|RuP<sup>2+</sup> can be obtained.

Another focus is on oxide-surface modification with Perylene Di-imide derivatives as light absorbers. PDI dyes are a class of chromophores that have strong absorption in the visible and high photochemical stabilities. We have synthesized a substituted PDI chromophore with phosphonate anchors. The PDI bay positions are substituted at 1,7 positions with 2,6-bis (3,3-dimethylbutyloxy) phenyl. The bis(butyloxyphenyl) groups are introduced for adding bulk around the perylene plane thus reducing its tendency for aggregation due to  $\pi$ - $\pi$  stacking. The compound shows absorption around 450-600 nm. In solution, it undergoes oxidation at 1.32 V and reductions at -0.81 V -0.99 V vs NHE. These potentials are suitable for both H<sub>2</sub>O oxidation and H<sup>+</sup> reduction. Further studies of this chromophore for electron/hole injection to semiconductor metal oxides, and constructing chromophore-catalyst assemblies, are currently in

progress.

### **DOE Sponsored Publications 2017**

1. Bing Shan, Byron H. Farnum, Kyung-Ryang Wee, and Thomas J. Meyer. Generation of Long-Lived Redox Equivalents in Self-Assembled Bilayer Structures on Metal Oxide Electrodes. *J. Phys. Chem. C*, **2017**, Article ASAP. DOI: [10.1021/acs.jpcc.6b12416](https://doi.org/10.1021/acs.jpcc.6b12416).
2. Degao Wang, Matthew V. Sheridan, Bing Shan, Byron H. Farnum, Seth L. Marquard, Benjamin D. Sherman, Michael S. Eberhart, Animesh Nayak, Atanu K. Das, R. Morris Bullock, Thomas J. Meyer. Layer-by-layer, Chromophore/Catalyst Assemblies for Dye-Sensitized Photoelectrosynthesis Cells by Atomic Layer Deposition. *Angew. Chem.* Submitted.

## Electron/hole selectivity in organic semiconductor contacts for solar energy conversion

Chris D. Weber, D. Westley Miller, Colin Bradley, Kira Egelhofer, and Mark C. Lonergan  
 Department of Chemistry and Biochemistry  
 University of Oregon  
 Eugene, OR, 97403

The direct conversion of solar energy to electricity or fuels requires the selective collection of one of an electron or hole at an interface. The development of contacts that form such interfaces to solar absorbers presents significant challenges to our fundamental understanding of the integrated action of charge transfer processes at interfaces. The action of these processes in determining the selectivity and recombination characteristics of semiconductor interfaces is of particular interest. We present studies on the relation of fundamental rate processes at semiconductor interfaces to their solar energy conversion properties, the integrated measurement of these rate processes for organic semiconductor contacts in a silicon model system using the interdigitated back contact (IBC) solar cell, and progress on understanding bulk recombination centers in lead halide perovskite solar cells to lay a foundation for better understanding their interplay with recombination processes at contacts.

We use a three contact geometry based on the IBC solar cell to simultaneously measure electron and hole transfer processes at semiconductor contacts containing interfacial layers based on organic semiconductors. A schematic of the IBC cell is shown in Fig. 1; it consists of a near intrinsic layer of silicon contacted on one side (the back side) with heavily doped n- and p-type regions ( $n^+$  and  $p^+$ ). A third contact, the one under study, is made to the front side and its electrical properties characterized against either the  $n^+$  or  $p^+$  contact. Aided by numerical simulation, the combination of these measurements can be used to determine the exchange current densities for electrons and holes ( $J_{on}$  and  $J_{op}$ ) at the interface under study.

Figure 2 shows results from an IBC cell study for 5-10 nm thick anionically (PFFA) and cationically (PFFC) functionalized polyfluorene-based interfacial layers (shown in Fig. 1)

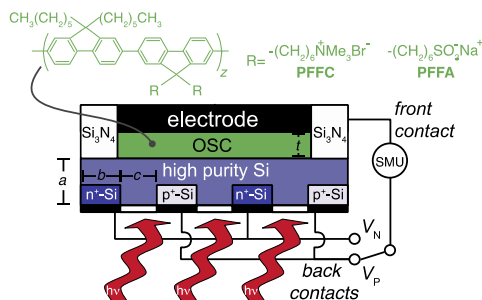


**Figure 1 - Schematic of interdigitated back contact solar cell and polyfluorene interfacial layers, which are examples of organic semiconductors being studied.**

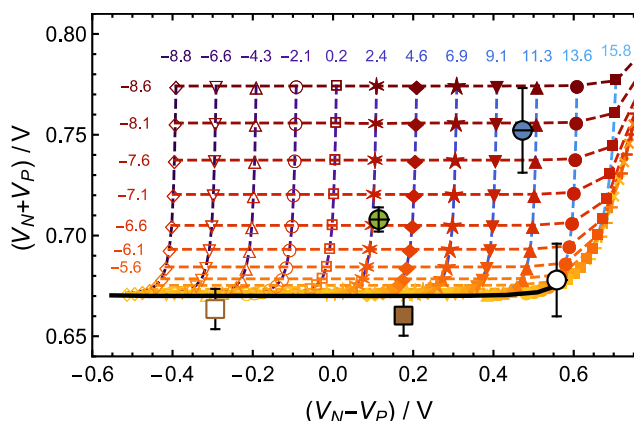


**Figure 2 - Comparison of numerical simulation of  $V_N + V_P$  versus  $V_N - V_P$  data to experiments for contacts to the IBC cell. The red/orange symbols connected by dashed lines are simulation results. The large symbols with error bars are the experimental data for PEDOT-PSS (black open circle), PFFA (blue filled circle minus), PFFC (green filled circle plus), Au (open brown square), and Ag (solid brown square).**

subsequently contacted with a PEDOT-PSS electrode. Plotted is the sum and difference of  $V_N$  and  $V_P$ , where  $V_N$  is the open-circuit voltage measured between the contact under study against the  $n^+$  contact, and  $V_P$  that against the  $p^+$  contact. The experimental data are the large symbols with error bars, and the small data points connected with a grid of dashed lines are the result of numerical simulation. The difference and sum report on parameters relating to the selectivity and recombination characteristics of the interface, where the selectivity ( $S$ ) is defined as  $S = J_{on} / J_{op}$  and the recombination parameter ( $R$ ) as  $R = J_{on} J_{op}$ . In regards to the simulation data, symbols of the same type and connected with a dashed blue line have the same value of  $\log S$ , as specified by the top blue labels. Data points connected by horizontal red/orange dashed lines have the same value of  $\log R$ , as specified by the left red/orange labels. The formation of a near regular grid demonstrates the ability of IBC cell measurements to separate  $S$  from  $R$ . A change in selectivity results in one of  $V_N$  or  $V_P$  increasing and the other decreasing (no change in sum), whereas a change in recombination results in both  $V_N$  and  $V_P$  either increasing or decreasing (no change in difference). Comparison of the experimental data to the simulation grid shows that modifying a PEDOT-PSS interface with polyfluorene-based polyelectrolytes reduces recombination at the interface with  $R$  decreasing six or seven orders of magnitude, presumably due to its action as a tunneling barrier. The selectivity of the interface is also significantly modified in a way that depends on the sign of the ionic functional group. The value of  $S$  for PFFA is some eight orders of magnitude greater than for PFFC. These results show that both selectivity and recombination must be considered in determining the action of interfacial layers. Results will also be presented that demonstrate the precise relation between interface selectivity and recombination in determining the properties of a solar cell.

The above studies highlight the importance of contact recombination. As our studies of organic semiconductor contacts extend to lead halide perovskite and related absorber materials, it is important to understand the balance of recombination processes in the entire system. Toward this end, we present results characterizing bulk defects in lead halide perovskite absorbers,

which can act as recombination centers, using sub-band gap external quantum efficiency (EQE) and junction capacitance methods. We have characterized the presence of gap-states in methylammonium lead halide perovskite absorbers as a function of synthesis method and halide composition. Figure 3 shows an example of sub-band gap EQE measurements on  $\text{CH}_3\text{NH}_3\text{Pb}(\text{I}_{1-x}\text{Br}_x)_3$  absorbers as a function of halide composition. All maintain sharp Urbach edges but also show an extended band of sub-bandgap electronic states that can be fit with one or two point defects for pure  $\text{CH}_3\text{NH}_3\text{PbI}_3$  or mixed  $\text{CH}_3\text{NH}_3\text{Pb}(\text{I}_{1-x}\text{Br}_x)_3$  compositions, respectively.

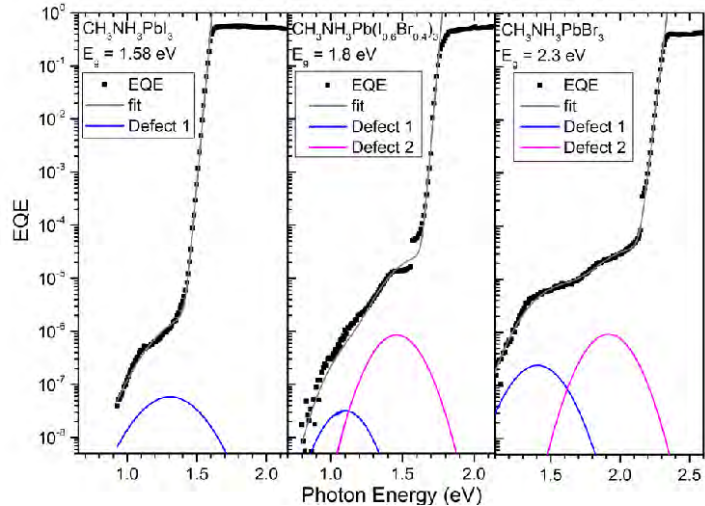


**Figure 3 - Sub-bandgap EQE spectra for  $\text{CH}_3\text{NH}_3\text{Pb}(\text{I}_{1-x}\text{Br}_x)_3$ . Fits to the data are shown as solid grey lines, with the underlying gaussian defect distributions shown as solid blue and magenta lines.**

## DOE Sponsored Publications 2014-2017

1. Carolin M. Sutter-Fella, D. Westley Miller, Quynh P. Ngo, Ellis T. Roe, Francesca M. Toma, Ian D. Sharp, Mark C. Lonergan, and Ali Javey, Band Tailing and Deep Defect States in  $\text{CH}_3\text{NH}_3\text{Pb}(\text{I}_{1-x}\text{Br}_x)_3$  Perovskites As Revealed by Sub-Bandgap Photocurrent, *ACS Energy Letters* **2**, 709 (2017).
2. D Westley Miller, Giles E Eperon, Ellis T Roe, Charles W Warren, Henry J Snaith, Mark C Lonergan, Defect states in perovskite solar cells associated with hysteresis and performance, *Applied Physics Letters* **109**, 153902 (2016).
3. Colin Bradley and Mark C. Lonergan, "Limits on anion reduction in an ionically functionalized fullerene by cyclic voltammetry with in situ conductivity and absorbance spectroscopy" *J. Mater. Chem. A* **4**, 8777 (2016).
4. Christopher D Weber, David P Stay, Mark C Lonergan, "The Effects of Polyfluorene Polyelectrolyte Interfacial Layers on Selectivity and Recombination Measured Using the Interdigitated Back Contact Solar Cell," *The Journal of Physical Chemistry C* **120**, 19951 (2016).
5. Ethan M. Walker and Mark C. Lonergan, "Extracting electrode space charge limited current: Charge injection into conjugated polyelectrolytes with a semiconductor electrode," *Applied Physics Letters* **108**, 213301 (2016)
6. Evan R. Darzi, Elizabeth S. Hirst, Christopher D. Weber, Lev N. Zakharov, Mark C. Lonergan, and Ramesh Jasti, "Synthesis, Properties, and Design Principles of Donor–Acceptor Nano hoops," *ACS Central Science* **6**, 335–342 (2015).
7. K.J. Karki, J. R. Widom, J. Seibt, I. Moody, M.C. Lonergan, T. Pullerits, A.H. Marcus, "Coherent two-dimensional photocurrent spectroscopy in a PbS quantum dot photocell," *Nature Communications* **5**, 5869 (2014).
8. C.D. Weber, C. Bradley, E.M. Walker, S.G. Robinson, M.C. Lonergan, "Increased Performance of Inverted Organic Photovoltaics Using a Cationically functionalized Fullerene Interfacial Layer," *Solar Energy Materials and Solar Cells* **129**, 90 (2014).
9. C.D. Weber, C. Bradley, M.C. Lonergan, "Solution phase n-doping of  $\text{C}_{60}$  and PCBM using tetrabutylammonium fluoride," *J. Mater. Chem. A* **2**, 303 (2014).



## *Session III*

### *First Row Chromophores*



# Towards Control of Electronic Excited State Phenomena in 3d Metal Complexes: Ultrafast x-ray laser studies of chemical dynamics

Kelly J. Gaffney

Stanford Synchrotron Radiation Lightsource and PULSE Institute  
SLAC National Accelerator Laboratory and Stanford University, Menlo Park, CA 94025  
kgaffney@slac.stanford.edu

Electronic excited state phenomena provide a compelling intersection of fundamental and applied research interests in the chemical sciences. This holds true for coordination chemistry, where harnessing the strong optical absorption and photocatalytic activity of compounds depends on our ability to control fundamental physical and chemical phenomena associated with electronic excited states. Unlike electronic ground state phenomena where Born-Oppenheimer potentials often suffice to understand molecular and chemical dynamics, non-adiabatic dynamics with strong coupling between electronic and vibrational motion often dominate the dynamics of electronic excited states. For 3d transition metal containing materials, intersystem crossing and internal conversion, as well as solvation, greatly influence the meta-stability of electron transfer excited states.

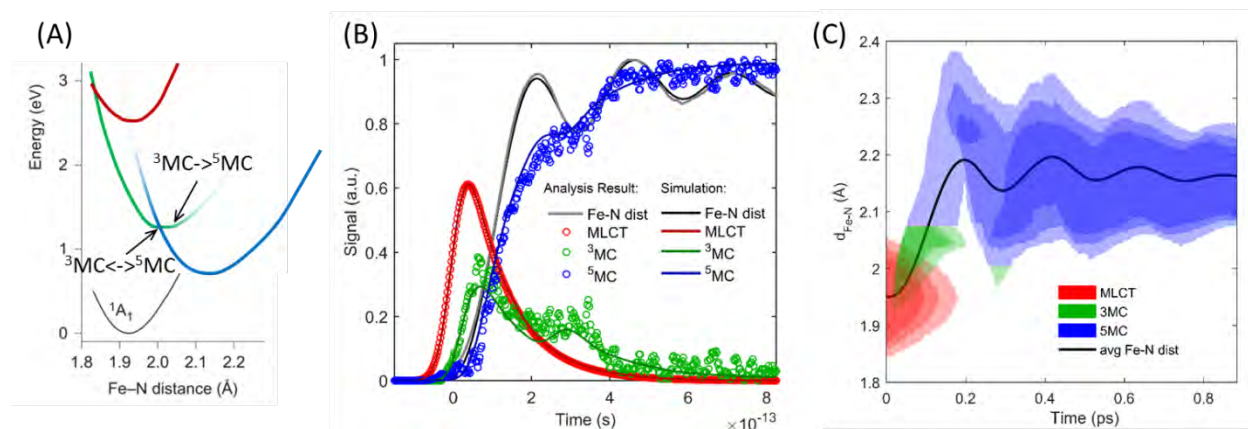


Figure 1: (A) Potential energy surface showing the key electronic states involved in photo-induced spin crossover in  $[\text{Fe}(\text{bpy})_3]^{2+}$ . (B) Time dependent populations of the  $^{1,3}\text{MLCT}$  (red),  $^3\text{MC}$  (green), and  $^5\text{MC}$  excited states, as well as the mean Fe-N bond length as a function of time for the full ensemble of excited molecules. (3) Time dependent distribution of Fe-N bond lengths for excited state populations extracted from a fit to the experimental results. Note that the results enable the determination of the Fe-N bond lengths associated with the non-adiabatic transitions between the  $^3\text{MC}$  and  $^5\text{MC}$  excited states.

For the non-adiabatic dynamics of electronic excited states, the location of conical intersections and seams between electronic states play a role to understanding excited state phenomena analogous to the transition state for the electronic ground state. Consequently, developing techniques capable of determining the non-equilibrium trajectories of electronic excited states and the locations of conical intersections is fundamental to harnessing photo-induced excited states. The diversity of non-equilibrium electronic and nuclear configurations, however, makes this a challenging task. In particular, experimental methods capable of disentangling the coupled motion of electrons and nuclear dynamics warrant emphasis. As I will discuss, the combination

of ultrafast hard x-ray absorption spectroscopy (XAS), emission-fluorescence spectroscopy (XES), and diffuse x-ray scattering (XDS) has enabled the complex evolution of the charge, spin, and coordination geometry to be investigated with unprecedented detail.

I will use the photo-induced spin crossover in  $[\text{Fe}(\text{bpy})_3]^{2+}$ , where bpy = 2,2'-bipyridine, as an archetypical system for understanding the chemical and physical properties that govern the lifetime of charge transfer excited states.  $[\text{Fe}(\text{bpy})_3]^{2+}$  has also proven to be an excellent system for the development of femtosecond resolution hard x-ray spectroscopy and x-ray scattering. The spin crossover process begins with the generation of a metal-to-ligand charge transfer (MLCT) excited state. In these studies, we have been able to definitively show the MLCT excited state transitions to a triplet metal centered excited state ( $^3\text{MC}$ ) before creating the high spin excited state ( $^5\text{MC}$ ). [1-4] In more recent unpublished work, we have combined the electronic structure information of XES with the nuclear structure information of XAS and XDS, to identify the Fe-N mean bond lengths where transition occur between the  $^3\text{MC}$  and the  $^5\text{MC}$  excited states. Interestingly, the bond length is different for the forward and back reactions, demonstrating that additional structural degrees of freedom must be critical to the non-adiabatic dynamics. A summary of these results can be found in Figure 1.

Using  $[\text{Fe}(\text{bpy})_3]^{2+}$  as a starting point, we have been able to apply the same methods to investigate how ligand substitution and solvent strongly influence the relaxation dynamics. In the mixed ligand complex,  $[\text{Fe}(\text{CN})_4(\text{bpy})]^{2-}$ , we observe MLCT excited state lifetimes of 19 ps in non-hydrogen bonding solvents. This represents more than a one hundred-fold increase over the MLCT lifetime in  $[\text{Fe}(\text{bpy})_3]^{2+}$ . [5] When dissolved in water, the dynamics are significantly different. In water, the MLCT state of  $[\text{Fe}(\text{CN})_4(\text{bpy})]^{2-}$  decays on the 100 fs time scale, but forms a metastable  $^3\text{MC}$ , instead of a  $^5\text{MC}$  (unpublished). Only by combining ultrafast optical UV-visible and XES spectroscopy have we been able to robustly characterize the relaxation mechanism and begin to contribute to the understanding of how ligand and solvent modifications influence excited state phenomena.

## References:

- [1] H.T. Lemke, C. Bressler, L.X. Chen, D.M. Fritz, K.J. Gaffney, A. Galler, W. Gawelda, K. Haldrup, R.W. Hartsock, H. Ihee, J. Kim, K.H. Kim, J.H. Lee, M.M. Nielsen, A.B. Stickrath, W.K. Zhang, D.L. Zhu, M. Cammarata, "Femtosecond X-ray Absorption Spectroscopy at a Hard X-ray Free Electron Laser: Application to Spin Crossover Dynamics," *J. Phys. Chem. A* 117 (4), 735 (2013).
- [2] W.K. Zhang, R. Alonso-Mori, U. Bergmann, C. Bressler, M. Chollet, A. Galler, W. Gawelda, R.G. Hadt, R.W. Hartsock, T. Kroll, K.S. Kjaer, K. Kubicek, H.T. Lemke, H.W. Liang, D.A. Meyer, M.M. Nielsen, C. Purser, J.S. Robinson, E.I. Solomon, Z. Sun, D. Sokaras, T.B. Van Driel, G. Vanko, T.C. Weng, D. Zhu, K.J. Gaffney, "Tracking Excited State Charge and Spin Dynamics in Iron Coordination Complexes " *Nature* 509 345 (2014).
- [3] W.K. Zhang, K.J. Gaffney, "Mechanistic Studies of Photoinduced Spin Crossover and Electron Transfer in Inorganic Complexes," *Acc. Chem. Res.* 48 (4), 1140 (2015).
- [4] H. Lemke, K.S. Kjaer, R.W. Hartsock, T.B. van Driel, M. Chollet, J.M. Glowonia, S.H. Song, D.L. Zhu, E. Pace, S.F. Matar, M.M. Nielsen, M. Benfatto, K.J. Gaffney, E. Collet, M. Cammarata, "Coherent structural trapping through wave packet dispersion during photoinduced spin state switching," *Nature Comm.* 8 15342 (2017).
- [5] W.K. Zhang, K.S. Kjaer, R. Alonso-Mori, U. Bergmann, M. Chollet, L.A. Fredin, R.G. Hadt, R.W. Hartsock, T. Harlang, T. Kroll, K. Kubicek, H.T. Lemke, H.W. Liang, Y.Z. Liu, M.M. Nielsen, P. Persson, J.S. Robinson, E.I. Solomon, Z. Sun, D. Sokaras, T.B. van Driel, T.C. Weng, D.L. Zhu, K. Warnmark, V. Sundstrom, K.J. Gaffney, "Manipulating charge transfer excited state relaxation and spin crossover in iron coordination complexes with ligand substitution," *Chem. Sci.* 8 (1), 515 (2017).

## Redefining the Photophysics of Fe(II)-based Chromophores

James K. McCusker  
Department of Chemistry  
Michigan State University  
East Lansing, Michigan 48824

The goal of our research program focuses on the development of chromophores based on first-row transition metal ions for use as light harvesters in solar energy conversion strategies. The underlying motivation for the work hinges on the issue of scalability and the limited potential for the widespread use of traditional second- and third-row chromophores due to their elemental scarcity. Based in large part on work we have carried out through our DOE-supported research, a key scientific issue impeding the utility of most first-row metal complexes in the context of solar energy conversion is the profound difference that exists in their intrinsic photophysics relative to their second- and third-row congeners. These differences are particularly problematic on ultrafast time scales: with the notable exception of complexes of Cu(I), the ultrafast relaxation processes that arise due to the presence of low-lying ligand-field excited-states in first-row metal complexes undercuts their use in virtually any application that relies on charge separation following photon capture. We believe this represents an important problem in fundamental science in general and energy science in particular. The focus of our research program is therefore to understand the factors that determine the dynamics associated with the charge-transfer excited-states of first-row transition metal-based chromophores, with the ultimate goal of circumventing and/or redefining their intrinsic photophysics in order to make feasible their use as light-harvesting components in solar energy conversion strategies. This presentation will cover two areas of our research that we have advanced during the previous funding period, as well as provide a brief prospectus of areas that we envision pursuing in the near future.

**A. Identification and Control of the Reaction Coordinate for Ultrafast MLCT Relaxation.** One can view the issue of ultrafast MLCT-state deactivation in first-row transition metal-based chromophores as a problem of relative rates, namely the rate of intramolecular relaxation from the charge-transfer to ligand-field-state manifold versus the rate of reaction out of the CT state. Control of these kinetics requires an understanding of the reaction coordinate coupled to the ultrafast CT-to-LF non-radiative decay process. One major thrust of our research

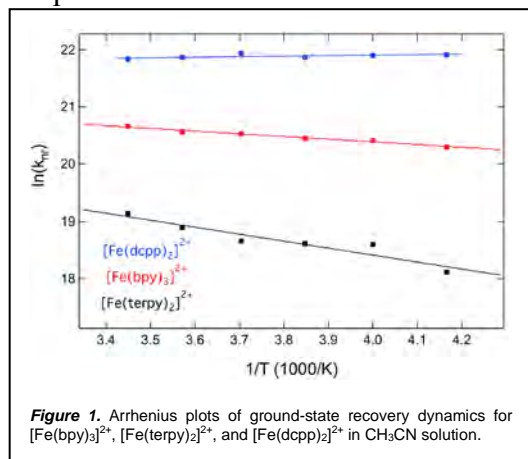


Figure 1. Arrhenius plots of ground-state recovery dynamics for [Fe(bpy)<sub>3</sub>]<sup>2+</sup>, [Fe(terpy)<sub>2</sub>]<sup>2+</sup>, and [Fe(dcpp)<sub>2</sub>]<sup>2+</sup> in CH<sub>3</sub>CN solution.

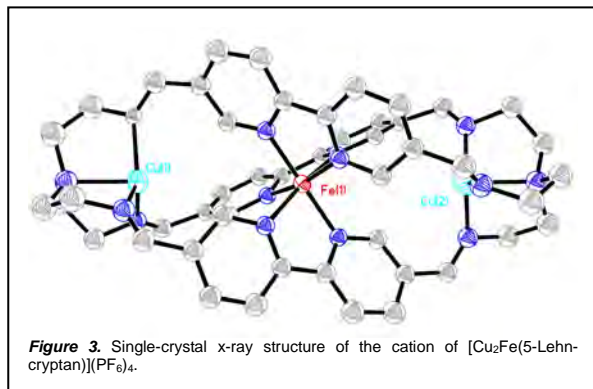
is therefore to identify and effectively redesign the reaction coordinate associated with these dynamics. We are tackling this problem by coupling information about reorganization energies associated with excited-state evolution with computational efforts to piece together the normal mode(s) known to undergo net displacement that are also energetically competent to contribute to these (experimentally determined) energies.

To achieve this goal, we have recently developed the capability to carry out variable-temperature sub-nanosecond time-resolved spectro-

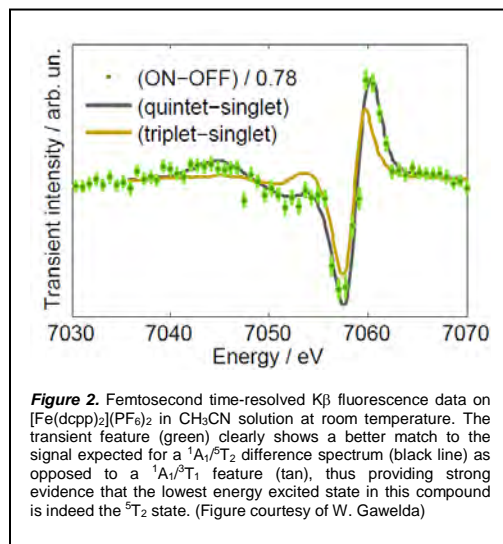
scopy. The first experiments utilizing this variable temperature ultrafast set-up involved measuring the temperature dependence of ground-state recovery dynamics in a number of Fe(II) polypyridyl complexes. This is a necessary first step in mapping out the reaction coordinate for the overall transformation of interest, but also represents a long-standing problem in the photophysics of this class of chromophores. Data acquired on several compounds are illustrated in Figure 1 in the form of an Arrhenius plot. A particularly intriguing result is the fact that, despite some fairly significant differences among these three compounds in terms of their molecular structures, the intercept of the Arrhenius plots for all three complexes were found to be approximately the same at  $\sim 250 \text{ ps}^{-1}$ . The pre-exponential term is essentially the rate constant expected in the limit of zero barrier; recasting this in terms of semi-classical Marcus theory enabled us to experimentally determine a relationship between the electronic coupling and reorganization energy for this process. Efforts to further quantify these parameters using compounds whose zero-point energies (i.e.,  $\Delta G_0$ ) can be independently measured are ongoing.

**B. Reshaping the Energy Landscape.** In addition to identifying the geometric factors that help to define the photophysics of Fe(II)-based chromophores,

we are working on synthetic approaches to invert the relative energies of their ligand-field and MLCT excited states; in this way, we hope to create a series of Fe(II)-based complexes whose electronic structures (and by extension excited-state reactivities) resemble that of Ru(II). One avenue of research involves synthetic elaboration of  $[\text{Fe}(\text{dcpp})_2]^{2+}$  (where dcpp is di(carboxypyridyl)pyridine), a compound that we developed through our research program that exhibits unprecedented optical and electrochemical properties for an Fe(II) polypyridyl complex. Work along these lines includes the development of new ligands that enhance  $\sigma$  donation and attenuate  $\pi$  donation to the metal in order to increase ligand-field strength, incorporation of electron withdrawing substituents to stabilize the MLCT manifold, and the use of ultrafast x-ray spectroscopy to determine the nature of the lowest-energy excited state as a function of ligand



spectroscopic measurements on this compound will be described, along with an overview of future directions of our research program.



composition (Figure 2). We have also recently pursued a new motif to explore the possibility of trapping a reactive excited state. The trinuclear assembly shown in Figure 3 consists of an Fe(II) tris-bpy core (in pseudo- $D_{3h}$  symmetry as opposed to  $D_3$ ) flanked by two Cu(I) ions. This system is thus set up as an intramolecular “flash-quench” assembly in which the MLCT excited state of the Fe(II) chromophore can be reductively quenched by Cu(I), resulting in the formation of a  $\text{bpy}^-$  species. Time-resolved

## DOE Sponsored Publications 2014-2017

1. Allison M. Brown, Catherine E. McCusker, and James K. McCusker, "Spectroelectrochemical Identification of Charge-Transfer Excited States in Transition Metal-based Polypyridyl Complexes", *Dalton Transactions*, **2014**, 43, 17635-17646.
2. Lindsey L. Jamula, Allison M. Brown, Dong Guo, and James K. McCusker, "Synthesis and Characterization of a High-Symmetry Ferrous Polypyridyl Complex: Approaching the  $^5T_2/{}^3T_1$  Crossing Point for Fe(II)", *Inorg. Chem.* **2014**, 53, 15-17.
3. Allison M. Brown, Catherine E. McCusker, Ana Maria Blanco-Rodriguez, Michael Towrie, Ian P. Clark, Antonin Vlcek, Jr. and James K. McCusker, "Vibrational Relaxation and Redistribution Dynamics in Ru(II) Polypyridyl-based Charge-Transfer Excited States: A Combined Ultrafast Electronic and Infrared Absorption Study", *J. Am. Chem. Soc.*, submitted for publication.
4. James K. McCusker, "The Photophysics of Fe(II) Complexes: Fundamental Issues, Perspectives, and Applications in Solar Energy Conversion", submitted for publication as a Perspective in *Chemical Science*.
5. Monica Carey and James K. McCusker, "Correlating Electronic Coupling and Reorganization Energy in the Excited-state Dynamics of Fe(II) Polypyridyl Complexes using Variable-temperature Ultrafast Spectroscopy", manuscript in preparation for submission to *Chemical Science*
6. Jennifer N. Miller and James K. McCusker, "Outer-sphere Effects on the Ground-state Recovery Dynamics of  $[\text{Fe}(\text{bpy})_3]^{2+}$ ", manuscript in preparation for submission to *Inorganic Chemistry*.
7. Monica Carey and James K. McCusker, "Solvent and Excitation Wavelength-dependent Dynamics in the Excited-state Evolution of  $[\text{Ru}(\text{dpb})_3]^{2+}$ : The Role of Charge Distribution in Solvent-Solute Coupling", manuscript in preparation for submission to the *Journal of Physical Chemistry A*.



*Session IV*

*Photoelectrochemical Nanostructures*



## Sensitization of Oxide Single Crystals with Quantum Confined Semiconductors

Lenore Kubie\*, Kevin Watkins\*, Mark Spitler, Jeff Blackburn<sup>+</sup>, William Rice<sup>#</sup>, Henry Wladkowski<sup>#</sup>, Laurie A. King\*, Meghan E. Kern\*, Subash Kattel<sup>#</sup>, Qian Yang\* and Bruce Parkinson\*

Department of Chemistry\* and Department of Physics<sup>#</sup>  
University of Wyoming, 1000 E. University  
Laramie, WY , 82071

and

<sup>+</sup>National Renewable Energy Laboratory

### CdSe Quantum Dot Photosensitization

We have extended our studies of the fundamentals of electron injection into large bandgap metal oxide semiconductors to further test the theoretical model proposed by Spitler that predicts that the photocurrent yields and photocurrent-voltage behavior are controlled by the doping density that then determines the field gradient of the Schottky barrier at the electrode/electrolyte interface. The model was earlier shown to be applicable to sensitization by both thiocyanine and ruthenium based sensitizing dyes with the difference of the behavior between the two classes of dyes being attributed to the different distance of the photogenerated hole on the dye from the injected electron that influences the rate of the back reaction. We have extended these studies to monolayers of adsorbed CdSe quantum dots of various sizes on well-characterized TiO<sub>2</sub> single crystals (Figure 1a) with varying doping densities. The results indicate that now, due to the much larger size of the injecting particle, the back reaction between the injected electron and the hole on the CdSe QD is reduced resulting in less sensitivity of the photocurrent yield on doping density as would be predicted by the model (Figure 1b) and more rapid onset of the photocurrent plateau in the photocurrent-voltage curves.

### Ag<sub>2</sub>S Nanoplatelets

Ultrathin silver sulfide (Ag<sub>2</sub>S) platelets were synthesized via a one-pot method in ethylene glycol with 3-mercaptopropionic acid serving as both the sulfur precursor and platelet ligand (Figure 2A and 2B). The thinnest platelets, with a height of only 3.5±0.2 Å, are quantum-confined with a 1S exciton Bohr diameter to confinement ratio of ~12.6. Transmission electron microscopy (TEM) and atomic force microscopy (AFM) reveal that during synthesis the nanoplatelets (NPLs) are encapsulated in a web-like polymer or gel. However, excess ligand, ethylene glycol, and the polymer/gel can be removed after synthesis, and the platelets can be readily resuspended in water. The growth of these NPLs is quantized by layer thickness as indicated by UV-vis and steady-state fluorescence spectra. TEM, XRD and AFM analyses of these NPLs support formation along the (202) plane of the □Ag<sub>2</sub>S structure (Figure 2C). Unlike previous Ag<sub>2</sub>S studies, the sensitized photocurrent spectroscopy measurements mimic the distinct absorption spectral shapes of the NPLs.

## Sensitization of SnO<sub>2</sub> and TiO<sub>2</sub> with Semiconducting Single Wall Nanotubes

After years of unsuccessful attempts we have finally demonstrated, with collaboration from NREL and the Rice group at UW, that photoexcited single wall semiconducting nanotubes can produce sensitized photocurrents on both TiO<sub>2</sub> and SnO<sub>2</sub> single crystal electrodes. The key to this success appears to be the use of cholate to solubilize the nanotubes that provides a carboxylate group to bond directly to the oxide surface that increases the electronic coupling. Figure 3 shows the absorption spectra of the nanotube suspension and the IPCE spectrum of the adsorbed nanotubes. Hints of multiple exciton generation will be discussed as well.

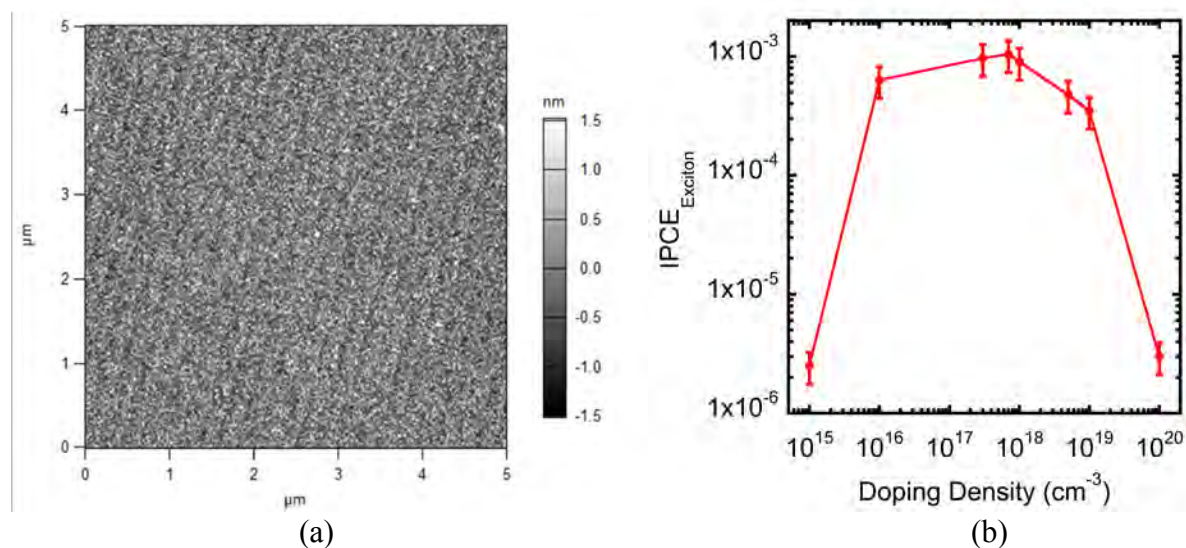
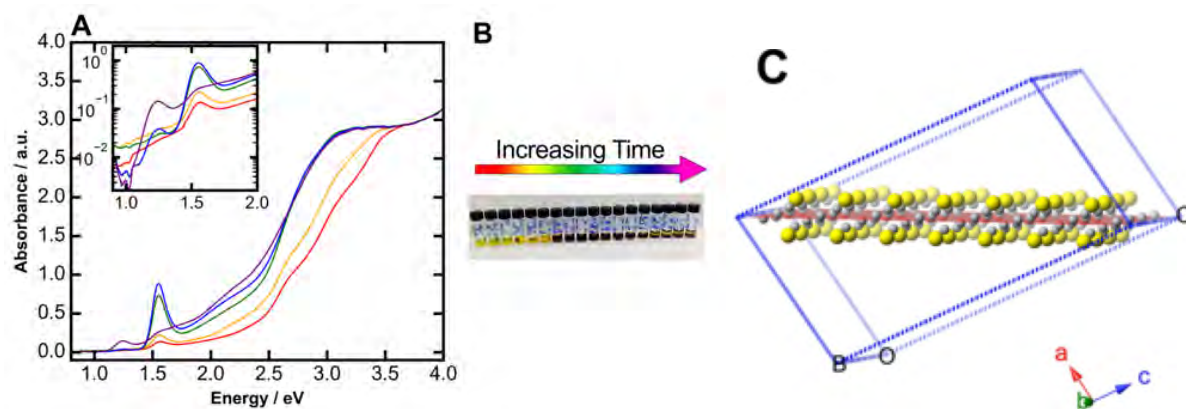


Figure 1 (a) AFM image of a monolayer of CdSe QDs on a single crystal TiO<sub>2</sub> (110) face. Note that the terraces of the surface structure can be seen below the QDs. (b) Incident photon current efficiencies for a range of doping densities of TiO<sub>2</sub> crystals (note the log scale).



**Figure 2.** A) UV-Vis spectra of Ag<sub>2</sub>S NPLs during synthesis in ethylene glycol. Time proceeds from red to purple. The first features to appear are an onset of absorbance at around 2 eV and a shoulder at around 2.5 eV (red). Over time, the 1.55 eV exciton band grows in (orange), and then begins to disappear as another peak at 1.25 eV begins to grow in (yellow). Further growth increases the OD of the peak at 1.25 eV (green and blue) until overgrowth causes flocculation of particles (purple). Inset shows an enlargement of the exciton region on a logarithmic scale for enhancement of the 1.55 eV peak. B) Photograph of aliquots from the reaction over time. The precursor solution is cloudy white, but turns yellow upon beginning to heat. The solutions turn from yellow to brown as the reaction proceeds until all particles crash out upon overgrowth. C) Model of a single layer of the Ag<sub>2</sub>S structure that is the proposed nanoplatelet structure.

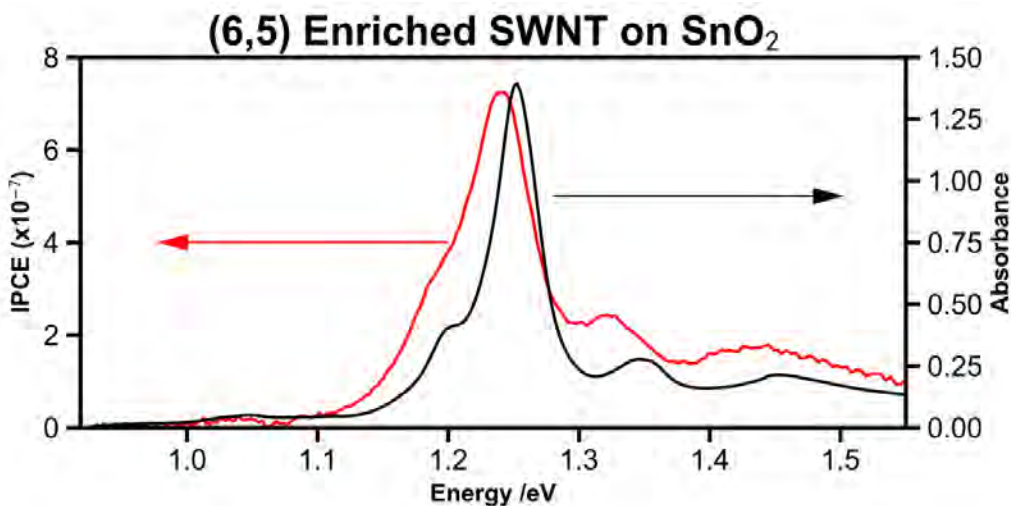


Figure 3 Incident photon current efficiency (left axis) as a function of energy and absorption spectrum (right axis) for highly enriched (6,5) semiconducting nanotubes on a SnO<sub>2</sub> (110) single crystal surface and in solution.

### DOE Sponsored Publications 2014-2017

1. Laurie King, Meghan Kern and B. A. Parkinson, "Sensitization of Single Crystal Substrates", In *Photoinduced Processes at Surfaces and in Nanomaterials*; ACS Symposium Series; American Chemical Society, Vol. 1196, pp 1–45, (2015).
2. Laurie A. King, Qian Yang, Michael L. Grossett, Zbigniew Galazka, Reinhard Uecker and B. A. Parkinson, "Photosensitization of Natural and Synthetic SnO<sub>2</sub> Single Crystals with Dyes and Quantum Dots", *J. Phys. Chem C*, 120(29), 15735-15742, (2016), DOI: 10.1021/acs.jpcc.5b11071\
3. Kevin J. Watkins, B. A. Parkinson and M. T. Spitler, "Physical Models for Charge Transfer at Single Crystal Oxide Semiconductor Surfaces as Revealed by the Doping Density Dependence of Collection Efficiency of Dye Sensitized Photocurrents", *J. Phys. Chem B*, 119(24), 7579-7588, (2015), DOI: 10.1021/jp511438j

4. Alexander B. Nepomnyashchii and B. A. Parkinson, “Contrasting Electrogenerated Chemiluminescence for a Dissolved and Surface Attached Carbazole Thiophene Cyanoacrylate Dye”, Applied Materials and Interfaces, 6, 14881-14885, (2014), DOI: 10.1021/am503743v
5. Y. Huang, E. Sutter, J.T. Sadowski, M. Cotlet, O.L.A. Monti, D.A. Racke, M. Neupane, R. Lake, B.A. Parkinson, and P. Sutter “Tin Disulfide – An emerging layered metal dichalcogenide semiconductor: Materials properties and device characteristics”, *ACS Nano*, 8(10), 10743-10755, (2014)
6. Paul F. Newhouse and B. A. Parkinson, “Combinatorial optimization of spinel  $\text{Co}_{3-x}\text{M}_x\text{O}_4$   $\text{M} = (\text{Al}, \text{Ga}, \text{In})$  alloyed thin films prepared by ink jet printing: photoelectrochemical, structural, and optical properties”, *J. Mater. Chem. A*, 3, 5901-5907, (2015).
7. Theodore J. Kraus, Alexander B. Nepomnyashchii and B. A. Parkinson, “Atomic Layer Deposition of Epitaxial Layers of Anatase  $\text{TiO}_2$  on Strontium Titanate Single Crystals: Morphological and Photoelectrochemical Studies”, *J. Vac. Sci. Technol. A* 33, 01A135 (2015)
8. Theodore J. Kraus, Alexander B. Nepomnyashchii and B. A. Parkinson, “Homo-epitaxial Growth on Single Crystal Anatase (101) and Rutile (110)  $\text{TiO}_2$  with Atomic Layer Deposition”, ACS Applied Materials and Interfaces, Applied Materials and Interfaces, 6(13), 9946-9949, (2014).
9. Yongqi Liang, Thomas Novet, James E. Thorne and B. A. Parkinson, “Photo-sensitization of ZnO Single Crystal Electrodes with PbS Quantum Dots”, Phys. Stat. Solidi A, 1-6, (2014) DOI 10.1002/pssa.201330602
10. Yongqi Liang, Meghan Kern, James E. Thorne, B. A. Parkinson, “Sensitization of ZnO Single Crystal Electrodes with CdSe Quantum Dots”, Langmuir, 30, 12551-12558, (2014)
11. John G. Rowley, Thanh D. Do, David A. Cleary and B. A. Parkinson, “Combinatorial Discovery Through a Distributed Outreach Program: Investigation of the Photoelectrolysis Activity of p-type Fe, Cr, Al Oxides”, Applied Materials and Interfaces, 6, 9046-9052, (2014)
12. Justin B. Sambur and B. A. Parkinson, “Size Selective Photoetching of CdSe Quantum Dot Sensitizers on Single Crystal  $\text{TiO}_2$ ”, Applied Materials and Interfaces, 6(24), 21916-21920, (2014)
13. Kevin J. Watkins, B. A. Parkinson and M. T. Spitler, “Physical Models for Charge Transfer at Single Crystal Oxide Semiconductor Surfaces as Revealed by the Doping Density Dependence of Collection Efficiency of Dye Sensitized Photocurrents”, *J. Phys. Chem B*, 119(24), 7579-7588, (2015), DOI: 10.1021/jp511438j
14. Kirill Sliozberg, Helge S. Stein, Chinmay Khare, Bruce A. Parkinson, Alfred Ludwig and Wolfgang Schuhmann, “Fe-Cr-Al containing oxide semiconductors as potential solar water splitting materials”, *ACS Applied Materials and Interfaces*, 7 (8), pp 4883–4889, (2015)

15. Philip Reckers, Mariel Dimamy, Joachim Klett, Sara Trost, Kirill Zilberberg,; Thomas Riedl, Bruce Parkinson, Joachim Brötz, Wolfram Jaegermann, Thomas Mayer, “Deep and Shallow TiO<sub>2</sub> Gap States on Cleaved Anatase Single Crystal (101) Surfaces, Nanocrystalline Anatase Films, and ALD Titania Ante and Post Annealing”, J. Phys. Chem. C., 119(18), 9890-9898, (2015).
16. Katarzyna Skorupska and B. A. Parkinson, “Combinatorial Synthesis and Screening of Oxide Materials for Photoelectrochemical Energy Conversion”, Book Chapter in “Photoelectrochemical solar fuel production. From basic principles to advanced devices”, Editors: Sixto Giménez and Juan Bisquert. Publisher: Springer. ISBN 978-3-319-29639-5, p427-462, Switzerland (2016)
17. Ilina Kondofersky, Alexander Müller, Halina Dunn, Alesja Ivanova, Goran Stefanic, Martin Ehrensperger, Christina Scheu, Bruce Parkinson, Dina Fattakhova-Rohlfing and Thomas Bein, "Nanostructured ternary FeCrAl oxide photocathodes for water photoelectrolysis", J. Am. Chem. Soc., 138(6), 1860-1868, (2016), DOI: 10.1021/jacs.5b08040
18. Laurie A. King and B. A. Parkinson, “Photosensitization with Iodide Capped PbSe Quantum Dots”, J. Phys. Chem. Letters, 7(14), 2844-2848, 2016, DOI: 10.1021/acs.jpcclett.6b01133
19. Brandon Durant and B. A. Parkinson, “Photovoltaic Response of Natural Kesterite Crystals”, Solar Energy Materials, Volume 144, Pages 586–591, 2016
20. Laurie A. King and B. A. Parkinson, “Probing the Relative Photoinjection Yields of Monomer and Aggregated Dyes into ZnO Crystals”, Langmuir, DOI: 10.1021/acs.langmuir.6b03395

# Spatial and Temporal Imaging of Multi-Scale Interfacial Charge Transport in Two-Dimensional Heterostructures

Long Yuan, Tong Zhu, Ti Wang, Shibin Deng, and Libai Huang  
 Department of Chemistry  
 Purdue University  
 West Lafayette, IN 47907

**Scope of the Project:** Controlling charge transfer and transport at the interfaces of nanostructures is an important challenge for their utilization in solar energy applications. Atomically thin and two-dimensional (2D) nanostructures provide a new platform to create architectures with sharp interfaces for directing charge transport. Elucidating mechanisms for multi-scale charge transfer, separation, and transport processes at the interfaces of 2D heterostructures is the overarching goal of this project.

## Recent Results:

**1. Photocarrier Generation by Interlayer Transitions.** Interlayer interactions could be significant in the 2D heterostructures, however, it remains unclear whether they can be utilized to facilitate carrier generation. We will first discuss our recent study to address charge generation directly from interlayer transitions in WS<sub>2</sub>/graphene heterostructures (Figure 1). The interlayer transitions are selectively excited with pump energy well below the A exciton resonance of WS<sub>2</sub> as schematically shown in Figure 1A. The heterostructures show transient absorption (TA) signal that tracks the WS<sub>2</sub> A exciton resonance at ~ 2.0 eV by pump energies below the band gap (Figure 1E).

The bleaching of the WS<sub>2</sub> A exciton in the heterostructures by excitation as low as 0.8 eV below the bandgap provides direct evidence for the existence of interlayer transitions. The magnitude of  $\Delta R/R_0$ , as plotted in Figure 1F, is proportional to the interlayer absorption. The absorption onset of 1.24 eV is in excellent agreement with the transition of electron from the K point of graphene to the conduction band of WS<sub>2</sub> near the  $\Lambda$  point predicted by theoretical calculation. Interlayer-coupling dependent charge population and dynamics has been imaged using ultrafast transient absorption microscopy (TAM) (Figure 1D). TA

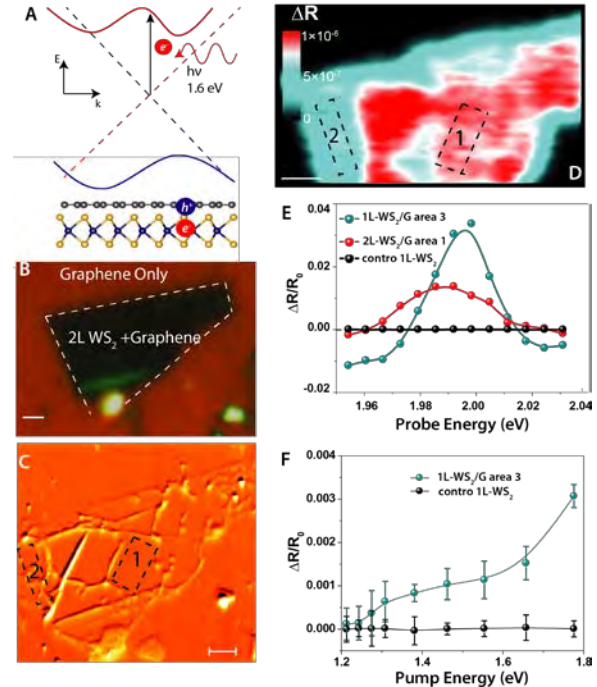


**Figure 1:** (A) Schematic illustration of the interlayer transition in a WS<sub>2</sub>/G heterostructure. (B) Optical image of a 2L-WS<sub>2</sub>/G heterostructure. (C) AFM height imaging of the 2L-WS<sub>2</sub>/G heterostructure. (D) Correlated TAM image of the 2L-WS<sub>2</sub>/G heterostructure measured at 0 ps probing the A exciton resonance when pump photon energy = 1.6 eV exciting only the interlayer transitions. Scale bar, 1  $\mu$ m. (E) TA spectrum of A exciton resonance in the 1L-WS<sub>2</sub>/G, 2L-WS<sub>2</sub>/G heterostructures, and the control 1L-WS<sub>2</sub> at 0 delay time with 1.6 eV pump photon energy. (F) TA signal at 0 ps probed at 2.0 eV (A exciton resonance) for the 1L-WS<sub>2</sub>/G heterostructure when varying the pump photon energy from 1.2 eV to 1.8 eV.

signal is higher at the strong-coupling area 1 than the weak-coupling area 2 (Figure 1D). TA signal in the 1L-WS<sub>2</sub>/G heterostructure is higher than the 2L-WS<sub>2</sub>/G heterostructure (Figure.1E), due to stronger interlayer coupling in the 1L-WS<sub>2</sub>/G heterostructure. These results suggest that interlayer interactions make graphene/2D semiconductor heterostructures even more attractive for photovoltaic applications than previously envisioned, because of the combined benefits of enhanced broadband photocarrier generation and high carrier mobility.

**2. Transport of Charge Transfer Excitons at 2D Organic-Inorganic Interfaces.** Molecular and polymeric organic solids are free of dangling bonds, offering potential to be integrated with 2D semiconductors to form van der Waals heterostructures. The organic/2D heterostructures, in principle, provide a more flexible platform to manipulate the interlayer excitonic states, because the momentum requirements for exciton emission should be relaxed. In addition, the atomically sharp nature of these interfaces serves as a model system for detailed investigation of the dissociation and transport of the interfacial charge transfer states.

We will discuss our initial efforts on imaging the transport of charge transfer excitons at the interfaces of tetracene (Tc) and WS<sub>2</sub> (Figure 2) using TAM. Emission of long-lived interlayer charge transfer excitons is observed in the heterostructure fabricated with monolayer WS<sub>2</sub> and Tc thin film, with lifetime of ~ 7 ns (Figure 2B). The electron transfer from monolayer Tc to WS<sub>2</sub> and the hole transfer in the opposite direction are found both to occur on a ps timescale. Rapid diffusion of charges has been observed following charge transfer suggesting that efficient charge separation can be achieved at these interfaces despite the formation of charge transfer excitons (Figure 2C,D, and E).

**Future Plans:** 1. To control interlayer charge transfer absorption *via* interlayer distance and layer orientation. 2. To further elucidate charge separation and transport mechanisms by visualizing charge transport across interfaces under an external electric field.

#### DOE Sponsored Publications 2016-2017

1. Long Yuan, Ting-Fung Chung, Agnieszka Kuc, Yong P. Chen, Thomas Heine, Libai Huang, Enhanced Photocarrier Generation at Graphene/WS<sub>2</sub> interfaces by Interlayer Coupling, in revision for *Science Advances*, 2017.
2. Long Yuan, Tong Zhu, Ti Wang, Mingwei Zhou, and Libai Huang, Exciton Structure, Dynamics, and Transport in Atomically Thin 2D Semiconductors, submitted 2017.
3. Tong Zhu, Long Yuan, Yan Zhao, Jianguo Mei, Libai Huang, Charge Transfer Excitons at 2D Organic-Inorganic Interfaces, Submitted, 2017.

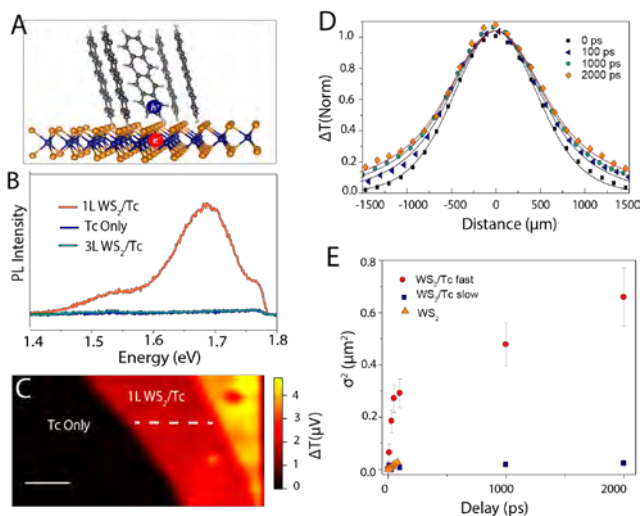


**Figure 2:** (A) Schematic illustration of charge-transfer excitons at WS<sub>2</sub>/Tc interface. (B) Photoluminescence measurement on 1L WS<sub>2</sub>/Tc, 3L WS<sub>2</sub>/Tc and Tc thin film with excitation wavelength of 590 nm (700 nm Long-pass filter), allowing selectively excite WS<sub>2</sub> in the heterostructure. (C) TAM image with pump= 3.14 eV, probe= 2.0 eV of the 1L WS<sub>2</sub>/Tc heterostructure, scale bar = 1μm. (D) 1D Spatial profiles of TA signal along the dashed line indicated in (C) at different pump-probe time delays. Solid lines are fits with sum of two Gaussian functions. (E) The variances of Gaussian profiles for the fast and slow population along with a WS<sub>2</sub> control.

## The role of surface motifs in group VI dichalcogenide photoelectrodes and two-dimensional materials as protective layers

Fan Yang, Jesús Velázquez, Jimmy John, Joshua D. Wiensch, Ellen X. Yan and Nathan S. Lewis  
 Department of Chemistry and Chemical Engineering  
 California Institute of Technology  
 Pasadena, CA 91125

Our recent work has been focused on the protection of gallium arsenide (GaAs) from photocorrosion using a monolayer of graphene, and controlling and characterizing the surfaces of layered transition metal dichalcogenides (TMDCs) of molybdenum and tungsten ( $\text{MX}_2$ ; M = Mo, W, X = S, Se). We have also studied the photoelectrochemical activity of  $\text{WSe}_2$  surface motifs using scanning photocurrent microscopy as well as the electrocatalysis of  $\text{MoS}_2$  in alkaline vs. acidic solution.

GaAs, a III-V semiconductor with a direct bandgap of  $\sim 1.4$  eV, passivates in aqueous pH 4-10 photoelectrochemical conditions and dissolves in strongly alkaline or acidic electrolytes. We have demonstrated a method that substantially increases the stability of n-GaAs (100) toward passivation under photoanodic conditions in a non-aqueous electrolyte containing 0.1% (v/v) water under AM1.5 illumination. Limited protection was observed in aqueous solutions of  $\text{Fe}(\text{CN})_6^{3-/4-}$ . The open-circuit voltages for n-GaAs and n-GaAs/Gr electrodes in contact with dry acetonitrile containing 1.0 M  $\text{LiClO}_4$  and a series of one-electron redox couples under AM1.5 illumination indicate that partial Fermi-level pinning is present in the system over the wide range of solution potentials investigated. Notably, the presence of graphene did not appear to affect the degree of Fermi-level pinning, indicating that the sources of pinning were independent of the interfacial graphene layer. (Figure 1)

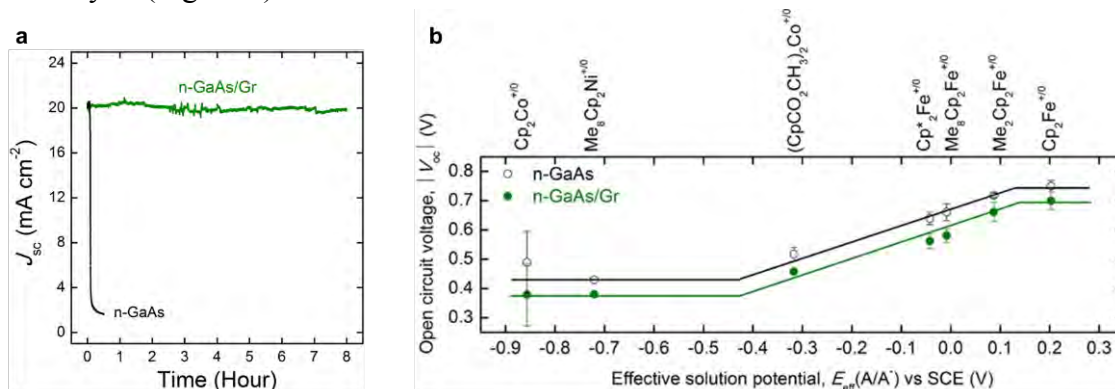
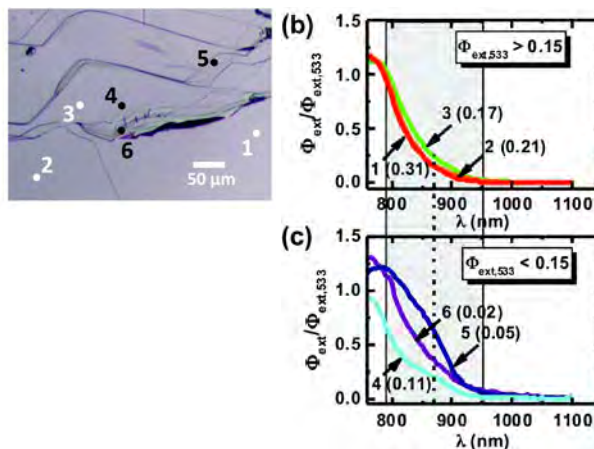


**Figure 1.** (a) Comparison of the  $J$ - $t$  behavior of potentiostatically controlled n-GaAs (black) and n-GaAs/Gr (green) electrodes ( $E = 0$  V vs solution) in contact with a  $\text{CH}_3\text{CN-Fc}^{+/0}$  system containing 0.1% (v/v) water under AM1.5 illumination. (b) Open-circuit voltage,  $V_{oc}$ , vs the effective solution redox potential,  $E_{eff}$  (A/A $^-$ ), in 1.0 M  $\text{LiClO}_4/\text{CH}_3\text{CN}$  for n-GaAs (black, open circles) and n-GaAs/Gr (green, filled circles). The corresponding lines serve as guides to indicate the observed trends in the different regions of  $V_{oc}$ , vs  $E_{eff}$  (A/A $^-$ ).

TMDCs have bandgap energies in the range of 1.0 eV to 1.5 eV (indirect, bulk) and 1.4 eV to 2.3 eV (direct, monolayer), and have large absorption coefficients ( $\sim 10^5 \text{ cm}^{-1}$  and  $\sim 10^6 \text{ cm}^{-1}$  for photon energies above  $E_{g,indirect}$  and  $E_{g,direct}$ , respectively), and can be doped n-type or p-type. These properties make TMDCs attractive for use in solar-driven water-splitting devices and integration of Pt/Ru catalysts onto p- $\text{WSe}_2$  photocathodes for the hydrogen evolution reaction (HER) yielded

**Figure 2.** (a) Optical image of a bare p-WSe<sub>2</sub> (a) electrode where local spectral measurements were carried out. (b) and (c) Local spectral response curves obtained at locations shown in (a) of bare p-WSe<sub>2</sub> electrode in contact with 10 mM Ru(NH<sub>3</sub>)<sub>6</sub><sup>3+</sup>/0.5 M KH<sub>2</sub>PO<sub>4</sub>(aq). Location number and external quantum yield ( $\Phi_{\text{ext}}$ ) at 533 nm ( $\Phi_{\text{ext},533}$ ) in brackets are shown beside each curve. Applied potential: -0.05 V vs. sat. Ag/AgCl. The area highlighted in grey represents the wavelength region below the direct bandgap of WSe<sub>2</sub> ( $E_{\text{g,direct}} = 1.57$  eV or 790 nm). The dotted vertical line indicates the wavelength around which the shoulder feature is observed in the spectral response.



hydrogen-evolving photocathodes with ideal regenerative cell efficiencies greater than 7% under mildly acidic conditions (pH = 4.2). The surfaces of TMDCs consist of multiple terraces separated by step edges. Previous work suggests that edge sites and chalcogen vacancies are deleterious to the photoconversion efficiency because under-coordinated atoms on the edges and defect sites are reactive toward surface corrosion processes and act as sites for charge-carrier recombination. However, edge-sites have also been shown to be the active sites for HER catalysis. Therefore, we were interested in using scanning photocurrent microscopy to probe the relationship between the surface morphology and the aqueous photoelectrochemical performance of single-crystal p-WSe<sub>2</sub> photocathodes.

We evaluated the electrochemical performance of p-WSe<sub>2</sub> photocathodes in contact with an aqueous solution containing a reversible one-electron redox couple (Ru(NH<sub>3</sub>)<sub>6</sub><sup>3+</sup>), and a solution of 0.5 M H<sub>2</sub>SO<sub>4</sub> (aq) with electrodeposited Pt on the electrode surface. Photocurrent measurements across macroscopic terraces and edges revealed variation in photoactivity among terraces. Terraces with low photocurrent were correlated with local spectral response measurements with spectral features below the bandgap for terraces with relatively poor photoconversion efficiencies, indicative of the presence of surface states. Local spectral response measurements showed inconsistent photocurrent and increased spectral features at sub-bandgap wavelengths at macroscopic edge sites compared to terraces. These results suggest that sub-bandgap states are responsible for the lower photocurrent at low-performing terraces and edge sites. (Figure 2)

In addition to investigating the photoelectrochemical performance of TMDCs as light absorbers, we have also been interested in examining the electrocatalytic activity of MoS<sub>2</sub> for the HER as an earth-abundant catalyst. Although MoS<sub>2</sub> has been well-established as an HER catalyst in acidic electrolytes, electrocatalysis of MoS<sub>2</sub> in alkaline electrolytes remains relatively unexplored. We compared the electrocatalytic activities of single crystal, polycrystalline, and amorphous MoS<sub>2</sub> in acidic vs. alkaline solution and found differences in the effect of morphology on overpotential. In acidic solution, increasing edge site density progressively decreased the overpotential at 10 mA/cm<sup>2</sup>, while the edge density does not appear to affect the overpotential in alkaline solution. These results suggest that step edges may not be the active sites for HER on MoS<sub>2</sub> electrodes in contact with alkaline electrolytes.

Our ongoing and future work focuses on using covalent functionalization to modify the surface electronic properties of TMDCs, and using graphene protection to stabilize TMDC photoanodes.

## DOE Sponsored Publications 2014-2017

1. Yang, F.; Nielander, A. C.; Grimm, R. L.; Lewis, N. S., Photoelectrochemical Behavior of n-Type GaAs(100) Electrodes Coated by a Single Layer of Graphene. *J. Phys. Chem. C* **2016**, *120* (13), 6989-6995.
2. Velazquez, J. M.; John, J.; Esposito, D. V.; Pieterick, A.; Pala, R.; Sun, G.; Zhou, X.; Huang, Z.; Ardo, S.; Soriaga, M. P.; Brunschwig, B. S.; Lewis, N. S., A scanning probe investigation of the role of surface motifs in the behavior of p-WSe<sub>2</sub> photocathodes. *Energy Environ. Sci.* **2016**, *9*, 164-175.
3. Lewis, N.S., Research opportunities to advance solar energy utilization. *Science* **2016**, *351*, doi: 10.1126/science.aad1920.
4. Nielander, A. C.; Shaner, M.; Papadantonakis, K. M.; Francis, S. A.; Lewis, N. S., A taxonomy for solar fuels generators. *Energy Environ. Sci.* **2015**, *8*, 16-25.
5. Hu, S.; Lewis, N. S.; Ager, J. W.; Yang, J.; McKone, J. R.; Strandwitz, N. C., Thin film materials for the protection of semiconducting photoelectrodes in solar-fuel generators. *J. Phys. Chem. C* **2015**, *119* (43), 24201-24228.
6. Warren, E. L.; Atwater, H. A.; Lewis, N. S., Silicon microwire arrays for solar energy-conversion applications. *J. Phys. Chem. C* **2014**, *118* (2), 747-759.
7. Santori, E. A.; Strandwitz, N. C.; Grimm, R. L.; Brunschwig, B. S.; Atwater, H. A.; Lewis, N. S., Operation of lightly doped Si microwires under high-level injection conditions. *Energy Environ. Sci.* **2014**, *7* (7), 2329-2338.

*Session V*

*Photons and Electrons-  
Designed Interactions*



## Design and Photophysics of Next Generation Cu(I) MLCT Excited States and Photochemical Upconversion in Water

Catherine E. McCusker, Sofia Garakyaraghi, Petr Koutnik, Karim El Roz,  
and Felix N. Castellano

Department of Chemistry  
North Carolina State University  
Raleigh, NC 27695-8204

Earth-abundant copper(I) *bis*-phenanthroline complexes represent alternatives to the more familiar 2<sup>nd</sup> and 3<sup>rd</sup> row transition metal containing photosensitizers. Copper(I) diimine complexes feature metal-to-ligand charge transfer (MLCT) properties similar to [Ru(bpy)<sub>3</sub>]<sup>2+</sup>, without the deactivating ligand field states found in other first row transition metal complexes. However, upon excitation, Cu(I) diimine complexes undergo a significant structural rearrangement, leading to excited states which are highly susceptible to exciplex formation and possess very short lifetimes. These properties limit their utility as photosensitizers, especially in donor solvents. To overcome these challenges, directed ligand design to sterically restrict the excited state distortion is necessary.

The 2,9- and the 3,8- positions on the phenanthroline ligand both play an important structural role in extending the excited state lifetime. Methyl groups in the 3,8- positions of the phenanthroline ligand, combined with bulky *sec*-butyl (or *iso*-propyl) groups in the 2,9- positions have been shown to cooperatively restrict the degree of structural distortion in the Cu(I) MLCT excited state. As a result, microsecond

excited state lifetimes were achieved and maintained in coordinating solvents. By preserving the cooperative steric substitutions in the 2,9 and 3,8 positions, and varying the substituents at the

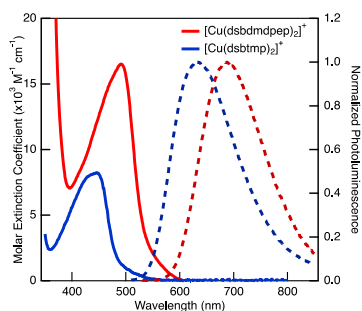
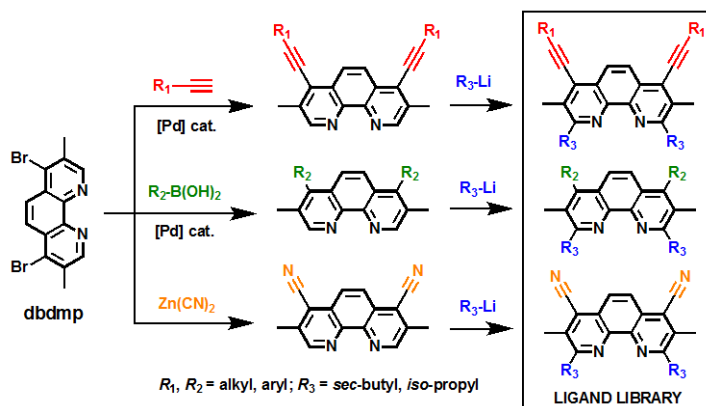


**Figure 1.** UV-Vis absorption and PL spectra of new Cu(I) MLCT chromophores.

4,7- positions of the phenanthroline ring, a new series of long-lifetime Cu(I) MLCT complexes have been synthesized with designer photophysical, electrochemical, and solubility properties; two examples are shown in Figure 1. The ligands were prepared in six steps starting from commercially available materials. Utilizing simple synthetic transformations, readily accessible 4,7-dibromo-3,8-dimethyl-1,10-phenanthroline (dbdmp), permit the generation of new libraries of ligands. These designer, earth-abundant chromophores can be implemented in a variety of solar energy conversion schemes including photochemical upconversion and solar fuels photochemistry.

More comprehensive analysis of the photo-induced structural distortions and singlet-triplet intersystem crossing dynamics in these Cu(I) chromophores are in progress. Femtosecond



optically gated fluorescence spectroscopy provides a means, complementary to ultrafast transient absorption, to monitor the excited state trajectory and surface crossings of these chromophores following laser excitation by monitoring photoluminescence (PL) decays. Here, upconverted fluorescence decay kinetics were collected at wavelengths along the blue side of the PL spectrum. The results display a strong wavelength dependence of the singlet emission, with rapid sub-picosecond decay dominating at higher energies. At lower emission energies, increasing contribution of a longer decay component was revealed. Figure 2 displays representative data of the wavelength dependent PL decay of  $[\text{Cu}(\text{dsbp})_2]^+$  (dsbp = 2,9-di-*sec*-butyl phenanthroline) in dichloromethane. This wavelength dependence is a signature of the excited state structural rearrangement of the phenanthroline ligands - these distortions lower the energy of the excited state surface concomitantly. Evaluating the decay kinetics using sums of exponential functions revealed two time components in excellent agreement with those measured in the complementary ultrafast transient absorption experiments. The sub-picosecond component (prompt fluorescence) is the time constant associated with the photo-induced structural change that modulates the singlet excited state surface to lower energy. The longer decay component represents the lifetime of the  $S_1$  state, and thus the time-scale of singlet-triplet intersystem crossing. As similarly observed in the ultrafast transient absorption data, the obtained time constants systematically lengthen as a function of structure; the molecule most structurally hindered and resistant to flattening distortions had the fastest dynamics, whereas the complex most susceptible to distortion (less steric bulk), possessed the slowest dynamics. The systematic variation in the PL decay time scales across the series illustrates that strongly impeded structural distortion in Cu(I) MLCT excited state enables more rapid surface crossings.

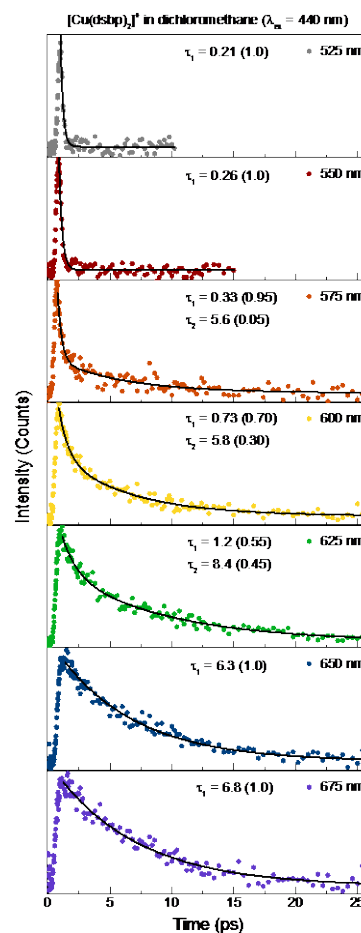


**Figure 2.** Fluorescence decay kinetics of  $[\text{Cu}(\text{dsbp})_2]^+$  in dichloromethane following 440 nm pulsed excitation. Black lines represent fits.

Upconversion photochemistry based on sensitized triplet-triplet annihilation (TTA) represents a means for generating high-energy excited states from low-energy excitation, having potential applications in a variety of energy conversion schemes including solar fuels photochemistry. Data obtained using a variety of Cu(I) MLCT sensitizers that drive both light-producing and product-forming chemical reactions will be presented. Photochemical upconversion schemes executed homogeneously in water have also been realized for the first time. Four representative donor-acceptor pairs generalizing this phenomenon were examined, namely, 9-anthracenecarboxylate ( $\text{AnCO}_2^-$ ) and 1-pyrenecarboxylate ( $\text{PyCO}_2^-$ ) serving as acceptors/annihilators along with the water-soluble Ru(II) MLCT triplet photosensitizers  $[\text{Ru}(\text{bpy})_3]^{2+}$  (bpy = 2,2'-bipyridine) and  $[\text{Ru}(\text{BPS})_3]^{4+}$  (BPS = bathophenanthroline disulfonate). In all instances, the bimolecular triplet-triplet energy transfer and TTA processes were investigated using static and transient PL along with nanosecond transient absorption experiments.

## DOE Sponsored Publications 2014-2017

1. *Advances in the Light Conversion Properties of Cu(I)-based Photosensitizers*. Lazorski, M.S.; Castellano, F.N. *Polyhedron* **2014**, *82*, 57-70.
2. *Excited State Equilibrium Induced Lifetime Extension in a Dinuclear Platinum(II) Complex*. McCusker, C.E.; Chakraborty, A.; Castellano, F.N. *J. Phys. Chem. A* **2014**, *118*, 10391-10399.
3. *Triplet State Formation in Homo- and Heterometallic Diketopyrrolopyrrole Chromophores*. McCusker, C.E.; Hablot, D.; Ziessel, R.; Castellano, F.N. *Inorg. Chem.* **2014**, *53*, 12564-12571.
4. *Enhancing Molecular Photophysics by Merging Organic and Inorganic Chromophores*. Castellano, F.N. *Acc. Chem. Res.* **2015**, *48*, 828-839.
5. *Transient Absorption Dynamics of Sterically Congested Cu(I) MLCT Excited States*. Garakyaraghi, S.; Danilov, E.O.; McCusker, C.E.; Castellano, F.N. *J. Phys. Chem. A* **2015**, *119*, 3181-3193.
6. *Efficient Visible to Near-UV Photochemical Upconversion Sensitized by a Long Lifetime Cu(I) MLCT Complex*. McCusker, C.E.; Castellano, F.N. *Inorg. Chem.* **2015**, *54*, 6035-6042.
7. *MLCT Sensitizers in Photochemical Upconversion: Past, Present, and Potential Future Directions*. Castellano, F.N.; McCusker, C.E. *Dalton Trans.* **2015**, *44*, 17906-17910.
8. *Exposing the Excited State Equilibrium in an Ir(III) Bichromophore: A Combined Time Resolved Spectroscopy and Computational Study*. Yarnell, J.E.; McCusker, C.E.; Leeds, A.J.; Breaux, J.M.; Castellano, F.N. *Eur. J. Inorg. Chem.* **2016**, 1808-1818.
9. *Materials Integrating Photochemical Upconversion*. McCusker, C.E.; Castellano, F.N. *Top. Curr. Chem.* **2016**, *374*(2), 19.
10. *Enhanced Photophysics from Self-Assembled Cyclometalated Ir(III) Complexes in Water*. McGoorty, M.M.; Khnayzer, R.S.; Castellano, F.N. *Chem. Commun.* **2016**, *52*, 7846-7849.
11. *Cuprous Phenanthroline MLCT Chromophore Featuring Synthetically Tailored Photophysics*. Garakyaraghi, S.; Crapps, P.D.; McCusker, C.E.; Castellano, F.N. *Inorg. Chem.* **2016**, *55*, 10628-10636.
12. Deaton, J.C.; Castellano, F.N. *Archetypal Iridium(III) Compounds for Optoelectronic and Photonic Applications: Photophysical Properties and Synthetic Methods in Iridium (III) in Optoelectronic and Photonics Applications*. John Wiley and Sons: New York (2017). E. Zysman-Colman, Editor.

13. *Charge Localization after Ultrafast Photoexcitation of Rigid Perylene Perylenediimide Dyad Visualized by Transient Stark Effect.* Koch, M.; Myahkostupov, M.; Oblinsky, D.G.; Wang, S.; Garakyaraghi, S.; Castellano, F.N.; Scholes, G.D. *J. Am. Chem. Soc.* **2017**, ASAP.
14. *Photochemical Upconversion in Water.* El Roz, K.A.; Castellano, F.N. *Chem. Sci.* **2017**, submitted.
15. *Photo-induced Structural Distortions and Singlet-Triplet Intersystem Crossing in Cu(I) MLCT Excited States Monitored by Femtosecond Optically Gated Fluorescence Spectroscopy.* Garakyaraghi, S.; Koutnik, P.; Castellano, F.N. *Phys. Chem. Chem. Phys.* **2017**, submitted.
16. *Enriching the Light Absorption and Photophysical Properties of Cu(I) MLCT Excited States.* Koutnik, P.; McCusker, C.E.; Garakyaraghi, S.; Castellano, F.N. Manuscript in preparation.
17. *Visible-light Catalyzed Dimerization of Aromatic Hydrocarbons Sensitized by Cu(I) MLCT Excited States.* Ogawa, T.; McCusker, C.E.; Castellano, F.N. Manuscript in preparation.

## Direct Observation of Charge Transfer and Quintet State Intermediates in Singlet Fission

Michael R. Wasielewski  
Department of Chemistry  
Northwestern University  
Evanston, IL 60208-3113

**Scope of the project.** We are investigating molecular solids in which photogenerated singlet excitons fission to generate two triplet excitons, which in turn, efficiently charge separate to produce two electron-hole pairs. We are also developing self-ordering molecular assemblies (SOMAs) that produce segregated charge conduits that will be able to independently carry electrons and holes to either catalysts or electrodes. We are focusing on how these assemblies can be grown on solid supports and electrodes to utilize their light-harvesting and photodriven charge separation capabilities. Finally, we are investigating how SOMAs can be used to provide multiple electrons or holes to catalysts for solar fuels formation by designing structures to prevent unproductive competitive quenching of excited states by energy transfer, spin exchange, and unquenched angular momentum involving the nearby metal catalysts.

**Recent Results.** Singlet exciton fission (SF) in ensembles of molecular chromophores down-converts one singlet exciton ( $S_1$ ) produced by single-photon absorption into two triplet excitons ( $T_1$ ) provided that the overall process is exoergic, i.e.  $E(S_1) > 2E(T_1)$ . There is great interest in this phenomenon because of its potential for increasing the maximum efficiency of photovoltaics from the 33% Shockley-Queisser limit for single-junction devices to nearly 45%. Charge transfer (CT) states have been frequently implicated in the mechanism of singlet exciton fission in molecular materials, but up until now their role has remained uncertain. We have prepared a series of covalently-linked terylene-3,4:11,12-bis(dicarboximide) (TDI) dimers in which triptycene spacers hold two TDI molecules in  $\pi$ -stacked geometries (Fig. 1). TDI is a highly stable and strong visible absorber ( $\epsilon_{650} = 93000 \text{ M}^{-1} \text{ cm}^{-1}$ ,  $E(S_1) = 1.87 \text{ eV}$ ) with a suitably low energy  $T_1$  state ( $E(T_1) = \leq 0.77 \text{ eV}$ ) to enable SF in the absence of entropic effects. The early time femtosecond transient absorption (fsTA) spectra of slip-stacked dimer **2** in polar  $\text{CH}_2\text{Cl}_2$  (Fig. 2a) closely match the  $S_n \leftarrow S_1$  spectra of TDI monomer **M**. The  $S_1$  state quickly decays in  $\tau = 8.1 \text{ ps}$  by symmetry-breaking charge separation to form  $\text{TDI}^{+\bullet}\text{-TDI}^{-\bullet}$ , while in toluene only  $^3\text{TDI}$  forms in 2.2 ps (Fig. 2b) as indicated by the triplet-triplet absorption features at 620 nm. The data also show that an excited state equilibrium occurs between  $^1(S_1S_0)$  and  $^1(T_1T_1)$ . Our results show for the first time that controlling the  $\text{TDI}^{+\bullet}\text{-TDI}^{-\bullet}$  CT state energy relative to that of  $^1(S_1S_0)$  results in the CT state serving as either a virtual state promoting SF or a trap state inhibiting it; thus, highlighting the critical role of the CT state in the SF mechanism.

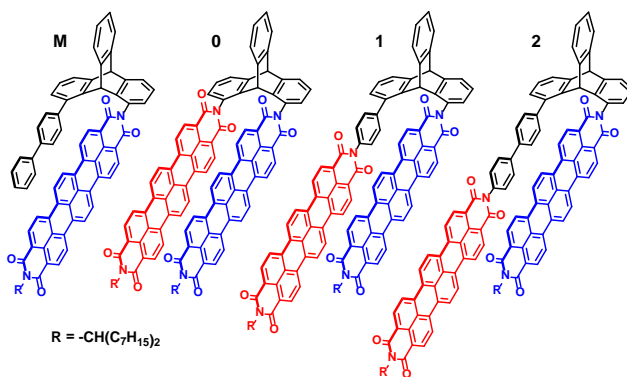


**Figure 1.** Structures of TDI monomer and dimers.

We have also investigated SF in thin polycrystalline films of two TDI derivatives **3** and **4**, which

crystallize into two distinct  $\pi$ -stacked structures (Fig. 3). The TDI molecules in **3** are rotated along an axis perpendicular to their  $\pi$  systems by  $23^\circ$ , while in **4**, a modest amount of slip-stacking along the N-N axis direction of the TDI molecules occurs. Vapor-deposited thin films of **3** and **4** preserve the essential single-crystal structural features. FsTA spectra of a solid film of **3** shows that the initial state produced following photon absorption has substantial CT character with spectra similar to those of dimer **2** in solution leading to near-quantitative SF, while that of **4** shows primarily excimer formation and a modest 50% SF yield.

As with CT states, the role of the  $^5(T_1T_1)$  quintet state in the SF mechanism has also been uncertain. We have employed a pentacene dimer linked by a rigid, non-conjugated 1,3-diethynyladamantyl spacer (**5**, Fig. 4) to probe the role of this state. The pentacenes in **5** are coupled just strongly enough to allow efficient SF before any other excited state processes occur, but weakly enough that the  $^1(T_1T_1)$  state formed by SF can undergo spin-mixing to form the  $^5(T_1T_1)$  on a time scale sufficiently slow to allow time-resolved electron paramagnetic resonance (TREPR) spectroscopy to observe both its formation and decay into independent triplet states ( $T_1 + T_1$ ). This allows us to use complementary time-resolved optical and TREPR spectroscopy to observe the intermediates and kinetics for the entire  $^1(S_1S_0) \rightleftharpoons ^1(T_1T_1) \rightleftharpoons ^5(T_1T_1) \rightarrow (T_1 + T_1)$  sequence. Fig. 4 shows the formation and decay of the spin-polarized  $^5(T_1T_1)$  state followed by formation of the spin-polarized ( $T_1 + T_1$ ) pair. Using these combined data, we have developed a single kinetic model that describes the data over seven temporal orders of magnitude both at room and cryogenic temperatures.

**Future Plans.** Our goal is to understand photodriven redox systems well enough to produce integrated artificial photosynthetic

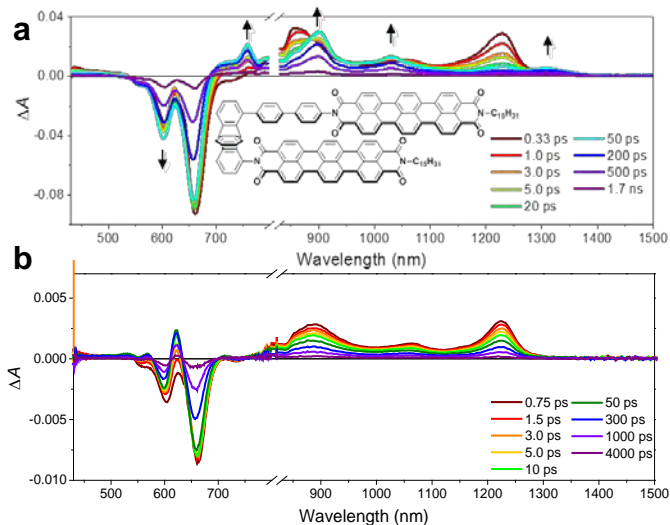


**Figure 2.** Transient absorption spectra of TDI dimer **2** a) in  $\text{CH}_2\text{Cl}_2$  where the arrows indicate the appearance of the 759, 900, 1030, and 1310 nm features characteristic of the  $\text{TDI}^{+}\text{-TDI}^{-}$  CT state, and b) in toluene showing the rapid formation of a triplet absorption signature at 620 nm.

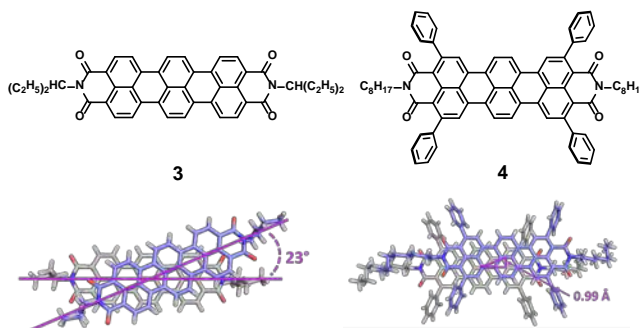


**Figure 3.** Chemical and single crystal X-ray diffraction structures of **3** and **4**.

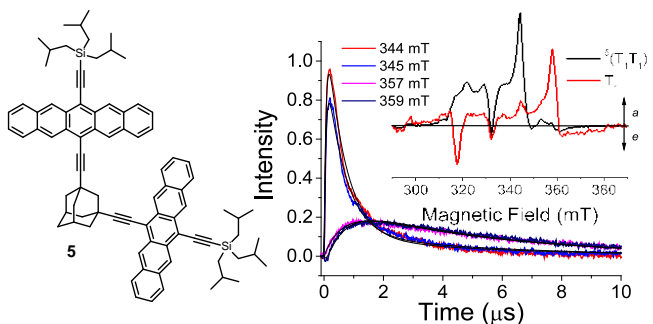


**Figure 4.** TREPR kinetics for the formation and decay of the  $^5(T_1T_1)$  and ( $T_1 + T_1$ ) states for **5** at 105 K in butyronitrile measured at the indicated magnetic field values corresponding to the species-associated spectra of the  $^5(T_1T_1)$  and separated  $T_1$  states shown in the inset.

systems that harvest light, separate charge and deliver that charge to electrodes for immediate use and to catalysts for fuels formation that store solar energy.

## DOE Sponsored Publications 2014-2017

1. Ground and Excited State Electronic Spectra of Perylenediimide Dimers with Flexible and Photodriven Charge Separation and Transport in Self-assembled Zinc Tetrabenzotetraphenylporphyrin and Perylenediimide Charge Conduits, V. V. Roznyatovskiy, R. Carmieli, S. M. Dyar, K. E. Brown, and M. R. Wasielewski, *Angew. Chem. Int. Ed.* **53**, 3457-3461 (2014).
2. Radical Anions of Trifluoromethylated Perylene and Naphthalene Imide and Diimide Electron Acceptors, V. V. Roznyatovskiy, D. M. Gardner, S. W. Eaton, and M. R. Wasielewski, *Org. Lett.* **16**, 696-699 (2014).
3. Rigid Geometries in DNA Conjugates, P. P. Neelekandan, T. A. Zeidan, M. McCullagh, G. C. Schatz, J. Vura-Weis, R. F. Kelley, C. H. Kim, M. R. Wasielewski, and F. D. Lewis, *Chem. Sci.* **5**, 973-981 (2014).
4. Gated Electron Sharing Within Dynamic Naphthalene Diimide-Based Oligorotaxanes, A.-J. Avestro, D. M. Gardner, N. A. Vermeulen, E. A. Wilson, S. T. Schneebeli, A. C. Whalley, M. E. Belowich, R. Carmieli, M. R. Wasielewski, and J. F. Stoddart *Angew. Chem. Int. Ed.* **53**, 4442-4449 (2014).
5. Electron Transfer and Multi-Electron Accumulation in ExBox<sup>4+</sup>, S. M. Dyar, J. C. Barnes, M. Juriček, J. F. Stoddart, D. T. Co, R. M. Young, M. R. Wasielewski, *Angew. Chem. Int. Ed.* **53**, 5371-5375 (2014).
6. Self-assembly of Supramolecular Light-harvesting Arrays from Symmetric Perylene-3,4-dicarboximide Trefoils, K. M. Lefler, C. H. Kim, Y.-L. Wu, and M. R. Wasielewski, *J. Phys. Chem. Lett.* **5**, 1608-1615 (2014).
7. Rh(I) as a Photoreductant in Bodipy Photoredox Switches, A. M. Lifschitz, R. M. Young, J. Mendez-Arroyo, V. V. Roznyatovskiy, C. M. McQuirk, M. R. Wasielewski, and C. A. Mirkin, *Chem. Commun.* **50**, 6850-6852 (2014).
8. Solid-State Characterization and Photoinduced Intramolecular Electron Transfer in a Nanoconfined Octacationic Homo[2]Catenane, J. C. Barnes, M. Frasconi, R. M. Young, N. H. Khdary, W.-G. Liu, S. M. Dyar, P. R. McGonigal, I. C. Gibbs-Hall, C. S. Diercks, A. A. Sarjeant, C. L. Stern, W. A. Goddard, M. R. Wasielewski, and J. F. Stoddart, *J. Am. Chem. Soc.* **2014**, *136*, 10569-10572.
9. Direct Observation of Ultrafast Excimer Formation in Covalent Perylenediimide Dimers using Near-Infrared Transient Absorption Spectroscopy, K. E. Brown, W. A. Salamant, L. E. Shoer, R. M. Young, and M. R. Wasielewski, *J. Phys. Chem. Lett.* **5**, 2588-2593 (2014).

10. Electron Delocalization in a Rigid Cofacial Naphthalene-1,8:4,5-bis(dicarboximide) Dimer, Y. Wu, M. Frasconi, D. M. Gardner, P. R. McGonigal, S. T. Schneebeli, M. R. Wasielewski, and J. F. Stoddart, *Angew Chem. Int. Ed.* **53**, 9476-9481 (2014).
11. Symmetrized Photoinitiated Electron Flow within the [Myoglobin:Cytochrome b5] Complex on Singlet and Triplet Timescales: Energetics vs Dynamics, N. Co, R. M. Young, A. L. Smeigh, M. R. Wasielewski, and B. M. Hoffman, *J. Am. Chem. Soc.* **136**, 12730-12736 (2014).
12. Excimer Formation in Cofacial and Slip-Stacked Perylene-3,4:9,10-bis(dicarboximide) Dimers on a Redox-Inactive Triptycene Scaffold, E. A. Margulies, L. E. Shoer, S. W. Eaton, and M. R. Wasielewski, *Phys. Chem. Chem. Phys.* **16**, 23735-23742 (2014).
13. Spin-Selective Charge Recombination in Complexes of CdS Quantum Dots and Organic Hole Acceptors, D. J. Weinberg, S. M. Dyar, Z. Khademi, M. Malicki, S. R. Marder, M. R. Wasielewski, and E. A. Weiss, *J. Am. Chem. Soc.* **136**, 14513-14518 (2014).
14. Energy Flow Dynamics within Cofacial and Slip-Stacked Perylene-3,4-dicarboximide Dimer Models of  $\pi$ -Aggregates, R. J. Lindquist, K. M. Lefler, K. E. Brown, S. M. Dyar, D. T. Co, R. M. Young, and M. R. Wasielewski, *J. Am. Chem. Soc.* **136**, 14912-14923 (2014).
15. Unusually Short Excited State Lifetimes of Indenofluorene and Fluorenofluorene Derivatives Result from a Conical Intersection, B. D. Rose, L. E. Shoer, A. G. Fix, M. R. Wasielewski, and M. M. Haley, *Chem. Phys. Lett.* **616-617**, 137-141 (2014).
16. Photoinduced Electron Transfer within a Zinc Porphyrin-Cyclobis(paraquat-*p*-phenylene) Donor-Acceptor Dyad, M. Fathalla, J. C. Barnes, R. M. Young, K. J. Hartlieb, S. M. Dyar, S. W. Eaton, B. K. Rugg, A. A. Sarjeant, D. T. Co, M. R. Wasielewski, J. F. Stoddart, *Chem. Eur. J.* **20**, 14690-14697 (2014).
17. Long-lived Charge Carrier Generation in Ordered Films of a Covalent Perylenediimide-Diketopyrrolopyrrole-Perylenediimide Molecule, P. E. Hartnett, S. M. Dyar, E. A. Margulies, L. E. Shoer, A. W. Cook, S. W. Eaton, T. J. Marks, and M. R. Wasielewski, *Chem. Sci.* **6**, 402-411 (2015).
18. Molecular Excited States: Accurate Calculation of Relative Energies and Electronic Coupling Between Charge Transfer and Non-Charge Transfer States, B. S. Veldkamp, X. Liu, M. R. Wasielewski, J. E. Subotnik, and M. A. Ratner, *J. Phys. Chem. A* **119**, 253-262 (2015).
19. Bias-switchable Permselectivity and Redox Catalytic Activity of a Ferrocene-Functionalized, Thin-Film Metal Organic Framework Compound, I. Hod, W. Bury, D. M. Gardner, P. Deria, V. Roznyatovskiy, M. R. Wasielewski, O. K. Farha, and J. T. Hupp, *J. Phys. Chem. Lett.* **6**, 586-591 (2015).

20. Photoinduced Hole Injection into a Self-assembled  $\pi$ -Extended G-quadruplex, Y.-L. Wu, K. E. Brown, D. M. Gardner, S. M. Dyar, and M. R. Wasielewski, *J. Am. Chem. Soc.* **137**, 3981-3990 (2015).
21. Post-Assembly Atomic Layer Deposition of Ultrathin Metal-Oxide Coatings Enhances the Performance of an Organic Dye-Sensitized Solar Cell by Suppressing Dye Aggregation, H.-J. Son, C. H. Kim, D. W. Kim, N. C. Jeong, C. Prasittichai, L. Luo, J. Wu, O. K. Farha, M. R. Wasielewski, and J. T. Hupp, *ACS Appl. Mater. Interfaces* **7**, 5150-5159 (2015).
22. Electronic Interactions of Michler's Ketone with DNA Bases in Synthetic Hairpins, A. S. Jalilov, R. M. Young, S. W. Eaton, M. R. Wasielewski, and F. D. Lewis, *Photochem. Photobiol.* **91**, 739-747 (2015).
23. Singlet Exciton Fission in Thin Films of *t*-Butyl-Substituted Terrylenes, S. W. Eaton, S. A. Miller, E. A. Margulies, L. E. Shoer, R. D. Schaller, and M. R. Wasielewski, *J. Phys. Chem. A* **119**, 4151-4161 (2015).
24. Fast Triplet Formation via Singlet Exciton Fission in a Covalent Perylenediimide- $\beta$ -Apocarotene Dyad Aggregate, C. M. Mauck, K. E. Brown, N. E. Horwitz, and M. R. Wasielewski, *J. Phys. Chem. A* **119**, 5587-5596 (2015).
25. Sub-Picosecond Singlet Exciton Fission in Cyano-Substituted Diaryltetracenes, E. A. Margulies, Y.-L. Wu, P. Gawel, S. A. Miller, L. E. Shoer, R. D. Schaller, F. Diederich, and M. R. Wasielewski, *Angew. Chem. Int. Ed.* **54**, 8679-8683 (2015).
26. Photoinduced Electron Transfer in 2,5,8,11-Tetrakis-Donor-Substituted Perylene-3,4:9,10-bis(dicarboximides), L. E. Shoer, S. W. Eaton, E. A. Margulies, and M. R. Wasielewski, *J. Phys. Chem. B* **119**, 7635-7643 (2015).
27. Charge and Spin Transport in an Organic Molecular Square, Y. Wu, S. K. Mohan Nalluri, R. M. Young, M. D. Krzyaniak, E. A. Margulies, J. F. Stoddart, and M. R. Wasielewski, *Angew. Chem. Int. Ed.* **54**, 11971-11977 (2015).
28. Ultrafast Photoinduced Symmetry Breaking Charge Separation and Electron Sharing in Perylenediimide Molecular Triangles, Y. Wu, M. Frasconi, R. M. Young, S. T. Schneebeli, P. Spenst, D. M. Gardner, F. Würthner, J. F. Stoddart, and M. R. Wasielewski, *J. Am. Chem. Soc.* **137**, 13236-13239 (2015).
29. Supramolecular Explorations: Exhibiting the Extent of Extended Cationic Cyclophanes, E. J. Dale, N. A. Vermeulen, M. Juriček, J. C. Barnes, R. M. Young, M. R. Wasielewski, and J. F. Stoddart, *Acc. Chem. Res.* **49**, 262-273 (2016).
30. Photoinduced Charge and Energy Transfer within *meta*- and *para*-Linked Chlorophyll *a*-Perylene-3,4:9,10-bis(dicarboximide) Donor-Acceptor Dyads, G.-J. Huang, M. A. Harris, M.

- D. Krzyaniak, E. A. Margulies, S. M. Dyar, R. J. Lindquist, Y. Wu, V. V. Roznyatovskiy, Y.-L. Wu, R. M. Young, and M. R. Wasielewski, *J. Phys. Chem B* **120**, 756-765 (2016).
31. Effects of Crystal Morphology on Singlet Exciton Fission in Diketopyrrolopyrroles P. E. Hartnett, E. A. Margulies, C. M. Mauck, S. A. Miller, Y. Wu, Y.-L. Wu, T. J. Marks, and M. R. Wasielewski, *J. Phys. Chem B* **120**, 1357-1366 (2016).
  32. Chiral Redox-Active Isosceles Triangles, S. K. M. Nalluri, Z. Liu, Y. Wu, K. R. Hermann, A. Samanta, D. J. Kim, M. R. Wasielewski and J. F. Stoddart, *J. Am. Chem. Soc.* **138**, 5968-5977 (2016).
  33. Nanoscale Chemical Imaging of a 2D Dynamic Phase Boundary with Ultrahigh Vacuum Tip-Enhanced Raman Spectroscopy, N. Jiang, N. Chiang, L. R. Madison, E. A. Pozzi, M. R. Wasielewski, T. Seideman, M. A. Ratner, M. C. Hersam, G. C. Schatz, and R. P. Van Duyne, *Nano Lett.* **16**, 3898-3904 (2016).
  34. Guest and Solvent Modulated Photo-driven Charge Separation and Triplet Generation in a Perylene Bisimide Cyclophane, P. Spent, R. M. Young, M. R. Wasielewski and F. Würthner, *Chem. Sci.* **7**, 5428-5434 (2016).
  35. Tuning Singlet Fission Efficiency via Sidechain Substitution in 3,6-Bis-(Thiophen-2-yl)-Diketopyrrolopyrrole, C. M. Mauck, P. E. Hartnett, E. A. Margulies, L. Ma, T. J. Marks, and M. R. Wasielewski, *J. Am. Chem. Soc.* **138**, 11749-11761 (2016).
  36. Enabling Singlet Fission by Controlling Intramolecular Charge Transfer in  $\pi$ -Stacked Covalent Terrylenediimide Dimers, E. A. Margulies, C. E. Miller, Y. Wu, L. Ma, G. C. Schatz, R. M. Young, and M. R. Wasielewski, *Nature Chem.* **8**, 1120-1125 (2016).
  37. Toward Metal-Organic Framework Based Solar Cells: Enhancing Directional Exciton Transport by Collapsing Three-Dimensional Film Structures, S. Goswami, L. Ma, M. R. Wasielewski, O. K. Farha, and J. T. Hupp, *ACS Appl. Mater. Interfaces* **8**, 30863-30870 (2016).
  38. Photoinduced Electron Transfer and Electrocatalytic Behavior of Perylene Covalently Linked to a [Pd(triphosphine)L]<sup>2+</sup> CO<sub>2</sub> Reduction Catalyst, R. E. Cook, B. T. Phelan, L. E. Shoer, M. B. Majewski, and M. R. Wasielewski, *Inorg. Chem.* **55**, 12281-12289 (2016).
  39. Singlet Fission via an Excimer-Like Intermediate in 3,6-Bis(thiophen-2-yl)diketopyrrolopyrrole Derivatives, C. M. Mauck, P. E. Hartnett, E. A. Margulies, L. Ma, C. E. Miller, G. C. Schatz, T. J. Marks, and M. R. Wasielewski, *J. Am. Chem. Soc.* **138**, 11749-11761 (2016).
  40. Direct Observation of a Charge Transfer State Preceding High Yield Singlet Fission in Terrylenediimide Thin Films, E. A. Margulies, C. E. Miller, L. Ma, E. Simonoff, G. C. Schatz, and M. R. Wasielewski, *J. Am. Chem. Soc.* **139**, 663-671 (2017).

41. G-Quadruplex Frameworks, Y.-L. Wu, N. E. Horwitz, K.-S. Chen, D. A. Gomez-Gualdron, N. S. Luu, L. Ma, T. C. Wang, M. C. Hersam, J. T. Hupp, O. K. Farha, R. Q. Snurr, and M. R. Wasielewski, *Nature Chem.* doi:10.1038/nchem.2689 (2017).
42. Characterization of Excimer Relaxation via Femtosecond Shortwave- and Mid-Infrared Spectroscopy, C. M. Mauck, R. M. Young, and M. R. Wasielewski, *J. Phys. Chem. A* **121**, 784–792 (2017).
43. Solvent-Templated Folding of Perylene Bisimide Macrocycles into Coiled Double-String Ropes with Solvent-Sensitive Optical Signatures, P. Spent, R. M. Young, B. T. Phelan, M., J. Dostál, T. Brixner, M. R. Wasielewski, and F. Würthner, *J. Am. Chem. Soc.* **139**, 2014–2021 (2017).
44. Excimer Formation and Symmetry-Breaking Charge Transfer in Cofacial Perylene Dimers, R. E. Cook, B. T. Phelan, R. J. Kamire, M. B. Majewski, R. M. Young, and M. R. Wasielewski, *J. Phys. Chem. A* **121**, 1607-1615 (2017).
45. Electron Hopping and Charge Separation within a Naphthalene-1,4:5,8-bis(dicarboximide) Chiral Covalent Organic Cage, T. Šolomek, N. E. Powers-Riggs, Y.-L. Wu, R. M. Young, M. D. Krzyaniak, N. E. Horwitz and M. R. Wasielewski, *J. Am. Chem. Soc.* **139**, 3348–3351 (2017).
46. Intramolecular Energy and Electron Transfer Within a Diazaperopyrenium-Based Cyclophane, X. Gong, R. M. Young, K. J. Hartlieb, C. Miller, Y. Wu, H. Xiao, P. Li, N. Hafezi, J. Zhou, L. Ma, T. Cheng, W. A. Goddard, O. K. Farha, J. T. Hupp, M. R. Wasielewski, and J. F. Stoddart, *J. Am. Chem. Soc.* **139**, 4107-4116 (2017).
47. Unified Model for Singlet Fission within a Non-conjugated Covalent Pentacene Dimer, B. S. Basel, J. Zirzmeier, C. Hetzer, B. T. Phelan, M. D. Krzyaniak, S. R. Reddy, P. B. Coto, N. E. Horwitz, R. M. Young, F. White, F. Hampel, T. Clark, M. Thoss, R. R. Tykwinski, M. R. Wasielewski, and D. M. Guldi, *Nature Comm.* (in press).

## Organic, Nanoscale, and Self-Assembled Structures Relevant to Solar Energy Conversion

Michael J. Therien  
 Department of Chemistry  
 French Family Science Center, 124 Science Drive  
 Duke University  
 Durham, NC 27708-0354

Understanding the molecular-level principles by which complex chemical systems carry out photochemical charge separation, transport, and storage will impact the design of practical solar energy conversion and storage devices. Towards this goal, this project focuses on several broad themes. This experimental effort aims to: (i) delineate new compositions of matter relevant to solar energy conversion, (ii) understand the basic photophysical properties of next-generation conjugated materials for excitonic solar cells, (iii) elucidate rules and principles that govern charge transfer, charge migration, photoconductivity, the extent of charge and exciton delocalization, and exciton diffusion dynamics in structures and assemblies relevant to light-driven energy transduction, (iv) probe and modulate the extent of electronic coupling between conjugated organic materials and nanoscale structures in both ground and excited states, and (v) engineer high quantum yield electron-hole pair production from initially prepared excitonic states in well-defined assemblies that feature nanoscale, electrooptically active components. Accomplishments over the current funding period include:

### *Developing Conjugated Structures that Provide Large Spatial Delocalization of Injected Charge.*

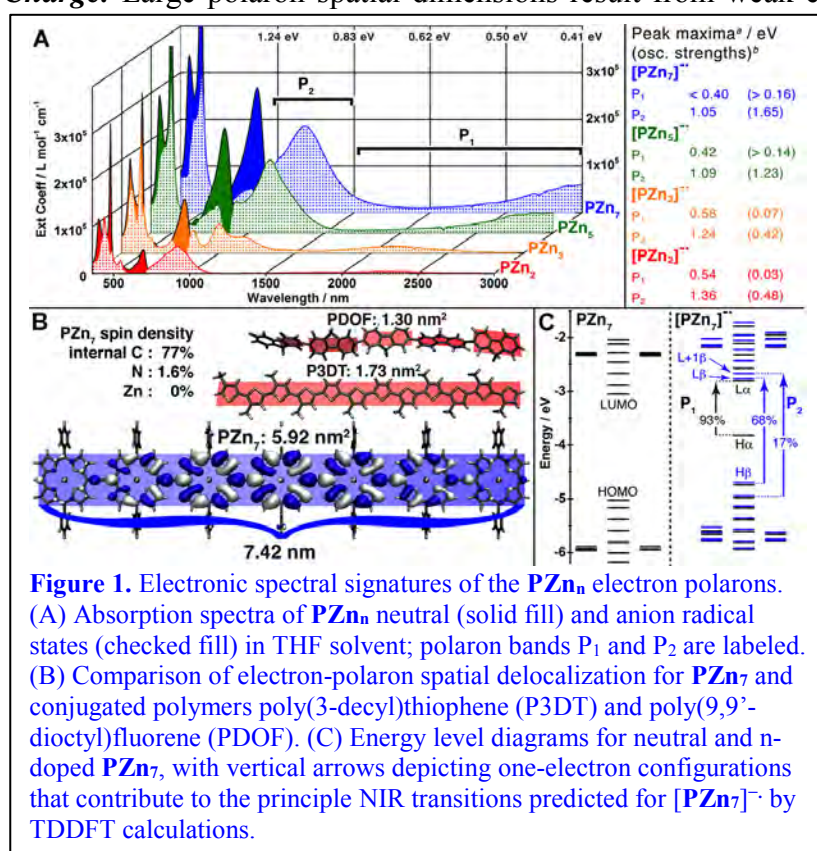
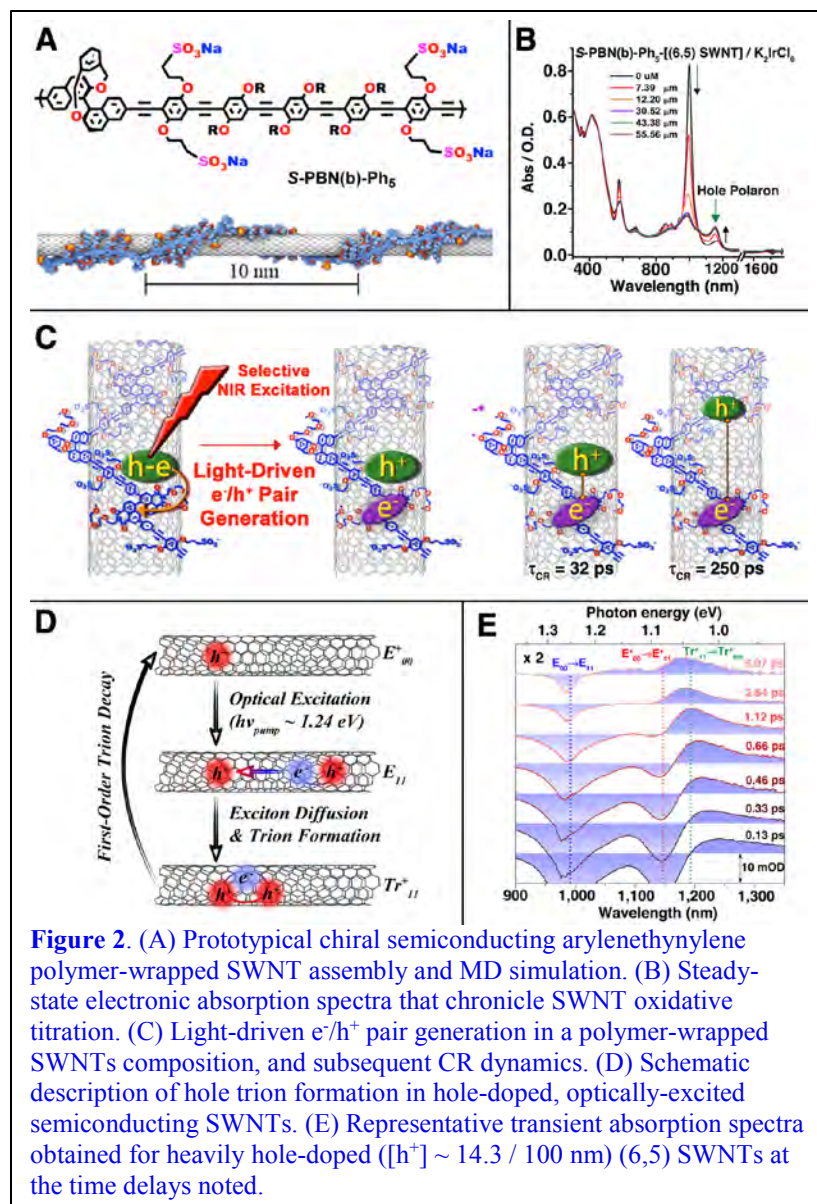


**Figure 1.** Electronic spectral signatures of the  $PZn_n$  electron polarons. (A) Absorption spectra of  $PZn_n$  neutral (solid fill) and anion radical states (checked fill) in THF solvent; polaron bands  $P_1$  and  $P_2$  are labeled. (B) Comparison of electron-polaron spatial delocalization for  $PZn_7$  and conjugated polymers poly(3-decyl)thiophene (P3DT) and poly(9,9'-dioctyl)fluorene (PDOF). (C) Energy level diagrams for neutral and n-doped  $PZn_7$ , with vertical arrows depicting one-electron configurations that contribute to the principle NIR transitions predicted for  $[PZn_7]^{•-}$  by TDDFT calculations.

identify materials with unusually low barriers for the charge transfer reactions that are central to electronic device applications. We demonstrated electron polarons in  $\pi$ -conjugated multiporphyrin arrays that feature vast areal delocalization. This finding is evidenced by concurrent optical and electron spin resonance measurements, coupled with electronic structure calculations that suggest atypically small reorganization energies for one-electron reduction of these materials. Species associated spectra for  $[PZn_2-7]^{•-}$  are displayed alongside the electronic absorption data for the neutral oligomers in **Figure 1A**. These data show:

(i) that the polaron states evince two principal absorption manifolds of lower energy than those of the neutral oligomers (labeled as  $P_1$  and  $P_2$ ), (ii) the transitions in the 1000 – 3000 nm (1.24 – 0.41 eV) spectral window show oscillator strengths that increase with the number of porphyrin repeat units, analogous to the vis-NIR electronic absorptions characteristic of their neutral counterparts, and (iii) the lowest energy transition  $P_1$  for  $[\text{PZn}_{2-7}]^-$  is progressively red-shifted and intensified with increasing oligomer length. In the context of Furukawa's modification of the FBC model,  $P_1$  and  $P_2$  are assigned as intragap transitions between levels whose energies are associated with the degree of polaronic structural relaxation. These polaron bands show dependences of their oscillator strengths and low energy electronic absorption maxima upon oligomer length that remain unsaturated for the range of compounds explored here, suggesting that the effective electron-polaron delocalization length is not yet reached for  $[\text{PZn}_7]^-$ . Time-dependent DFT (TD-DFT) calculations show that the absorption spectra of  $[\text{PZn}_n]^-$  are only well represented using a model that delocalizes the highest-occupied majority spin orbital ( $\text{HOMO}\alpha$ ) over the entire porphyrin oligomers. The most intense  $P_1$ -region transitions are of  $\text{HOMO}\alpha \rightarrow \text{LUMO}\alpha$  character, while the principal  $P_2$ -region transitions are dominated by  $\text{HOMO}\beta \rightarrow \text{LUMO}\beta$  configurations (**Figure 1C**). The combination of EPR, electronic spectral, and computational studies show that negative charges in these highly conjugated organic structures are dispersed over greater areas relative to any other organic material that has been studied to date (**Figure 1B**). These studies provide important insights, as organic materials that adeptly accommodate and transmit negative charges pose a significant design challenge for compositions that provide enhanced solar energy conversion efficiencies.

***Excitonic, Polaronic, Charge-Separated, and Trionic States in Semiconducting Polymer-Wrapped Single-Walled Carbon Nanotube Assemblies.*** We have established aryleneethynylene polymer designs that give rise to single-handed helical wrapping of single-walled carbon nanotubes (SWNTs; **Figure 2A**). Highly charged, chiral anionic semiconducting polymers helically wrap single-walled carbon nanotubes (SWNTs) at periodic and constant morphology. These polymers can be used as tools to modulate SWNT electronic properties, provide expansive solubility, or organize functional organic moieties at predefined intervals along the SWNT surface. We detailed (SWNT)-based nanohybrid compositions based on (6,5) chirality-enriched SWNTs ([6,5] SWNTs) and chiral semiconducting polymers that feature repeat units that contain electron acceptors. Such helically wrapped polymer-SWNT superstructures, for example, feature perylene diimide (PDI) electron acceptor unit positioned at 3 nm intervals along the nanotube surface, thus controlling rigorously SWNT–electron acceptor stoichiometry and organization. Potentiometric studies determine driving forces for photoinduced charge separation (CS) and thermal charge recombination (CR) reactions, as well as spectroscopic signatures of SWNT hole polaron and PDI radical anion states (**Figure 2B**). Femtosecond pump-probe transient absorption spectroscopic experiments determine driving force- and solvent-dependent photoinduced CS and thermal CR dynamics, and provide insights into the factors that govern photoinduced charge transfer reactions at soft matter-hard matter interfaces defined by polymers and SWNTs (**Figure 2C**). Related experiments probe the transient absorptive and dynamical properties of positively and negatively charged excitons (i.e., hole- and electron trions) in these semiconducting polymer-wrapped SWNT superstructures (**Figure 2D-E**); these studies determine trion transient absorptive signatures and dynamics as functions of absolute electron- or hole-doping levels. Global analysis of these data over the entire vis-NIR spectral domain, where these systems display characteristic transient absorptive spectral signatures, provide fundamental



carrier generation is influenced by the carrier population, (iv) probe how carrier-carrier or exciton-carrier interactions compete with electron-transfer or carrier-recombination processes, and (v) probe if carrier-carrier interactions give rise to unique spectroscopic signals. These studies provide insights into new designs that maximize the SWNT charge density that may be generated for a given excitation fluence, and opportunities to understand how charge-charge/charge-exciton interactions impact charge transfer reactions that occur at the nanotube-semiconducting polymer interface.

new understanding of trion formation and decay mechanisms. These photophysical studies of SWNT trion dynamics suggest new opportunities to manipulate and couple charges, spins, and excitons in carbon nanotubes important for solar energy conversion.

**Impact of Excitation Fluence Upon Charge Carrier Density in Polymer-Wrapped SWNT Assemblies.** We have utilized individualized, length-sorted chirality enriched single-walled carbon nanotubes having dimensions of 200 and 800 nm, femtosecond transient absorption spectroscopy, and variable excitation fluences, to modulate the exciton density per nanotube unit length. Using chiral semiconducting polymer-wrapped SWNT superstructures, we (i) explore how exciton density impacts photoinduced CS and thermal CR reaction dynamics, (ii) determine how carrier-carrier interactions influence charge-separated state lifetime, (iii) investigate the extent to which

### DOE Sponsored Solar Photochemistry Publications 2014-2017:

- 1) Fluence-Dependent Singlet Exciton Dynamics in Length-Sorted Chirality-Enriched Single-Wall Carbon Nanotubes, J. Park, P. Deria, J.-H. Olivier, and M. J. Therien, *Nano Lett.* **2014**, *14*, 504–511. DOI: 10.1021/nl403511s.
- 2) Potentiometric, Electronic, and Transient Absorptive Spectroscopic Properties of Oxidized Single-Walled Carbon Nanotubes Helically Wrapped by Ionic, Semiconducting Polymers in Aqueous and Organic Media, P. Deria, J.-H. Olivier, J. Park, and M. J. Therien, *J. Am. Chem. Soc.* **2014**, *136*, 14193–14199. DOI: 10.1021/ja507457z.
- 3) Electron Spin Relaxation of Hole and Electron Polarons in  $\pi$ -Conjugated Porphyrin Arrays: Spintronic Implications, J. Rawson, P. J. Angiolillo, P. R. Frail, I. Goodenough, and M. J. Therien, *J. Phys. Chem. B.* **2015**, *119*, 7681–7689. DOI: 10.1021/jp5122728.
- 4) Unambiguous Diagnosis of Photoinduced Charged Carrier Signatures in a Stoichiometrically Controlled Semiconducting Polymer-Wrapped Carbon Nanotube Assembly, J.-H. Olivier, J. Park, P. Deria, J. Rawson, Y. Bai, A. Kumbhar, and M. J. Therien, *Angew. Chem., Int. Ed. Engl.* **2015**, *54*, 8133–8138. DOI: 10.1002/anie.201501364.
- 5) Extreme Electron Polaron Spatial Delocalization in  $\pi$ -Conjugated Materials, J. Rawson, P. J. Angiolillo, and M. J. Therien, *Proc. Natl. Acad. Sci. U.S.A.* **2015**, *112*, 13779–13783. DOI: 10.1073/pnas.1512318112.
- 6) Valence Band Dependent Charge Transport in Bulk Molecular Electronic Devices Incorporating Highly Conjugated Multi[(Porphinato)Metal] Oligomers, R. C. Bruce, R. Wang, J. Rawson, M. J. Therien, and W. You, *J. Am. Chem. Soc.* **2016**, *138*, 2078–2081. DOI: 10.1021/jacs.5b10772.
- 7) First-Order Hyperpolarizabilities of Chiral, Polymer-Wrapped Single-Walled Carbon Nanotubes, G. Depotter, J.-H. Olivier, M. G. Glesner, P. Deria, Y. Bai, G. Bullard, A. S. Kumbhar, M. J. Therien, and K. Clays, *Chem. Commun.* **2016**, *52*, 12206–12209. DOI: 10.1039/C6CC06190G.
- 8) On the Importance of Electronic Symmetry for Triplet State Delocalization, S. Richert, G. Bullard, J. Rawson, P. J. Angiolillo, M. J. Therien, and C. R. Timmel, *J. Am. Chem. Soc.* **2017**, *139*. DOI: 10.1021/jacs.7b01204.
- 9) Alkyne-Bridged Multi[Copper(II) Porphyrin] Structures: Nuances of Orbital Symmetry in Long-Range, Through-Bond Mediated, Isotropic Spin Exchange Interactions, R. Wang, A. M. Brugh, J. Rawson, M. J. Therien, and M. D. E. Forbes, *J. Am. Chem. Soc.* Submitted.

## Carrier Delocalization and Long-lived Charges in Doped Conjugated Polymers

Garry Rumbles<sup>1,2,3</sup>, Michael Ortiz<sup>2</sup>, Natalie Pace<sup>2</sup>, Jessica Ramirez<sup>2</sup>, Jaehong Park<sup>1</sup>, Wei Zhang<sup>2</sup> and Obadiah Reid<sup>3</sup>

<sup>1</sup>Chemistry and Nanoscience Center,  
National Renewable Energy Laboratory, Golden, Colorado, 80401  
and

<sup>2</sup>Department of Chemistry and Biochemistry

<sup>3</sup>Renewable and Sustainable Energy Institute  
University of Colorado Boulder, Boulder, CO 80309

This presentation will focus on understanding the fundamental photoinduced electron transfer steps of excitations in thin films conjugated polymers that are doped with molecular electron acceptors. The goal is to understand how these systems produce very high yields of long-lived, separated charges when exciting the acceptor directly, or indirectly through the conjugated polymer, which serves as both a light harvesting system and electron donor. An unusual feature of these systems is the large discrepancy in timescales of the initial photoinduced electron transfer step, which is sub-picosecond, and the recombination process, which can take as long as milliseconds.

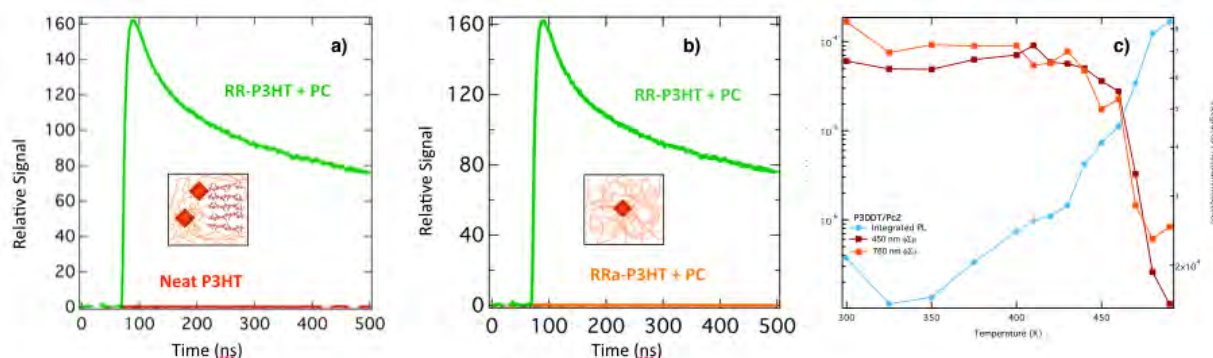


Figure 1 – Microwave absorption transients of carriers in a) RR-p3HT; b) RRa-p3HT; and c) the influence on the microwave absorption and photoluminescence of increasing temperature on the RR-p3HT sample.

Our recent work has shown that the solid-state microstructure of the conjugated polymer is a critical factor that influences the photophysics of these model systems. Using regioregular (RR-p3HT), and regiorandom (RRa-p3HT) poly(3-hexylthiophene) we have demonstrated that long-lived carriers are only present when crystallites (or ordered aggregates) are present in the RR-p3HT sample. Two polymer samples each containing a low concentration of a silicon phthalocyanine (SiPc) could be selectively excited through the prominent Q-band at 780 nm. While photoluminescence from the macrocycle was quenched in both cases, studies using time-resolved microwave conductivity (TRMC), revealed that long-lived charges were only observed in the sample that contained the aggregates (Figure 1a), while none were observed in the

amorphous RRa-p3HT (Figure 1b), which displayed only efficient geminate recombination. Using the new temperature-controlled capabilities of the TRMC experiment at NREL, we were able to similarly eliminate the crystallites from the RR-p3HT and suppress the carrier yield, as shown in Figure 1c). We attribute this effect to delocalization of the hole in the RR-p3HT facilitated by the presence of the aggregates, although it is unclear whether delocalization requires one or more of the extended, planar polymer chains. The delocalization effect provides access to a charge-separated (CS) state, which has a greater probability of dissociating into free carriers.<sup>10,23</sup> Similar effects have also been observed in poly(9,9'- dioctylfluorene), PFO, where we are also able to observe the emission from an exciplex state as the carriers recombine.

To examine further the relative role of charge-transfer (CT) and charge-separated (CS) states, as well as exciplex states in doped conjugated polymer films, we have studied a new C<sub>70</sub>-encapsulated bisporphyrin covalent organic polyhedron (COP-5:C<sub>70</sub>)<sup>1</sup> (Figure 2), which in a low dielectric toluene solvent demonstrates unusual photoinduced electron transfer kinetics. Transient absorption studies of this molecule have shown that electron transfer from one of the cage porphyrins to the encapsulated C<sub>70</sub> occurs in less than 400 fs, to create a CT state that has a lifetime of over 600 ps. We are now using this complex to study the effects of the CT state on carrier yields and lifetimes when it is used as a sensitizer for the conjugated polymers.

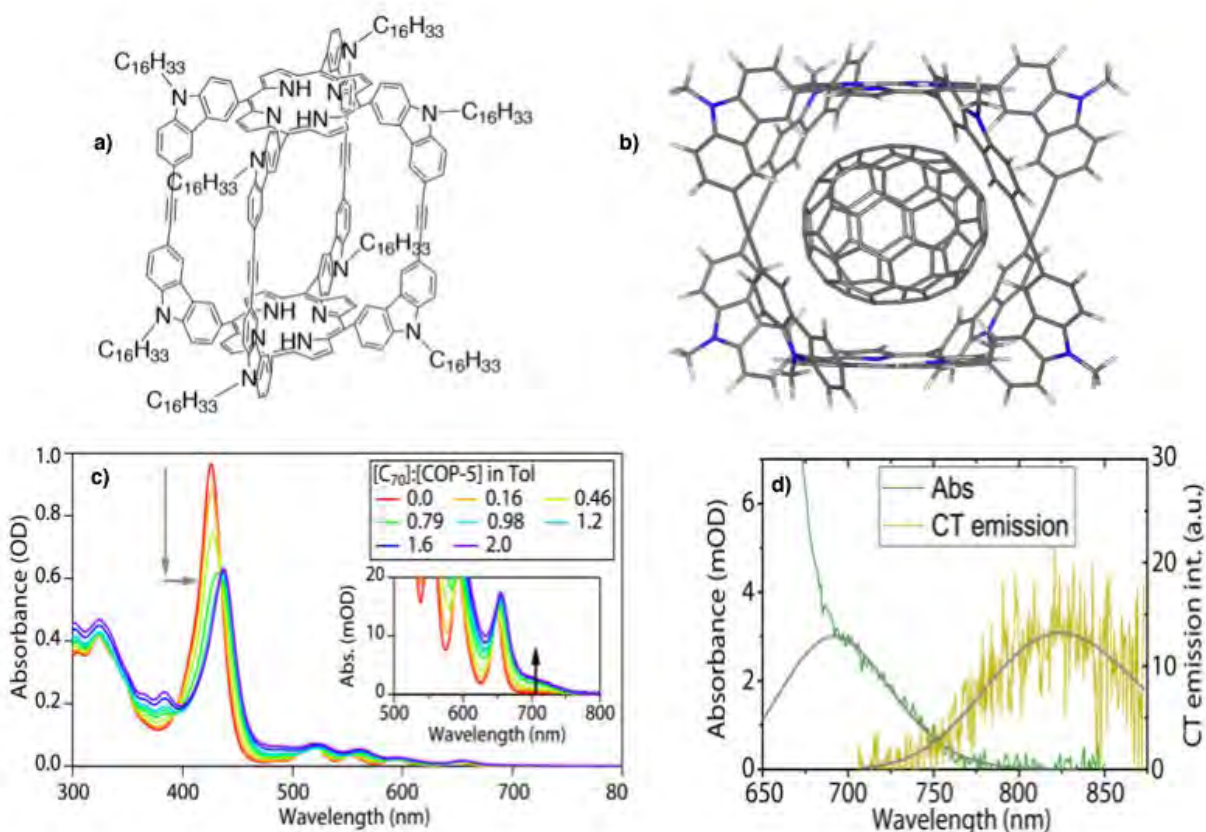


Figure 2 – a) Structure of bisporphyrin covalent organic polyhedron (COP-5); b) structure with encapsulated C<sub>70</sub> fullerene; c) absorption spectra as a function of COP-5:C<sub>70</sub> ratio (Association constant,  $K_{AS} = 1,5 \times 10^8 \text{ M}^{-1}$ ); d) absorption and emission spectra of the CT state.

## DOE Sponsored Publications 2014-2017

- (1) Ortiz, M.; Cho, S.; Niklas, J.; Kim, S.; Poluektov, O. G.; Zhang, W.; Rumbles, G.; Park, J. Through-Space Ultrafast Photoinduced Electron Transfer Dynamics of a C70-Encapsulated Bisporphyrin Covalent Organic Polyhedron in a Low-Dielectric Medium. *J Am Chem Soc* **2017**, *139* (12), 4286–4289.
- (2) Nayak, P. K.; Moore, D. T.; Wenger, B.; Nayak, S.; Haghhighirad, A. A.; Fineberg, A.; Noel, N. K.; Reid, O. G.; Rumbles, G.; Kukura, P.; et al. Mechanism for Rapid Growth of Organic-Inorganic Halide Perovskite Crystals. *Nat Comms* **2016**, *7*, 13303.
- (3) Larson, B. W.; Reid, O. G.; Coffey, D. C.; Avdoshenko, S. M.; Popov, A. A.; Boltalina, O. V.; Strauss, S. H.; Kopidakis, N.; Rumbles, G. Inter-Fullerene Electronic Coupling Controls the Efficiency of Photoinduced Charge Generation in Organic Bulk Heterojunctions. *Adv. Energy Mater.* **2016**, *6* (24), 1601427.
- (4) Reid, O. G.; Yang, M.; Kopidakis, N.; Zhu, K.; Rumbles, G. Grain-Size-Limited Mobility in Methylammonium Lead Iodide Perovskite Thin Films. *ACS Energy Lett.* **2016**, 561–565.
- (5) Beard, M. C.; Blackburn, J. L.; Johnson, J. C.; Rumbles, G. Status and Prognosis of Future-Generation Photoconversion to Photovoltaics and Solar Fuels. *ACS Energy Lett.* **2016**, *1* (2), 344–347.
- (6) Ihly, R.; Mistry, K. S.; Ferguson, A. J.; Clikeman, T. T.; Larson, B. W.; Reid, O. G.; Boltalina, O. V.; Strauss, S. H.; Rumbles, G.; Blackburn, J. L. Tuning the Driving Force for Exciton Dissociation in Single-Walled Carbon Nanotube Heterojunctions. *Nature Chemistry* | doi:10.1038/nchem.2354 **2016**, *8* (6), 603–609.
- (7) Reid, O. G.; Rumbles, G. Resonance Energy Transfer Enables Efficient Planar Heterojunction Organic Solar Cells. *J Phys Chem C* **2016**, *120* (1), 87–97.
- (8) Park, J.; Ramirez, J. J.; Clikeman, T. T.; Larson, B. W.; Boltalina, O. V.; Strauss, S. H.; Rumbles, G. Variation of Excited-State Dynamics in Trifluoromethyl Functionalized C<sub>60</sub> Fullerenes. *Phys Chem Chem Phys* **2016**, *18* (33), 22937–22945.
- (9) Pascoe, A. R.; Yang, M.; Kopidakis, N.; Zhu, K.; Reese, M. O.; Rumbles, G.; Fekete, M.; Duffy, N. W.; Yi-Bing, C. Planar Versus Mesoscopic Perovskite Microstructures: the Influence of CH<sub>3</sub>NH<sub>3</sub>PbI<sub>3</sub> Morphology on Charge Transport and Recombination Dynamics. *Nano Energy* **2016**, *22*, 439–452.
- (10) Feier, H. M.; Reid, O. G.; Pace, N. A.; Park, J.; Bergkamp, J. J.; Sellinger, A.; Gust, D.; Rumbles, G. Local Intermolecular Order Controls Photoinduced Charge Separation at Donor/Acceptor Interfaces in Organic Semiconductors. *Adv. Energy Mater.* **2016**, *6* (6), 1502176.
- (11) Crisp, R. W.; Callahan, R.; Reid, O. G.; Dolzhenkov, D. S.; Talapin, D. V.; Rumbles, G.; Luther, J. M.; Kopidakis, N. Photoconductivity of CdTe Nanocrystal-Based Thin Films: Te<sub>2</sub>-Ligands Lead to Charge Carrier Diffusion Lengths Over 2 μm. *The Journal of Physical Chemistry Letters* **2015**, *6* (23), 4815–4821.
- (12) Park, J.; Reid, O. G.; Blackburn, J. L.; Rumbles, G. Photoinduced Spontaneous Free-Carrier Generation in Semiconducting Single-Walled Carbon Nanotubes. *Nat Comms* **2015**, *6*, 8809.

- (13) Clikeman, T. T.; Bukovsky, E. V.; Wang, X.-B.; Chen, Y.-S.; Rumbles, G.; Strauss, S. H.; Boltalina, O. V. Core Perylene Diimide Designs via Direct Bay- and Ortho-(Poly)Trifluoromethylation: Synthesis, Isolation, X-Ray Structures, Optical and Electronic Properties. *Eur J Org Chem* **2015**, 2015 (30), 6641–6654.
- (14) Park, J.; Reid, O. G.; Rumbles, G. Photoinduced Carrier Generation and Recombination Dynamics of a Trilayer Cascade Heterojunction Composed of Poly(3-Hexylthiophene), Titanyl Phthalocyanine, and C 60. *J Phys Chem B* **2015**, 119 (24), 7729–7739.
- (15) LaCount, M. D.; Weingarten, D.; Hu, N.; Shaheen, S. E.; van de Lagemaat, J.; Rumbles, G.; Walba, D. M.; Lusk, M. T. Energy Pooling Upconversion in Organic Molecular Systems. *J Phys Chem A* **2015**, 119 (17), 4009–4016.
- (16) Nogueira, A. F.; Rumbles, G. Special Section Guest Editorial: Hybrid Organic-Inorganic Solar Cells. *J. Photon. Energy* **2015**, 5 (1), 057401–057401.
- (17) Bird, M.; Mauro, G.; Zaikowski, L.; Li, X.; Reid, O. G.; Karten, B.; Asaoka, S.; Chen, H.-C.; Cook, A. R.; Rumbles, G.; et al. Singlet, Triplet, Electron and Hole Transport Along Single Polymer Chains; Hayes, S. C., Bittner, E. R., Eds.; International Society for Optics and Photonics, 2015; Vol. 9549, pp 95490E–95490E–10.
- (18) Dayal, S.; Zhong, H.; Kopidakis, N.; Scholes, G. D.; Rumbles, G. Improved Power Conversion Efficiency for Bulk Heterojunction Solar Cells Incorporating CdTe-CdSe Nanoheterostructure Acceptors and a Conjugated Polymer Donor. *J. Photon. Energy* **2015**, 5 (1), 057409.
- (19) Park, J.; Reid, O. G.; Rumbles, G. Photo-Induced Carrier Generation and Recombination Dynamics Probed by Combining Time-Resolved Microwave Conductivity and Transient Absorption Spectroscopy. *SPIE Nanoscience + Engineering* **2015**, 9549, 954900–954900–7.
- (20) San, L. K.; Bukovsky, E. V.; Larson, B. W.; Whitaker, J. B.; Deng, S. H. M.; Kopidakis, N.; Rumbles, G.; Popov, A. A.; Chen, Y.-S.; Wang, X.-B.; et al. A Faux Hawk Fullerene with PCBM-Like Properties. *Chem Sci* **2015**, 6 (3), 1801–1815.
- (21) Wojciechowski, K.; Stranks, S. D.; Abate, A.; Sadoughi, G.; Sadhanala, A.; Kopidakis, N.; Rumbles, G.; Li, C.-Z.; Friend, R. H.; Jen, A. K.-Y.; et al. Heterojunction Modification for Highly Efficient Organic - Inorganic Perovskite Solar Cells. *Acs Nano* **2014**, 8 (12), 12701–12709.
- (22) O'Connor, B. T.; Reid, O. G.; Zhang, X.; Kline, R. J.; Richter, L. J.; Gundlach, D. J.; DeLongchamp, D. M.; Toney, M. F.; Kopidakis, N.; Rumbles, G. Morphological Origin of Charge Transport Anisotropy in Aligned Polythiophene Thin Films. *Adv Funct Mater* **2014**, 24 (22), 3422–3431.
- (23) Marsh, H. S.; Reid, O. G.; Barnes, G.; Heeney, M.; Stingelin, N.; Rumbles, G. Control of Polythiophene Film Microstructure and Charge Carrier Dynamics Through Crystallization Temperature. *Journal of Polymer Science Part B-Polymer Physics* **2014**, 52 (10), 700–707.
- (24) Niklas, J.; Holt, J. M.; Mistry, K.; Rumbles, G.; Blackburn, J. L.; Poluektov, O. G. Charge Separation in P3HT:SWCNT Blends Studied by EPR: Spin Signature of the Photoinduced Charged State in SWCNT. *The Journal of Physical Chemistry Letters* **2014**, 5 (3), 601–606.

- (25) Callahan, R. A.; Coffey, D. C.; Chen, D.; Clark, N. A.; Rumbles, G.; Walba, D. M. Charge Generation Measured for Fullerene–Helical Nanofilament Liquid Crystal Heterojunctions. *Acs Appl Mater Inter* **2014**, *6* (7), 4823–4830.
- (26) Buchaca-Domingo, E.; Ferguson, A. J.; Jamieson, F. C.; McCarthy-Ward, T.; Shoaee, S.; Tumbleston, J. R.; Reid, O. G.; Yu, L.; Madec, M.-B.; Pfannmöller, M. Additive-Assisted Supramolecular Manipulation of Polymer: Fullerene Blend Phase Morphologies and Its Influence on Photophysical Processes. *Materials Horizons* **2014**, *1* (2), 270–279.
- (27) Bird, M. J.; Reid, O. G.; Cook, A. R.; Asaoka, S.; Shibano, Y.; Imahori, H.; Rumbles, G.; Miller, J. R. Mobility of Holes in Oligo-and Polyfluorenes of Defined Lengths. *The Journal of Physical Chemistry C* **2014**, *118* (12), 6100–6109.
- (28) Larson, B. W.; Whitaker, J. B.; Popov, A. A.; Kopidakis, N.; Rumbles, G.; Boltalina, O. V.; Strauss, S. H. Thermal [6, 6]→[6, 6] Isomerization and Decomposition of PCBM (Phenyl-C61-Butyric Acid Methyl Ester). *Chem Mater* **2014**, *26* (7), 2361–2367.



## *Session VI*

### *Small Molecule Activation I*



## Catalytic Reduction of Nitrogen to Ammonia with Molybdenum Catalysts

Lasantha A. Wickramasinghe, Takaya Ogawa, and Richard R. Schrock

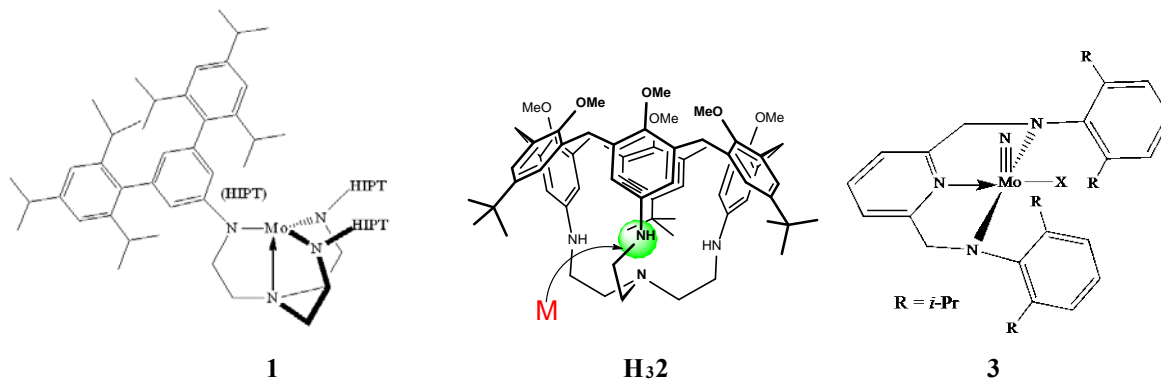
Department of Chemistry

Massachusetts Institute of Technology

77 Massachusetts Avenue, Room 6-331

Cambridge, Massachusetts 02139

There are now three published homogeneous systems that will reduce molecular nitrogen to ammonia with protons and electrons under mild conditions, all homogeneously. (No heterogeneous system that operates under mild conditions is known.) The first (2003) was a molybdenum catalyst that contains a tetradentate tren-based triamidoamine(3-) ligand ( $[\text{N}(\text{CH}_2\text{CH}_2\text{N}(\text{HIPT}))_3]^{3-}$ ) in which HIPT is 3,5-(2,4,6-triisopropylphenyl) $_2\text{C}_6\text{H}_3$  (**1**).<sup>1,2</sup> The second system, and now several variations, was published by Nishibayashi in 2011.<sup>3</sup> The catalyst precursor in this case is a bimetallic Mo(0) complex that contains a neutral "PNP pincer"



ligand, 2,6-(*t*-Bu<sub>2</sub>PCH<sub>2</sub>)<sub>2</sub>(NC<sub>5</sub>H<sub>3</sub>); the catalytic cycle is proposed to involve monomeric intermediates in which the lowest oxidation state of Mo is not Mo(0). The third system was discovered by Peters; in this case the reduction is catalyzed by an iron complex in which the ligand scaffold is a tetradentate neutral trisphosphine-based "tripodal" ligand.<sup>4</sup> All three systems are most efficient with a metallocene as a reducing agent and a nitrogen-based acid such as lutidinium<sup>+</sup> or Ph<sub>2</sub>NH<sub>2</sub><sup>+</sup> as the proton source. As proposed in the original system based on **1**, some form of proton-coupled electron transfer (PCET) is a key feature of the reduction. For example, it was first shown in 2002 that  $[\text{N}(\text{CH}_2\text{CH}_2\text{N}(\text{HIPT}))_3]\text{MoN}_2$  could not be reduced by CoCp<sub>2</sub> or protonated by lutidinium, but both together in benzene produced  $[\text{N}(\text{CH}_2\text{CH}_2\text{N}(\text{HIPT}))_3]\text{Mo-N=NH}$  in high yield. (Delivery of the first proton and electron is the most difficult step in the reduction based on **1**.) In all systems loss of ligand from the metal is often a limiting factor in terms of turnover.

We have turned to the synthesis of a ligand variation of that found in **1** (**H32**) that we felt should be relatively stable toward removal through protonation under reducing conditions. It is based on a calix[6]arene ligand in which a tren system has been installed on the "lower rim" of the calix[6]arene. We have now prepared **[2]Mo≡N** and shown that under the conditions

successful for **1** as a catalyst for nitrogen reduction, [2]Mo≡N is does *not* reduce nitrogen catalytically, a problem that we think is related to the slow rate of exchange of ammonia for dinitrogen along with a restricted access of the metal by reagents. A variation in which three of the methoxides in the "linkers" in the ligand have been removed and replaced by H is currently being explored. We then turned to a Mo-based catalyst (**3**) that contains a conformationally rigid pyridine-based diamido ligand, [2,6-(ArNCH<sub>2</sub>)<sub>2</sub>NC<sub>5</sub>H<sub>3</sub>]<sup>2-</sup> (Ar = 2,6-disopropylphenyl; X = *t*-Bu, Cl, OTf, OC<sub>6</sub>F<sub>5</sub>).<sup>5</sup> We found that the conditions most recently used by Peters (CoCp\*<sub>2</sub> and Ph<sub>2</sub>NH<sub>2</sub>OTf in diethyl ether) produced ~8 equivalents of ammonia in a batch-wise reduction of dinitrogen. The fact that the only variation that leads to a convincingly catalytic reduction of dinitrogen is that in which X = O-*t*-Bu has led to the search for what the actual catalyst for the catalytic reduction might be. These efforts are ongoing and will be updated.

Three of the four known systems for reducing dinitrogen are based on molybdenum catalysts. In all cases metallocenes as reducing agents and amines or anilinium salts as proton sources are optimum.

## References

- <sup>1</sup> Yandulov, D. V.; Schrock, R. R. *Science* **2003**, *301*, 76-78. (a) Schrock, R. R. *Angew. Chem. Int. Ed.* **2008**, *47*, 5512-5522. (b) Hettterscheid, D. G. H.; Hanna, B. S.; Schrock, R. R. *Inorg. Chem.* **2009**, *48*, 8569-8577. (c) Schrock, R. R. in *Catalysis Without Precious Metals*, Bullock, R. M., Ed., Wiley-VCH, 2010, page 25. (d) Munisamy, T.; Schrock, R. R. *Dalton Trans.* **2012**, *41*, 130-137.
- <sup>2</sup> (a) Thimm, W.; Gradert, C.; Broda, H.; Wennmohs, F.; Neese, F.; Tuczek, F. *Inorg. Chem.* **2015**, *54*, 9248-9255. (b) Schenk, S.; Le Guennic, B.; Kirchner, B.; Reiher, M. *Inorg. Chem.* **2008**, *47*, 3634-3650. (c) Reiher, M.; Le Guennic, B.; Kirchner, B. *Inorganic Chemistry* **2005**, *44*, 9640-9642.
- <sup>3</sup> (a) Arashiba, K.; Miyake, Y.; Nishibayashi, Y. *Nat. Chem.* **2011**, *3*, 120. (b) Nishibayashi, Y. *Dalton Trans.* **2012**, *41*, 7447-7453. (c) Kinoshita, E.; Arashiba, K.; Kuriyama, S.; Eizawa, A.; Nakajima, K.; Nishibayashi, Y., *Eur. J. Inorg. Chem.* **2015**, *2015*, 1789-1794. (d) Arashiba, K.; Kinoshita, E.; Kuriyama, S.; Eizawa, A.; Nakajima, K.; Tanaka, H.; Yoshizawa, K.; Nishibayashi, Y. *J. Am. Chem. Soc.* **2015**, *137*, 5666-5669. (e) Nishibayashi, Y. *Accs. Chem. Res.* **2016**, *49*, 987-995.
- <sup>4</sup> (a) Anderson, J. S.; Rittle, J.; Peters, J. C. *Nature* **2013**, *501*, 84-87. (b) Chalkley, M. J.; Del Castillo, T. J.; Matson, B. D.; Roddy, J. P.; Peters, J. C. *ACS Cent. Sci.* **2017**, *3*, 217-223.
- <sup>5</sup> Guérin, F.; McConville, D. H.; Vittal, J. J. *Organometallics* **1996**, *15*, 5586-5590.

## DOE Sponsored Publications 2014-2017 (DOE support for N<sub>2</sub> reduction began in 2015)

"A Calix[6]azacryptand Ligand with a Sterically Protected Tren-based Coordination Site for Metal Ions"  
Zahim, S.; Wickramasinghe, L. A.; Evano, G.; Jabin, I.; Schrock, R. R.; Müller, P. *Org. Lett.* **2016**, *18*, 1570-1573; DOI: 10.1021/acs.orglett.6b00410.

## Molecular Photoelectrocatalysts for Hydrogen Evolution

Alexander J. M. Miller, Matthew B. Chambers, Catherine L. Pitman, Daniel A. Kurtz  
 Department of Chemistry  
 University of North Carolina at Chapel Hill  
 Chapel Hill, NC 27599-3290

Light-driven fuel synthesis is typically accomplished by systems comprised of separate components that absorb light, separate charge, and catalyze bond-forming reactions. This project introduces *molecular photoelectrocatalysts* as an alternative approach that integrates light-harvesting and bond-forming steps for efficient photon-to-fuel conversion. We recently discovered that the iridium hydride  $[\text{Cp}^*\text{Ir}(\text{bpy})(\text{H})]^+$  (**1**) mediates sustained visible light-driven water splitting in aqueous media across a wide pH range with high Faradaic and quantum efficiency at low electrochemical overpotential. In this presentation, I will share recent progress on our mechanism-guided development of molecular photoelectrocatalysts for  $\text{H}_2$  synthesis.

While light-driven  $\text{H}_2$  release from monometallic and bimetallic dihydrides is well-understood, photochemical  $\text{H}_2$  release from monohydrides is unusual — and relatively unstudied. Photoexcitation of **1** generates a metal-to-ligand charge transfer (MLCT) triplet excited state  $[\text{Cp}^*\text{Ir}(\text{bpy})(\text{H})]^{+*}$  (**1**<sup>\*</sup>) featuring broad orange emission (Figure 1). Time-Dependent Density Functional Theory (TD-DFT) studies are consistent with electronic excitation from an Ir-based HOMO to a bpy- $\pi^*$ -based LUMO. Although an excited state that shifts electron density away from the metal center might indicate a more *acidic* metal hydride, the net reactivity of complex **1** is *hydridic*. Thermodynamic analysis reveals that hydride **1** is *both* more acidic *and* more hydridic (Figure 1), in analogy to the ambiphilic reactivity of  $[\text{Ru}(\text{bpy})_3]^{2+}$  as a photo-oxidant and a photo-reductant.

Kinetic studies in acetonitrile solution have revealed an unprecedented, exceptionally efficient pathway for photochemical  $\text{H}_2$  evolution from **1**<sup>\*</sup> via bimolecular self-quenching of the excited state by electron transfer (Scheme 1). The bimetallic nature of the reaction is clear from isotopic labeling studies and quantum yield measurements that show a strong iridium concentration

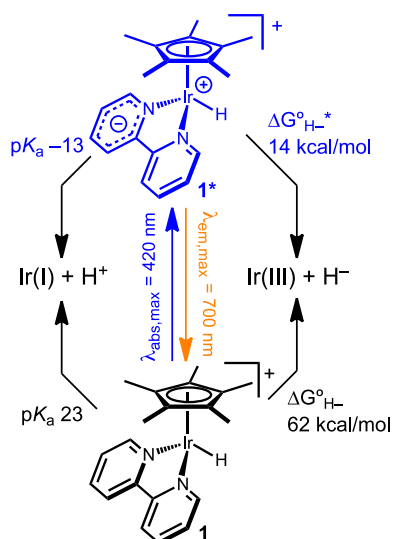
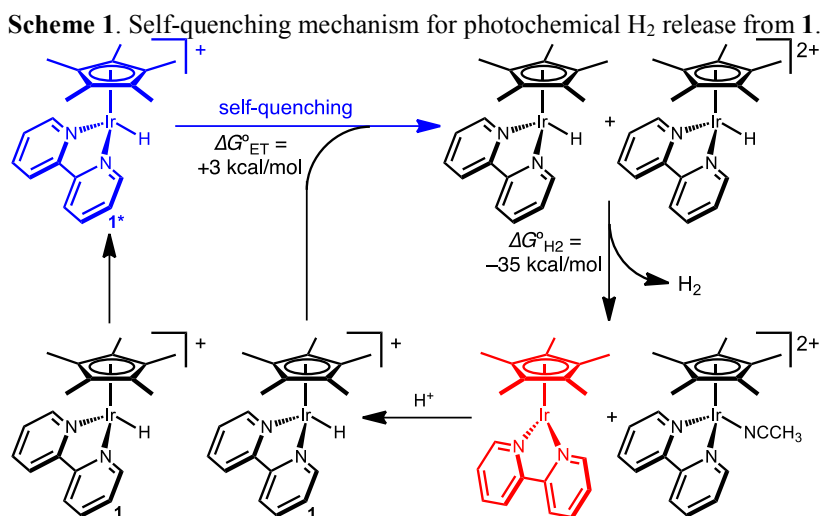


**Figure 1.** Ground state and excited state thermochemistry of **1**.



dependence. Above 15 mM concentrations of **1**, H<sub>2</sub> release occurs with essentially *unity quantum efficiency*. Self-quenching of **1**\* by a ground state molecule of **1** occurs at rates near the diffusion limit. The lack of any measureable kinetic isotope effect or dependence on the acid concentration indicates that the Ir–H bond does not break during self-quenching. Scheme 1 shows the proposed mechanism, wherein **1**\* undergoes rate-limiting bimetallic self-quenching via electron transfer, followed by rapid bimetallic H<sub>2</sub> release. The self-quenching electron transfer is slightly unfavorable, but the following H<sub>2</sub> release step is highly exergonic. Preliminary studies in water suggest that a similar mechanism is operating. In dichloromethane, however, only dehydrohalogenation to form chloromethane is observed (with no evidence for H<sub>2</sub> release). Kinetic studies are still consistent with self-quenching of the excited state, but we hypothesize that the solvent intercepts the Ir(IV)–H and/or Ir(II)–H intermediates.

The self-quenching mechanism for H<sub>2</sub> evolution provides clear guidance for catalyst design: a single bimetallic molecule should provide more efficient photoelectrochemical catalysis under conditions where bimolecular reactivity is limited, such as at low catalyst loadings or in surface-tethered systems. Three new bimetallic iridium catalysts containing alkyl linkers of varying length (4, 8, and 12 carbons) were synthesized and found to catalyze photoelectrochemical H<sub>2</sub> evolution in neutral water. Rate constants (from chronoamperometry, Figure 2 inset) for the tethered systems are roughly 3-fold higher than the monometallic complex at low concentrations (Figure 2). As expected, the rates converge at higher concentrations as bimolecular quenching becomes more efficient.

Efforts to establish design principles for “photohydride” catalysts will be discussed in the last part of the talk. In the context of probing the generality of self-quenching pathways, we prepared a new iridium methyl complex, [Cp\*Ir(bpy)(CH<sub>3</sub>)]<sup>+</sup> (**2**). The spectroscopic, structural and photophysical signatures of methyl **2** are almost identical to the analogous hydride **1**. It seemed plausible that self-quenching could initiate ethane formation, so samples of **2** were illuminated in the presence of CH<sub>3</sub><sup>+</sup> or H<sup>+</sup> sources. C–C bond formation is indeed observed, but ethane is formed along with methane, propionitrile, and succinonitrile. Mechanistic studies reveal that, despite spectroscopic similarities, the excited state of **2** homolyzes to form methyl radical (CH<sub>3</sub>•). We suspect homolysis outcompetes self-quenching, but rapid recombination lowers the quantum efficiency for ethane formation. Our deeper mechanistic understanding of light-triggered H<sub>2</sub> evolution from organometallic monohydrides is now guiding the development of new catalyst candidates, including ruthenium arene complexes with multiple ligand tuning opportunities.

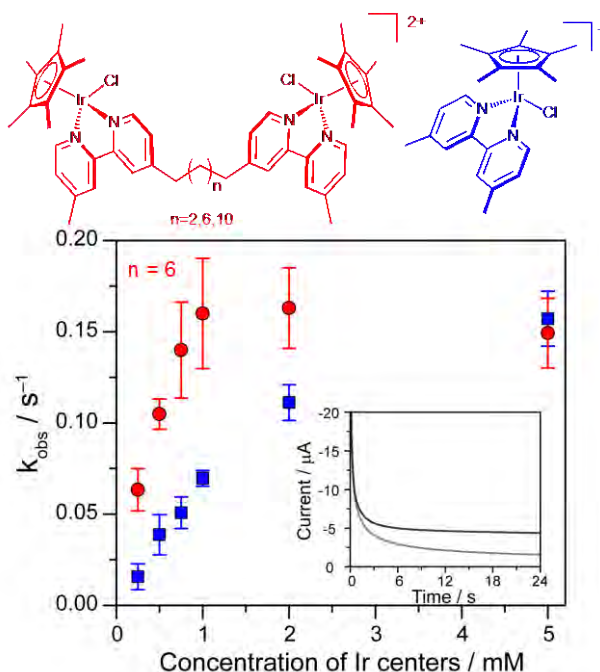


**Figure 2.** Structures and rate constants for photoelectrocatalytic H<sub>2</sub> evolution as a function of concentration for bimetallic (red) and monometallic catalysts (blue). Inset: typical chronoamperometry trace from which  $k_{\text{obs}}$  is extracted, showing current response in the dark (gray) and in the light (black).

### **DOE Sponsored Publications 2014-2017**

1. Chambers, M. B.; Kurtz, D. A.; Pitman, C. L.; Brennaman, M. K.; Miller, A. J. M. “Efficient Photochemical Dihydrogen Generation Initiated by a Bimetallic Self-Quenching Mechanism.” *J. Am. Chem. Soc.* **2016**, *138*, 13509.
2. Wiedner, E. S.; Chambers, M. B.; Pitman, C. L.; Bullock, R. M.; Miller, A. J. M.; Appel, A. M. “Thermodynamic Hydricity of Transition Metal Hydrides.” *Chem. Rev.* **2016**, *116*, 8655.
3. Pitman, C. L.; Miller, A. J. M. “Photochemical Production of Ethane from an Iridium Methyl Complex.” *Submitted*.

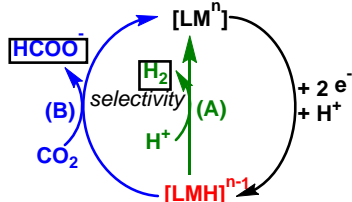
# Design of Efficient Molecular Electrocatalysts for Water and Carbon Dioxide Reduction Using Predictive Models of Thermodynamic Properties

Jenny Y. Yang, Charlene Tsay, Bianca M. Ceballos, Zachary Thammavongsy, Juliet F. Khosrowabadi Kotyk, Samantha Ruelas, Drew Cunningham, Brooke Livesay, Ivy M. Kha  
Department of Chemistry  
University of California, Irvine  
Irvine, California, 92697-2025

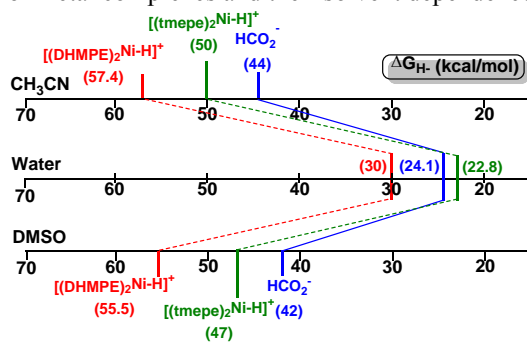
The overall goals of this project are to 1) develop a thermochemical framework to guide the design of efficient molecular catalysts for aqueous  $\text{H}^+$  to  $\text{H}_2$  at various pH conditions or selective  $\text{CO}_2$  reduction to  $\text{HCO}_2^-$  and 2) design new ligand architectures with functional groups in the secondary coordination sphere to orchestrate proton movement in multi-electron, multi-proton redox reactions.

We approached the first goal by experimentally measuring the hydricity of transition metal hydrides, a common intermediate in both  $\text{H}_2$  and  $\text{HCO}_2^-$  formation (**Scheme 1**). We have investigated how hydricity changes in magnitude in different solvents, supporting initial work by C. Cretuz and E. Fujita that the reduction of  $\text{CO}_2$  by transition metal hydrides is more thermodynamically favorable in water (**Scheme 2**). (**Pub #8**) We have also demonstrated how hydricity can be used to determine the functional or optimal pH range of hydrogen evolution, as well as the conditions for the selective electrochemical

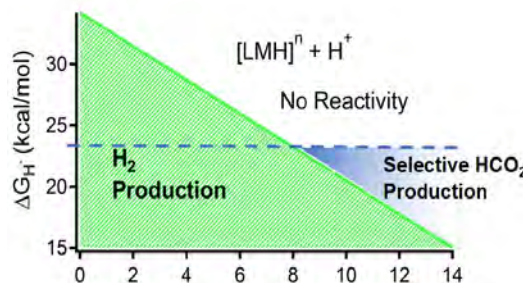
Scheme 1



Scheme 2. Experimentally measured hydricities of metal complexes and their solvent dependence



$\text{H}_2$  and  $\text{HCO}_2^-$  formation in water.

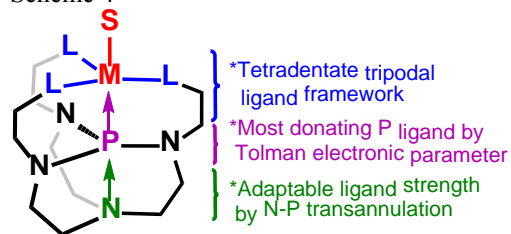


generation of metal hydride intermediates for reduction of alternative substrates without concomitant hydrogen formation. (**Pub #2 & 3**) Additionally, we also have evidence the rate determining step for catalysis is protonation of the metal hydride to form the H-H bond. (**Pub #2**) The results from our initial study were used to develop a new highly stable catalyst for the electrocatalytic aqueous production of  $\text{H}_2$  at pH 1, with no evidence of catalyst degradation after an 18 hour controlled potential electrolysis. (**Pub #4**) Our thermochemical studies guided a step-wise mechanistic study of the catalyst using stoichiometric proton and electron transfer reagents. We are currently leveraging our thermochemical measurements to guide the rational design of new complexes for aqueous reduction of protons at various pH values and the selective reduction of  $\text{CO}_2$  (**Scheme 3**). (**Pub #3**) These studies will also provide insight to how the ligand can be used to tune the hydricity to achieve targeted

values according to our thermochemical guidelines. Our longer-term goal is to apply our understanding of how to tailor hydricity in transition metal complexes so that we can develop new selective catalysts for more challenging reduction reactions.

We have also been developing new ligands to support multi-proton, multi-electron transition metal catalyzed reactions. We have synthesized a new series of ligands that incorporate a super base in the secondary coordination sphere. The ligand is based on Verkade's superbases (**Scheme 3**). (**Pub #5 & 7**) The motivation behind the ligand design is to promote orthogonal proton and electron transfer to CO<sub>2</sub> to generate formate without proceeding through a metal hydride intermediate. This is similar to the mechanism proposed for the enzyme formate dehydrogenase, and is believed to be the source of the high product selectivity exhibited by the enzyme.

Scheme 4



Another new ligand is the tetradentate diamine-dipyridal ligand, or L<sup>DMA</sup>, which incorporates two dimethylamines bases in the secondary coordination sphere. We initially used the diamagnetic Cu(I) complex to investigate the

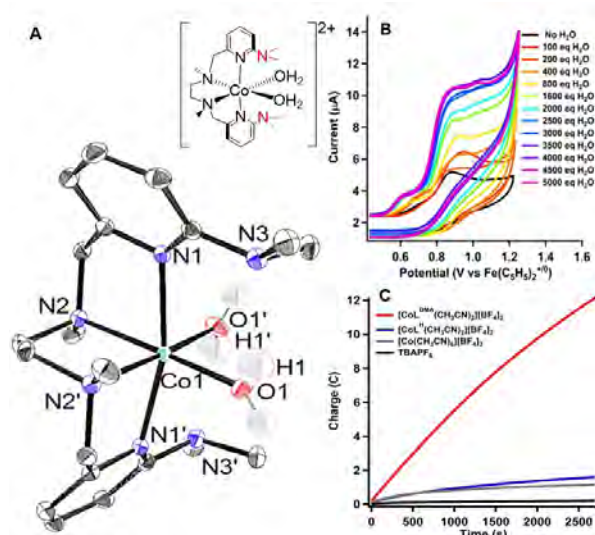


Figure 1. A) ORTEP of [CoL<sup>DMA</sup>(H<sub>2</sub>O)<sub>2</sub>][BF<sub>4</sub>]<sub>2</sub>. Thermal ellipsoids are drawn at the 50% probability level. The counter anions, solvent molecules and hydrogen atoms other than those on the aquo ligands have been removed for clarity. B) Cyclic voltammogram upon addition of water to 1.0 mM solutions to [CoL<sup>DMA</sup>(CH<sub>3</sub>CN)<sub>2</sub>][BF<sub>4</sub>]<sub>2</sub> (**2**) in 0.10 M Bu<sub>4</sub>NBF<sub>4</sub> in CH<sub>3</sub>CN at 100 mV/s. C) Charge passed vs time in the controlled potential electrolysis of a 1 mM solution of [CoL<sup>DMA</sup>(CH<sub>3</sub>CN)<sub>2</sub>][BF<sub>4</sub>]<sub>2</sub> (**2**) in 95:5 CH<sub>3</sub>CN:H<sub>2</sub>O (v/v) at 1.07 V vs Fe(C<sub>5</sub>H<sub>5</sub>)<sub>2</sub><sup>+0</sup> (red trace). Equivalent electrolyses under the same conditions; [CoL<sup>H</sup>(CH<sub>3</sub>CN)<sub>2</sub>][BF<sub>4</sub>]<sub>2</sub> (no pendant bases) (**1**, blue trace), [Co(CH<sub>3</sub>CN)<sub>6</sub>][BF<sub>4</sub>]<sub>2</sub> (gray trace), and TBAPF<sub>6</sub> (Bu<sub>4</sub>NPF<sub>6</sub>, black trace).

diamagnetic Cu(I) complex to investigate the pK<sub>a</sub> of the pendant amines using <sup>1</sup>H NMR spectroscopy. Our study demonstrated that the ligand backbone is more basic than the pendant functionalities. (**Pub #6**) More recently we have been investigating the Co(II) complex (**Figure 1**). Addition of water to a solution of the Co(II) complex in acetonitrile gives rise to a catalytic current (**Figure 1b**). Analysis of the headspace after controlled potential electrolysis found O<sub>2</sub> as the product with > 95% Faradaic efficiency. The activity (charge passed) over time of [CoL<sup>DMA</sup>(CH<sub>3</sub>CN)<sub>2</sub>][BF<sub>4</sub>]<sub>2</sub> (red trace) compared to equivalent electrolyses at 1.07 V vs Fe(C<sub>5</sub>H<sub>5</sub>)<sub>2</sub><sup>+0</sup> with [CoL<sup>H</sup>(CH<sub>3</sub>CN)<sub>2</sub>][BF<sub>4</sub>]<sub>2</sub> (analogue with no pendant bases, blue trace), [Co(CH<sub>3</sub>CN)<sub>6</sub>][BF<sub>4</sub>]<sub>2</sub> (gray trace), and no Co complexes (black trace) in 95:5 CH<sub>3</sub>CN:H<sub>2</sub>O (v/v) is shown in **Figure 1c**. The high activity compared to the analogue with no pendant bases demonstrates the importance of proton management in water oxidation. (**Pub # 1**) We are currently studying mechanistic details related to water oxidation by this complex and modifying the ligand for greater stability under oxidative conditions. We will continue to investigate this ligand set to determine how controlling proton movement can minimize

kinetic barriers in redox catalysis.

### DOE Sponsored Publications 2014-2017

1. Kotyk, J. F. K.; Ziller, J. W.; Yang, J. Y., *in preparation*.  
“Intramolecular Hydrogen-Bonding in a Cobalt Aquo Complex and Electrochemical Water Oxidation Activity”
2. Tsay, C.; Yang, J. Y. *in preparation*.  
“Hydricity as an Activity Descriptor for Homogeneous Hydrogen Evolution Catalysis”
3. Ceballos, B. M.; Tsay, C.; Yang, J. Y. *submitted, in review*.  
“CO<sub>2</sub> Reduction or HCO<sub>2</sub><sup>-</sup> Oxidation? Solvent-Dependent Thermochemistry of a Nickel Hydride Complex”
4. Tsay, C.; Yang, J. Y.\*, *J. Am. Chem. Soc.*, **2016**, *138*(43), 14174-14177.  
“Electrocatalytic Hydrogen Evolution Under Acidic Aqueous Conditions and Mechanistic Studies of a Highly Stable Molecular Catalyst”
  - Cover article
  - Highlighted in [Spotlights on Recent JACS Publications](#)
5. Thammavongsy, Z.; Kha, I. M.; Ziller, J. W.; Yang, J. Y.\*, *Dalton Trans.*, **2016**, *45*, 9853-9859. (invited to “New Talent: Americas” special issue)  
“Electronic and Steric Tolman Parameters for Proazaphosphatranes, the Superbase Core of the Tri(pyridylmethyl)azaphosphatrane (TPAP) Ligand”
6. Kotyk, J. F. K.; Ziller, J. W.; Yang, J. Y.\*, *J. Coord. Chem.*, **2016**, *69*(11-13), 1990-2002. (invited to "Emerging Leaders in Coordination Chemistry Issue")  
"Copper Tetradentate N<sub>2</sub>Py<sub>2</sub> Complexes with Pendant Bases in the Secondary Coordination Sphere: Improved Ligand Synthesis and Protonation Studies"
7. Thammavongsy, Z.; Kotyk, J. F. K.; Tsay, C.; Yang, J. Y.\*, *Inorg. Chem.*, **2015**, *54*(23), 11505-11510.  
"Flexibility is Key: Synthesis of a Tripyridylamine (TPA) Congener with a Phosphorus Apical Donor and Coordination to Cobalt(II)"
8. Tsay, C.; Livesay, B.; Ruelas, S.; Yang, J. Y.\*, *J. Am. Chem. Soc.* **2015**, *137*(44), 14114-14121.  
"Solvation Effects on Transition Metal Hydricity"
  - Selected for JACS virtual issue “The Way Forward in Molecular Electrocatalysis”

*Session VII*

*Small Molecule Activation II*



## C-H Bond Formation with CO<sub>2</sub>: Insights for Designing Selective (Electro)catalysts

Atefeh Taheri, Natalia D. Loewen, Louise A. Berben  
Department of Chemistry  
University of California Davis  
Davis, CA 95616

The formation and subsequent reaction of metal-hydride species, in proton-containing reaction solutions, are key steps in reaction pathways for electrocatalytic generation of reduced CO<sub>2</sub> products, such as formate and methanol. However, these proton-containing reaction solutions and metal hydride catalyst intermediates can also readily promote H<sub>2</sub> evolution or CO formation unless reactions conditions and catalysts are properly designed (Scheme 1). Therefore, to selectively produce C-H bonds from CO<sub>2</sub> in water, it is important to understand which kinetic and thermodynamic parameters are important, and how we should design (electro)catalysts to promote desired reaction outcomes.

[Fe<sub>4</sub>N(CO)<sub>12</sub>]<sup>-</sup> (**1**<sup>-</sup>) selectively produces formate from CO<sub>2</sub> at -1.2 V vs. SCE in aqueous buffered solutions, at 4.0 mAcm<sup>-2</sup> and is stable for over 24 h (Figure 1). Insights into the kinetic and thermochemical contributors to the selectivity for formate production observed with **1** are being obtained. Our current working hypothesis is that the reduced hydride, [H-Fe<sub>4</sub>N(CO)<sub>12</sub>]<sup>-</sup> (**H-1**<sup>-</sup>) is generated by reduction and protonation of **1**, and transfers H<sup>-</sup> to CO<sub>2</sub> to afford formate (Figure 1). Evidence derived from electrochemical, X-ray crystallographic, and reactivity studies supports involvement of (**H-1**<sup>-</sup>).

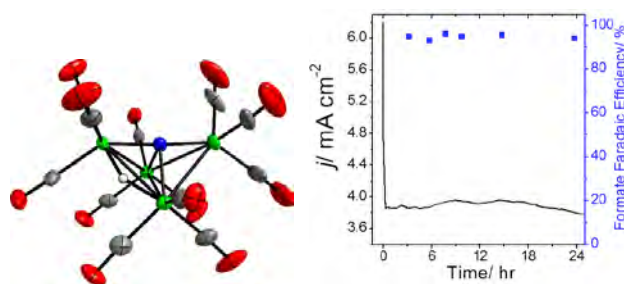
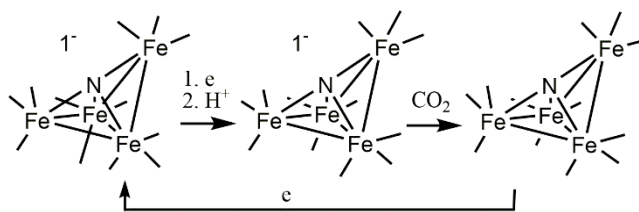


**Figure 1.** (left) Structure of [H-Fe<sub>4</sub>N(CO)<sub>12</sub>]<sup>-</sup>. (right) pH 7, -1.2 V vs. SCE, GC electrode.

**Probing the Nature of the Interaction Between (H-1)<sup>-</sup> and CO<sub>2</sub>.** Using electrochemical techniques, we measured the rates of each elementary step in the catalytic cycle for formate formation from CO<sub>2</sub>, including the rates of electron transfer, and proton transfer, and the subsequent transfer of hydride to CO<sub>2</sub>. We established that hydride transfer to CO<sub>2</sub> is rate determining, and we then measured this rate at various temperatures in both water and water/acetonitrile (5:95). Using Eyring analysis entropy and enthalpy of activation for hydride transfer were determined. The large negative value for entropy indicates an ordered transition state, and future experiments will use variable temperature IR spectroelectrochemistry to gain more information about the structure of this ordered transition state.



**Scheme 1.** Mechanism for CO<sub>2</sub> reduction to formate.

**Synthesis of Next Generation Catalysts.** Development of modified iron clusters based on the structure of **1**<sup>-</sup> will yield information on reaction mechanism and improve catalytic performance

in specific areas. Carbonyl ligands can be replaced by phosphino donors that are substituted with a wide array of functional groups, and this strategy will allow us to address different questions. *Installation of a Proton Relay.* This work, using alcohol-substituted phosphine resulted in formation of H<sub>2</sub> and suppression of C-H bond formation. This is further

evidence for the hydride intermediate. *Installation of Hydrogen Bonding Functional Groups.* In another approach, we are incorporating functional groups that could interact directly with CO<sub>2</sub> to facilitate a bi-functional approach to reduction. For example pyridine is known to interact with CO<sub>2</sub>, and thiofuran has potential for similar reactivity: [Ph<sub>2</sub>pyP-1]<sup>-</sup>, [Phpy<sub>2</sub>P-1]<sup>-</sup>, and [(C<sub>4</sub>H<sub>4</sub>S)<sub>3</sub>P-1]<sup>-</sup> have been synthesized (Figure 2), and their electrochemistry and reactivity will be investigated.

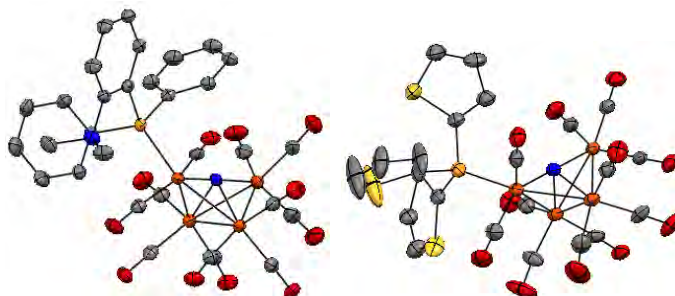


**Figure 3.** Structures of (left) [Ph<sub>2</sub>pyP-1]<sup>-</sup>, and (right) [(C<sub>4</sub>H<sub>4</sub>S)<sub>3</sub>P-1]<sup>-</sup>. Green, grey, blue, orange, and yellow colors are Fe, C, N, P, and S atoms.

*Enhancement of Aqueous Solubility and Hydrogen Bond Donor Ability.* The PTA ligand and methylated analog, MePTA<sup>+</sup> have been added to 1<sup>1-</sup> to afford [PTA<sub>2</sub>-1]<sup>-</sup> and [(MePTA)<sub>2</sub>-1]<sup>+</sup> (Figure 2). These positively charged ligands suitable for hydrogen bonding were designed to favor transport of neutral CO<sub>2</sub> while disfavoring transport of positively charged H<sup>+</sup>. CV and CPE experiments show two reversible one-electron reductions of [Fe<sub>4</sub>N(CO)<sub>10</sub>(MePTA)<sub>2</sub>]<sup>+</sup> at -1.2 and -1.4 V vs. V vs. SCE, and that formate is produced. We have not yet investigated possible changes in CO<sub>2</sub> binding constant or potential enhanced rates of CO<sub>2</sub> reduction that could result from this modification of [Fe<sub>4</sub>N(CO)<sub>12</sub>]<sup>-</sup> but synthesis of the catalyst and observation of CO<sub>2</sub> conversion to formate is significant initial progress. Future work will address these experiments, probe positively charged pendants that are oriented more directly at the site of the reduced hydride, explore more highly charged pendants such as Me<sub>2</sub>PTA<sup>2+</sup>, related pendants with larger bites angles for positioning of charged groups, and explore addition of MePTA<sup>+</sup> and other pendants to carbide-containing [Fe<sub>4</sub>C(CO)<sub>12</sub>]<sup>2-</sup>.

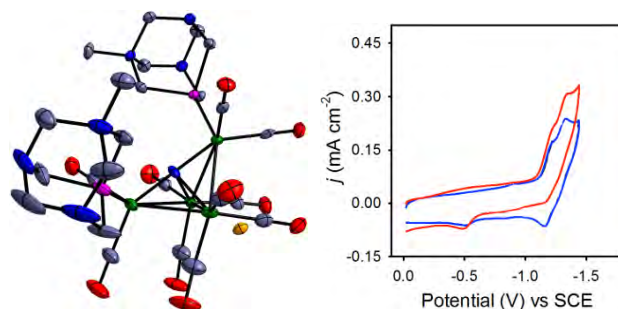


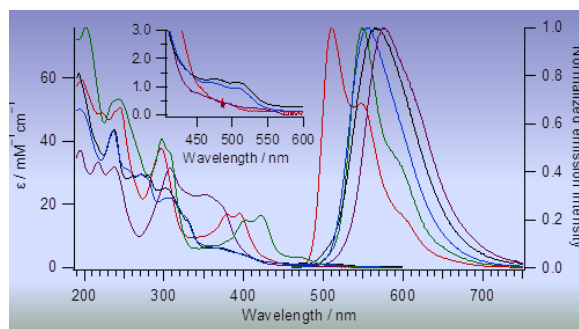
**Figure 3.** (left) Structure of [Fe<sub>4</sub>N(CO)<sub>10</sub>(N-MePTA)<sub>2</sub>]<sup>+</sup>I<sup>-</sup>. Green, grey, blue, red, pink, and orange colors are Fe, C, N, O, P, and I atoms. (right) CV's of [Fe<sub>4</sub>N(CO)<sub>10</sub>(N-MePTA)<sub>2</sub>]<sup>+</sup>I<sup>-</sup> in 0.1 M Bu<sub>4</sub>NPF<sub>6</sub> MeCN (blue), with CO<sub>2</sub> (red). GC electrode, 100 mV/s.

## Artificial Photosynthesis for Fuel Generation in Solution and at Interfaces

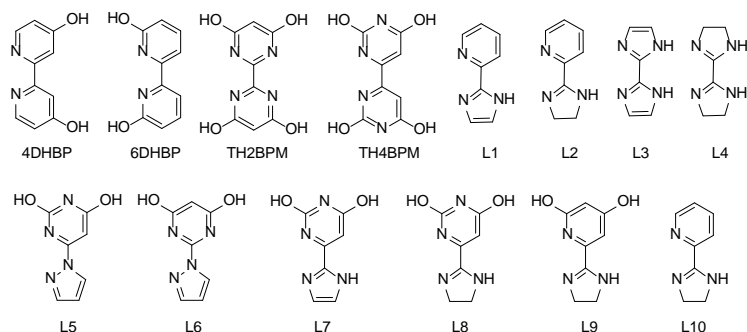
Etsuko Fujita, Javier. J. Concepcion, Mehmed Z. Ertem, David C. Grills, Gerald F. Manbeck, James T. Muckerman and Dmitry E. Polyansky  
Chemistry Division  
Brookhaven National Laboratory  
Upton, NY 11973-5000

We are carrying out fundamental research involving coordinated experimental and theoretical studies of factors that must be considered in designing artificial photosynthetic systems for the generation of fuels and oxygen from water. The work is aimed at unraveling kinetic and mechanistic details of various processes including: (1) photo-initiated proton-coupled electron-transfer reactions; (2) reversible interconversion of CO<sub>2</sub> and formic acid using Cp\*Ir complexes bearing proton responsive ligands; (3) electrochemical CO<sub>2</sub> reduction in organic solvents, or ionic liquids using Re, Mn, and Ru complexes; (4) photochemical CO<sub>2</sub> and/or proton reduction using Ir and Co complexes; (5) nano-structured carbide/nitride composites and oxynitrides with non-precious metals for HER and ORR/OER catalysts, respectively; (6) water oxidation using ruthenium molecular catalysts with multifunctional ligands; and (7) water oxidation at semiconductor interfaces. At this meeting, we will report on several selected topics.

*Hydricity, Electrochemistry, and Excited-State Chemistry of Ir Complexes for CO<sub>2</sub> Reduction:* Transition-metal hydrides play crucial roles in the hydrogenation/dehydrogenation of organic substrates including CO<sub>2</sub>, formate and methanol, H<sub>2</sub> production/oxidation, etc. The hydricity, i.e., hydride-transfer ability, is an important thermodynamic property together with the acidity, i.e., proton-transfer ability for the design of catalysts, especially for fuel generation reactions. In an efficient photocatalytic system with [Ir(tpy)(ppy)Cl]<sup>+</sup> (tpy = 2,2':6',2''-terpyridine, ppy = 2-phenylpyridine), for CO<sub>2</sub> reduction to CO under visible light, the hydride species was proposed as an important intermediate. We have isolated two isomers of the Ir-H, where the hydride is *trans* to either N of ppy or to C of ppy, and have studied their distinct reactivity in the ground and excited states. While *C-trans*-Ir-H is a strong hydride donor that can convert CO<sub>2</sub> to formate, we found that neither hydride is a key intermediate, but [Ir(tpy)(ppy)]<sup>0</sup> bearing a vacant site is an intermediate in the photocatalytic reaction. In order to obtain stronger hydride donors to go beyond formate or CO for the reduction of CO<sub>2</sub> via hydride transfer reactions, we have explored hydricities, photochemistry and CO<sub>2</sub> reduction with several Ir complexes with more electron-donating ligands.



*CO<sub>2</sub> Hydrogenation and Formic Acid Dehydrogenation:* Our investigations of the interconversion of CO<sub>2</sub>/H<sub>2</sub> and formic acid (FA) using Cp\*Ir(III) complexes with a series of proton responsive ligands (see figure below) in water has led to both the reaction rates and catalyst stabilities having been significantly improved. Complemented by DFT calculations, kinetic isotope effect studies of the rates of formate production reveal that the rate-determining



step for CO<sub>2</sub> hydrogenation is H<sub>2</sub> heterolysis involving a proton relay to the deprotonated pendant –O<sup>−</sup> base via a water bridge. The dehydrogenation of formic acid in acidic solution is likely to occur by a mechanism with a pH-dependent rate-determining step (e.g., CO<sub>2</sub> elimination or Ir–H protonation). We

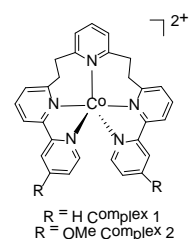
achieved complete dehydrogenation of FA (20 mol) with 10 μM Cp\*Ir(L10)(OH<sub>2</sub>)<sup>2+</sup> at 50 °C to produce 1.0 m<sup>3</sup> CO<sub>2</sub>/H<sub>2</sub> mixture without any additives or pH adjustment (avg. TOF 7,000 h<sup>−1</sup>, TON > 2,000,000). This result opens future opportunities for on-board or on-site H<sub>2</sub> generation from 10 M FA (pH ~1.6) or neat FA.

*Earth-Abundant HER, OER and ORR Catalysts:* The electrolysis of water presents an alternative for hydrogen generation from natural gas when the electricity for water electrolysis is produced by renewable energy, especially with the use of non-noble metal catalysts. We investigated nano-structured Mo or W carbide/nitride composites for the HER, and CoMn oxynitrides as bifunctional catalysts for the ORR and OER. All these durable and efficient catalysts can be prepared by simple environmentally benign methods.

*Reduction of CO<sub>2</sub> using Metal Complexes with Proton-Responsive Ligands:* [Re(CO)<sub>3</sub>LCI] and [Ru(tpy)L(NCCH<sub>3</sub>)]<sup>2+</sup> (L = 4DHBP or 6DHBP, see above figure) surprisingly facilitate reductive deprotonation of L via 1 equiv. of H<sub>2</sub> production. Contrary to our expectation of the effect of bases in the second-coordination sphere, complexes with *ortho*-OH groups hinder CO<sub>2</sub> reduction by forming, e.g., a Ru(CO)(tpy) complex with 6,6'-(O<sub>2</sub>CO)<sub>2</sub>-2,2'-bipyridine. While OH groups near a metal center are known to accelerate CO<sub>2</sub> reduction with FeTPP-type complexes, the formation of a stable keto-type ligand by a reductive deprotonation should be avoided because both the metal center and the ligand react with CO<sub>2</sub> leading to deactivation of the catalyst.

*Reduction of CO<sub>2</sub> using Trigonal Bipyramidal Polypyridyl Co(II) Complexes:*

While a considerable number of cobalt molecular complexes have been studied for their binding of CO<sub>2</sub>, electrochemical and photochemical CO<sub>2</sub> reduction, to our knowledge trigonal bipyramidal (TBP) polypyridyl cobalt (II) complexes have not been used as catalysts for CO<sub>2</sub> reduction. X-ray structures of the cobalt complexes with pentadentate ligands (see figure) showed that all five nitrogen atoms are coordinated to the Co<sup>2+</sup> ion and the geometry is TBP without any coordinated solvent molecules. We investigated spin states of the Co(II) center, as well as experimental and theoretical studies of the binding of CO<sub>2</sub>, CO or proton to the reduced Co complexes. For photocatalytic CO<sub>2</sub> reduction, we employed the conditions reported by Schmehl,<sup>1</sup> which use [Ru(bpy)<sub>3</sub>]<sup>2+</sup> as a photosensitizer, tri-*p*-tolylamine as a commercially available efficient reductive quencher and triethylamine as a sacrificial electron donor. Because cobalt(II) complexes with a TBP geometry are very rare, we believe detailed mechanistic studies of their reduction of CO<sub>2</sub> to CO are warranted.



We especially thank Drs. Yuichiro Himeda (AIST), Takuji Hirose (Saitama U.) and Koichi

Kodama (Saitama U.) for their contributions to our collaborative work.

### DOE Sponsored Publications of the AP Group 2014-2017

1. Interconversion of CO<sub>2</sub>/H<sub>2</sub> and Formic Acid under Mild Conditions in Water: Ligand Design for Effective catalysis, In *Advances in Inorganic Chemistry*, Vol. 66, CO<sub>2</sub> Chemistry, Wang, W.-H.; Himeda, Y.; Muckerman, J. T.; Fujita, E. pp. 189-222, Eds. Van Eldik, R.; Aresta, M. Burlington, Elsevier, 2014.
2. Water Oxidation by Ruthenium Catalysts Having Non-innocent Ligands, a book chapter in *Molecular Water Oxidation Catalysis*, Wada, T.; Tanaka, K.; Muckerman, J. T.; Fujita, E. Ed. Antoni Llobet, pp 77-111, Wiley & Sons, Ltd. 2014.
3. Reactivity of a *fac*-ReCl( $\alpha$ -diimine)(CO)<sub>3</sub> Complex with an NAD<sup>+</sup> Model Ligand toward CO<sub>2</sub> Reduction, Matsubara, Y.; Hightower, S. H.; Chen, J.; Grills, D. C.; Polyansky, D. E.; Muckerman, J. T.; Tanaka, K.; Fujita, E. *Chem. Commun.* **2014**, 50, 728-730.
4. Efficient H<sub>2</sub> Generation from Formic Acid using Azole Complexes in Water, Manaka, Y.; Wang, W.-H.; Suna, Y.; Kambayashi, H.; Muckerman, J. T.; Fujita, E.; Himeda, Y. *Catal. Sci. Technol.* **2014**, 4, 34-37.
5. Efficient Water Oxidation with Organometallic Iridium Complexes as Precatalysts at Neutral pH, Lewandowska-Andralojc, A.; Polyansky, D. E.; Wang, C.-H.; Wang, W.-H.; Himeda, Y.; Fujita, E. *Phys. Chem. Chem. Phys.* **2014**, 16, 11976-11987.
6. Kinetic and Mechanistic Studies of Carbon-to-Metal Hydrogen Atom Transfer Involving Os-Centered Radicals Evidence for Tunneling, Lewandowska-Andralojc, A.; Grills, D.C.; Zhang, J.; Bullock, R. M.; Miyazawa, A.; Kawanishi, Y.; Fujita, E. *J. Am. Chem. Soc.* **2014**, 136, 3572-3578.
7. Formic Acid Dehydrogenation with Bio-Inspired Iridium Complexes: A Kinetic Isotope Effect Study and Mechanistic Insight, Wang, W.-H.; Xu, S.; Manaka, Y.; Suna, Y.; Kambayashi, H.; Muckerman, J. T.; Fujita, E.; Himeda, Y. *ChemSusChem* **2014**, 7, 1976-1983.
8. New Water Oxidation Chemistry of a Seven-Coordinate Ruthenium Complex with a Tetradentate Polypyridine-type Ligand, Muckerman, J. T.; Kowalczyk, M.; Badiei, Y. M.; Polyansky, D. E.; Yang, Y.; Concepcion, J. J.; Zong, R.; Thummel, R. P.; Fujita, E. *Inorg. Chem.* **2014**, 53, 6904-6913.
9. Tungsten Carbide-Nitride on Graphene Nanoplatelets as a Durable Hydrogen Evolution Electrocatalyst, Chen, W.-F.; Schneider, J. M.; Sasaki, S.; Wang, C.-H.; Schneider, S.; Iyer, S.; Iyer, S.; Chu, Y.; Muckerman, J. T.; Fujita, E. *ChemSusChem* **2014**, 7, 2414-8.
10. Theoretical Modeling of Low Energy Electronic Transitions in Reduced Cobaloximes, Bhattacharjee, A.; Chavaroy-Kerlidou, M.; Dempsey, J. L.; Gray, H. B.; Fujita, E.; Muckerman, J. T.; Fontecave, M.; Artero, V.; Arantes, G. M.; Field, M. T. *ChemPhysChem*, **2014**, 15, 2951-2958.
11. Positional Effects of Hydroxy Groups on Catalytic Activity of Proton-Responsive Half-Sandwich Cp\*Iridium(III) Complexes, Suna, Y.; Ertem, M. Z.; Wang, W. -H.; Kambayashi,

- H.; Manaka, Y.; Muckerman, J. T.; Fujita, E.; Himeda, Y. *Organometallics* **2014**, *33*, 6519-6530.
12. Electrocatalysts for Carbon Dioxide Reduction, Polyansky, D. E. In *Encyclopedia of Applied Electrochemistry*; Kreysa G., Ota K., Savinell R., Eds.; Springer Science: New York, **2014**; Vol. 1, pp 431-436.
  13. Application of Pulse Radiolysis to Mechanistic Investigations of Water Oxidation Catalysis, Polyansky, D. E.; Hurst, J. K.; Lymar, S. V. *Eur. J. Inorg. Chem.* **2014**, 619-634.
  14. Computational Investigation of Structural and Electronic Properties of Aqueous Interfaces of GaN, ZnO, and GaN/ZnO Alloy, Kharche, N.; Hybertsen, M. S.; Muckerman, J. T. *Phys. Chem. Chem. Phys.* **2014**, *16*, 12057-12066.
  15. Electrocatalytic CO<sub>2</sub> Reduction with a Homogeneous Catalyst in Ionic Liquid: High Catalytic Activity at Low Overpotentia, Grills, D. C.; Matsubara, Y.; Kuwahara, Y.; Golisz, S. R.; Kurtz, D. A.; Mello, B. A. *J. Phys. Chem. Lett.* **2014**, *5*, 2033-2038.
  16. Mechanism of the Formation of a Mn-Based CO<sub>2</sub> Reduction Catalyst Revealed by Pulse Radiolysis with Time-Resolved Infrared Detection, Grills, D. C.; Farrington, J. A.; Layne, B. H.; Lymar, S. V.; Mello, B. A.; Preses, J. M.; Wishart, J. F. *J. Am. Chem. Soc.* **2014**, *136*, 5563-5566.
  17. The Reaction of Cobaloximes with Hydrogen: Products and Thermodynamics, Estes, D. P.; Grills, D. C.; Norton, J. R. *J. Am. Chem. Soc.* **2014**, *136*, 17362-17365.
  18. First-Principles Approach to Calculating Energy Level Alignment at Aqueous Semiconductor Interfaces, Kharche, N.; Muckerman, J. T.; Hybertsen, M. S. *Phys. Rev. Lett.* **2014**, *113*, 176802.
  19. Mechanism of Water Oxidation by [Ru(bda)(L)<sub>2</sub>]: the Return of the “Blue Dimer”, Concepcion, J. J.; Zhong, D. K.; Szalda, D. J.; Muckerman, J.T.; Fujita, E. *Chem. Commun.* **2015**, *51*, 4105-4108.
  20. Push or Pull? Proton Responsive Ligand Effects in Rhenium Tricarbonyl CO<sub>2</sub> Reduction Catalysts, Manbeck, G. F.; Muckerman, J. T.; Szalda, D. J.; Himeda, Y.; Fujita, E. *J. Phys. Chem. B*, **2015**, *119*, 7457-7466.
  21. A Review of Iron and Cobalt Porphyrins, Phthalocyanines, and Related Complexes for Electrochemical and Photochemical Reduction of Carbon Dioxide, Manbeck, G. F.; Fujita, E. *J. Porphyrins Phthalocyanines*, **2015**, *19*, 45-64.
  22. Hierarchical Heterogeneity at the CeO<sub>x</sub>-TiO<sub>2</sub> Interface: Electronic and Geometric Structural Influence on the Photocatalytic Activity of Oxide on Oxide Nanostructures, Luo, S; Nguyen-Phan, T.-D.; Johnston-Peck, A.; Barrio, L.; Sallis, S.; Arena, D.; Kundu, S.; Xu, W.; Piper, L.; Stach, E.; Polyansky, D. E. ; Fujita, E.; Rodriguez, J. A.; Senanayake, S. *J. Phys. Chem. C*, **2015**, *119*, 2669-2679
  23. Mechanistic Studies of Hydrogen Evolution in Aqueous Solution Catalyzed by a Terpyridine-Amine Cobalt Complex, Lewandowska-Andralojc, A; Baine, T.; Zhao, X.; Muckerman, J. T.; Fujita, E.; Polyansky, D.E. *Inorg. Chem.* **2015**, *54*, 4310-4021.

24. Photo-induced Water Oxidation at the Aqueous GaN (10 $\bar{1}$ 0) Interface: Deprotonation Kinetics of the First Proton-Coupled Electron-Transfer Step, Ertem, M.Z.; Kharche, N.; Batista, V. S.; Hybertsen, M. S.; Tully, J. C.; Muckerman, J. T. *ACS Catal.* **2015**, *5*, 2317-2323.
25. CO<sub>2</sub> Hydrogenation Catalyzed by Iridium Complexes with a Proton-responsive Ligand, Onishi, N.; Xu, S.; Manaka, Y.; Suna, Y.; Wang, W. -H.; Muckerman, J. T.; Fujita, E.; Himeda, Y., *Inorg. Chem.* **2015**, *54*, 5114-5123.
26. Preface for Small-Molecule Activation: Carbon-Containing Fuels, Fujita, E.; Goldman A. S. *Inorg. Chem.* **2015**, *54*, 5040-5042.
27. Highly Robust Hydrogen Generation by New Bioinspired Ir Complexes for Dehydrogenation of Formic Acid in Water, Wang, W.-H.; Ertem, M. Z.; Xu, S.; Onishi, N.; Manaka, Y.; Suna, Y.; Kambayashi, H.; Muckerman, J. T.; Fujita, E.; Himeda, Y. *ACS Catal.* **2015**, *5*, 5496-5504.
28. CO<sub>2</sub> Hydrogenation to Formate and Methanol as an Alternative to Photochemical CO<sub>2</sub> Reduction. Wang, W.-H.; Himeda, Y.; Muckerman, J. T.; Manbeck, G. F.; Fujita, E. *Chem. Rev.* **2015**, *115*, 12936-12973.
29. Striving towards Noble-Metal-Free Photo-Catalytic Splitting of Water: The Hydrogenated-Graphene-TiO<sub>2</sub> Prototype, Nguyen-Phan, T.-D.; Luo, S.; Liu, Z.; Pham, V. H.; Gamalski, A. D.; Xu, W.; Stach, E. A.; Dickersons, J. H.; Polyansky, D. E.; Senanayake, S. D.; Fujita, E.; Rodriguez, J. A. *Chem. Mater.*, **2015**, *27*, 6282-6296.
30. Biomass-Derived High-Performance Tungsten-Based Electrocatalysts on Graphene for Hydrogen Evolution, Meng, F.; Hu, E.; Zhang, L.; Sasaki, K.; Muckerman, J. T.; Fujita, E. *J. Mater. Chem. A*, **2015**, *3*, 18572-18577.
31. Striking Differences in Properties of Geometric Isomers of [Ir(tpy)(ppy)H]<sup>+</sup>: Experimental and Computational Studies of their Hydricities, Interaction with CO<sub>2</sub>, and Photochemistry, Garg, K.; Matsubara, Y.; Ertem, M. Z.; Lewandowska-Andralojc, A.; Sato, S.; Szalda, D. J.; Muckerman, J. T.; Fujita, E. *Angew. Chem. Int. Ed.* **2015**, *54*, 14128-14132.
32. Intramolecular proton transfer boosts water oxidation catalyzed by a Ru complex, Matheu, R.; Ertem, M. Z.; Benet-Buchholz, J.; Coronado, E.; Batista, V. S.; Sala, X.; Llobet, A. *J. Am. Chem. Soc.* **2015**, *137*, 10786-11549.
33. Thermodynamic Aspects of Electrocatalytic CO<sub>2</sub> Reduction in Acetonitrile and with an Ionic Liquid as Solvent or Electrolyte, Matsubara, Y.; Grills, D. C.; Kuwahara, Y. *ACS Catal.* **2015**, *5*, 6440-6452.
34. Mechanism of Manganese-Catalyzed Oxygen Evolution from Experimental and Theoretical Analyses of <sup>18</sup>O Kinetic Isotope Effects, Khan, S.; Yang, K.; Ertem, M. Z.; Batista, V. S.; Brudvig, G. W. *ACS Catal.* **2015**, *5*, 7104-7113.
35. Highly Efficient Cp\*Ir Catalysts with Imidazoline Ligands for CO<sub>2</sub> Hydrogenation, Xu, S.; Onishi, N.; Tsurusaki, A.; Manaka, Y.; Wang, W.-H.; Muckerman, J. T.; Fujita, E.; Himeda, Y. *Eur. J. Inorg. Chem.*, **2015**, 5591-5594.

36. The Effect of Chloride Anions on the Formation and Reactivity of Nanoporous Silver Catalysts for CO<sub>2</sub> Electroreduction, Hsieh, Y.-C.; Senanayake, S. D.; Zhang, Y.; Xu W.; Polyansky, D. E. *ACS Catal.* **2015**, *5*, 5349-5356.
37. Ultrafast Transient Absorption Spectrum of the Room Temperature Ionic Liquid 1-Hexyl-3-Methylimidazolium bromide: Confounding Effects of Photo-Degradation, Musat, R. M.; Crowell, R. A.; Polyansky, D. E.; Thomas, M. F.; Wishart, J. F.; Katsumura, Y.; Takahashi, K. *Radiat. Phys. Chem.* **2015**, *117*, 78-82.
38. Artificial Photosynthesis, Kunwar, N.; Sharma, S.; Benjamin, S.; Polyansky, D. E. In *Solar Energy Conversion and Storage. Photochemical Modes*, Suresh C. Ameta; Ameta, R., Eds. CRC Press: Boca Raton, **2015**; pp187-218. Book chapter.
39. Interconversion of Formic Acid and Carbon Dioxide by Proton-Responsive, Half Sandwich Cp\*Ir(III) Complexes: A Computational Mechanistic Investigation, Ertem, M. Z.; Himeda, Y.; Fujita, E.; Muckerman, J. T. *ACS Catal.* **2016**, *6*, 600-609.
40. Direction to Practical Production of Hydrogen by Formic Acid Dehydrogenation with Cp\*Ir Complexes Bearing Imidazoline Ligands, Onishi, N.; Ertem, M. Z.; Xu, S.; Tsurusaki, A.; Manaka, Y.; Muckerman, J. T.; Fujita, E.; Himeda, Y. *Catal. Sci. Tech.* **2016**, *6*, 988-992.
41. Unravelling the Hydrogenation of TiO<sub>2</sub> and Graphene Oxide/TiO<sub>2</sub> Composites in Real Time by *In Situ* Synchrotron X-ray Powder Diffraction and Pair Distribution Function Analysis, Nguyen-Phan, T.-D.; Liu, Z.; Luo, S.; Gamalski, A. D.; Vovchok, D.; Xu, W.; Stach, E. A.; Polyansky, D. E.; Fujita, E.; Rodriguez, J. A.; Senanayake, S. D. *J. Phys. Chem. C* **2016**, *120*, 3472-3482.
42. Visible Light-Driven H<sub>2</sub> Production over Highly Dispersed Ruthenium on Rutile TiO<sub>2</sub> Nanorods, Nguyen-Phan, T.-D.; Luo, S.; Vovchok, D.; Llorca, J.; Graciani, J.; Sanz, J. F.; Sallis, S.; Xu, W.; Bai, J.; Piper, L. F. J.; Polyansky, D. E.; Fujita, E.; Senanayake, S. D.; Stacchiola, D. J.; Rodriguez, J. A. *ACS Catal.* **2016**, *6*, 407-417.
43. Electrocatalytic Reduction of Carbon Dioxide with a Well-Defined PN<sup>3</sup>-Ru Pincer Complex, Min, S.; Rasul, S.; Li, H.; Grills, D. C.; Takanabe, K.; Li, L.-J.; Huang, K.-W. *ChemPlusChem* **2016**, *81*, 166-171.
44. Experimental Insight into the Thermodynamics of the Dissolution of Electrolytes in Room-Temperature Ionic Liquids: From the Mass Action Law to the Absolute Standard Chemical Potential of a Proton, Matsubara, Y.; Grills, D. C.; Koide, Y. *ACS Omega* **2016**, *1*, 1393-1411.
45. Noninnocent Proton-Responsive Ligand Facilitates Reductive Deprotonation and Hinders CO<sub>2</sub> Reduction Catalysis in [Ru(tpy)(6DHBP)(NCCH<sub>3</sub>)]<sup>2+</sup> (6DHBP = 6,6'-(OH)<sub>2</sub>bpy), Duan, L.; Manbeck, G. F.; Kowalczyk, M.; Szalda, D. J.; Muckerman, J. T.; Himeda, Y.; Fujita, E. *Inorg. Chem.* **2016**, *55*, 4582-4594.
46. Water Oxidation by Ruthenium Complexes Incorporating Multifunctional Bipyridyl Diphosphonate Ligands, Xie, Y.; Shaffer, D. W.; Lewandowska-Andralojc, A.; Szalda, D. J.; Concepcion, J. J., *Angew. Chem. Int. Ed.* **2016**, *55*, 8067-8071

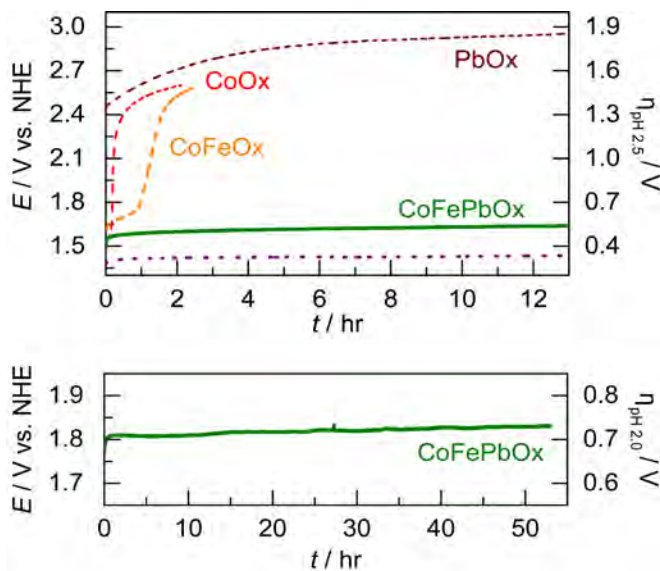
47. Proton-Coupled Electron Transfer in a Strongly Coupled Photosystem II-Inspired Chromophore–Imidazole–Phenol Complex: Stepwise Oxidation and Concerted Reduction, Manbeck, G. F.; Fujita, E.; Concepcion, J. J. *J. Am. Chem. Soc.* **2016**, *138*, 11536-11549.
48. Manipulating the Rate-Limiting Step in Water Oxidation Catalysis by Ruthenium Bipyridine-Dicarboxylate Complexes, Shaffer, D. W.; Xie, Y.; Szalda, D. J.; Concepcion, J. J. *Inorg. Chem.* **2016**, *55*, 12024-12035.
49. Three-Dimensional Ruthenium-Doped TiO<sub>2</sub> Sea Urchins for Enhanced Visible-Light-Responsive H<sub>2</sub> Production, Nguyen-Phan, T. D.; Luo, S.; Vovchok, D.; Llorca, J.; Sallis, S.; Kattel, S.; Xu, W. Q.; Piper, L. F. J.; Polyansky, D. E.; Senanayake, S. D.; Stacchiola, D. J.; Rodriguez, J. A. *Phys. Chem. Chem. Phys.* **2016**, *18*, 15972-15979.
50. Calculating Free Energy Changes in Continuum Solvation Models, Ho, J.; Ertem, M. Z. *J. Phys. Chem. B* **2016**, *7*, 1319-1329.
51. Mechanism of Photocatalytic Reduction of CO<sub>2</sub> by Re(bpy)(CO)<sub>3</sub>Cl from Differences in Carbon Isotope Discrimination, Schneider, T. W.; Ertem, M. Z.; Muckerman, J. T.; Angeles-Boza, A. M. *ACS Catal.* **2016**, *6*, 5473-5481.
52. Enhancing Electrocatalytic Performance of Bifunctional Cobalt Manganese Oxynitride Nanocatalysts on Graphene, Li, Y.; Kuttiyiel, K. A.; Lijun Wu, L.; Zhu, Y.; Fujita, E.; Adzic, R. R.; Sasaki, K. *ChemSusChem*. **2017**, *10*, 68-73.
53. Turning on the Protonation-First Pathway for Electrocatalytic CO<sub>2</sub> Reduction by Manganese Bipyridyl Tricarbonyl Complexes, Ngo, K. T.; McKinnon, M.; Mahanti, B.; Narayanan, R. P.; Grills, D. C.; Ertem, M. Z.; Rochford, J. *J. Am. Chem. Soc.* **2017**, *139*, 2604-2618.
54. Electrochemical Reduction of CO<sub>2</sub> Catalyzed by Re(pyridine-oxazoline)(CO)<sub>3</sub>Cl Complexes, Nganga, J. K.; Samanamu, C. R.; Tanski, J. M.; Pacheco, C.; Saucedo, C.; Batista, V. S.; Grice, K. A.; Ertem, M. Z.; Angeles-Boza, A. M., *Inorg. Chem.* **2017**, *56*, 3214-3226.
55. Light-Driven Water Splitting by a Covalently Linked Ruthenium-Based Chromophore-Catalyst Assembly, Sherman, B. D.; Xie, Y.; Sheridan, M. V.; Wang, D.; Shaffer, D. W.; Meyer, T. J.; Concepcion, J. J. *ACS Energy Lett.* **2017**, *2*, 124-128.
56. Efficient Hydrogen Storage and Production using an Iridium Catalyst with an Imidazoline-Based Proton-Responsive Ligand in Water, Wang, L.; Onishi, N.; Murata, K.; Hirose, T.; Muckerman, J. T.; Fujita, E.; Himeda, Y. *ChemSusChem*, **2017**, in press, DOI: 10.1002/cssc.201601437.
57. Hydricity, Electrochemistry, and Excited-State Chemistry of Ir Complexes for CO<sub>2</sub> Reduction, Manbeck, G. F.; Garg, K.; Shimoda, T.; Szalda, D. J.; Ertem, M. Z.; Muckerman, J. T.; Fujita, E. *Faraday Discuss.* **2017**, in press, DOI: 10.1039/c6fd00223d.
58. Mechanistic and Kinetic Studies of Ruthenium-Based Oxygen Evolution Catalysts Using a Dissolved-Oxygen Optical Probe, Badiei, Y. M.; Xie, Y.; Concepcion, J. J.; Renderos, G.; Gutierrez, K.; Aquino, T. *Inorg. Chem.* under review.
59. Tetra- and Heptametallic Ru(II), Rh(III) Supramolecular Hydrogen Production Photocatalysts, Manbeck, G. F.; Fujita, E.; Brewer, K. *Submitted to J. Am. Chem. Soc.*

60. Fast Single-Site Molecular Water Oxidation Catalysts: One Site is Still Enough, Shaffer, D. W.; Xie, Y.; Szalda, D. J.; Concepcion, J. J., *Submitted to Nature Chem.*
61. O-O Coupling: From Detailed Mechanistic Understanding to Enhanced Water Oxidation Catalysis, Xie, Y.; Shaffer, D. W.; Concepcion, J. J., *Submitted to ACS Catal.*

## Exploiting Templating to Engender Acid Stability for OER Catalysts

Daniel G. Nocera  
Department of Chemistry and Chemical Biology  
Harvard University  
Cambridge, MA 02138

Understanding how to control oxygen evolution reaction catalysis in the acidic pH regime is important to us because it challenges our abilities to manipulate proton-coupled electron transfer to confer stability to metal oxides in acid and in doing so to open new avenues for further catalyst design and assessment. Additionally, the knowledge gained from optimizing catalysis in acid may be applied to other reactions at low pH including hydrohalic acid splitting, oxygen reduction and formic/phosphoric acid oxidation. Accordingly, we have sought design principles for developing active, stable, and earth-abundant acidic OER catalysts. The experimental design has begun with electrodeposited manganese oxide (MnOx), which we are able to stabilize in concentrated nitric acid by inserting an equilibrium for catalyst self-assembly that is driven by  $Mn^{2+}$  comproportionation. While stable, the catalyst activity is low, though it may be improved through potential cycling deposition. To advance beyond activated MnOx, we have turned to a design principle to incorporate different co-interacting metals to fulfill specific roles to achieve desired functionality. To this end, OER activity and stability have been de-coupled such that each property may be furnished by separate metals and optimized independently. Mixed metal oxide films have been constructed with Co as the catalytic metal and Mn as the structural metal (denoted CoMnOx). These films exhibit similar OER activity as that of electrodeposited Co oxide (CoOx), but the catalyst is much more stable (remaining intact over 12 h of continuous operation in acid vs minutes for CoOx); the 12 hr limitation on stability at high anodic potential is due to transformation to permanganate ( $MnO_4^-$ ). Further, exploiting the ability to optimize the structural metal independently, Pb oxide was utilized to furnish high anodic stability at low pH. Mixed metal oxides were electrodeposited with Co as the catalytic component and Pb (with Fe dopant) as the structural element. These films exhibit the activity of CoOx but they do not dissolve when operated at current densities of  $1 \text{ mA/cm}^2$  in acid continuously for over 50 h at pH 2.0. Depending on our experimental progress



Electrochemical stability for acidic OER measured by sustained chronoamperometry at (top)  $1.0 \text{ mA/cm}^2$  in pH 2.5  $P_i$  for CoOx (red  $\dashrightarrow$ ), CoFeOx (orange  $\dashrightarrow$ ), and CoFePbOx (dark green  $\dashrightarrow$ ) with PbOx (purple  $\dashrightarrow$ ) shown for comparison; and at (bottom)  $1.0 \text{ mA/cm}^2$  in pH 2.0 sulfate for CoFePbOx (dark green  $\dashrightarrow$ ). The inflection of potential in the plots indicates film dissolution.

to the meeting date, discussion may be extended to oxidic Ni catalysts. These results demonstrate that an approach of using a stable metal oxide as a scaffold for active OER metals provides a promising path for the development of active, stable, and earth-abundant OER catalysts.

### DOE Sponsored Publications 2014-2017

1. A functionally stable manganese oxide oxygen evolution catalyst in acid. Michael Huynh, D. Kwabena Bediako and Daniel G. Nocera, *J. Am. Chem. Soc.* **2014**, *136*, 6002–10.
2. Role of pendant proton relays and proton-coupled electron transfer on the hydrogen evolution reaction by nickel hangman porphyrins. D. Kwabena Bediako, Brian H. Solis, Dilek K. Dogutan, Manolis M. Roubelakis, Andrew G. Maher, Chang Hoon Lee, Matthew B. Chambers, Sharon Hammes-Schiffer and Daniel G. Nocera, *Proc. Natl. Acad. Sci. U.S.A.* **2014**, *111*, 15001–6.
3. Nucleation and growth mechanisms of an electrodeposited manganese oxide oxygen evolution catalyst. Michael Huynh, D. Kwabena Bediako, Yi Liu and Daniel G. Nocera, *J. Phys. Chem. C* **2014**, *118*, 17142–52.
4. Electrocatalytic H<sub>2</sub> evolution by proton-gated hangman iron porphyrins. Daniel J. Graham and Daniel G. Nocera, *Organometallics* **2014**, *33*, 4994–501.
5. Water oxidation catalysis by Co(II) impurities in Co(III)<sub>4</sub>O<sub>4</sub> cubanes. Andrew M. Ullman, Yi Liu, Michael Huynh, D. Kwabena Bediako, Hongsen Wang, Bryce L. Anderson, David C. Powers, John J. Breen, Héctor D. Abruña and Daniel G. Nocera, *J. Am. Chem. Soc.* **2014**, *136*, 17681–8.
6. Theoretical analysis of cobalt hangman porphyrins: Ligand dearomatization and mechanistic implications for hydrogen evolution. Brian H. Solis, Andrew G. Maher, Tatsuhiko Honda, David C. Powers, Daniel G. Nocera and Sharon Hammes-Schiffer, *ACS Catal.* **2014**, *4*, 4516–26.
7. Spectroscopic studies of nanoparticulate thin films of a cobalt-based oxygen evolution catalyst. Yi Liu and Daniel G. Nocera, *J. Phys. Chem. C* **2014**, *118*, 17060–6.
8. Post-synthetic modification of hangman porphyrins synthesized on the gram scale. Daniel J. Graham, Shao-Liang Zheng and Daniel G. Nocera, *ChemSusChem* **2014**, *7*, 2449–52.
9. Electron transfer studies of a peroxide dianion. Andrew M. Ullman, Xianru Sun, Daniel J. Graham, Nazario Lopez, Matthew Nava, Rebecca De Las Cuevas, Peter Müller, Elena V. Rybak-Akimova, Christopher C. Cummins and Daniel G. Nocera, *Inorg. Chem.* **2014**, *53*, 5384–91.
10. Nature of activated manganese oxide for oxygen evolution. Michael Huynh, Chenyang Shi, Simon J. L. Billinge and Daniel G. Nocera, *J. Am. Chem. Soc.* **2015**, *137*, 14887–904.
11. Proton-coupled electron transfer chemistry of hangman macrocycles: Hydrogen and oxygen evolution reactions. Dilek K. Dogutan, D. Kwabena Bediako, Daniel J. Graham, Christopher M. Lemon and Daniel G. Nocera, *J. Porph. Phthal.* **2015**, *19*, 1–8

12. Ultrafast photoinduced electron transfer from peroxide dianion. Bryce L. Anderson, Andrew G. Maher, Matthew Nava, Nazario Lopez, Christopher C. Cummins and Daniel G. Nocera, *J. Phys. Chem. B* **2015**, *119*, 7422–29.
13. Electrochemical polymerization of pyrene derivatives on functionalized carbon nanotubes for pseudocapacitive electrodes. John C. Bachman, Reza Kaviani, Daniel J. Graham, Dong Young Kim, Suguru Noda, Daniel G. Nocera, Yang Shao-Horn and Seung Woo Lee, *Nature Commun.* **2015**, *6*, 7040/1–9.
14. Oxygen evolution catalysis by cobalt oxido thin films. D. Kwabena Bediako, Andrew M. Ullman and Daniel G. Nocera, *Top. Curr. Chem.* **2015**, *371*, 173–214.
15. Anion-receptor mediated oxidation of carbon monoxide to carbonate by peroxide dianion. Matthew Nava, Nazario Lopez, Peter Müller, Gang Wu, Daniel G. Nocera and Christopher C. Cummins, *J. Am. Chem. Soc.* **2015**, *137*, 14562–5.
16. Micelle-encapsulated quantum dot-porphyrin assemblies as in vivo two-photon oxygen sensors. Christopher M. Lemon, Elizabeth Karnas, Xiaoxing Han, Oliver T. Bruns, Dai Fukumura, Mounqi G. Bawendi, Rakesh K. Jain, Dan G. Duda and Daniel G. Nocera, *J. Am. Chem. Soc.* **2015**, *137*, 9832–42.
17. Pushing single-oxygen-atom-bridged bimetallic systems to the right: A cryptand encapsulated Co–O–Co unit. Julia M. Stauber, Eric D. Bloch, Konstantinos D. Vogiatzis, Shao-Liang Zheng, Ryan G. Hadt, Dugan Hayes, Lin X. Chen, Laura Gagliardi, Daniel G. Nocera, and Christopher C. Cummins, *J. Am. Chem. Soc.* **2015**, *137*, 15354–7.
18. Comparison of self-assembled and micelle encapsulated QD chemosensor constructs for biological sensing. Christopher M. Lemon and Daniel G. Nocera, *Faraday Discuss.* **2015**, *185*, 249–266.
19. Photophysical properties of  $\beta$ -substituted free-base corroles. Christopher M. Lemon, Robert L. Halbach, Michael Huynh and Daniel G. Nocera, *Inorg. Chem.* **2015**, *54*, 2713–25.
20. Nickel phlorin intermediate formed by proton-coupled electron transfer in hydrogen evolution mechanism. Brian H. Solis, Andrew G. Maher, Dilek K. Dogutan, Daniel G. Nocera and Sharon Hammes-Schiffer, *Proc. Natl. Acad. Sci. U.S.A.* **2016**, *113*, 485–492.
21. Electronic structure of copper corroles. Christopher M. Lemon, Michael Huynh, Andrew G. Maher, Bryce L. Anderson, Eric D. Bloch, David C. Powers and Daniel G. Nocera, *Angew. Chem. Int. Ed.* **2016**, *55*, 2176–80.
22. Oxygen reduction catalysis at a dicobalt center: The relationship of faradaic efficiency to overpotential. Guillaume Passard, Andrew M. Ullman, Casey N. Brodsky and Daniel G. Nocera, *J. Am. Chem. Soc.* **2016**, *138*, 2925–28.
23. Activation of electron-deficient quinones through hydrogen-bond-donor-coupled electron transfer. Amanda K. Turek, David J. Hardee, Andrew M. Ullman, Daniel G. Nocera and Eric N. Jacobsen, *Angew. Chem. Int. Ed.* **2016**, *55*, 539–544.

24. Probing edge site reactivity of oxidic cobalt water oxidation catalysts. Andrew M. Ullman, Casey N. Brodsky, Nancy Li, Shao-Liang Zheng and Daniel G. Nocera, *J. Am. Chem. Soc.* **2016**, *138*, 4229–36.
25. Monodispersed MgO nanocrystals for H<sub>2</sub> production from room-temperature photodecomposition of liquid methanol. Zhengqing Liu, Zongyou Yin, Casandra Cox, Michel Bosman, Xiaofeng Qian, Na Li, Dong Yan, Daniel G. Nocera, Yaping Du and Ju Li, *Science Adv.* **2016**, *2*, e1501425/1–8.
26. X-ray spectroscopic and computational studies of a Co<sub>4</sub>O<sub>4</sub> cubane: Electronic structure contributions to the formation of high-valent states relevant to the oxygen-evolution reaction. Ryan G. Hadt, Dugan Hayes, Casey N. Brodsky, Andrew M. Ullman, Bryce L. Anderson, Diego M. Casa, Mary H. Upton, Daniel G. Nocera and Lin X. Chen, *J. Am. Chem. Soc.* **2016**, *138*, 11017–30.
27. Influence of iron doping on tetravalent nickel content in catalytic oxygen evolving films. Nancy Li, D. Kwabena Bediako, Ryan G. Hadt, Dugan Hayes, Thomas J. Kempa, Felix von Cube, Casey N. Brodsky, David C. Bell, Lin X. Chen and Daniel G. Nocera, *Proc. Natl. Acad. Sci. U.S.A.* **2017**, *114*, 1486–91.
28. *In situ* characterization of cofacial Co(IV) centers in a Co<sub>4</sub>O<sub>4</sub> cubane: Modeling the high-valent active site in oxygen evolving catalysts. Casey N. Brodsky, Ryan G. Hadt, Dugan Hayes, Benjamin J. Reinhart, Nancy Li, Lin X. Chen and Daniel G. Nocera, *Proc. Natl. Acad. Sci. U.S.A.* **2017**, *114*, 3855–60.
29. Hydrogen evolution catalysis by a sparsely substituted cobalt chlorin. Andrew G. Maher, Guillaume Passard, Dilek K. Dogutan, Robert L. Halbach, Bryce L. Anderson, Christopher J. Gagliardi, Masahiko Taniguchi, Jonathan S. Lindsey and Daniel G. Nocera, *ACS Catal.* **2017**, *6*, ASAP, DOI: 10.1021/acscatal.7b00969.

*Session VIII*

*Models in Electron Transfer*



## Proton-Coupled Electron Transfer Processes Underpinning the Electrocatalytic Generation of Hydrogen

Jillian L. Dempsey, Noémie Elgrishi, Banu Kandemir, Katherine J. Lee, Brian D. McCarthy, and Eric S. Rountree  
Department of Chemistry  
University of North Carolina  
Chapel Hill, NC 27516

Proton-coupled electron transfer (PCET) processes underpin the efficiency of molecular catalysts that mediate electrochemical fuel-forming reactions like hydrogen evolution. By leveraging electroanalytical methods with time-resolved spectroscopy, work in our research group has focused on elucidating the reaction pathways by which proton and electron transfers proceed in catalytic systems (and related model complexes). This talk will discuss recent progress towards understanding PCET in catalysis, specifically highlighting how we have 1) gained new understanding of the thermochemical parameters controlling PCET reactions in non-aqueous solvents, 2) revealed that pendant bases in the secondary coordination sphere can lead to catalytic onset potentials that are dependent on effective pH of the solution, and 3) identified the non-trivial role of acid choice on the reaction kinetics of a cobalt-hydride formation.

We have recognized that proton-coupled electron transfer (PCET) reactions are not a purely aqueous phenomenon and molecular catalysts for the electrochemical reduction of acids to H<sub>2</sub> are often studied in non-aqueous solvents. As such, we have carried out systematic studies to extend the potential-pK<sub>a</sub> relationships (Pourbaix Theory) used to describe the thermochemistry of aqueous PCET reactions to non-aqueous solvents. The relationship derived predicts that a plot of  $E^{0'}$  for a molecular species that undergoes a PCET reaction will vary with both the pK<sub>a</sub> of the proton source and the ratio of acid and base in solution. While often PCET reactions in non-aqueous solvents are kinetically controlled, we identified coordination complexes for which Nernstian equilibria are accessed on the electrochemical timescale, and validate this potential-pK<sub>a</sub> theory through construction of two experimental diagrams. One example is provided by MoCp<sub>2</sub>(S<sub>2</sub>C<sub>2</sub>(H)-4-pyridin-yl), which features a redox non-innocent dithiolate ligand with a pendant pyridine. Clear shifts in the  $E^{0'}$  for oxidation are observed when acid is added to solution (Figure 1), the magnitude of which is directly correlated to acid pK<sub>a</sub>.

Interest in examining potential-pK<sub>a</sub> relationships in catalysis, we have carried out mechanistic studies of [Ni(P<sub>2</sub><sup>Ph</sup>N<sub>2</sub><sup>Bn</sup>)<sub>2</sub>(CH<sub>3</sub>CN)][BF<sub>4</sub>]<sub>2</sub> (P<sub>2</sub><sup>Ph</sup>N<sub>2</sub><sup>Bn</sup> = 1,5-dibenzyl-3,7-diphenyl-1,5-diaza-3,7-

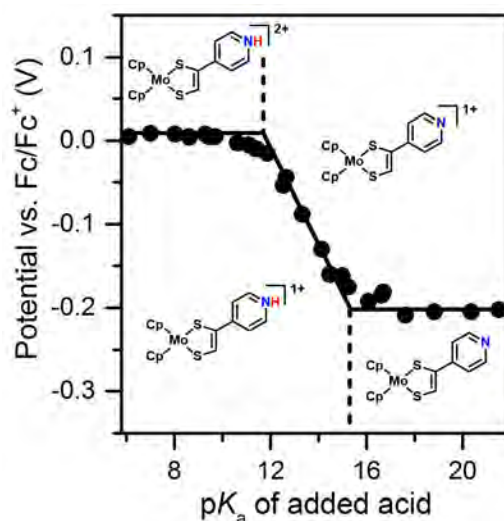


**Figure 1.** The  $E^{0'}$  of MoCp<sub>2</sub>(S<sub>2</sub>C<sub>2</sub>(H)-4-pyridin-yl) shifts as a function of the pK<sub>a</sub> of the acid present in solution. From these data, a non-aqueous potential-pK<sub>a</sub> diagram can be generated.

diphosphacyclooctane). The applied potential at which this complex catalyzes proton reduction has previously been observed to shift 60 mV per effective pH unit across a limited range in acetonitrile, indicative of a thermodynamically controlled n-electron, n-proton PCET reaction. Subsequent computational investigation outlined a complete potential- $pK_a$  diagram which identified the most thermochemically stable species as a function solution free energy and applied potential and suggested that the experimentally observed potential- $pK_a$  dependence corresponds to a two-electron, two-proton transfer. In order to more deeply probe the PCET reaction pathways that give rise to the potential- $pK_a$  relationship observed for this catalyst, cyclic voltammograms were recorded for acids with  $pK_a$  values spanning 15 units. Comparison between the computationally- and experimentally-derived diagrams reveals that the observed potentials for catalysis do not align with the predicted potential- $pK_a$  relationships (Figure 2). Through complementary stopped-flow rapid mixing experiments, the elementary reaction steps of hydrogen evolution were examined. Optical detection of ligand-protonated intermediates, in addition to hydride species known to be key intermediates in hydrogen production, suggest that the pendant amines play key roles in both mediating proton transfer and in promoting  $pK_a$ -dependent catalytic activity. From these data, we demonstrate that the equilibria forming at the surface of the electrode can occur between kinetically accessible reaction intermediates, not just the most thermodynamically stable species.

Transition metal hydride complexes, like those noted above, are key intermediates in hydrogen evolution and  $CO_2$  reduction cycles. With an interest in understanding the parameters influencing the mechanism and kinetics of transition metal hydride formation we identified a model system,  $[Co(Cp)(dppe)]^{2+}$  (Cp = cyclopentadienyl, dppe = 1,2-bis(diphenylphosphino)ethane), that forms a stable cobalt hydrides. By decoupling hydride formation from catalyst turnover, we have examined how various acid parameters dictate the reaction rate and mechanism of hydride formation. From cyclic voltammetry experiments, we diagnosed a stepwise PCET mechanism and determined the second order rate constants for the protonation step ( $k_{PT}$ ) for a series of 22 acids (Figure 3). The relationship between  $k_{PT}$  and acid  $pK_a$  revealed that acid choice has a non-trivial effect on reaction kinetics, underscoring the crucial and often overlooked role of the nature of the proton source in fuel forming catalysis operating through metal hydrides.

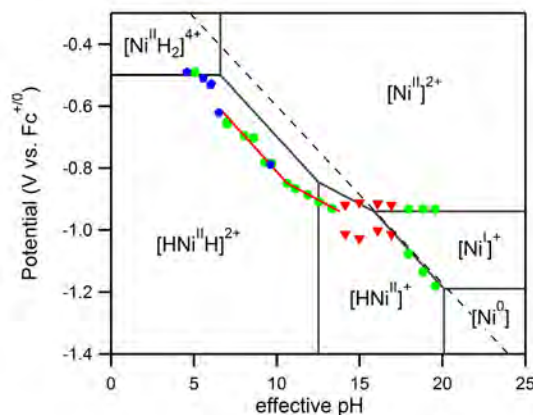


**Figure 2.** Potential- $pK_a$  diagram for  $[Ni(P_2^{Ph}N_2^{Bz})_2]^{2+}$  in acetonitrile based on experimental measurements of thermochemical values and computational investigation, overlain with of redox potentials determined from catalytic cyclic voltammograms recorded as a function of solution free energy.

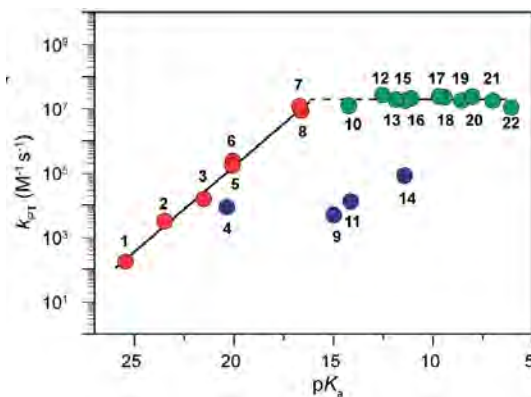


**Figure 3.** Rate constants for protonation of Co(I) ( $k_{PT}$ ) as a function of acid  $pK_a$  in  $CH_3CN$ .

### DOE Sponsored Publications 2016-2017

1. Rountree, E. S.; McCarthy, B. D.; Dempsey, J. L. Experimental Access to Non-Aqueous Potential- $pK_a$  Diagrams of Catalytic Systems. *Submitted*.
2. Elgrishi, N.; Rountree, K. J.; McCarthy, B. D.; Rountree, E. S.; Eisenhart, T. T.; Dempsey, J. L. A Practical Beginner's Guide to Cyclic Voltammetry. *Submitted*.
3. Lee, K. J.; Elgrishi, N.; Kandemir, B.; Dempsey, J. L. Applications of electrochemical and spectroscopic methods for evaluating molecular electrocatalysts. *Nat. Rev. Chem.* **2017**, *In Press*.
4. Lee, K. J.; McCarthy, B. D.; Rountree, E. S.; Dempsey, J. L. Identification of an Electrode-Adsorbed Intermediate in the Catalytic Hydrogen Evolution Mechanism of a Cobalt Dithiolene Complex. *Inorg. Chem.* **2017**, *56*, 1988–1998.
5. McCarthy, B. D.; Dempsey, J. L. Decoding Proton-Coupled Electron Transfer with Potential- $pK_a$  Diagrams. *Inorg. Chem.* **2017**, *56*, 1225–1231.
6. Elgrishi, N.; Kurtz, D. A.; Dempsey, J. L. Reaction Parameters Influencing Cobalt Hydride Formation Kinetics: Implications for Benchmarking  $H_2$ -Evolution Catalysts. *J. Am. Chem. Soc.* **2017**, *139*, 239–244.

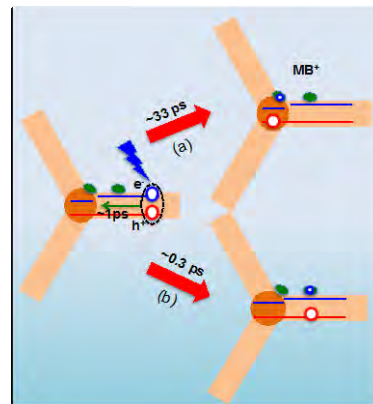
## Plasmon Induced Interfacial Charge Transfer Transition: A New Mechanism for Efficient Hot Electron Transfer

Tianquan Lian  
Department of Chemistry  
Emory University  
1515 Dickey Dr. NE, Atlanta, Georgia 30222

The objectives of our research program are three fold: 1) to examine Auger-assisted and hole transfer mechanisms in nanomaterials beyond quantum dots; 2) to under the mechanism of long distance charge separation and charge recombination in nanorod-metal heterostructures; and 3) to further investigate the mechanism of plasmon induced interfacial charge transfer transition as a new pathways for efficient hot electron transfer in plasmonic metal/semiconductor interface. In the following, we summarize the key progresses in these areas.

**1.) Auger assisted hole transfer from nanorods.** We have showed that the rates of electron transfer (ET) from CdX (X=S, Se and Te) quantum dots (QDs) to molecular acceptors increased monotonically with the driving force (0 ~ 1.3 eV), lacking the inverted regime behavior expected from the Marcus ET theory. We proposed that electron transfer from QDs followed an Auger-assisted ET model, in which, the excess energy of the electron can be transfer to the hole, which overcomes the unfavorable Franck-Condon overlap in the Marcus inverted regime (see pub. 2). We believe that the proposed Auger-assisted ET model is generally applicable to many excitonic nanomaterials. We have extend this model to hole transfer from CdSe/CdS nanorods. In this case, hole transfer leads to excitation of electrons in the conduction band, which can be directly observed by transient absorption spectroscopy. This work is ongoing.

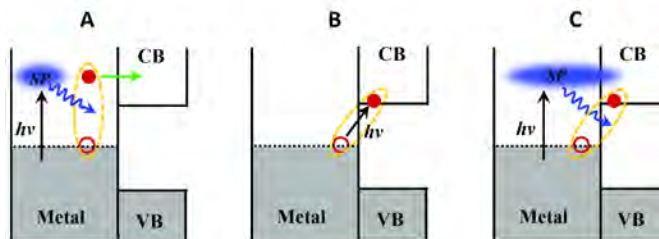
**2) Long-distance charge separation:** Quantum confined nanorod heterostructures offer the opportunity to control the energy of electrons and holes by rod diameters and the spatial location of carriers along the long axis through their length. In CdSe/CdS nanorods, we showed that excitons generated in CdS rod can be transported efficiently to CdSe seed, with CdS rod functioning as an antenna for efficient light absorption (see pub. 3, 7). Furthermore, CdSe/CdS-Pt nanorods, the long distance between the CdSe seed and the Pt tip allows for long distance charge separation to slow down recombination (see Pub 1 and 6). We have extended these studies to CdSe tetrapods, in which four arms can further enhance the light absorption cross-section. We showed that CdSe tetrapods has a quasi-type II band alignment between the Zinc Blend CdSe quantum dot core and four Wurtzite CdSe nanorod branches and 88% of the excitons generated in the CdSe branches localized to the core with a time constant of  $1.01 \pm 0.06$  ps, driven by the lower conduction band energy in the core. We demonstrated that ET to methylene blue molecules (with an average time constant of  $33 \pm 8$  ps) occurred after the exciton is localized to the core, while ultrafast ET ( $0.31 \pm 0.01$  ps) to methyl viologen occurs prior to the localization of the exciton. Thus, the competition of exciton interfacial dissociation and transport along the rod enables the control of the nature of charge separated states in nanorod-electron acceptor complexes. In collaboration with Jeff Pyun at Univ. Arizona, we have showed that similar to CdSe/CdS nanorods, the band alignment in CdSe@CdS tetrapods can also be tuned by the size of the CdSe



seed to achieve type I and quasi-type II alignment (see pub. 15). The enhanced charge separation in the small seeded tetrapods, coupled with the excellent light-absorbing capabilities of these systems, enabled the preparation of Janus-type Au-tetrapod NCs on large scale (2.5 g) in under 90 seconds using only sunlight as the irradiation source.

### 3) Plasmon induced hot electron transfer:

Surface plasmon resonance (SPR) has been used to increase light absorption of semiconductors through enhanced local fields near the metal nanostructures. In more recent years, there have been reports of plasmon-induced hot electron or hole transfer from the excited metal into semiconductors. The reported efficiencies of such processes are typically low. Hot electron transfer is believed to follow a conventional mechanism (PHET, Scheme 1A), in which the plasmon decay by exciting hot electron-hole pairs within the metal on the few to 10s femtosecond time scale. Because of the rapid relaxation of hot electrons (or holes) to their Fermi levels on the 100s fs time scale, transfer of hot electrons is often inefficient.



Scheme 1. Metal-to-semiconductor hot-electron transfer pathways. A) Conventional plasmon induced hot electron transfer (PHET), B) Direct interfacial charge transfer transition (DICTT), C) Plasmon induced interfacial charge transfer transition (PICTT).

We proposed plasmon-induced metal-to-semiconductor interfacial charge transfer transition (PICTT) as a pathway for efficient hot electron transfer in strongly coupled metal/semiconductor heterojunctions (Scheme 1C). In this scheme, the metal plasmon serves as an efficient light absorber due to its large extinction coefficient. The strong coupling of the metal and semiconductor provides a new plasmon decay process, in which an electron in the metal is excited into the semiconductor conduction band across the interface as a result of plasmon decay. We experimentally demonstrated the proposed PICTT pathway in CdSe-Au nanorod heterostructures, and reported a highly efficient plasmon induced Au-to-CdSe charge separation with a quantum efficiency of > 24% (pub. 9). We argued that this pathway differs from the direct metal-to-semiconductor interfacial charge-transfer transition (DICTT, Scheme 1B) because of the superior light harvesting ability of the plasmon. In ongoing work, we are investigating what the key material properties that lead to the presence of the PICTT pathway and how to rationally design heterostructures efficient plasmon induced hot electron transfer. Preliminary results suggest that PICTT pathways may exist in Au/TiO<sub>2</sub> and Ag/TiO<sub>2</sub> interfaces.

We proposed plasmon-induced metal-to-semiconductor interfacial charge transfer transition (PICTT) as a pathway for efficient hot electron transfer in strongly coupled metal/semiconductor heterojunctions (Scheme 1C). In this scheme, the metal plasmon serves as an efficient light absorber due to its large extinction coefficient. The strong coupling of the metal and semiconductor provides a new plasmon decay process, in which an electron in the metal is excited into the semiconductor conduction band across the interface as a result of plasmon decay. We experimentally demonstrated the proposed PICTT pathway in CdSe-Au nanorod heterostructures, and reported a highly efficient plasmon induced Au-to-CdSe charge separation with a quantum efficiency of > 24% (pub. 9). We argued that this pathway differs from the direct metal-to-semiconductor interfacial charge-transfer transition (DICTT, Scheme 1B) because of the superior light harvesting ability of the plasmon. In ongoing work, we are investigating what the key material properties that lead to the presence of the PICTT pathway and how to rationally design heterostructures efficient plasmon induced hot electron transfer. Preliminary results suggest that PICTT pathways may exist in Au/TiO<sub>2</sub> and Ag/TiO<sub>2</sub> interfaces.

### DOE Sponsored Publications 2014-2017

1. Kaifeng Wu, Zheyuan Chen, Hongjin Lv, Haiming Zhu, Craig L Hill, Tianquan Lian, "Hole Removal Rate Limits Photo-driven H<sub>2</sub> Generation Efficiency in CdS-Pt and CdSe/CdS-Pt Semiconductor Nanorod-metal tip Heterostructures", **J. Am. Chem. Soc.** (2014), 136, 7708-7716, DOI: 10.1021/ja5023893.
2. Haiming Zhu, Ye Yang, Kim Hyeon-Deuk, Marco Califano, Nianhui Song, Youwei Wang, Wenqing Zhang, Oleg V Prezhdo, Tianquan Lian, "Auger-Assisted Electron Transfer from Photoexcited Semiconductor Quantum Dots". **Nano Letters** (2014), 14(3), 1263-1269.
3. Haiming Zhu, Zheyuan Chen, Kaifeng Wu, and Tianquan Lian, Wavelength Dependent Efficient Photoreduction of Redox Mediators Using Type II ZnSe/CdS Nanorod

- Heterostructures”, **Chem. Sci.** (2014), 5, 3905-3914.
4. Kaifeng Wu, William Rodríguez-Córdoba and Tinaquan Lian, “Exciton Localization and Dissociation Dynamics in CdS and CdS-Pt Quantum Confined Nanorods: Effect of Non-uniform Rod Diameters”, **J. Phys. Chem. B** (2014), 118, 14062-14069
  5. Jing Gu, Yong Yan, Brian J. Helbig, Zhuangqun Huang, Tianquan Lian, Russell H. Schmehl, “The influence of ligand localized excited states on the photophysics of second row and third row transition metal terpyridyl complexes: Recent examples and a case study”, **Coord. Chem. Rev.** (2015), 282, 100-109
  6. Kaifeng Wu, Haiming Zhu, Tianquan Lian, “Ultrafast Exciton Dynamics and Light-driven H<sub>2</sub> Evolution in Colloidal Semiconductor Nanorods and Pt-tipped Nanorods”, **Acc. Chem. Res.** (2015), 48, 851-859.
  7. Kaifeng Wu, Lawrence J Hill, Jinquan Chen, James R McBride, Nicholas G Pavlopoulos, Nathaniel E Richey, Jeffrey Pyun, Tianquan Lian, “Universal Length-Dependence of Rod-to-Seed Exciton Localization Efficiency in Type I and Quasi Type II CdSe@ CdS Nanorods”, **ACS Nano** (2015), 9, 4591-4599, DOI: 10.1021/acsnano.5b01245.
  8. Kaifeng Wu, Yongling Du, Hua Tang, Zheyuan Chen, Tianquan Lian, “Efficient Extraction of Trapped Holes from Colloidal CdS Nanorods”, **J. Am. Chem. Soc.** (2015), 137 (32), pp 10224–10230, DOI: 10.1021/jacs.5b04564
  9. Kaifeng Wu, Jinquan Chen, James R. McBride, Tianquan Lian, “Efficient hot-electron transfer by a plasmon-induced interfacial charge-transfer transition”, **Science** (2015), 349 (6248): 632 DOI: 10.1126/science.aac5443
  10. Kaifeng Wu, Tianqun Lian, “Quantum Confined Colloidal Nanorod Heterostructures for Solar-to-Fuel Conversion”, **Chem. Soc. Rev.** (2016), 45, 3781-3810 (DOI: 10.1039/C5CS00472A)
  11. Ye Yang, Kaifeng Wu, A. Shabaev, Al. L. Efros, Tianquan Lian, and Matthew C. Beard, “Direct Observation of Photo-Excited Hole Localization in CdSe Nanorods”, **ACS Energy Letters**, (2016) 1, 76-81.
  12. Ye Yang, PhD; Kaifeng Wu; Zheyuan Chen, PhD; Ban-Seok Jeong; Tianquan Lian, “Competition of Branch-to-core Exciton Localization and Interfacial Electron Transfer in CdSe Tetrapods”, **Chem. Phys.** (2016) 47, 32-38 (Special issue on Quantum Dots).
  13. Sooho Lee, Yimeng Wang, Yawei Liu, Dongkyu Lee, Kangha Lee, Doh C. Lee, Tianquan Lian, “Exciton Dynamics within Cation-exchanged CdSe/PbSe Nanorods: The Role of Defects”, **Chem. Phys. Lett.** Special Memorial Issue for Ahmed Zewail), under review.
  14. Bryant Chica, Chang-Hao Wu, Yuhgene Liu, Michael W.W. Adams, Tianquan Lian, and R. Brian Dyer, “Downhill Redox Shuttle for Efficient Photocatalytic Hydrogen Production in CdSe/CdS Nanorod-[NiFe] Hydrogenase Assemblies”, **Nature Energy**, under review.
  15. Nicholas G. Pavlopoulos, Yawei Liu, Jeffrey T. Dubose, Nicola Pinna, Marc-Georg Willinger, Kookheon Char, Tianquan Lian, and Jeffrey Pyun, “Type I vs Type II Modulation in CdSe@CdS Tetrapods: Ramifications for Noble Metal Tipping”, **ACS Nano**, Under Review
  16. Taghinejad, Mohammad; Taghinejad, Hossein; Malak, Sidney; Moradinejad, Hesam; Xu, Zihao; Liu, Yawei; Woods, Eric; Eftekhari, Ali ; Lian, Tianquan; Tsukruk, Vladimir; Adibi, Ali, “Ultrasharp and Tunable Crystal/Fano-Type Resonances Enabled by Out-of-Plane Dipolar Coupling in Plasmonic Nanopatch Arrays”, **submitted**

## Temperature and solvent polarizability in electron-transfer reactions

M. M. Waskasi,<sup>1</sup> M. D. Newton,<sup>2</sup> and D. V. Matyushov<sup>1</sup>

<sup>1</sup>School of Molecular Sciences, Arizona State University, Tempe, AZ 85287

<sup>2</sup>Brookhaven National Laboratory, Chemistry Department, Upton, NY 11973-5000

The goal of this study is to identify and describe theoretically experimentally testable effects of thermodynamic conditions and solvent identity on the kinetics of electron transfer reactions. In the first year of the project we have focused on the temperature effect [1-2] and on the effect of the solvent polarizability [3-4].

Temperature affects rates of activated transitions according to the Arrhenius law. However, the transition-state theory puts the free energy of activation in place of the activation “energy” in this empirical law. Since the free energy involves a complex dependence on temperature, the overall temperature law can be non-Arrhenius. At high barriers, only the activation enthalpy is important and a straight line in the Arrhenius coordinates (log of the rate vs inverse temperature) is typically observed. When the barrier is low, close to the top of the Marcus inverted parabola, entropic effects become important and one observes unusual temperature laws for the activated kinetics. In this regime, one can distinguish between predictions of different models for the solvent reorganization of electron transfer.

A major result of molecular models of solvation is the prediction of the special effect of the density fluctuations of molecular solvents on the temperature dependence of the reorganization energy (reorganization entropy). Dipolar rotations produce only a weak temperature dependence of the reorganization energy, in line with the continuum solvation models. On the contrary, dipolar translations (density fluctuations) produce a hyperbolic temperature term. The overall dependence of the reorganization energy, and of the reaction Gibbs energy, is hyperbolic. The observable prediction of this effect is the bell-shaped temperature law for the reaction rate in the Arrhenius coordinates.

The bell-shaped temperature law was confirmed by experiments on charge-transfer dyads [1] and

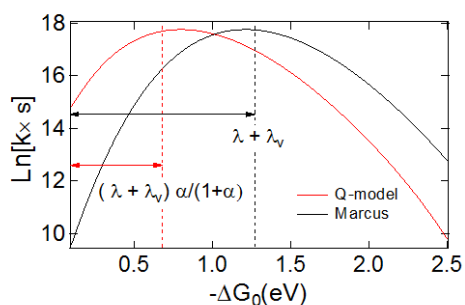


**Figure 1** Energy gap law in the Marcus theory and in the Q-model. The parameters are from the fit to the kinetic data of Miller et al.

by the analysis of the kinetic electron-transfer data from Miller and co-workers [2]. In both cases, upward curved Arrhenius plots are observed, with the top of the curve corresponding to the activationless transition. This point, analogous to the top of the inverted Marcus parabola, is now reached by altering temperature instead of altering the driving force in the traditional Marcus paradigm. In the case of charge separation in Miller’s donor-acceptor complexes we have found that

the standard Gaussian Marcus model does not provide a consistent analysis of both the reaction rates and the reaction free energies. The two data sets were reconciled [2] within the Q-model of electron transfer, which incorporates the non-Gaussian statistics of the energy gap in the modeling. The main

qualitative result of this analysis is a significant change in the energy-gap law under the Q-model scenario. Specifically, the top of the Marcus energy-gap law is achieved at a value about half of the reorganization energy when the Q-model is used (Figure 1). This is in contrast with the maximum position at the driving force equal to the reorganization energy in the Marcus model.

Traditional models of electron transfer connect the effect of the solvent polarizability on the reaction kinetics with the Pekar factor, which enters the reorganization energy of electron transfer. The overall result of this perspective is that the reorganization energy is reduced by about a factor of two in polarizable liquids compared to non-polarizable ones. We have studied the problem from the perspective of microscopic models of polar liquids. In this approach, we used microscopic susceptibilities of polar liquids depending on the wave vector. They were derived by combining simulations with liquids state theories. The transition to continuum was achieved by taking the limit of zero wavevector [3]. We found that although an analog of the Pekar factor can be obtained as the corresponding continuum limit of the microscopic susceptibility functions, there are two novel features to the problem: (i) the functionality in terms of the high-frequency and static dielectric constants is different from the Pekar factor and (ii) the reorganization energies calculated for realistic system parameters do not follow the standard continuum predictions [3]. The main qualitative distinction of the new perspective is a much weaker dependence of the reorganization energy on the polarizability of the solvent. This is a very significant result for computer simulations of electron transfer since most of them are done with non-polarizable force fields for the solvent. Our results suggest that essentially no polarizability corrections are required in applying those simulations to experimental data.

We have applied the general ideas developed in Ref. [3] to the problem of the solvent-induced shift of optical spectral lines [4]. We have obtained a new functional form for the solvent-induced shift in the continuum limit. The dependence of the shift on the solvent polarizability is much more gentle than predicted by the Lippert-McRae equation traditionally used to analyze optical spectral band-shapes.

1. M. M. Waskasi, G. Kodis, A. L. Moore, T. Moore, D. Gust, D. V. Matyushov, "Marcus bell-shaped electron transfer kinetics observed in an Arrhenius plot", *J. Am. Chem. Soc.* **138** (2016) 9251.
2. M. M. Waskasi, M. D. Newton, and D. V. Matyushov, "Impact of temperature an non-Gaussian statistics on electron transfer in donor-bridge-acceptor molecules", *J. Phys. Chem. B* **121** (2017) 2665.
3. H. Dinpajoo, M. D. Newton, and D. V. Matyushov, "Free energy functionals for polarization fluctuations: Pekar factor revisited". *J. Chem. Phys.* **146** (2017) 064504
4. D. V. Matyushov and M. D. Newton, "Solvent-induced shift of spectral lines in polar-polarizable solvents", *J. Phys. Chem. A* **121** (2017) 2232.

*Session IX*

*Novel Semiconducting Solids*



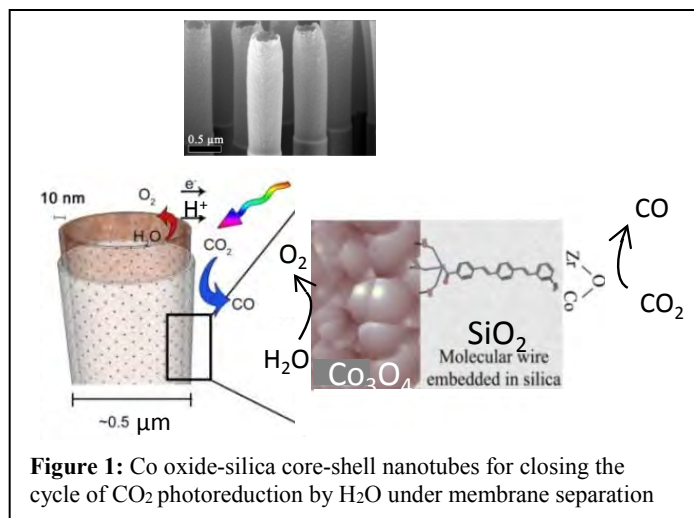
## Silica Nanolayers with Embedded Molecular Wires for Closing the Cycle of CO<sub>2</sub> Photoreduction by H<sub>2</sub>O under Membrane Separation

Heinz Frei

Molecular Biophysics and Integrated Bioimaging Division  
Lawrence Berkeley National Laboratory  
Berkeley, CA 94720

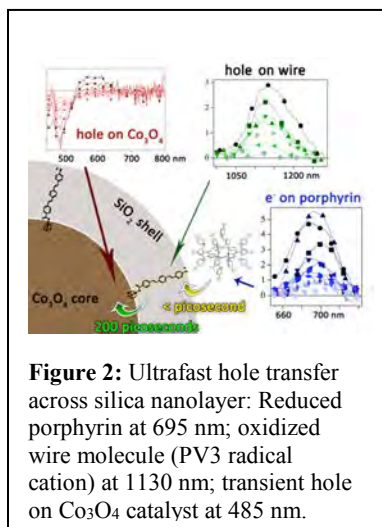
The overall goal of our research is to complete the photosynthetic cycle of CO<sub>2</sub> reduction by H<sub>2</sub>O under membrane separation of the half reactions on the nanoscale, a key design aspect of natural photosynthesis, by using functionalized inorganic oxide based core-shell nanotubes. Co oxide nanotubes surrounded by ultrathin silica shells with embedded molecular wires for tight control of electron transport are being developed as water oxidation catalyst-membrane assemblies driven by heterobinuclear light absorbers (Figure 1).<sup>10,11</sup> Photodeposition methods afford spatially directed light absorber-nanocatalyst coupling, and atomic layer deposition techniques allow for the assembly of core-shell nanotube arrays that provide product separation across all length scales from nano to macro. Transient optical spectroscopy reveals insight into charge-transfer mechanisms across multiple interfaces, while identification of surface intermediates by time-resolved FT-IR spectroscopy under reaction conditions guide photocatalyst improvement.

*Ultrafast hole transfer from light absorber to Co<sub>3</sub>O<sub>4</sub> water oxidation catalyst across molecular wires embedded in silica membrane:* Femtosecond transient absorption spectroscopy of photo-induced hole transfer from a molecular light absorber, here free base porphyrin electrostatically adsorbed on the silica, to Co oxide catalyst across the silica-embedded *para*-oligo(phenylene vinylene) (3 aryl units, PV3) allowed the direct observation of charge arrival on the wire



molecule, which takes place in less than a ps (excitation at 430 nm).<sup>19</sup> For achieving sufficient spectroscopic sensitivity, aqueous colloids of spherical core-shell nanoparticles were employed. Charge separation was indicated by the emerging PV3 radical cation and reduced porphyrin bands (Figure 2). Subsequent forward transfer of the positive charge to the Co oxide particle occurred in 250 ps, exceeding known hole transfer rates from anchored molecular light absorbers to metal oxide catalyst particles for water oxidation by several orders of magnitude. Arrival of

holes on Co<sub>3</sub>O<sub>4</sub> was indicated by bleach at 485 nm. The finding indicates that molecular light absorbers coupled to metal oxide catalysts by silica-embedded oligo(phenylene vinylene) offers an approach for integrated artificial photosystems featuring efficient hole transfer while enabling product separation on the nanoscale. Corresponding charge transfer studies using ZrOCo light absorber are in progress.



*Electronic control of charge flow across nanoscale silica membrane by embedded molecular wires:* Few nanometer-thin dense phase silica layers with embedded PV3 wires covalently anchored on the surface of Co oxide catalyst for water oxidation are shown by visible light sensitized electrochemical measurements to transport charges across the proton conducting, O<sub>2</sub> impermeable membrane.<sup>9</sup> For these measurements, planar constructs were prepared by low temperature ALD methods. Characterization of the Co<sub>3</sub>O<sub>4</sub>(7 nm) – SiO<sub>2</sub>(2 nm)/PV3 layers on a 100 nm Pt electrode by STEM-EDX, XPS, and grazing angle ATR FT-IR demonstrates conformal coverage and a density of 1 wire nm<sup>-2</sup>. Visible light sensitization of electrodes with silica embedded PV3 using Ru(bpy)<sub>3</sub> resulted in short circuit current (27 e<sup>-</sup>s<sup>-1</sup>wire<sup>-1</sup>), consistent with favorable alignment of the [Ru(bpy)<sub>3</sub>]<sup>3+</sup> potential with respect to the

HOMO energy of the wire. By contrast, visible light-generated reduced Sn porphyrin did not induce current because the potential is situated in the HOMO-LUMO gap of PV3. The finding demonstrates tight control of charge transport by the wire orbital energetics. The ultrathin silica membrane offers an approach for separating fuel forming from water oxidation catalysis on the length scale of nanometers. Given the flexibility of nanofabrication and ALD methods, this type of membrane is suitable for implementation in a variety of artificial photosystem designs.

*Coupling of ZrOCu<sup>II</sup> binuclear light absorber to Cu nanocatalyst for CO<sub>2</sub> reduction, observation of transient one-electron surface intermediate at aqueous nanoparticle interface:* The directionality of charge transfer upon excitation of ZrOCu light absorbers was utilized to assemble a Cu<sub>x</sub>O<sub>y</sub> nanocluster for CO<sub>2</sub> reduction coupled to the Zr acceptor site of the light absorber, and the photoreduction of CO<sub>2</sub> to CO by the photocatalytic unit demonstrated.<sup>8</sup> With the goal of exploring reaction pathways beyond CO, we sought to detect and structurally identify the primary CO<sub>2</sub> reduction intermediate on Cu<sub>x</sub>O<sub>y</sub> as well as metallic Cu nanocatalyst surfaces. For metallic Cu particles at the aqueous/solid interface driven by visible light-sensitized electron injection (Sn porphyrin excited at 514 nm), a surface species with  $\nu_{\text{sym}}(\text{CO}_2)$  at 1356 cm<sup>-1</sup> (<sup>13</sup>C: 1323 cm<sup>-1</sup>, no D isotope shift) was observed to grow in with first order kinetics by rapid-scan ATR FT-IR spectroscopy. While 2-electron products were not generated with this sensitizer, the same Cu metal particles are known to produce CO under electrocatalytic conditions. By contrast, visible light excitation of CdSe nanoparticles in aqueous solution led to first order growth of a surface species with very similar spectral signature, namely at 1370 cm<sup>-1</sup> (<sup>13</sup>C: 1333 cm<sup>-1</sup>) along with bands at 1575 cm<sup>-1</sup> (<sup>13</sup>C: 1548 cm<sup>-1</sup>) and 1336 cm<sup>-1</sup> (<sup>13</sup>C: 1297 cm<sup>-1</sup>). Two-electron co-products CO and HCO<sub>3</sub><sup>-</sup> appeared with an induction period. Based on these first infrared spectrokinetic observations, a primary surface intermediate with OCOCO<sub>2</sub><sup>-</sup> structure is proposed.

*Future work:* Methods for coupling two heterobinuclear light absorbers in 2-photon tandem configuration inside the Co oxide-silica core-shell nanotube structure for optimal solar coverage and potential matching will be explored. In parallel, control of electron/hole transfer across ultrathin silica membranes for artificial photosynthesis by tuning the orbital energetics of embedded molecular wires through synthetic modification will be expanded, and detailed mechanistic understanding sought by transient spectroscopy. Approaches for steering CO<sub>2</sub> to more deeply reduced products by catalyst redesign guided by insights from surface intermediates monitored by transient infrared spectroscopy will be pursued.

## DOE Solar Photochemistry Sponsored Publications 2014-2017

1. M. Zhang, M. de Respinis, and H. Frei. Time Resolved Observation of Water Oxidation Intermediates on Cobalt Oxide Nanoparticle Catalyst in Aqueous Solution. *Nature Chem.* **6**, 362-367 (2014).
2. M.L. Macnaughtan, H.S. Soo, and H. Frei. Binuclear ZrOCo Metal-to-Metal Charge-Transfer Unit in Mesoporous Silica for Light-Driven CO<sub>2</sub> Reduction to CO and Formate. *J. Phys. Chem. C* **118**, 7874-7885 (2014).
3. S. Helveg, C.F. Kisielowski, J.R. Jinschek, P. Specht, G. Yuan, and H. Frei. Observing Gas-Catalyst Dynamics at Atomic Resolution and Single Atom Sensitivity. *Micron* **68**, 176-185 (2014).
4. B.A. McClure and H. Frei. Excited State Electron Transfer of All-Inorganic Heterobinuclear TiOMn<sup>II</sup> Chromophore Anchored on Silica Nanoparticle Surface. *J. Phys. Chem. C* **118**, 11601-11611 (2014).
5. W. Kim, G. Yuan, B.A. McClure, and H. Frei. Light-Driven Carbon Dioxide Reduction by Water at Binuclear ZrOCo<sup>II</sup> Unit Coupled to Ir oxide Nanocluster Catalyst. *J. Am. Chem. Soc.* **136**, 11034-11042 (2014).
6. G. Yuan, A. Agiral, N. Pellet, W. Kim, and H. Frei. Inorganic Core-Shell Assemblies for Closing the Photosynthetic Cycle. *Faraday Discuss.* **176**, 233-249 (2014).
7. M. Zhang and H. Frei. Towards a Molecular Level Understanding of the Multi-Electron Catalysis of Water Oxidation on Metal Oxide Surfaces. *Catal. Lett.* **145**, 420-435 (2015).
8. W. Kim and H. Frei. Directed Assembly of Cuprous Oxide Nanocluster Catalyst for CO<sub>2</sub> Reduction Coupled to Heterobinuclear ZrOCo<sup>II</sup> or TiOCo<sup>II</sup> Light Absorber in Mesoporous Silica. *ACS Catal.* **5**, 5627-5635 (2015).
9. E. Edri and H. Frei. Charge Transport through Organic Molecular Wires Embedded in Ultrathin Insulating Inorganic Layer. *J. Phys. Chem. C* **119**, 28326-28334 (2015).
10. W. Kim, B.A. McClure, E. Edri, and H. Frei. Coupling of Carbon Dioxide Reduction with Water Oxidation in Nanoscale Photocatalytic Assemblies. *Chem. Soc. Rev.* **45**, 3221-3243 (2016).
11. W. Kim, E. Edri, and H. Frei. Hierarchical Inorganic Assemblies for Artificial Photosynthesis. *Acc. Chem. Res.* **49**, 1634-1645 (2016).
12. C.F. Kisielowski, H. Frei, P. Specht, I.D. Sharp, J.A. Haber, and S. Helveg. Revisiting the Structure of Spinel Co<sub>3</sub>O<sub>4</sub> Catalysts by Controlling Beam-Induced Sample Alterations in the Vacuum of a Transmission Electron Microscope. *Adv. Struct. Chem. Imag.* **2**, 13 (2016).
13. H. Frei. Water Oxidation Investigated by Rapid-Scan FT-IR Spectroscopy. *Curr. Opin. Chem. Eng.* **12**, 91-97 (2016).
14. H.H. Pham, M.J. Cheng, H. Frei, and L.W. Wang. Surface Proton Hopping and Fast-Kinetics Pathway of Water Oxidation on Co<sub>3</sub>O<sub>4</sub>(001) Surface. *ACS Catal.* **6**, 5610-5617 (2016).

15. R. Alonso-Mori *et al.* Towards Characterization of Photo-Excited Electron Transfer and Catalysis in Natural and Artificial Systems Using XFELs. *Faraday Discuss.* (2017). DOI:10.1039/C6FD00084C.
16. M. Zhang, and H. Frei. Water Oxidation Mechanisms of Metal Oxide Catalysts by Vibrational Spectroscopy of Transient Intermediates. *Annu. Rev. Phys. Chem.* **68** (2017). DOI:10.1146/annurev-physchem-052516-050655
17. H. Frei. Coupling of Metal Oxide Nanoparticle Catalysts for Water Oxidation to Molecular Light Absorbers. *J. Energy. Chem.* **25** (2017). DOI:10.1016/j.jechem.2017.03.001
18. H. Frei. Photocatalytic Fuel Production. *Curr. Opin. Electrochem.* **2** (2017). DOI:10.1016/j.coelec.2017.03.009
19. E. Edri, J. K. Cooper, I. D. Sharp, D. Guldi, and H. Frei. Ultrafast Charge Transfer between Light Absorber and  $\text{Co}_3\text{O}_4$  Water Oxidation Catalyst across Molecular Wires Embedded in Silica Membrane. *J. Am. Chem. Soc.* **139** (2017). DOI:10.1021/jacs.7b01070

## Intriguing Excited State Behavior of Ternary Semiconductor and Hybrid Perovskite Nanostructures

Jacob B. Hoffman, Danilo H. Jara, Seog J. Yoon, Subila Balakrishna  
and Prashant V. Kamat

Radiation Laboratory, and Department of Chemistry and Biochemistry  
University of Notre Dame, Notre Dame, IN 46556

Ternary semiconductor quantum dots (QDs) such as  $\text{CuInS}_2$  recently have gained prominence because of their tunable excited state properties. Their visible photoluminescence, well matched bandgap to the solar spectrum (1.5 eV) and exclusion of heavy metals make them attractive for light harvesting applications. Despite the increased interest in  $\text{CuInS}_2$  QDs, its optical properties are yet to be understood fully. The difficulty of proposing a universal physical model for the charge carrier dynamics of multinary QDs arises from the uncertainties associated with various internal defect states located within the bandgap. Although the reason behind such complexity is not clear, unique electronic properties of I-III-IV semiconductors have been ascribed to nonhomogeneous distribution of elements, size/shape variation and active sub-bandgap states.

$\text{CuInS}_2$  nanocrystals prepared in our laboratory by hot injection method exhibit absorption and emission spectral features that are strongly dependent on the  $[\text{Cu}]:[\text{In}]$  ratio (Figure 1). The excitation and emission spectra indicate presence of two independent optical transitions. These two independent excited states can be resolved by varying excitation laser wavelength in a transient absorption spectrometer. The bleaching of band edge absorption and broad tail absorption bands in the subpicosecond–nanosecond time scale were probed to establish the bandgap and sub-bandgap transitions. The recombination process as monitored by photoemission decay indicated a strong involvement of surface traps. Better understanding of the origin of the optical transitions

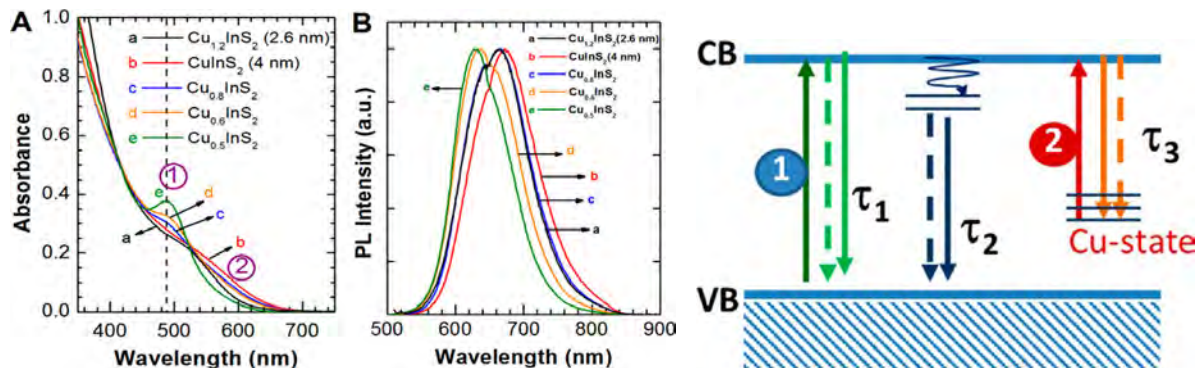


**Figure 1** (A) Absorption spectra, (B) emission spectra ( $\lambda_{\text{ex}} = 490 \text{ nm}$ ), and (C) energy level diagram of  $\text{Cu}_x\text{InS}_2$  QDs with different  $[\text{Cu}]:[\text{In}]$  ratio, dispersed in chloroform. The circled numbers 1 and 2 in panel A indicate the excitonic and Cu-related sub-bandgap transitions, respectively. Scheme on the right shows possible deactivation pathways following excitation of  $\text{Cu}_x\text{InS}_2$ .

and their influence on the photodynamics will enable effective utilization of ternary semiconductor quantum dots in designing new energy conversion systems.

Another class of ternary semiconductors with unusual excited state properties is lead halide perovskite ( $\text{CH}_3\text{NH}_3\text{PbX}_3$  or  $\text{CsPbX}_3$ ). This hybrid perovskite exhibits halide ion composition dependent photochemistry and enables bandgap tuning for selective visible light response. By varying the ratio of Br:I in the mixed halide perovskite ( $\text{CH}_3\text{NH}_3\text{PbBr}_x\text{I}_{3-x}$ ) it was possible to tune the bandgap between 1.55 -2.43 eV. When subjected to visible light irradiation such mixed halide perovskites exhibit migration of halide ions to create iodide-rich and bromide-rich regions. This intriguing aspect of halide ion movement in mixed halide films can be probed through emission and transient absorption spectroscopy. These spectroscopy measurements have allowed us to establish the time scale with which such segregation occurs under laser (405 nm, 25  $\text{mW}/\text{cm}^2$ –1.7  $\text{W}/\text{cm}^2$ ) irradiation as well as dark recovery. While the phase segregation occurs with a rate constant of 0.1-0.3  $\text{s}^{-1}$ , the recovery occurs over a time period of several minutes-hour. The kinetics of the photoinduced segregation and dark recovery becomes slower

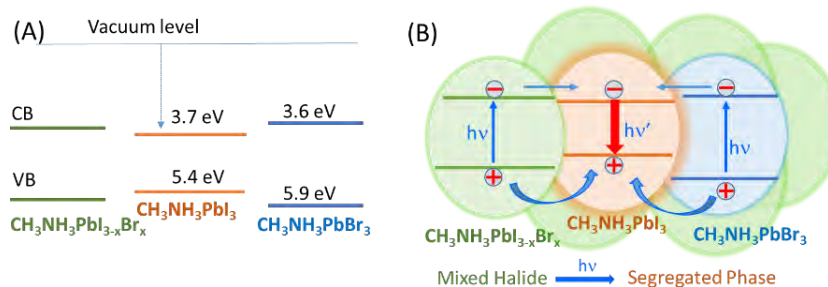


Figure 2. (A) Energy band diagram for mixed halide and phase segregated pairs. Energy level estimates for  $\text{CH}_3\text{NH}_3\text{PbI}_3$  and  $\text{CH}_3\text{NH}_3\text{PbBr}_3$ . (B) Charge separation in phase segregated pairs and transfer of charge carriers to  $\text{CH}_3\text{NH}_3\text{PbI}_3$  sites. I-rich domains serve as charge recombination sites and thus contribute to the observed emission.

in halide deficient films suggesting the involvement of halide defects in the phase segregation. The relative photoluminescence quantum yield for I-rich region (em. max. 760 nm) is nearly two orders of magnitude greater than that of Br-rich region (em. max. 530 nm), thus indicating the dominance of I-rich region to serve as charge recombination centers (Figure 2). We have also prepared nanostructured  $\text{CsPbBr}_{3-x}\text{I}_x$  by selectively exchanging bromide with iodide in a  $\text{CsPbBr}_3$  film. By employing transient absorption spectroscopy we are able to probe transfer of charges through the mixed halide gradient finally accumulating at lower energetic conduction and valence bands of the I-rich region. Understanding such cascading charge transfer from Br-rich region to localized I-rich region is important for designing gradient halide structures in mixed halide systems.

Future efforts will focus on elucidating the excited state properties of  $\text{CsPbBr}_3$  nanocrystals synthesized by hot injection method. Our ability to anchor well-defined Au nanoparticles on cubic perovskite nanocrystals will further allow us to explore the excited state interaction between  $\text{CsPbBr}_3$  and Au nanoparticles and explore their photocatalytic properties. Both solar cell performance evaluation as well as spectroscopic studies will allow us to establish the effectiveness of mixed halide perovskites in solar cells. The ability to vary the gradient composition by halide exchange will allow us to study the effects of light capture and charge transport properties.

## DOE Sponsored Publications 2017-2014

### Invited Reviews (Peer Reviewed, 2016 - 2014):

1. Kamat, P. V., Semiconductor Surface Chemistry as Holy Grail in Photocatalysis and Photovoltaics. *Acc. Chem. Res.* 2017, 50, 527-531
2. Manser, J. S.; Christians, J. A.; Kamat, P. V. Intriguing Optoelectronic Properties of Metal Halide Perovskites *Chem. Rev.* 2016, 116 12956–13008.
3. Manser, J. S.; Saidaminov, M. I.; Christians, J. A.; Bakr, O. M.; Kamat, P. V. Making and Breaking of Lead Halide Perovskites *Acc. Chem. Res.* 2016, 49, 330-338
4. Christians, J. A.; Manser, J. S.; Kamat, P. V., Multifaceted Excited State of  $\text{CH}_3\text{NH}_3\text{PbI}_3$ . Charge Separation, Recombination, and Trapping. *J. Phys. Chem. Lett.*, 2015, 6, 2086-2095
5. Kamat, P. V.; Christians, J. A.; Radich, J. G., *Quantum Dot Solar Cells. Hole Transfer as a Limiting Factor in Boosting Photoconversion Efficiency.* *Langmuir*, 2014, 30, 5716–5725
6. Hines, D. A.; Kamat, P. V., *Recent Advances in Quantum Dot Surface Chemistry.* *ACS Appl Mater. & Interfaces*, 2014, 6, 3041–3057

### Peer Reviewed Research Papers (2016 - 2014):

1. Kobosko, S. M.; Jara, D. H.; Kamat, P. V.,  $\text{AgInS}_2$ – $\text{ZnS}$  Quantum Dots: Excited State Interactions with  $\text{TiO}_2$  and Photovoltaic Performance. *ACS Appl. Mater. & Interfaces* 2017, 9, ASAP, DOI: 10.1021/acsami.1026b14604
2. Hoffman, J. B.; Alam, R.; Kamat, P. V., Why Surface Chemistry Matters for QD–QD Resonance Energy Transfer. *ACS Energy Lett.* 2017, 2, 391-396
3. Balakrishnan, S. K.; Kamat, P. V., Au– $\text{CsPbBr}_3$  Hybrid Architecture: Anchoring Gold Nanoparticles on Cubic Perovskite Nanocrystals. *ACS Energy Lett.* 2017, 2, 88-93
4. Huang, W.; Manser, J. S.; Sadhu, S.; Kamat, P. V.; Ptasinska, S., Direct Observation of Reversible Transformation of  $\text{CH}_3\text{NH}_3\text{PbI}_3$  and  $\text{NH}_4\text{PbI}_3$  Induced by Polar Gaseous Molecules. *J. Phys. Chem. Lett.* 2016, 7, 5068-5073
5. Hoffman, J. B.; Schleper, A. L.; Kamat, P. V. Transformation of Sintered  $\text{CsPbBr}_3$  Nanocrystals to Cubic  $\text{CsPbI}_3$  and Gradient  $\text{CsPbBr}_x\text{I}_{3-x}$  through Halide Exchange *J. Am. Chem. Soc.* 2016, 138, 8603-8611
6. Yoon, S. J.; Draguta, S.; Manser, J. S.; Sharia, O.; Schneider, W. F.; Kuno, M.; Kamat, P. V. Tracking Iodide and Bromide Ion Segregation in Mixed Halide Lead Perovskites during Photoirradiation *ACS Energy Lett.* 2016, 1, 290-296
7. Guo, Z.; Yoon, S. J.; Manser, J. S.; Kamat, P. V.; Luo, T. Structural Phase- and Degradation-Dependent Thermal Conductivity of  $\text{CH}_3\text{NH}_3\text{PbI}_3$  Perovskite Thin Films *J. Phys. Chem. C* 2016, 120, 6394-6401
8. Jara, D. H.; Stamplecoskie, K. G.; Kamat, P. V. Two Distinct Transitions in  $\text{Cu}_x\text{InS}_2$  Quantum Dots. Bandgap versus Sub-Bandgap Excitations in Copper-Deficient Structures. *J. Phys. Chem. Lett.* 2016, 7, 1452-1459
9. Yoon, S. J.; Stamplecoskie, K. G.; Kamat, P. V. How Lead Halide Complex Chemistry Dictates the Composition of Mixed Halide Perovskites *J. Phys. Chem. Lett.* 2016, 7, 1368-1373
10. Huang, W.; Manser, J. S.; Kamat, P. V.; Ptasinska, S., Evolution of Chemical Composition, Morphology, and Photovoltaic Efficiency of  $\text{CH}_3\text{NH}_3\text{PbI}_3$  Perovskite under Ambient Conditions. *Chem. Mater* 2016, 28, 303–311

11. Manser, J. S.; Reid, B.; Kamat, P. V., Evolution of Organic-Inorganic Lead Halide Perovskite from Solid-State Iodoplumbate Complexes. *J. Phys. Chem. C*, 2015, 119, 17065-17073
12. Grigioni I.; Stamplecoskie K.G.; Selli E.; Kamat P.V. Dynamics of photogenerated charge carriers in WO<sub>3</sub>/BiVO<sub>4</sub> heterojunction photoanodes. *J. Phys. Chem. C* 2015, 119, 20792–800
13. Hines, D. A.; Darzi, E. R.; Hirst, E. S.; Jasti, R.; Kamat, P. V., Carbon Nanohoops: Excited Singlet and Triplet Behavior of Aza 8 CPP and 1,15-Diaza 8 CPP *J. Phys. Chem. A*, 2015, 119, 8083-8089
14. Guo, Z.; Manser, J. S.; Wan, Y.; Kamat, P. V.; Huang, L. B., Spatial and temporal imaging of long-range charge transport in perovskite thin films by ultrafast microscopy. *Nature Communications*, 2015, 6, Article No. 7471
15. Stamplecoskie, K. G.; Kamat, P. V., Synergistic Effects in the Coupling of Plasmon Resonance of Metal Nanoparticles with Excited Gold Clusters. *J. Phys. Chem. Lett.*, 2015, 6, 1870-1875
16. Christians, J. A.; Miranda Herrera, P. A.; Kamat, P. V., Transformation of the Excited State and Photovoltaic Efficiency of CH<sub>3</sub>NH<sub>3</sub>PbI<sub>3</sub> Perovskite upon Controlled Exposure to Humidified Air. *J. Am. Chem. Soc.* 2015, 137, 1530–1538
17. Chen, Y.-S.; Manser, J. S.; Kamat, P. V., All Solution-Processed Lead Halide Perovskite-BiVO<sub>4</sub> Tandem Assembly for Photolytic Solar Fuels Production. *J. Am. Chem. Soc.* 2015, 137, 974-981
18. Hines, D. A.; Forrest, R. P.; Corcelli, S. A.; Kamat, P. V., Predicting the Rate Constant of Electron Tunneling Reactions at the CdSe-Linker-TiO<sub>2</sub> Interface. *The Journal of Physical Chemistry B* 2015, 119, 7439-7446
19. Choi, H.; Chen, Y.-S.; Stamplecoskie, K. G.; Kamat, P. V., Boosting the Photovoltage of Dye-Sensitized Solar Cells with Thiolated Gold Nanoclusters. *J. Phys. Chem. Lett.* 2015, 6, 217–223
20. Stamplecoskie, K. G.; Manser, J. S.; Kamat, P. V., Dual Nature of the Excited State in Organic-Inorganic Lead Halide Perovskites. *Energy & Environ.Sci.* 2015, 8, 208 - 215
21. Jara, D. H.; Yoon, S. J.; Stamplecoskie, K. G.; Kamat, P. V., Size-Dependent Photovoltaic Performance of CuInS<sub>2</sub> Quantum Dot-Sensitized Solar Cells. *Chem. Mater.* 2014, 26, 7221–7228.
22. Manser, J. S.; Kamat, P. V., *Band Filling with Charge Carriers in Organometal Halide Perovskites*. *Nature Photonics*, 2014, 8, 737–743
23. Hoffman, J.; Choi, H.; Kamat, P. V., *Size Dependent Energy Transfer Pathways in CdSe Quantum Dot-Squaraine Light Harvesting Assemblies: Förster versus Dexter*. *J. Phys. Chem. C*, 2014, **118**, 18453–18461
24. Stamplecoskie, K. G.; Kamat, P. V., *Size-Dependent Excited State Behavior of Glutathione-Capped Gold Clusters and Their Light-Harvesting Capacity*. *J. Am. Chem. Soc.*, 2014, **136**, 11093–11099
25. Radich, J. G.; Krenselewski, A. L.; Zhu, J.; Kamat, P. V., *Is Graphene a Stable Platform for Photocatalysis? Mineralization of Reduced Graphene Oxide with UV-Irradiated TiO<sub>2</sub> Nanoparticles*. *Chem. Mater.*, 2014, **26**, 4662–4668
26. Radich, J. G.; Peeples, N. R.; Santra, P. K.; Kamat, P. V., *Charge Transfer Mediation through Cu<sub>x</sub>S. The Hole Story of CdSe in Polysulfide*. *J. Phys. Chem. C*, 2014, **118**, 16463–16471
27. Becker, M. A.; Radich, J. G.; Bunker, B. A.; Kamat, P. V., *How does a SILAR CdSe film grow? Tuning the deposition steps to suppress interfacial charge recombination in solar cells*. *J Phys Chem Lett.*, 2014, **5**, 1575–1582
28. Kim, J.-P.; Christians, J. A.; Choi, H.; Krishnamurthy, S.; Kamat, P. V., *CdSeS Nanowires. Compositionally Controlled Band Gap and Exciton Dynamics*. *J. Phys. Chem. Lett.*, 2014, **5**, 1103-1109

29. Wang, Y.; Liu, K.; Mukherjee, P.; Hines, D. A.; Santra, P.; Shen, H. Y.; Kamat, P.; Waldeck, D. H., *Driving charge separation for hybrid solar cells: photo-induced hole transfer in conjugated copolymer and semiconductor nanoparticle assemblies*. *Phys Chem Chem Phys*, 2014, **16**, 5066-5070
30. Chen, Y.-S.; Kamat, P. V., *Glutathione Capped Gold Nanoclusters as Photosensitizers. Visible Light Induced Hydrogen Generation in Neutral Water*. *J. Am. Chem. Soc.*, 2014, **136**, 6075–6082
31. Hines, D. A.; Darz, E. R.; Jasti, R.; Kamat, P. V., *Carbon Nanohoops: Excited Singlet and Triplet Behavior of [9]- and [12]-Cycloparaphenylene*. *J Phys Chem A*, 2014, **118**, 1595–1600
32. Christians, J. A.; Fung, R.; Kamat, P. V., *An Inorganic Hole Conductor for Organo-Lead Halide Perovskite Solar Cells. Improved Hole Conductivity with Copper Iodide*. *J. Am. Chem. Soc.*, 2014, **136**, 758–764
33. Christians, J. A.; Leighton, D. T.; Kamat, P. V., *Rate Limiting Interfacial Hole Transfer in Sb<sub>2</sub>S<sub>3</sub> Solid-State Solar Cells*. *Energy & Environmental Science*, 2014, **7**, 1148 - 1158
34. Stampelcoskie, K. G.; Chen, Y.-S.; Kamat, P. V., *Excited-State Behavior of Luminescent Glutathione-Protected Gold Clusters*. *The Journal of Physical Chemistry C*, 2014, **118**, 1370-1376
35. An, T.; Gao, Y.; Li, G.; Kamat, P. V.; Peller, J.; Joyce, M. V., *Kinetics and Mechanism of •OH Mediated Degradation of Dimethyl Phthalate in Aqueous Solution: Experimental and Theoretical Studies*. *Environmental Science & Technology*, 2014, **48**, 641-648

# Structurally-correlated charge carrier dynamics in disordered semiconductors

Erik M. Grumstrup, Eric S. Massaro, Andy H. Hill, Casey L. Kennedy  
Department of Chemistry and Biochemistry  
Materials Science Program  
Montana State University  
Bozeman, MT 59717

Solution-processed, disordered semiconductors have long held promise as low-cost and chemically tunable alternatives to conventional inorganic semiconductors for photovoltaic and photochemical applications, however a fundamental understanding of their optoelectronic properties is often hampered by chemical and structural heterogeneity intrinsically to the fabrication/synthesis approach. To overcome these challenges, we use ultrafast spectroscopy, coupled to far-field optical microscopy to improve spatial resolution beyond what is achievable with ensemble spectroscopic methods. In this talk I'll discuss recent results from structure-correlated ultrafast measurements of individual organic-inorganic and all-inorganic perovskite crystals. I'll also discuss ongoing work aimed at improving spatial resolution in far-field optical techniques to sub-100 nm length scales.

**CH<sub>3</sub>NH<sub>3</sub>PbI<sub>3</sub> Perovskites.** While the excited state dynamics of organic-inorganic hybrid perovskites have been heavily studied in recent years, little is known about what specific parameters influence the charge carrier mobility of the material. We utilized pump-probe microscopy to directly image charge carrier diffusion in 25 single-crystal domains. The measured diffusion constant is directly proportional to the ambipolar charge carrier mobility through the Einstein relation. Our measurements show that, provided transport occurs far from grain boundaries, carrier mobilities in a thin film morphology are on average comparable to those found in carefully grown single crystals. By performing transport measurements as a function of pump power, we also find that mobility is not reduced by carrier-carrier scattering at high excitation densities ( $> 10^{18} \text{ cm}^{-3}$ ). These results point to a combination of a large static relative permittivity and strong carrier-phonon coupling as the primary material parameters which limit carrier transport through the lattice. Because

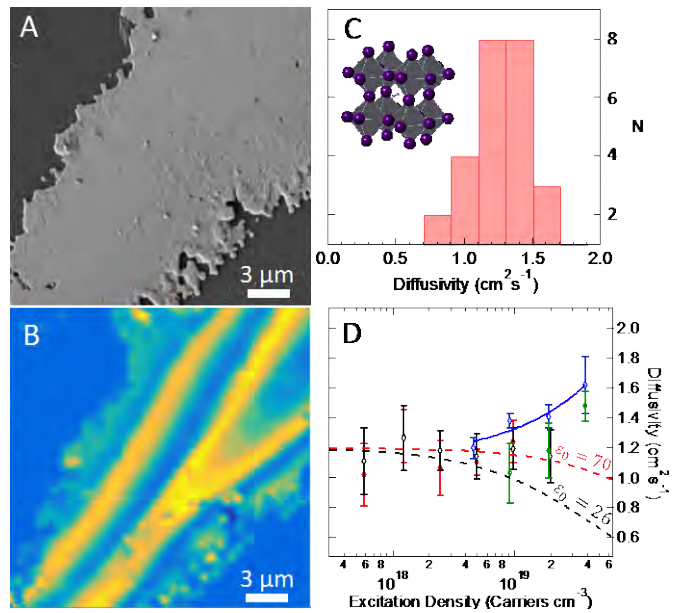


**Figure 1.** (A) SEM image of a single CH<sub>3</sub>NH<sub>3</sub>PbI<sub>3</sub> domain. (B) Correlated transient microscopy image collected at  $\Delta t = 5$  ps. (C) Diffusion constants measured on 25 individual domains. (D) Excitation density-dependent diffusion constants determined for 4 individual domains. Error bars show 90% confidence intervals. Dashed lines show modeled reduction in carrier mobility due to carrier-carrier scattering for two values of the static permittivity. Solid blue line reflects the expected increase in diffusivity as thermally excited conduction band states are occupied at high densities.

carrier-carrier scattering and carrier-trap scattering share a common interaction potential, these results also suggest that trap sites in the lattice play a minimal role in the overall transport characteristics of  $\text{CH}_3\text{NH}_3\text{PbI}_3$  perovskites.

**CsPbI<sub>2</sub>Br Perovskites.** To establish the impacts of chemical substitution on the system of semiconducting perovskites, we have also performed a series of time-resolved microscopy

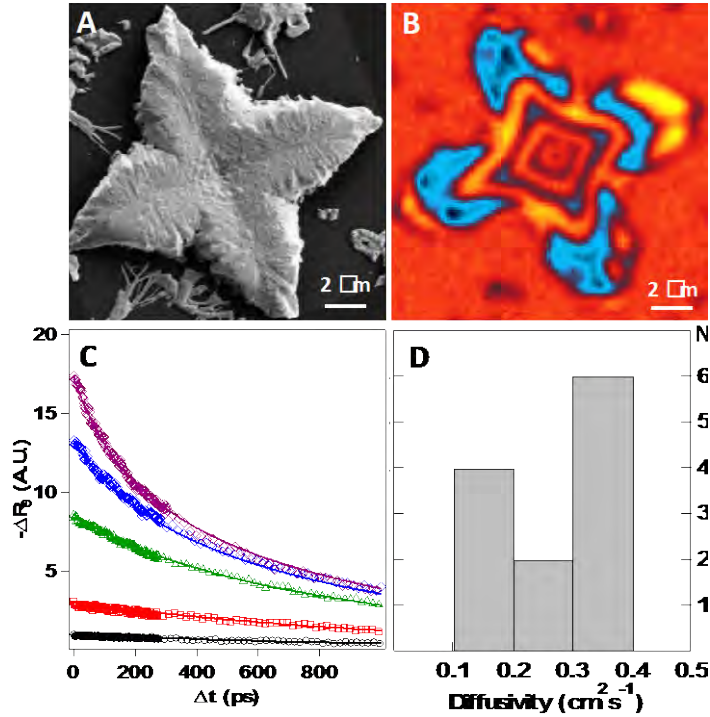


**Figure 2.** (A) SEM image of an individual  $\text{CsPbI}_2\text{Br}$  domain with its corresponding transient reflectivity image in (B). The distinct fringe pattern arises from Fabry-Perot modes supporting the probe wavelength. (C) Global fits (lines) to the data (points) of recombination dynamics in an individual domain. (D) Histogram of diffusion constants collected from 12 individual  $\text{CsPbI}_2\text{Br}$  domains.

measurements on the all-inorganic perovskite  $\text{CsPbI}_2\text{Br}$ . This work focused on the mixed halide perovskite as the pure iodide system,  $\text{CsPbI}_3$ , is stable in its perovskite phase only at elevated temperatures. Despite similar processing conditions as the  $\text{CH}_3\text{NH}_3\text{PbI}_3$  films,  $\text{CsPbI}_2\text{Br}$  forms a qualitatively different morphology, with polycrystalline domains comprised of grains oriented symmetrically around the center. Distinct fringe patterns in transient reflectivity images (Fig. 2) arise from pump-induced shifts to the probe beam Fabry-Perot modes supported in the domain. I'll discuss two key findings that distinguish  $\text{CsPbI}_2\text{Br}$  from its organic-inorganic analogue. First, global fits to power-dependent recombination dynamics do not show a significant contribution from bimolecular, direct recombination at high excitation densities. Rather, a third order Auger recombination mechanism is relevant for excitation densities greater than  $\sim 5 \times 10^{18} \text{ cm}^{-3}$ . Second, we find that the average ambipolar diffusivity is reduced by a factor of five relative to  $\text{CH}_3\text{NH}_3\text{PbI}_3$ . I'll discuss ongoing efforts to determine the morphological and dynamical factors that reduce carrier transport in these  $\text{CsPbI}_2\text{Br}$  domains relative to organic-inorganic hybrids.

**Sub-Diffraction Limited Spectroscopies.** The enhanced spatial resolution provided by optical microscopy enables structural and compositional correlation on length scales greater than  $\sim 200$  nm, however many morphological and chemical heterogeneities in disordered semiconductors fall below the diffraction limit. To provide further insight into this nanoscale regime, our group is developing a variety of techniques which improve the spatial resolution of time-resolved, far-field spectroscopies. We have developed and demonstrated structured pump-probe microscopy, which improves spatial resolution over the diffraction limit by a factor of two and enables sample probe volumes of  $\sim 100$  nm fwhm without relying on highly nonlinear light-matter interactions. We are also developing multi-pulse techniques which we anticipate will provide the ability to measure excited state diffusion lengths on the sub-20 nm length scale.

## DOE Sponsored Publications 2014-2017

1. Massaro, E. S.; Hill, A. H.; Grumstrup, E. M., Super-Resolution Structured Pump–Probe Microscopy. *ACS Photonics* **2016**, 3 (4), 501-506.
2. Massaro, E. S.; Hill, A. H.; Kennedy, C. L.; Grumstrup, E. M., Imaging theory of structured pump-probe microscopy. *Optics Express* **2016**, 24 (18), 20868.
3. Hill, A. H.; Smyser, K. E.; Kennedy, C. L.; Massaro, E. S.; Grumstrup, E. M., Screened Charge Carrier Transport in Methylammonium Lead Iodide Perovskite Thin Films. *Journal of Physical Chemistry Letters* **2017**, 8 (5), 948-953.
4. Massaro, E. S.; Grumstrup, E. M., Label-Free Saturated Structured Excitation Microscopy. *Photonics* **2017**, Submitted.
5. Kennedy, C. L.; Hill, A. H.; Massaro, E. S.; Grumstrup, E. M., Ultrafast Excited State Transport and Decay Dynamics in Cesium Lead Mixed-Halide Perovskites. *ACS Energy Letters* **2017**, Submitted.

*Session X*

*Spectral Sensitization*



## Development of p-GaP Photocathodes for Dye-Sensitization and Ultramicroelectrode Platforms for the Measurement of Heterogeneous Charge-Transfer Kinetics

Elizabeth Brown, Sudarat Lee, Sofiya Hlynchuk, Molly MacInnes, Mitchell Lancaster, Saurabh Acharya, and Stephen Maldonado  
Department of Chemistry  
University of Michigan  
Ann Arbor, MI, 48109-1055

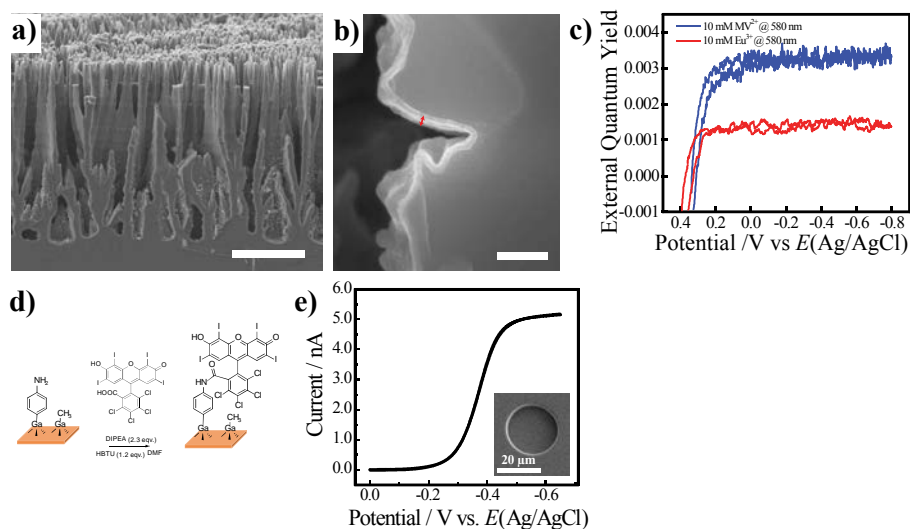


**Figure 1.** Scanning electron micrographs of (a) 40 μm-deep macroporous GaP after 150 cycles ZnO deposition at growth rate of 1.92 Å s<sup>-1</sup> and (b) conformal ZnO films produced by ALD (indicated by red arrows) on the macroporous structures. Scale bars: 20 μm and 200 nm, respectively. c) A comparison of the photocurrents elicited between two redox couples with similar  $E^0$  values ( $\sim -0.6$  V vs  $E(\text{Ag}/\text{AgCl})$ ) but substantially different self-exchange rates on p-GaP(100) coated with adsorbed rose bengal. d) Covalent attachment of an organic chromophore on planar p-GaP(111)A derivitized with  $-\text{CH}_3$  and  $-p$ -aniline groups. e) Representative response for a 10 micron radius n-Si ultramicroelectrode disk immersed in aqueous solution containing 0.1 M KCl and 0.002 M  $\text{Ru}(\text{NH}_3)_6\text{Cl}_3$ . Fit of the data correspond to  $k_{\text{et}} = 10^{-16}$  cm<sup>4</sup> s<sup>-1</sup>,  $E_{\text{cb}} = -0.45$  V, and a diode quality factor of 1.4.

This presentation will highlight the recent progress our group has made on advancing the concept of sensitized p-type gallium phosphide (p-GaP) photocathodes with high-aspect-ratio electrode form factors. The goal is to demonstrate a platform with two features. (1) Deleterious recombination processes are minimized by an electrode with a strong internal electric field that rapidly directs injected holes away from the semiconductor/electrolyte interface. (2) The electrode morphology still presents enough surface area that appreciable dye loading is possible that enables absorption of a large fraction of the visible spectrum. Three separate topics on these fronts will be described.

First, a route for the assembly of high-aspect-ratio GaP electrodes with controllable p-type doping will be presented. Macroporous p-GaP films have been prepared through a multi-step process involving anodic etching of intrinsic GaP wafers. Conformal coating of these materials with zinc oxide (ZnO) by atomic layer deposition (ALD) serves as a p-type dopant source upon thermal annealing (Figures 1a,b). Data will be shown to support the contention that the resultant

macroporous films retain a high surface area structure with sufficient p-type doping to sustain an appreciable internal electric field. Preliminary data where this strategy is applied to GaP nanowire films prepared by vapor-liquid-solid crystal growth with metal catalysts will be discussed.

Second, progress on the identification of ideal sensitizer/redox couple combinations will be described (Figure 1c). In addition, three distinct strategies to couple a molecular chromophore and/or electrocatalyst to the surface of crystalline GaP will be shown. (1) The utility in purposely derivitizing p-GaP surfaces with organic moieties bonded to the surface through Ga-C linkages will be presented. Data will be shown and discussed where GaP(111)A surfaces are functionalized with *p*-aniline groups that are then used to attach a species through a second surface reaction (Figure 1d). Additionally, the preparation of triarylmethane dyes as Grignard reagents will be discussed as a means to directly attach a chromophore on the surface of p-GaP. The benefits and limitations of each approach will be mentioned. (2) An alternative approach based on thin graphene or reduced graphene oxide (r-GO) coatings will be presented. With these coatings, it is possible to chemisorb aromatic species on the surface of any electrode coated with graphene or r-GO. We will demonstrate sensitization of p-GaP in this way as a means to bypass the necessity of forming bonds directly with atop Ga or P atoms. (3) We will present preliminary findings that suggest thin oxide coatings (e.g. ZnO coatings prepared by ALD) also enable the binding of, and hole injection from, dyes to the surface of p-GaP. The possible role of excess Zn<sup>2+</sup> in the film will be discussed.

Third, a new strategy for the measurement of heterogeneous charge-transfer reactions at semiconductor electrodes will be discussed. Motivated by difficult-to-interpret observations in the current-potential responses of modified, macroscale semiconductor electrodes, we have begun utilizing semiconductor ultramicroelectrode (UMEs) platforms for quantitative kinetic study. This work is inspired by the ample precedent with metal UMEs for measurement of heterogeneous charge-transfer rate constants through the analysis of steady-state current-potential responses. Although the microelectrode premise is general to all electrode material types, almost no work has been done to utilize the defined interplay between kinetic and radial diffusion at semiconductor/electrolyte processes. We first show a methodology to fabricate semiconductor disk ultramicroelectrodes (SUMEs) and discuss the advantages/limitations imposed by the chosen electrode geometry (Figure 1e). Second, we discuss basic predictions in the response characteristics of SUMEs for redox processes of outer-sphere, one electron couples, emphasizing both differences from metal UMEs and diagnostic features that describe the quality and energetics of the semiconductor interface. Third, we show preliminary measurements with n-Si SUMEs as a function of size, electrode condition, redox couple, and solvent. Time permitting, a description of how to utilize p-GaP SUMEs with finite-element modelling to measure sensitization processes and test microscopic models of charge transfer will be given.

#### **DOE Sponsored Publications 2014-2017**

1. Peczonczyk, S. L.; Brown E. S.; and Maldonado, S. "*Secondary Functionalization of Allyl-Terminated GaP(111)A Surfaces via Heck Cross-Coupling Metathesis, Hydrosilylation, and Electrophilic Addition of Bromine*" *Langmuir*, **2014**, *30*, 156-164
2. Brown, E. S.; Peczonczyk, S. L.; Wang, Z.; and Maldonado, S. "*Photoelectrochemical Properties of CH<sub>3</sub>-Terminated p-Type GaP(111)A*" *J. Phys. Chem. C.*, **2014**, *118*, 22, 11593-11600
3. Eady, S. C.; Peczonczyk, S. L.; Maldonado, S.; and Lehnert, N. "*Facile Heterogenization of a*

*Cobalt Catalyst via Graphene Adsorption: Robust and Versatile Dihydrogen Production Systems*" *Chem. Comm.*, **2014**, 50, 8065-8068

4. Brown, E. S.; Peczonczyk, S. L.; and Maldonado, S. "*Wet Chemical Functionalization of GaP(111)B Through a Williamson Ether-Type Reaction*" *J. Phys. Chem. C.*, **2014**, 119, 1338-1345

5. Brown, E. S.; Hlynchuk, S.; and Maldonado, S. "*Chemically Modified Si(111) Surfaces Simultaneously Demonstrating Hydrophilicity, Resistance Against Oxidation, and Low Trap State Densities*" *Surf. Sci.*, **2016**, 645, 49-55

6. Ilic, S.; Brown, E. S.; Xie, Y.; Maldonado, S.; and Glusac, K. D.; "*Sensitization of p-GaP with Monocationic Dyes: The Effect of Dye Excited-State Lifetime on Hole Injection Efficiencies*" *J. Phys. Chem. C.*, **2016**, 120, 3145-3155

7. Lee, S.; Bielinski, A. R.; Fahrenkrug, E.; Dasgupta, N. P.; and Maldonado, S.; "*Macroporous p-GaP Photocathodes Prepared by Anodic Etching and Atomic Layer Deposition Doping*" *ACS Appl. Mater. Interfaces.*, **2016**, 8, 16178-16185

8. Lee, S.; Wen, W.; and Maldonado, S. "*Comparison of GaP Nanowires Grown from Au and Sn Vapor-Liquid-Solid Catalysts as Photoelectrode Materials*" submitted **2017**

9. MacInnes, M.; Lehnert, N.; and Maldonado, S. "*Reduction of Graphene Oxide with Cobaltocenes*" submitted **2017**

10. Lancaster, M.; Acharya, S.; and Maldonado, S. "*Analysis of the Utility of Recessed Disk Ultramicroelectrodes for Quantitative Analysis of Heterogeneous Charge Transfer Kinetics*" submitted **2017**

11. Lancaster, M.; Acharya, S.; and Maldonado, S. "*Semiconductor Ultramicroelectrodes: Platforms for Studying Semiconductor Interfacial Processes*" in preparation

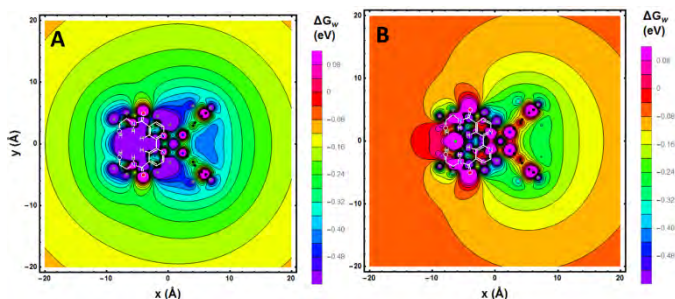
# Electron Transfer Dynamics in Efficient Molecular Solar Cells

Brian DiMarco, Tim Barr, William Ward and Gerald J. Meyer  
Department of Chemistry  
University of North Carolina at Chapel Hill  
Chapel Hill, NC 27510

An important objective of this Department of Energy supported research is to provide new mechanistic insights into surface mediated photochemical processes relevant to solar energy conversion. In this past three years our research has focused on oxidation photo-redox chemistry and on the role surface electric fields play on basic spectroscopic properties of molecular-semiconductor interfaces. Although this research is purely fundamental science, the results and their interpretation have relevance to applications in dye sensitized and photogalvanic solar cells as well as in the storage of solar energy in the form of chemical bonds.

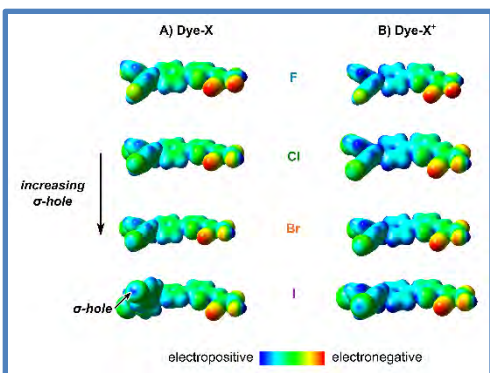
## Dynamic Excited State Electron Transfer in Ion-Pairs

Ion-pair interactions between a cationic ruthenium complex,  $[\text{Ru}(\text{dtb})_2(\text{dea})][\text{PF}_6]_2$ ,  $\text{C1}^{2+}$  where **dea** is 4,4'-diethanolamide-2,2'-bipyridine and **dtb** is 4,4'-di-*tert*-butyl-2,2'-bipyridine, and chloride, bromide, and iodide are reported. A remarkable result is that a 1:1 iodide:excited-state ion-pair,  $[\text{C1}^{2+}, \text{I}^-]^*$ , underwent diffusional electron-transfer oxidation of iodide that did not occur when ion-pairing was absent. The ion-pair equilibrium constants ranged  $10^4$ – $10^6$   $\text{M}^{-1}$  in  $\text{CH}_3\text{CN}$  and decreased in the order  $\text{Cl}^- > \text{Br}^- > \text{I}^-$ . The ion-pairs had longer-lived excited states, were brighter emitters, and stored more free energy than did the non-ion-paired states. The  $^1\text{H}$  NMR spectra revealed that the halides formed tight ion-pairs with the amide and alcohol groups of the **dea** ligand. Electron-transfer reactivity of the ion-paired excited state was not simply due to it being a stronger photooxidant than the non-ion-paired excited state. Instead, work term,  $\Delta G_w$  was the predominant contributor to the driving force for the reaction. Natural bond order calculations provided natural atomic charges that enabled quantification of  $\Delta G_w$  for all the atoms in  $\text{C1}^{2+}$  and  $[\text{C1}^{2+}, \text{I}^-]^*$  presented herein as contour diagrams that show the most favorable electrostatic positions for halide interactions. Part A of the accompanying figure shows the most favorable position in the **dea** ligand for the first halogen ion-pairing, and Part B shows the favorable sites for the second ion-pairing. The results were most consistent with a model wherein the non-ion-paired  $\text{C1}^{2+*}$  excited state traps the halide and prevents its oxidation, but allows for dynamic oxidation of a second iodide ion.



## Evidence for Halogen Bonding in Dye-Sensitized Solar Cells

An enhancement in the photovoltage from dye-sensitized solar cells was observed under conditions where halogen-bonding interactions existed between iodide and the photo-oxidized dye. The triarylamine-based dyes shown displayed larger rate constants for dye regeneration ( $k_{\text{reg}}$ ) by the nucleophilic electrolyte species when heavier halogen substituents were positioned on the

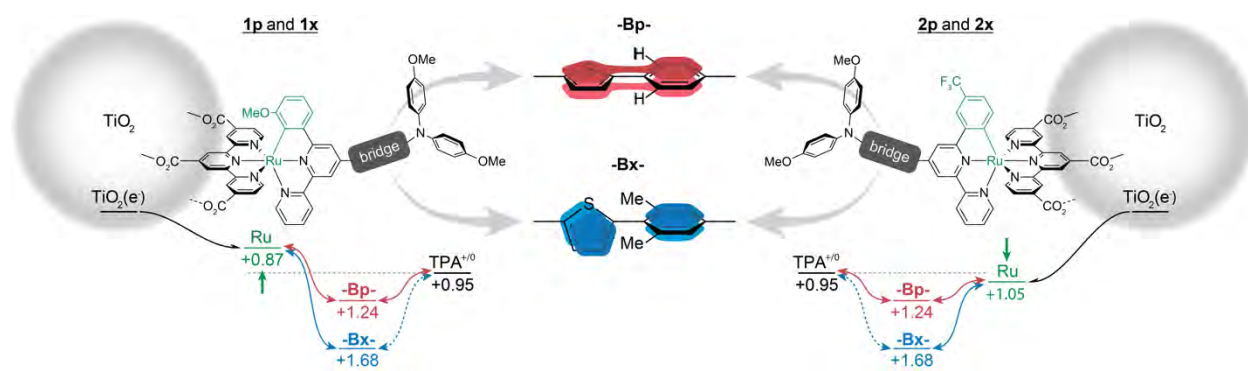


para-positions of the phenyl rings in the dye, Dye-X. The open-circuit voltages tracked these  $k_{\text{reg}}$  values. The density functional theory data shown reveals that the  $\sigma$ -hole responsible for halogen bonding was most pronounced Dye-I, particularly in its one electron oxidized state. This analysis of a homologous series of dyes that differ only in the identity of two halogen substituents provides compelling evidence that the DSSC photovoltage is sensitive to  $k_{\text{reg}}$ . This study also provides the first direct evidence that halogen-bonding interactions between a dye and the electrolyte can bolster

significantly influence light driven interfacial electron transfer reactions.

### Interfacial Electron Transfer Pathways

At molecular dye-semiconductor interfaces, optimization of interfacial electron transfer has previously been accomplished through control of the molecular-semiconductor distance and/or the



free energy that accompanies electron transfer. Recently it was shown that a kinetic *pathway* for electron transfer from a semiconductor to a molecular acceptor exist that can provide an alternative method for controlling interfacial kinetics. The pathway was identified by the rational design of two series of dye molecules where the distance and the driving force were held near parity while only the geometric torsion about a xylyl- (Bx) or phenyl- (Bp) thiophene bridge was varied. An intervalence charge transfer analysis of the one-electron oxidized dyes, revealed that the electronic coupling through the phenyl- bridge was a factor of ten greater than through the xylyl bridge. Comparative studies revealed a significant bridge dependence for electron transfer that could not be rationalized by a change in distance or driving force. Instead the data indicate an interfacial electron transfer pathway that utilizes the aromatic bridge orbitals, most likely by a hole superexchange mechanism. In future work, the electron transfer kinetics will be analyzed by adiabatic and non-adiabatic theoretical models. The magnitude of the electric field generated by the injected electrons is expected to influence the more proximate metal center to a greater extent than the remote triphenyl amine. Evidence for local electric fields comes from the interfacial energetics where it was found that the TPA<sup>+0</sup> redox chemistry was almost Nernstian, while the Ru<sup>III/II</sup> deviated significantly. More direct evidence for fields induced by the injected electrons

will be garnered from future Stark spectroscopic studies of these dyes and dye-sensitized interfaces.

**DOE Sponsored Publications 2014-2017:**

1. Intramolecular Hole Transfer Modulation and Lateral Hole Hopping at the Sensitized TiO<sub>2</sub> Interface. Hu, K.; Robson, K. C. D.; Beauvilliers, E. E.; Schott, E.; Zarate, X.; Arratia-Perez, R.; Berlinguette, C. P.; Meyer, G. J. *J. Am. Chem. Soc.* 2014, *136*, 1034-1046.
2. Donor- $\pi$ -Acceptor Organic Hybrid TiO<sub>2</sub> Interfaces for Solar Energy Conversion. Hu, K.; Robson, K.C.D.; Berlinguette, C.P.; Meyer, G.J. *Thin Solid Films* 2014, *560*, 49-54.
3. Electric Fields and Charge Screening in Dye Sensitized Mesoporous Nanocrystalline TiO<sub>2</sub> Thin Films. O'Donnell, R.M.; Sampaio, R.N.; Barr, T.J. Meyer, G.J. *J. Phys. Chem. C* 2014, *118*, 16976-16986.
4. Ostwald Isolation to Determine the Reaction Order for TiO<sub>2</sub>(e<sup>-</sup>)|S<sup>+</sup> → TiO<sub>2</sub>|S Charge Recombination at Sensitized TiO<sub>2</sub> Interfaces. Brigham, E.C.; Meyer, G.J. *J. Phys. Chem. C* 2014, *118*, 7886-7893.
5. Direct Spectroscopic Evidence for Constituent Heteroatoms Enhancing Charge Recombination at a TiO<sub>2</sub>-Ruthenium Dye Interface. Hu, K.; Severin, H.; Koivisto, B.; Robson, K.; Schott, E.; Arratia-Perez, R.; Meyer, G.J.; Berlinguette, C.P. *J. Phys. Chem. C* 2014, *118*, 17079-17089.
6. Electric Field Control of TiO<sub>2</sub>(e<sup>-</sup>) + I<sub>3</sub><sup>-</sup> → Charge Recombination Relevant to Dye-Sensitized Solar Cells. Sampaio, R.N.; O'Donnell, R.M.; Barr, T.J.; Meyer, G.J. *J. Phys. Chem. Lett.* 2014, *5*, 3265-3268.
7. Direct Spectroscopic Evidence for Constituent Heteroatoms Enhancing Charge Recombination at a TiO<sub>2</sub>-Ruthenium Dye Interface. Hu, K.; Severin, H.; Koivisto, B.; Robson, K.; Schott, E.; Arratia-Perez, R.; Meyer, G.J.; Berlinguette, C.P. *J. Phys. Chem. C* 2014, *118*, 17079-17089.
8. Temperature Dependent Iodide Oxidation by MLCT Excited States. Taheri, A; Meyer, G.J. *Dalton Trans.* 2014, *43*, 17856-17863.
9. Electric Field Control of TiO<sub>2</sub>(e<sup>-</sup>) + I<sub>3</sub><sup>-</sup> → Charge Recombination Relevant to Dye-Sensitized Solar Cells. Sampaio, R.N.; O'Donnell, R.M.; Barr, T.J.; Meyer, G.J. *J. Phys. Chem. Lett.* 2014, *5*, 3265-3268.
10. Iodide Ion-Pairing with Highly Charged Ru Polypyridyl Cations in CH<sub>3</sub>CN. Swords, W.; Li, G.; Meyer, G.J. *Inorg. Chem.* 2015, *54*, 4512-4519.
11. Visible Light Driven Nanosecond Bromide Oxidation by a Ru Complex with Subsequent Br-Br Bond Formation. Li, G.; Ward, W.W.; Meyer, G.J. *J. Am. Chem. Soc.* 2015, *137*, 8321-8323.

12. Kinetic Resolution of Charge Recombination and Electric Fields at the Sensitized TiO<sub>2</sub> Interface. Ward, C.; O'Donnell, R.M.; DiMarco, B.D.; Meyer, G.J. *J. Phys. Chem. C* 2015, *119*, 25273-25281.
13. Cation Dependent Charge Recombination in Dye-Sensitized Solar Cells. DiMarco, B.N.; O'Donnell, R.M.; Meyer, G.J. *J. Phys. Chem. C* 2015, *119*, 21599-21604.
14. A Kinetic Pathway for Interfacial Electron Transfer from a Semiconductor to a Molecule. Hu, K.; Blair, A.D.; Piechota, E.J.; Schauer, P.A.; Sampaio, R.N.; Meyer, G.J.; Berlinguette. C.P. *Nature Chem.* 2016, *8*, 853-859.
15. Interfacial Halogen Bonding. Swords, W.B.; Simon, S.J.C.; Hu, K.; Parlance, F.G.L.; Dean, R.K.; Meyer, G.J.; Berlinguette. C.P. *Angew. Chemie* 2016, *55*, 5956-5960.
16. Halogen Bonding Promotes Higher Dye-Sensitized Solar Cell Photovoltages. Simon, S.J.C.; Parlance, F.G.L.; Swords, W.B.; Kellett, C.W.; Du, C.; Lam, B.; Dean, R.K.; Hu, K.; Meyer, G.J.; Berlinguette, C.P. *J. Am. Chem. Soc.* 2016, *138*, 10406-10409.
17. A Continuous Surface Electric Field Contraction Accompanies Electron Transfer from TiO<sub>2</sub> to Oxidized Sensitizers. Sampaio, R.N.; Li, G.; Meyer, G.J. *ACS Energy Lett.* 2016, *1*, 846-851.
18. Redox Active Ion-Paired Excited States Undergo Dynamic Electron Transfer. Troian-Gautier, L; Beauvilliers, E.N.; Swords, W.B.; Meyer, G.J. *J. Am. Chem. Soc.* 2017, *138*, 16815-16826.

## Electronic and Vibrational Coherence in Heterogeneous Electron Transfer

Baxter Abraham<sup>1</sup>, Jesus Nieto-Pescador<sup>2</sup>, Jolie Blake<sup>1</sup>, Hao Fan<sup>3</sup>, Elena Galoppini<sup>3</sup> and  
Lars Gundlach<sup>1,2</sup>

<sup>1</sup> Department of Chemistry and Biochemistry, University of Delaware, Newark, DE 19716

<sup>2</sup> Department of Physics and Astronomy, University of Delaware, Newark, DE 19716

<sup>3</sup> Department of Chemistry, Rutgers University, Newark, NJ 07102

The objective of this research is to uncover coherence in heterogeneous electron transfer (HET). This task can be roughly split into three steps: Finding a suitable combination of methods, defining a suitable set of molecule/semiconductor combinations, and uncovering signatures of coherence in the 2D signals. These three steps go hand in hand and overlap strongly. The results of this project will lead to a new conceptual view of the first steps of charge separation in HET systems and will benefit a broad range of applied research among which are new approaches to solar energy conversion, photocatalysis and optoelectronics. I will present progress made towards these goals during the past year.

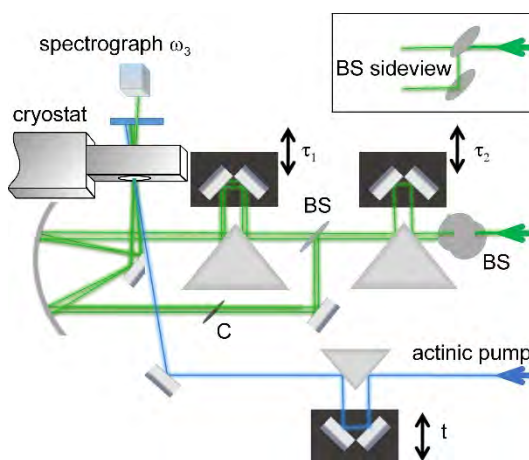


Fig.1 Improved phase stable pump-DFWM/2DES setup.

We developed and commissioned a passively phase-stable four-wave mixing setup (pump-DFWM) that is capable of measuring Raman active modes that couple to electronic excited states in solid-state HET systems in a picosecond time-window (Fig.1). The improved mechanical stability increased the signal-to-noise ratio by about a factor of 2 compared to our previous setup. In addition, the phase-stable design will be exploited during the next phase when we start exploring the addition of an external oscillator to the existing pump-DFWM experiment. A 10 kHz frame rate CCD polychromator based on a pentaprism design was built and commissioned. The camera is synchronized with a 5 kHz chopper and the 10 kHz repetition rate laser system and allows shot-to-shot subtraction of ground state and excited state spectra. Due to the mirrorless prism design the throughput of the polychromator is above 90%. Different schemes for pulse compression were realized and evaluated. Since we already achieved sub- 10 fs pulses with the previous setup, the goal was to simplify the setup and speed-up the alignment procedure for the DFWM NOPA. We now use a combination of chirped mirrors and a prism compressor to generate sub-15 fs pulses on a daily basis without major realignment.

Implementing pump-DFWM measurement on solid-state samples required a combined effort in nanoparticle synthesis and instrument development. Light scattering is a major issue for measurements on nanoparticle films even more so for background-free techniques like DFWM. We evaluated several schemes for reducing the amount of scattered light in the measurement that were mostly combinations of spatial filtering of the signal beam and post-subtraction of background by including additional choppers. We also strengthened our effort to reduce scattering in the film by increasing the homogeneity of particle size and optimizing annealing conditions. We

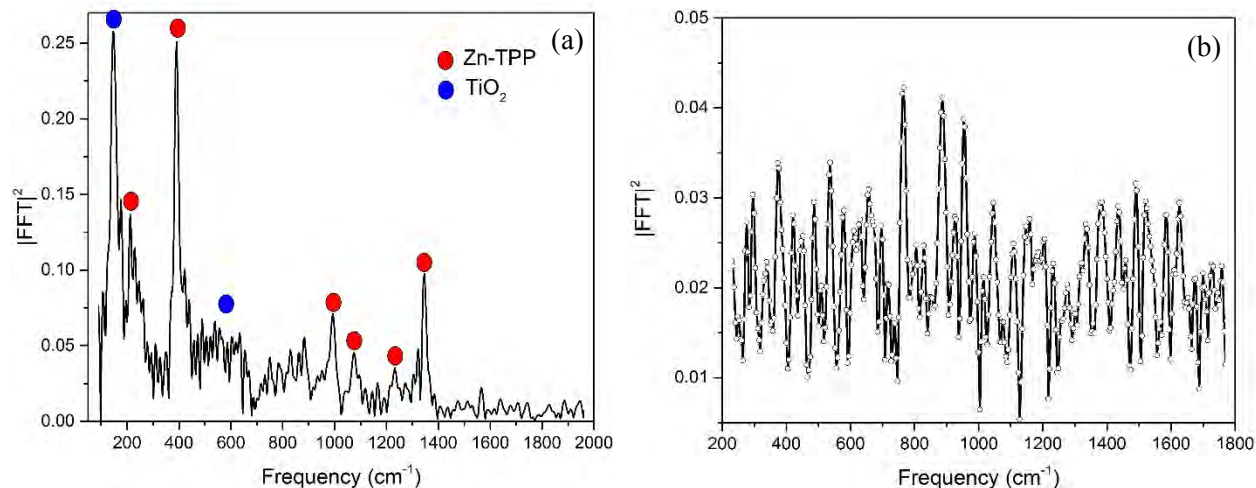


Fig. 2 (a) Solid-state ground state DFWM spectrum of Zn-TTP on TiO<sub>2</sub>. (b) Solid-state pump-DFWM spectrum of Soret band excited Zn-TTP on TiO<sub>2</sub>.

are now able to record ground-state DFWM signals that show Raman active modes of a Zn-TTP derivative photosensitizer adsorbed on TiO<sub>2</sub> colloidal films in vacuum with a signal-to-noise ratio that is only a factor of two smaller than measurements in solution (Fig.2 (a)). All molecular modes that are observed in steady state Raman measurements on solution phase Zn-TTP are found in the solid-state spectrum (red dots). The anatase phonon modes are also clearly visible (blue dots). Anatase TiO<sub>2</sub> shows several weak broad peaks in the region between 400 to 700 cm<sup>-1</sup> that are not clearly resolved. The chromophore is bound via a long bridge group that consist of three phenyl rings. Therefore, no significant shift of the ground state Raman signal was expected upon binding to TiO<sub>2</sub>.

Finally, first pump-DFWM measurements have been performed on a solid-state sample. Zn-TTP/TiO<sub>2</sub> is not an ideal system for initial pump-DFWM measurements due to its spectral and dynamic properties. The lifetime of the excited state is only about 80 fs. Neither the S<sub>2</sub> excited state nor the cation show clear absorption peaks in the excited state that could be exploited for resonance enhancement. Nevertheless, modes at 760 cm<sup>-1</sup> and 880 cm<sup>-1</sup> that cannot be associated with ground state Raman modes has been observed from the molecule after excitation in the Soret band. DFT calculations of the Zn-TTP cation show a vibrational mode between the ground state modes at 400 and 1000 cm<sup>-1</sup> at around 800 cm<sup>-1</sup>. We will start measuring on a perylene derivative (Pe-CH<sub>2</sub>-COOH) sensitized films shortly. DTP-Pe-CH<sub>2</sub>-COOH is planned to be used for initial pump-DFWM measurements because of its advantageous spectral and dynamic properties. Pump-DFWM on solid-state samples has been established and shows very promising first results.

### DOE Sponsored Publications 2014-2017

1. “Ultrafast Relaxation Dynamics of Photoexcited Zinc-Porphyrin: Electronic-Vibrational Coupling”, Baxter Abraham, Jesus Nieto-Pescador and Lars Gundlach, *J. Phys. Chem. Lett.*, (2016) **7**, 3151-3156
2. “Analyte-induced spectral filtering in femtosecond transient absorption spectroscopy”, Baxter Abraham, Jesus Nieto-Pescador and Lars Gundlach, *Journal of Luminescence*, (2017) **187**, 92-95



*Session XI*

*Natural Chromophores*



## **Two-Dimensional Electronic-Vibrational Spectroscopy**

G.R. Fleming, N.H.C.Lewis, T.A.A. Oliver, N.Gruenke  
Molecular Biophysics and Integrated Bioimaging Division  
Lawrence Berkeley National Laboratory  
and  
Department of Chemistry  
University of California Berkeley  
Berkeley CA 94720

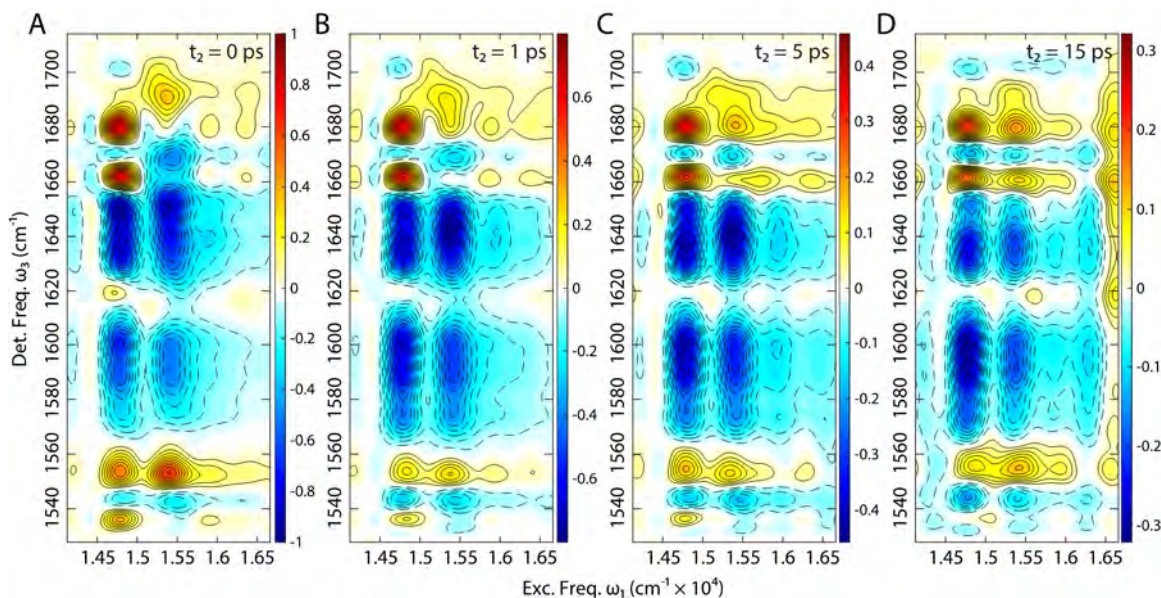
This project aims to reveal the physical and chemical design principles that are utilized in photosynthetic light harvesting and trapping. We rely heavily on ultrafast spectroscopy, theory and modeling. There has been much recent interest in the role of vibrations in ultrafast energy and electron transfer. Debate continues as to the relative importance of electronic, vibronic and vibrational coherences in 2D electronic spectra. Our contributions to this issue are both theoretical and experimental.

On the experimental front we have developed a new two-dimensional spectroscopic technique - two-dimensional electronic-vibrational spectroscopy (2DEV). This method has several unique advantages: it directly correlates the electronic and nuclear evolution potentially enabling clear assignment of specific modes in reactive pathways, and it enables site populations to be obtained without assumption, paving the way to mapping of excitations in real space as a function of time for example a movie of the flow of excitation or electrons in real time, i.e., a movie of the flow of excitation or electrons in real time. We have developed the theoretical models necessary to interpret to 2D spectra and have applied the method to Chla and Chlb in solution and to LHCI. In LHCI we are able to identify specific pathways of relaxation with timescales ranging from 50fs to 10ps. The spectra can be well described by four singular vectors that correspond to (a) overall relaxation of the spectrum, (b) Chlb to Chla transfer and Chla to Chla' relaxation, (c) equilibration to bottleneck states, and (d) resolved intermediates along the relaxation pathway. The data clearly show the Chlb to Chla transfer which is not possible in one- or two- D electronic spectroscopy because exciton levels of mostly Chlb character have very similar energies to excitons of mostly Chla character and their spectra overlap extensively. Our next target is electron transfer in the bacterial reaction center via 2DEV spectroscopy. We have obtained the reaction center in D<sub>2</sub>O (necessary for transmission of the IR wavelengths) through the generosity of Prof Richard Cogdell (Glasgow). With experience on this project we should be able to investigate Photosystem II to explore the role of vibrations in charge separation proposed by van Grondelle and Oglivly.

In collaboration with A. Ishizaki we have examined the role of vibrations in both 2D electronic spectra and in the underlying energy transfer dynamics. This work, which uses the same theory for both the dynamics and the spectroscopy, shows the important role of near resonant vibrations in creating ground state vibrational wave packets. However, when incorporated properly the environmental fluctuations destroy the fragile vibronic coherences very rapidly and they play very little role in the energy transfer dynamics. Our results stand in sharp contrast to the results of other groups and are based on a formally exact solution of the chosen Hamiltonian.

Finally, future plans involve beginning experiments with quantum light (aka entangled photon pairs). Such experiments have not yet been attempted on complex systems, but have the potential to shed light on questions of preparation of internal states, level structures and degrees of delocalization.

Figure 1.



**Two-dimensional electronic-vibrational spectra for LHCII trimers in D<sub>2</sub>O at 77K for a series of waiting times, T. The bands at lower and higher excitation frequency correspond to Chla and Chlb respectively. Sample was provided by Prof R Bassi (Verona).**

### DOE Sponsored Publications 2014-2017

Special note, the development of the apparatus for 2DEV spectroscopy required support by both DOE/BES and by NSF. Therefore several early publications acknowledge both sources and are marked by \*. Applications more easily fit to the specific sources and acknowledge a single supporter.

1. Role of Electronic-Vibrational Mixing in Enhancing Vibrational Coherences in the Ground Electronic States of Photosynthetic Bacterial Reaction Center, Ian S. Ryu, Hui Dong, G.R. Fleming, *J. Phys. Chem. B*, 2014, 3 118, pp 1381–1388.
2. Generalized Master Equation with non-Markovian Multichromophoric Förster Resonance Energy Transfer for Modular Exciton Densities, S. Jang, S. Hoyer, K.B. Whaley and G. R. Fleming, *Phys. Rev. Letters*, 113, 188102 (2014).
3. \*Correlating the Motion of Electrons and Nuclei with Two-Dimensional Electronic-Vibrational Spectroscopy, Thomas A. A. Oliver, Nicholas H. C. Lewis, G. R. Fleming *PNAS*, 111, 28, 10061-10066, doi: 10.1073/pnas.1409207111 (2014).

4. Inhomogeneous Broadening Induced Long-lived Integrated Two-Color Coherence Photon Echo Signal, Hui Dong, G. R. Fleming, *J. Phys. Chem. B*, 118, 30 8956-8961 (2014).
5. Interpreting Coherence Beats in Numerically Exact Simulations of 2D Spectra, D. Monahan, L. Whaley-Mayda, A. Ishizaki, G. R. Fleming, *Ultrafast Phenomena XIX*, pp553-556 (2015).
6. Coherent Exciton Dynamics in the Presence of Underdamped Vibrations, A. G. Dijkstra, C. Wang, J. Cao, G. R. Fleming, *Journal of Phys. Chem. Letters*, 6, 6
7. Determining the static electronic and vibrational energy correlations via two-dimensional electronic-vibrational spectroscopy, H. Dong, N. Lewis, T.A.A. Oliver, G. R. Fleming, *J. Chem. Phys.* 142, 17420 (2015)
8. \*Measuring Correlated Electronic and Vibrational Spectral Dynamics Using Line Shapes in Two-Dimensional Electronic-Vibrational Spectroscopy, N. Lewis, H. Dong, T.A.A. Oliver, G. R. Fleming, *J. Chem. Phys.* 142, 174202 (2015).
9. Impact of environmentally induced fluctuations on quantum mechanically mixed electronic and vibrational pigment states in photosynthetic energy transfer and 2D electronic spectra, Y. Fujihashi, A. Ishizaki, G. R. Fleming, *J. Chem. Phys.* 142, 212403 (2015).
10. Influences of Quantum Mechanically Mixed Electronic and Vibrational Pigment States in 2D Electronic Spectra of Photosynthetic Systems: Strong Electronic Coupling Cases, Y. Fujihashi, A. Ishizaki, G. R. Fleming, *Chinese Journal of Chemistry, Journal of the Chinese Chemical Society*, 63, Issue 1, pp 49-56, (2016).
11. Influence of Weak Vibrational-Electronic Couplings on 2D Electronic Spectra and Inter-Site Coherence in Photosynthetic complexes, D. Monahan, L. Whaley-Mayda, A. Ishizaki, G. R. Fleming, *Journal of Chemical Physics*, 143, 65101 (2015).
12. A Method for the Direct Measurement of Electronic Site Populations in a Molecular Aggregate Using Two-Dimensional Electronic-Vibrational Spectroscopy, N.H.C. Lewis, H. Dong, G. R. Fleming, *J. Chem. Phys.*, 143, 124203 (2015)
13. Quasi-Bell inequalities from symmetrized products of noncommuting qubit observables. O. Gamel and G.R. Fleming *J Math Phys* (In Press) (2017)
14. Disorder-Induced Quantum Beats in Two-Dimensional Spectra of Excitonically Coupled Molecules, V. Butkus, H. Dong, D. Abramavicius, L. Valkunas and G. R. Fleming, *J. Phys. Chem. Lett.*, 7, pp 277-282 (2016).
15. Molecular Science is Central to a Sustainable Future, G. R. Fleming, *IMS Letters*, 73, March (2016).
16. Renewables need a grand-challenge strategy. A. Bernstein, E.H. Sargent, A. Aspuru-Guzik, R. Cogdell, G.R. Fleming, R. Van Grondelle, M. Molina, et al, *Nature*, pp 538 (2016)

## Fundamental Studies of the Vibrational, Electronic, and Photophysical Properties of Tetrapyrrolic Architectures

David F. Bocian,<sup>1</sup> Dewey Holten,<sup>2</sup> Christine Kirmaier,<sup>2</sup> and Jonathan S. Lindsey<sup>3</sup>

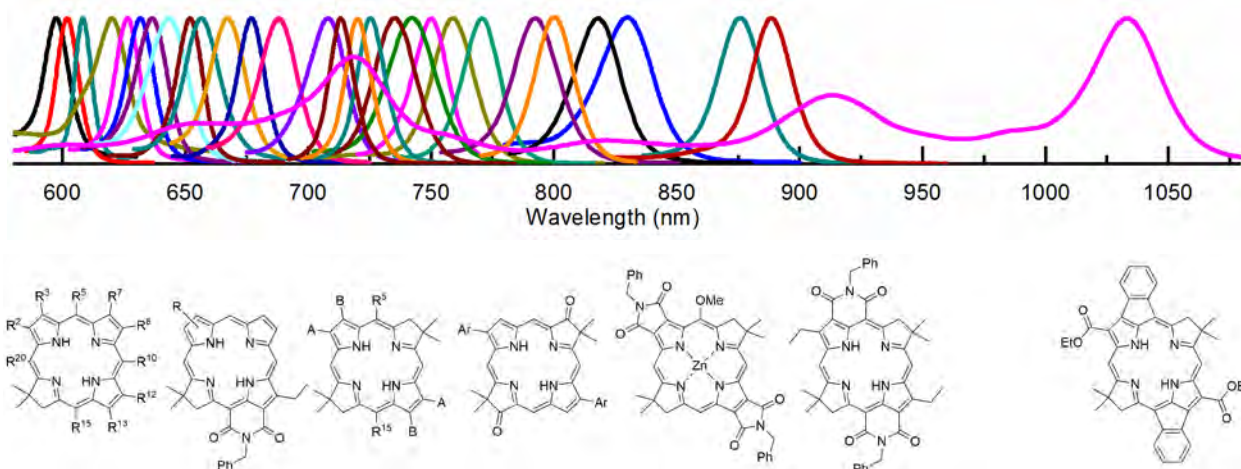
<sup>1</sup>Department of Chemistry, University of California Riverside, Riverside, CA 92521

<sup>2</sup>Department of Chemistry, Washington University, St. Louis, MO 63130

<sup>3</sup>Department of Chemistry, North Carolina State University, Raleigh, NC 27695

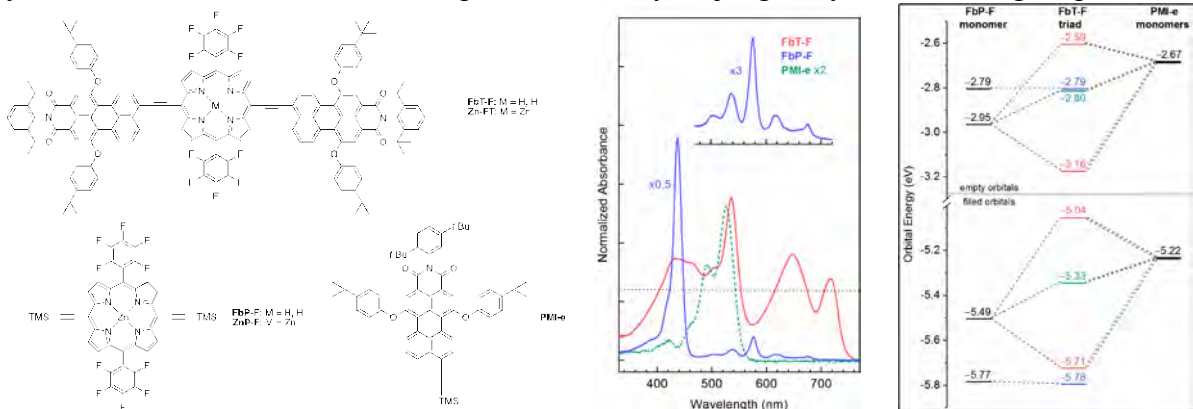
A long-term objective of our program is to design, synthesize, and characterize tetrapyrrole-based molecular architectures that absorb sunlight across the visible and near-infrared spectrum, funnel energy, and separate charge (hole, electron) with high efficiency and in a manner compatible with current and future solar-energy conversion schemes. Particularly noteworthy findings over the past three years are as follows:

Molecular design, synthesis, and characterization (photophysical, redox, molecular orbital) studies have afforded a palette of tunable absorbers spanning the photon-rich red and near-infrared spectral regions. Recent work has focused on novel tetrapyrroles that extend absorption deeper into the near-infrared, past the ~900 nm limit that we had previously attained. The new architectures include annulated bacteriochlorins, one of which has the intense long-wavelength (Q<sub>y</sub>) absorption band at 1033 nm. The near-ultraviolet to near-infrared absorption profiles have been analyzed via density functional theory and four-orbital-model simulations. The rate constants and yields of the singlet excited-state decay pathways (fluorescence, intersystem crossing, and internal conversion) have been characterized. The studies afford molecular design principles for tunable red/near-infrared absorbers for solar-conversion systems.



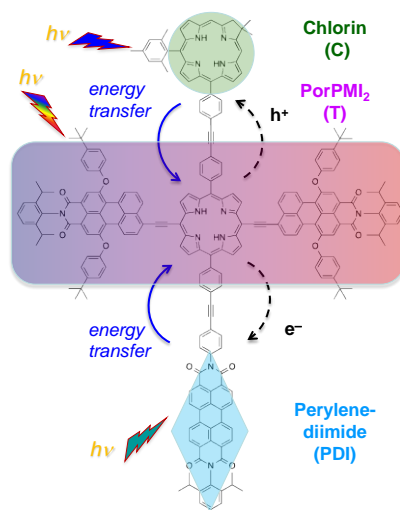
Panchromatic absorbers are potentially valuable for use in molecular-based energy-conversion schemes. An ideal construct would absorb strongly over a broad spectral window and the absorbed energy would flow quantitatively via internal conversion to the discrete lowest excited state, rather than by a stepwise energy cascade between individual sites as in photosynthetic antennas and most synthetic analogues. Our initial studies aimed at understanding the structural features that might lead to panchromatic absorption involved a dyad composed of a simple porphyrin and perylene-monoimide joined by an ethynyl linker. These

studies were extended to multiperylene–porphyrin arrays (triads to pentads) and a variety of tetrapyrrole–chromophore (boron dipyrin, perylene-monoimide, terylene-monoimide) and tetrapyrrole–tetrapyrrole (porphyrin, chlorin, bacteriochlorin, phthalocyanine) architectures. The arrays have variations in the extent of panchromaticity as judged by the wavelength spread and



uniformity of absorption intensity across the spectrum. The arrays generally show long (several nanoseconds) singlet excited-state lifetimes. Studies of the MO characteristics of the arrays reveal the interplay between the spectral properties, extent of inter-chromophore interactions, and the relative energies of the participating orbitals of the units and their electron densities at the attachment sites.

An ultimate goal of our program is to assemble a single architecture that exhibits panchromatic absorption, transfers energy to the lowest excited state, and contains additional components for excited-state electron transfer and ground-state hole transfer. An initial construct in this theme is a triad with two perylene-monoimides strongly coupled via ethynes to a porphyrin. This triad is elaborated with (i) a perylene-diimide (PDI; cyan diamond, bottom) that serves as an electron acceptor, and (ii) a chlorin (C; green circle, top) that serves as an hole trap. The pentad and all subunits (monomers to tetrads) have been studied by static and time-resolved spectroscopy in polar and nonpolar media at 295 and 77 K reveal fast energy transfer and varying degrees of charge separation depending on the array and conditions.



Our present focus concerns several interrelated themes: (i) Gain a deeper understanding of the spectral and electronic properties of bacteriochlorins – and tetrapyrroles in general – with an aim of elucidating the design principles to give wide latitude in tuning these properties for select applications. (ii) Synthesize and characterize the next-generation of integrated architectures that incorporate a panchromatic absorber unit and other molecular components to achieve efficient hole/electron migration and long-lived charge separation. (iii) Test the impact of coherence on photophysical and energy/electron-transfer properties of tetrapyrrole-based assemblies. Collectively, the proposed studies will provide fundamental insights into molecular properties, interactions, and processes relevant to the rational design of molecular architectures for solar-energy conversion.

### DOE Sponsored Publications 2014-2017

1. “Synthesis of 24 Bacteriochlorin Isotopologues, Each Containing a Symmetrical Pair of  $^{13}\text{C}$  or  $^{15}\text{N}$  Atoms in the Inner Core of the Macrocycle,” Chen, C.-Y.; Bocian, D. F.; Lindsey, J. S. *J. Org. Chem.* **2014**, *79*, 1001–1016.
2. “Probing Electronic Communication for Efficient Light-Harvesting Functionality: Dyads Containing a Common Perylene and a Porphyrin, Chlorin, or Bacteriochlorin,” Yang, E.; Wang, J.; Diers, J. R.; Niedzwiedzki, D. M.; Kirmaier, C.; Bocian, D. F.; Lindsey, J. S.; Holten, D. *J. Phys. Chem. B* **2014**, *118*, 1630–1647.
3. “Regioselective  $\beta$ -Pyrrolic Bromination of Hydrodipyrin–Dialkylboron Complexes Facilitates Access to Synthetic Models for Chlorophyll *f*,” Liu, M.; Ptaszek, M.; Mass, O.; Minkler, D. J.; Sommer, R. D.; Bhaumik, J.; Lindsey, J. S. *New J. Chem.* **2014**, *38*, 1717–1730.
4. “Photophysical Properties and Electronic Structure of Retinylidene–Chlorin–Chalcones,” Springer, J. W.; Taniguchi, M.; Krayner, M.; Ruzié, C.; Diers, J. R.; Niedzwiedzki, D. M.; Bocian, D. F.; Lindsey, J. S.; Holten, D. *Photochem. Photobiol. Sci.* **2014**, *13*, 634–650.
5. “NMR Spectral Properties of 16 Synthetic Bacteriochlorins with Site-Specific  $^{13}\text{C}$  or  $^{15}\text{N}$  Substitution,” Chen, C.-Y.; Taniguchi, M.; Lindsey, J. S. *J. Porphyrins Phthalocyanines* **2014**, *18*, 433–456.
6. “Vibronic Characteristics and Spin-Density Distributions in Bacteriochlorins as Revealed by Spectroscopic Studies of 16 Isotopologues. Implications for Energy- and Electron-Transfer in Natural Photosynthesis and Artificial Solar-Energy Conversion,” Diers, J. R.; Tang, Q.; Hondros, C. J.; Chen, C.-Y.; Holten, D.; Lindsey, J. S.; Bocian, D. F. *J. Phys. Chem. B* **2014**, *118*, 7520–7532.
7. “Panchromatic Absorbers for Solar Light-Harvesting,” Alexy, E. J.; Yuen, J. M.; Chandrashaker, V.; Diers, J. R.; Kirmaier, C.; Bocian, D. F.; Holten, D.; Lindsey, J. S. *Chem. Commun.* **2014**, *50*, 14512–14515.
8. “Effects of Substituents on Synthetic Analogs of Chlorophylls. Part 4: How Formyl Group Location Dictates the Spectral Properties of Chlorophylls *b*, *d* and *f*,” Yuen, J.; Harris, M. A.; Liu, M.; Diers, J. R.; Kirmaier, C.; Bocian, D. F.; Lindsey, J. S.; Holten, D. *Photochem. Photobiol.* **2015**, *91*, 331–342.
9. “Progress Towards Synthetic Chlorins with Graded Polarity, Conjugatable Substituents, and Wavelength Tunability,” Ra, D.; Gauger, K. A.; Muthukumaran, K.; Balasubramanian, T.; Chandrashaker, V.; Taniguchi, M.; Yu, Z.; Talley, D. C.; Ehudin, M.; Ptaszek, M.; Lindsey, J. S. *J. Porphyrins Phthalocyanines* **2015**, *19*, 547–572.
10. “Photophysical Properties and Electronic Structure of Chlorin–Imides: Bridging the Gap between Chlorins and Bacteriochlorins,” Faries, K. M.; Diers, J. R.; Springer, J. W.; Yang, E.; Ptaszek, M.; Lahaye, D.; Krayner, M.; Taniguchi, M.; Kirmaier, C.; Lindsey, J. S.; Bocian, D. F.; Holten, D. *J. Phys. Chem. B* **2015**, *119*, 7503–7515.

11. "Extending the Short and Long Wavelength Limits of Bacteriochlorin Near-Infrared Absorption via Dioxo- and Bisimide-Functionalization," Vairaprakash, P.; Yang, E.; Sahin, T.; Taniguchi, M.; Krayner, M.; Diers, J. R.; Wang, A.; Niedzwiedzki, D. M.; Lindsey, J. S.; Bocian, D. F.; Holten, D. *J. Phys. Chem. B* **2015**, *119*, 4382–4395.
12. "De Novo Synthesis of Gem-Dialkyl Chlorophylls for Probing and Emulating our Green World," Lindsey, J. S. *Chem. Rev.* **2015**, *115*, 6534–6620.
13. "Elaboration of an Unexplored Substitution Site in Synthetic Bacteriochlorins," Zhang, N.; Reddy, K. R.; Jiang, J.; Taniguchi, M.; Sommer, R. D.; Lindsey, J. S. *J. Porphyrins Phthalocyanines* **2015**, *19*, 887–902.
14. "Integration of Cyanine, Merocyanine, and Styryl Dye Motifs with Synthetic Bacteriochlorins," Yang, E.; Zhang, N.; Krayner, M.; Taniguchi, M.; Diers, J. R.; Kirmaier, C.; Lindsey, J. S.; Bocian, D. F.; Holten, D. *Photochem. Photobiol.* **2015**, *92*, 111–125.
15. "Effects of Strong Electronic Coupling in Chlorin and Bacteriochlorin Dyads," Kang, H. S.; Esemamoto, N. N.; Diers, J. R.; Niedzwiedzki, D. M.; Greco, J. A.; Akhighbe, J.; Yu, Z.; Pancholi, C.; Bhagavathy, G. B.; Nguyen, J. K.; Birge, R. R.; Kirmaier, C.; Ptaszek, M.; Holten, D.; Bocian, D. F., *J. Phys. Chem. A* **2016**, *120*, 379–395.
16. "Synthesis and Photophysical Characteristics of 2,3,12,13-Tetraalkylbacteriochlorins," Zhang, S.; Kim, H.-J.; Tang, Q.; Yang, E.; Bocian, D. F.; Holten, D.; Lindsey, J. S. *New J. Chem.* **2016**, *40*, 5942–5956.
17. "Bioconjugatable, PEGylated Hydroporphyrins for Photochemistry and Photomedicine. Narrow-Band, Red-Emitting Chlorins," Liu, M.; Chen, C.-Y.; Mandal, A. K.; Chandrashaker, V.; Evans-Storms, R. B.; Pitner, J. B.; Bocian, D. F.; Holten, D.; Lindsey, J. S. *New J. Chem.* **2016**, *40*, 7721–7740.
18. "Bioconjugatable, PEGylated Hydroporphyrins for Photochemistry and Photomedicine. Narrow-Band, Near-Infrared-Emitting Bacteriochlorins," Zhang, N.; Jiang, J.; Liu, M.; Taniguchi, M.; Mandal, A. K.; Evans-Storms, R. B.; Pitner, J. B.; Bocian, D. F.; Holten, D.; Lindsey, J. S. *New J. Chem.* **2016**, *40*, 7750–7767.
19. "Panchromatic Chromophore–Tetrapyrrole Light-Harvesting Arrays Constructed from Bodipy, Perylene, Terrylene, Porphyrin, Chlorin, and Bacteriochlorin Building Blocks," Hu, G.; Liu, R.; Alexy, E. J.; Mandal, A. K.; Bocian, D. F.; Holten, D.; Lindsey, J. S. *New J. Chem.* **2016**, *40*, 8032–8052.
20. "Photophysical Comparisons of PEGylated Porphyrins, Chlorins and Bacteriochlorins in Water," Mandal, A. K.; Sahin, T.; Liu, M.; Lindsey, J. S.; Bocian, D. F.; Holten, D. *New J. Chem.* **2016**, *40*, 9648–9656.
21. "Tuning the Electronic Structure and Properties of Perylene–Porphyrin–Perylene Panchromatic Absorbers," Amanpour, J.; Hu, G.; Alexy, E. J.; Mandal, A. K.; Kang, H. S.; Yuen, J. M.; Diers, J. R.; Lindsey, J. S.; Holten, D.; Bocian, D. F. *J. Phys. Chem. A* **2016**, *120*, 7434–7450.

22. “Photophysical Properties and Electronic Structure of Porphyrins Bearing Zero to Four *meso*-Phenyl Substituents: New Insights into Seemingly Well Understood Tetrapyrroles,” Mandal, A. K.; Taniguchi, M.; Diers, J. R.; Niedzwiedzki, D. M.; Kirmaier, C.; Lindsey, J. S.; Bocian, D. F.; Holten, D. *J. Phys. Chem. A* **2016**, *120*, 9719–9731.
23. “Northern-Southern Route to Synthetic Bacteriochlorins,” Liu, Y.; Lindsey, J. S. *J. Org. Chem.* **2016**, *81*, 11882–11897.
24. “Synthetic Chlorins, Possible Surrogates for Chlorophylls, Prepared by Derivatization of Porphyrins,” Taniguchi, M.; Lindsey, J. S. *Chem. Rev.* **2017**, *117*, 344–535. *Special issue on Light-Harvesting*
25. “Synthesis, Photophysics, and Electronic Structure of Oxobacteriochlorins,” Liu, M.; Chen, C.-Y.; Hood, D.; Taniguchi, M.; Diers, J. R.; Bocian, D. F.; Holten, D.; Lindsey, J. S. *New J. Chem.* **2017**, DOI:10.1039/c6nj04135c.
26. “Construction of the Bacteriochlorin Macrocyclic Ring with Concomitant Nazarov Cyclization To Form the Annulated Isocyclic Ring: Analogues of Bacteriochlorophyll *a*,” Zhang, S.; Lindsey, J. S. *J. Org. Chem.* **2017**, *82*, 2489–2504.

## *Posters*



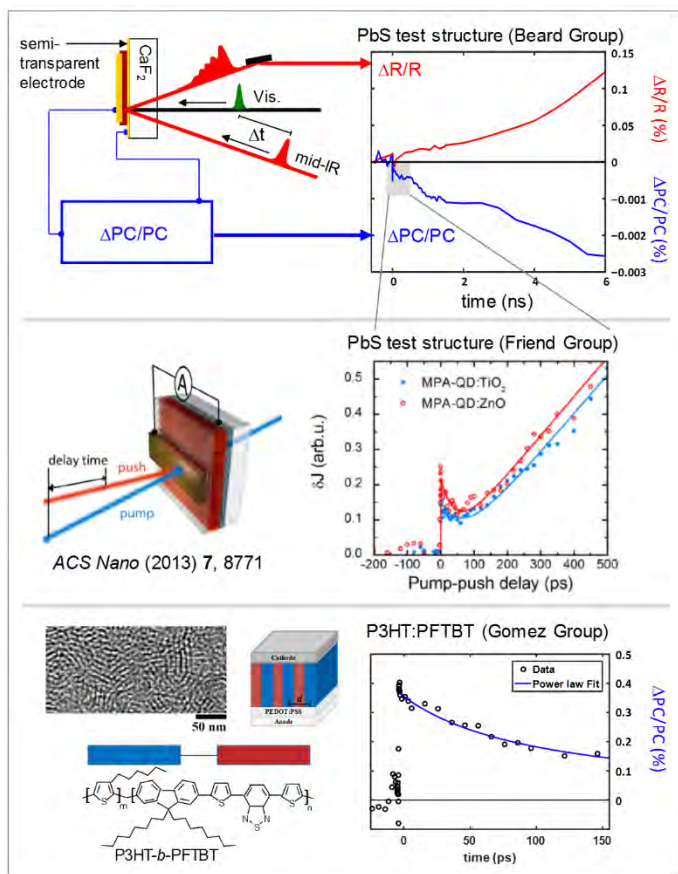
## Molecular and Structural Probes of Defect States in Quantum Dots for Solar Photoconversion

Christopher Grieco, Grayson Doucette, Kyle T. Munson and John B. Asbury  
Department of Chemistry  
The Pennsylvania State University  
University Park, PA 16802

The objective of this research is to develop new electro-optical spectroscopic techniques that allow a direct correlation of molecular structural information about ligand-nanocrystal interactions with the corresponding density and energetic distribution of surface defects and the influence that these defects have on charge transport and recombination in quantum confined nanocrystalline arrays. The insight that is gained will provide a molecular basis for the rational development of novel pathways for the use of quantum dots in systems for solar energy transduction.

Last year, we made significant strides toward realization of photocurrent detected infrared (PDIR) spectroscopy and demonstrated the technique using organic photovoltaic test structures. In these experiments, the ultrafast push pulse served to optically dissociate bound charge transfer states and trapped charge carriers, resulting in positive changes in photocurrent ( $\Delta PC/PC$ ) measured in the PDIR experiments. This year, we extended the technique to study PbS colloidal quantum dot (CQD) test structures provided by the Beard group at the National Renewable Energy Laboratory. Our findings are condensed in a collage of figures appearing below.

Briefly, our studies reveal that the transport and trapping mechanisms operative in organic photovoltaic materials that give rise to significant  $\Delta PC/PC$  signals are not applicable in PbS CQD materials. We believe the push pulse in the PDIR experiment has a positive influence on charge transport in organic materials because of their natively poor transport properties. In contrast, charge transport in PbS CQD materials does not appear to be trap-limited in the same way. The corresponding  $\Delta PC/PC$  signals are dominated by artifacts arising from transient reflectivity of the electrodes used in the test structures. Unfortunately, signals from such artifacts have been interpreted as evidence of push-induced detrapping of carriers in similar PbS CQD materials. We are currently working to develop methods to avoid transient reflectivity artifacts in an effort to realize the original program goals.



## Optoelectronic and Charge Injection Traits of Dyes for Photoelectrochemical Applications

Adam J. Matula, Svante Hedström, Shin Hee Lee, Jianbing Jiang, Robert. H. Crabtree, Gary W. Brudvig and Victor S. Batista

Department of Chemistry, Yale University, New Haven, CT 06520, U.S.A.  
Yale Energy Sciences Institute, Yale University, West Haven, CT 06516, U.S.A.

In any solar energy-driven system, the number of photons harvested limits the amount of energy available. This makes it important to maximize spectral coverage and to ensure that the photons absorbed can be utilized. In this study, we computationally model spectral coverage as well as interfacial electron transfer in two classes of model systems: porphyrin–phenazine dyes and Ru(bpy)<sub>3</sub> compounds with differentially conjugated linker groups.

Light-harvesting molecules that absorb across the entire visible region are known as panchromatic dyes. Porphyrins are successful sensitizer frameworks,<sup>1</sup> but absorb red photons poorly. Here, we have systematically studied the absorption properties of a series of porphyrin–linker–phenazine molecules using TD-DFT to calculate optical transitions. The porphyrin–ethyne–phenazine system shows excellent spectral coverage and a first-pass screening procedure based on its calculated  $\Delta G_{\text{oxidation}}$  and the outer-sphere reorganization energy indicates that the system has great promise as a sensitizer for photoelectrochemical cells.

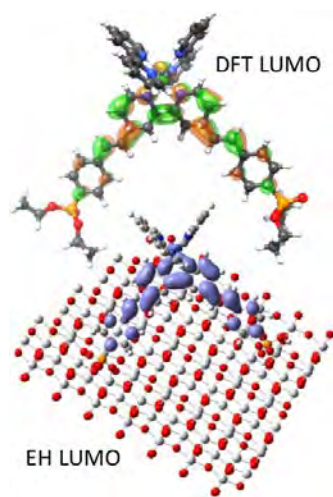


**Figure 2.** LUMO of the Ru<sub>3</sub> dye,<sup>2</sup> calculated with DFT and EH, respectively.

We have examined a series of sensitizers using the same Ru(bpy)<sub>3</sub> chromophoric core but linked to a TiO<sub>2</sub> surface via differentially conjugated linker moieties. Density functional theory was used to verify the character of orbitals calculated with semiempirical Extended Hückel (EH) calculations which were then used for electron-injection dynamics calculations. The conjugation across the linker was found to be vital in determining the interplay between injection and recombination. A delocalized LUMO is favorable for efficient injection, whereas a HOMO localized far from the anchoring group retards the efficiency-limiting recombination process.<sup>2</sup>

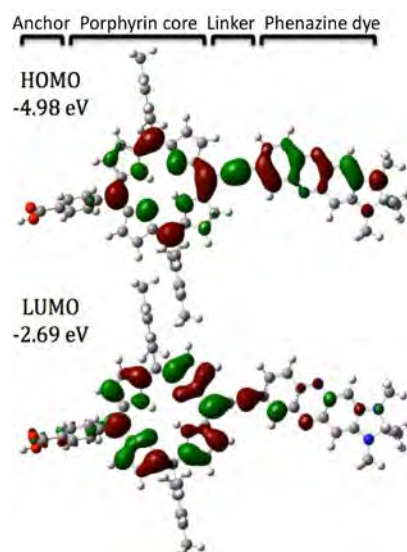


**Figure 1.** HOMO and LUMO of a panchromatic porphyrin–ethyne–phenazine sensitizing dye.

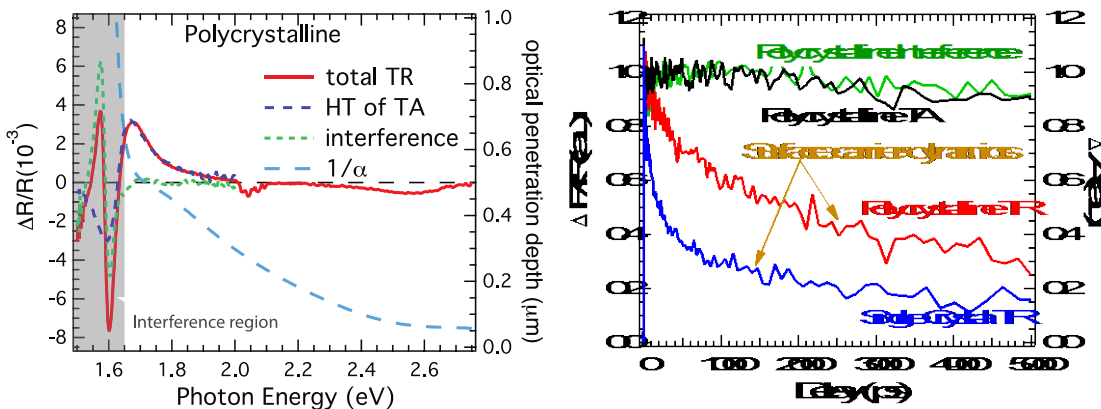
### References

1. Jiang, J; Sweirk, J. R.; Materna, K. L.; Hedström, S.; Lee, S. H.; Crabtree, R. H.; Schmuttenmaer, C. A.; Batista, V. S.; Brudvig, G. W. *J. Phys. Chem. C*, 2016, 120, 28971–28982.
2. Jiang, J; Sweirk, J. R.; Hedström, S.; Matula, A. J.; Crabtree, R. H.; Batista, V. S.; Schmuttenmaer, C. A.; Brudvig, G. W. *Phys. Chem. Chem. Phys.*, 2016, 18, 18678–18682.

## Time-resolved Optical Studies of Perovskite Polycrystalline Films, Single Crystals, Quantum Dots and their Surfaces

Matthew C. Beard, Kai Zhu, Jao van de Lagemaat, Elisa M. Miller, Joseph M. Luther, Ye Yang  
 Chemistry and Nanoscience Center,  
 National Renewable Energy Laboratory  
 Golden, CO 80401

Lead-iodide perovskites are emerging as promising light absorbers for solution-processed thin-film photovoltaic applications. In addition, these materials are also intensively studied for light-emitting diodes, photodetectors, and lasers. Understanding their photophysical properties is crucial for the better design and utilization of these applications. We have used time-resolved transient spectroscopies to better understand both bulk carrier dynamical processes as well as the surface carrier dynamics. We employed transient reflection spectroscopy to measure the surface carrier dynamics in methylammonium lead iodide perovskite single crystals and polycrystalline films. We find that the surface recombination velocity (SRV) in polycrystalline films is nearly an order of magnitude smaller than that in single crystals, likely due to unintended surface passivation of the films during synthesis. In spite of the low SRV, surface recombination limits the total carrier lifetime in polycrystalline thin films, meaning that recombination inside grains and at grain boundaries is less important than top and bottom surface recombination. The suppressed SRV in the polycrystalline films appears to be related to an excess of methylammonium compared to the single crystals surfaces, determined by X-ray photoelectron spectroscopy analysis.



Left Figure. Separating spectral components from bulk and surface in thin-film TR spectroscopy. The TR spectrum captured at a 5 ps delay (red-traces) for the polycrystalline thin films. The Hilbert transform of the transient absorption spectrum (blue-trace) and photo-induced interference (green-trace) deconvolved from the total TR. The cyan-trace is the optical penetration depth as function of photon energy and corresponds to the right axis. The spectral features in the grey shaded region result from the interference in the thin film. Right figure compares the surface dynamics to total carriers in polycrystalline and single crystalline samples.

## Controlling the Endohedral and Exohedral Environment of SWCNTs for Improved Energy Harvesting and Transport

**Jeff Blackburn**,<sup>1</sup> Rachele Ihly,<sup>1</sup> Dylan Arias,<sup>1</sup> Stein van Bezou,<sup>2</sup> Sofie Cambré,<sup>2</sup> Wim Wenseleers,<sup>2</sup> Andrew Ferguson,<sup>1</sup> Justin Johnson<sup>1</sup>

1. National Renewable Energy Laboratory, Golden, CO
2. University of Antwerp, Antwerp, Belgium

Semiconducting single-walled carbon nanotubes (s-SWCNTs) are strong near-IR and visible absorbers, and have high mobilities for excitons and charges. As such, thin films of s-SWCNTs can be used in solar energy harvesting schemes to produce electricity or fuels. While these s-SWCNT films are often depicted solely as networks of SWCNT bundles, devoid of other species, this idealized picture often does not match reality. The surfactants or polymers used to selectively extract s-SWCNTs often remain within the film, and the endohedral volume of the s-SWCNTs is often filled with solvent. This poster describes our recent efforts to *rationally control the endohedral and exohedral environment* of highly enriched s-SWCNTs in ways that are beneficial for energy harvesting and the transport of excitons and charges.

In the first study, we demonstrate the encapsulation of the squaraine dye, Squarylium III (Sqm), in highly enriched s-SWCNTs as a route to enhance light absorption *via* fast excitation energy transfer (EET) from encapsulated dyes to the s-SWCNTs (Figure 1). We demonstrate that encapsulation of small molecules within SWCNTs does not alter the selectivity of polyfluorene polymers for isolating s-SWCNTs, a requirement for efficient solar photoconversion schemes. By tracking the excited state transient absorption signatures of both components, we demonstrate sub-picosecond EET of excitons generated in dye molecules to the surrounding s-SWCNTs. Photoluminescence excitation maps demonstrate that the absorption of encapsulated dye molecules depends sensitively on the diameter of the s-SWCNT in which they are encapsulated. These observations are consistent with a model that considers the s-SWCNT diameter as a constraint that directs the precise geometries of J-aggregate structures that Sqm can adopt within s-SWCNTs. These studies demonstrate that s-SWCNTs have the potential to serve as a unique tool for guiding inter-molecular interactions of spatially-confined molecules and that encapsulation strategies enable hybrid systems with emergent optical and electronic properties, such as new optical transitions and directed energy transport (in the form of excitons or charge carriers), distinct from the individual entities.

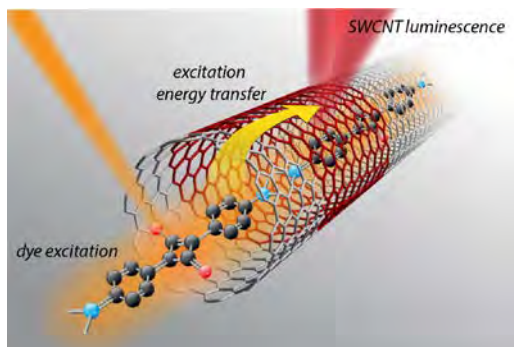


**Figure 1. Cartoon of excitation energy transfer from encapsulated squaraine dye to s-SWCNT**

In the second study, we synthesize “cleavable” polyfluorene-based semiconducting polymers to produce s-SWCNT thin films completely devoid of the sorting polymer. Polyfluorenes have emerged as highly selective agents for extracting s-SWCNTs with high yield, purity, and throughput. However, it has proven to be challenging to quantitatively remove these polymers after selective extraction of s-SWCNTs, so thin films prepared from polyfluorene-based dispersions typically have significant amounts of residual polymer. Since charge and exciton transport within s-SWCNT thin films can be sensitive to the degree of inter-nanotube electronic coupling, the ultimate effects of this residual polymer on transport are unclear although they are likely to be deleterious. Through the use of cleavable polymers, we develop a “solid-state” polymer removal approach that is analogous to the approach adopted in the semiconductor nanocrystal community to improve electronic coupling and charge-carrier mobility in nanocrystal thin films and ordered arrays. The resulting films show improved transport of charge carriers and excitons.

## Charge Transfer Processes in Catalyzed Photoelectrodes for Solar Water Splitting

Shannon W. Boettcher, Jingjing Qui, Michael Nellist, Forrest Laskowski  
Department of Chemistry and Biochemistry  
University of Oregon  
Eugene, OR 97403

Light-absorbing semiconductor electrodes coated with electrocatalysts are key components of photoelectrochemical energy conversion and storage systems. Efforts to optimize these systems have been slowed by an inadequate understanding of the semiconductor-electrocatalyst interface. The semiconductor-electrocatalyst interface is important because it separates and collects photoexcited charge carriers from the semiconductor. The photovoltage generated across the interface drives “uphill” photochemical reactions, such as water splitting to form hydrogen fuel.

In this poster I will describe our latest efforts to understand the microscopic processes and materials parameters governing interfacial electron transfer between light-absorbing semiconductors, electrocatalysts, and solution, using new experimental “dual-working-electrode photoelectrochemistry” approaches.<sup>1</sup> First, we illustrate the operating mechanism of Si photoelectrodes catalyzed/protected by thin Ni metal layers. Efficient photoelectrodes are possible with very thin Ni layers that largely oxidize to NiOOH under operating conditions but retain metallic Ni contacts for hole collection.<sup>2</sup> Second, we show using direct electrical measurements that NiFeO<sub>x</sub> catalyst layers deposited on  $\alpha$ -Fe<sub>2</sub>O<sub>3</sub> are efficient collectors of photoexcited holes, which then drive catalytic oxygen evolution. These measurements directly address a longstanding debate on whether such layers on  $\alpha$ -Fe<sub>2</sub>O<sub>3</sub> indeed are acting as catalysts or only affecting the interface energetics / passivating surface states.<sup>3</sup> Third, we report a new (photo)electrochemical atomic force microscopy technique to monitor hole accumulation, and the resulting potential changes, in catalyst layers in-situ with a conductive nanotip electrode probe. This technique enables the study of catalysts and photoelectrodes that were impossible to analyze by the macroscopic approach used previously.

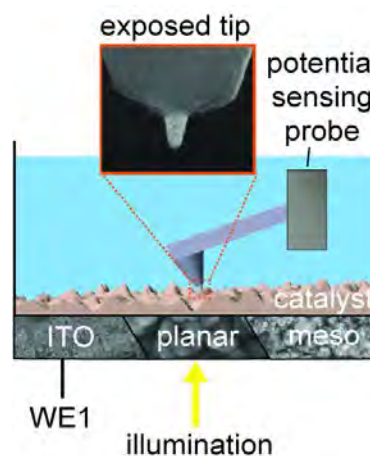


**Fig. 1.** Schematic illustration of (photo)electrochemical AFM technique developed to monitor interface electronic behavior and dynamics *in situ*.

1. Nellist, M. R.; Laskowski, F. A. L.; Lin, F.; Mills, T. J.; Boettcher, S. W., Semiconductor–Electrocatalyst Interfaces: Theory, Experiment, and Applications in Photoelectrochemical Water Splitting. *Acc. Chem. Res.* **2016**, *49* (4), 733-740.
2. Laskowski, F. A. L.; Nellist, M. R.; Venkatkarthick, R.; Boettcher, S. W., Junction behavior of n-Si photoanodes protected by thin Ni elucidated from dual working electrode photoelectrochemistry. *Energy Environ. Sci.* **2017**, *10* (2), 570-579.
3. Qiu, J.; Hajibabaei, H.; Nellist, M. R.; Laskowski, F. A. L.; Hamann, T. W.; Boettcher, S. W., Direct In Situ Measurement of Charge Transfer Processes During Photoelectrochemical Water Oxidation on Catalyzed Hematite. *Submitted*.

## Modular Nanoscale and Biomimetic Systems for Photocatalytic Hydrogen Generation

Kara L. Bren, Richard Eisenberg, Todd D. Krauss  
Department of Chemistry  
University of Rochester  
Rochester, NY14627-0216

The use of light to drive chemical reactions is a promising approach to the production of fuels such as hydrogen ( $H_2$ ). In this collaborative project, we are drawing on synthetic chemistry, materials science, photochemistry and biochemistry to develop integrated systems for light-driven fuel production. These systems include semiconductor quantum dots (QDs) as photosensitizers and synthetic and biomolecular catalysts.

Success with QD photosensitizers for  $H_2$  evolution has motivated our efforts to improve the performance of these systems by engineering QD heterostructures with improved internal charge separation. CdTe/CdSe nanobarbells (Fig. 1) are promising candidates because the staggered band alignment allows for spatial separation of the photoexcited electron and hole, while still allowing for facile charge transfer. Using a Ni-dihydrolipoic acid catalyst and ascorbic acid as the sacrificial electron donor,  $H_2$  evolution studies were performed in water using CdTe/CdSe nanobarbell photocatalysts and compared to results obtained using CdSe QDs of similar diameter. The nanobarbells demonstrated an order of magnitude increase in turnover number (TON) compared to QDs, illustrating a route to improving the performance of integrated solar fuels systems.

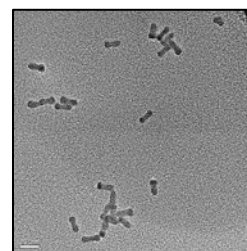


**Fig. 1:** TEM image of CdTe/CdSe/CdTe nanobarbells.

Synthetic molecular catalysts in development include Ni, Co, and Fe bis(dithiolene) complexes with redox-active ligands for charge storage. Pairing these catalysts with QDs capped with inert tridentate ligands has facilitated the analysis of reaction pathways. Biomolecular hydrogen evolution catalysts also are in development. Using biomolecules provides a route to catalysts with precisely tuned metal microenvironments (Fig. 2). We have found that pairing biomolecular catalysts with glutathione-capped QDs as electron donors yields extremely high TON values ( $>100,000$ ) for light-induced  $H_2$  production. Unlike solid-state catalysts and molecular catalysts that are formed in situ, these biological catalysts are well defined structurally, making this a promising system for detailed mechanistic study and optimization.



**Fig. 2:** Synthetic mimochrome artificial hydrogenase.

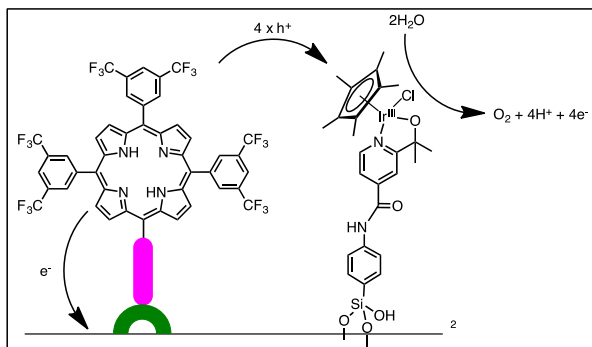
Through the systematic studies of these  $H_2$ -generating systems, a fundamental understanding of initial charge transfer steps, the mechanism(s) of  $H_2$  generation, and sources of system instability is being achieved. In addition, an approach with the goal of eliminating sacrificial electron donors is being pursued through the development of a photoelectrochemical  $H_2$ -generating assembly in which the photocathodes are constructed via sensitization of p-type semiconductor (e.g. NiO) with tunable QD light absorbers.

# Light-Driven Water Oxidation using a High-Potential Porphyrin Photosensitizer and a Molecular Iridium Catalyst

Kelly L. Materna, Jianbing Jiang, Kevin P. Regan, Charles A. Schmuttenmaer, Robert H. Crabtree and Gary W. Brudvig

Department of Chemistry, Yale University, New Haven, CT 06520, U.S.A.  
Yale Energy Sciences Institute, Yale University, West Haven, CT 06516, U.S.A.

The quest to produce renewable fuels using solar energy has focused interest in the development of water-splitting dye-sensitized photoelectrochemical cells, which mimic the processes occurring in photosynthesis. In these cells, the photoanode performs light-driven water-oxidation catalysis using light-harvesting dyes and water-oxidation catalysts. In this study, a series of eight high-potential CF<sub>3</sub>-substituted porphyrins have been designed and synthesized.



Four of these porphyrins bear the amidophenyl linker, but they differ in the anchoring groups: carboxylate, THP-protected hydroxamate, silatrane and phosphonate. The other four porphyrins have longer phenylamidophenyl linkers, and the same four types of anchors. Their electrochemical, photophysical and interfacial electron-transfer properties have been studied by steady-state and time-resolved absorption spectroscopies and THz spectroscopy. Computational work has also been done to evaluate how coupled/decoupled the different anchoring groups are to the semiconducting metal oxides. We assembled photoanodes by using a new high potential CF<sub>3</sub>-porphyrin dye with a THP-protected hydroxamic acid surface-anchoring group (1) and a Cp\*-iridium water-oxidation catalyst containing a silatrane anchoring group (2). These photoanodes have been optimized by choosing water-stable surface anchoring groups that maximize charge injection by the dye and slow charge recombination with the catalyst. Photoelectrochemistry, photostability measurements, transient absorption spectroscopy, and Clark-electrode O<sub>2</sub>-detection measurements were used to study photoanodes with varying surface dye:catalyst ratios in order to identify the optimal composition. Faster hole transfer to the catalyst was observed with lower dye:catalyst ratios using transient absorption spectroscopy, along with less photodegradation of the dye, as detected by IR and UV-visible spectroscopy. A lower dye:catalyst ratio also resulted in a higher rate of photocatalytic O<sub>2</sub> evolution, detected in real-time by using a Clark electrode. Samples prepared using a 2:1 or 8:1 dye:catalyst ratio showed sustained O<sub>2</sub> evolution over twenty hours.

## References

1. Jiang, J.; Swierk, J. R.; Materna, K. L.; Hedström, S.; Lee, S. H.; Crabtree, R. H.; Schmuttenmaer, C. A.; Batista, V. S.; Brudvig, G. W. *J. Phys. Chem. C* **2016**, *120*, 28971–28982.
2. Materna, K. L.; Rudshteyn, B.; Brennan, B. J.; Kane, M. H.; Bloomfield, A. J.; Huang, D. L.; Shopov, D. Y.; Batista, V. S.; Crabtree, R. H.; Brudvig, G. W. *ACS Catal.* **2016**, *6*, 5371–5377.

## Ultrafast Excited State Relaxation and Vibrational Wave-packet Motions in Pt Dimer Complexes

L. X. Chen,<sup>1,2</sup> P. Kim,<sup>1,2</sup> S. E. Brown-Xu,<sup>2</sup> M. S. Kelley,<sup>2</sup> A. Chacaborty,<sup>4</sup> X. Li,<sup>3</sup> F. N. Castellano,<sup>4</sup> G. C. Schatz,<sup>2</sup>

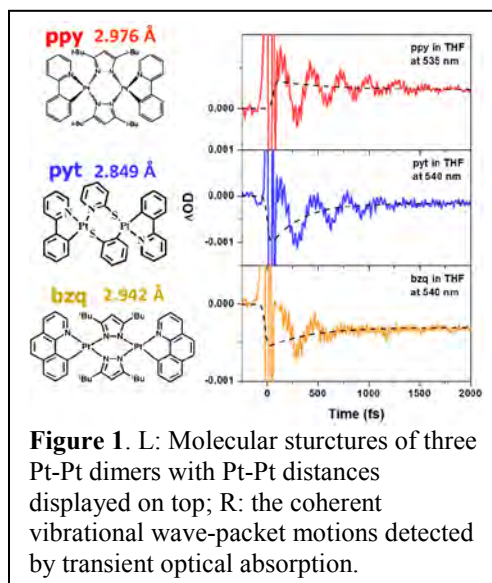
<sup>1</sup>Chemical Sciences and Engineering Division, Argonne National Laboratory, Lemont, IL 60439; <sup>2</sup>Department of Chemistry, Northwestern University, Evanston, IL 60208;

<sup>3</sup>Department of Chemistry, University of Washington, Seattle, WA 98195;

<sup>4</sup>Department of Chemistry, North Carolina State University, Raleigh, NC 27695

The long term goal of the research is to investigate effects of coherent electronic and nuclear motions in the excited state to the excited state relaxation pathways which if understood, can be used to guide synthesis to control excited state relaxation pathways in favor of driving photochemical reactions with minimal loss in the energy converted from photons. Pt(II) complexes may function as sensitizers in solar energy conversion and as catalysts for photochemical transformation. A series of platinum pyrazolate bridged dimers are selected as a platform of structural tuning for optimal excited state pathways for desirable functions. These complexes display progressing changes in optical properties, energy levels and excited state pathways with absorption/emission peaks strongly dependent upon the Pt-Pt distances in the ground state which determine the energy splitting of the  $\sigma$  bonding and  $\sigma^*$  antibonding MOs formed by overlapping the two  $5d_{z^2}$  MOs from the two Pt centers. When the photoexcitation induces electron depletion from  $\sigma^*$  antibonding MO, the apparent Pt-Pt order changes from 0 in the ground state to 0.5 in the excited state causing the shortening of the Pt-Pt distance by  $>0.2\text{\AA}$ , which has been detected via X-ray transient absorption spectroscopy in our previous studies with 100ps time resolution detecting the transient structure of the triplet state.

To follow the excited state trajectory, we recently carried transient absorption measurements on the aforementioned Pt-dimer complexes using sub-30 fs laser pulses in a transient grating setup and found long-lived wave-packet oscillations along the Pt-Pt stretching coordinate. These oscillations imply that the coherence prepared upon the excitation of the singlet MLCT state survives ISC and is transferred from the <sup>1</sup>MMLCT state to the <sup>3</sup>MMLCT state. As the Pt-Pt distance decreases, the lifetime of wave-packet motion is dramatically shortened, indicating a strong dependence of energy relaxation dynamics in the MMLCT state on the energy level of the excited state controlled by the Pt-Pt distance (**Figure 1**). The coherent vibrational wave-packet dynamics observed in this study suggest that the Pt-Pt distance controls the electronic coupling between singlet and triplet MMLCT states which could have significant influence on the excited state lifetime and dynamic energetics of the molecules. Future studies include wave-packet motion phase related photoinduced energy and electron transfer processes in these complexes.



## Photoelectrochemical properties of nanostructured Cu-based photoelectrodes prepared from copper hydroxy double salt precursor films

Allison C. Cardiel, Margaret A Lumley, and Kyoung-Shin Choi

Department of Chemistry  
University of Wisconsin-Madison  
Madison, WI 53706

We have developed new electrochemical synthesis conditions to produce copper hydroxy double salt (Cu-HDS) films. Cu-HDSs are composed of  $\text{Cu}(\text{OH})_2$  layers with a portion of the  $\text{OH}^-$  ions replaced by other anions such as  $\text{Cl}^-$ ,  $\text{NO}_3^-$ , and  $\text{SO}_4^{2-}$ . These layers are held together by Van der Waals interactions. Due to the atomic-level layered structure, HDSs can be grown as films composed of 2D crystals (Figure 1a). These films can serve as precursor films to prepare Cu-containing semiconductors with 3D crystal structures as films with unique nanostructured morphologies, which may not be easily obtained by direct synthesis. In this presentation, we report the electrochemical synthesis of Cu-HDS films and their conversions to CuO and  $\text{Cu}_{11}\text{V}_6\text{O}_{26}$  photoelectrodes. CuO is a p-type semiconductor with a bandgap of 1.2-1.8 eV, which along with its abundance and non-toxicity, makes CuO ideal for use in solar energy conversion. However, CuO suffers from poor charge transport properties, which is typical for oxide-based photoelectrodes. Therefore, nanostructuring can be a useful strategy to shorten the distance that the minority carriers need to travel to reach the interface and thus minimize electron-hole recombination (Figure 1b).  $\text{Cu}_{11}\text{V}_6\text{O}_{26}$  (Figure 1c) is an n-type semiconductor with a bandgap of 1.8 eV that has not been systematically investigated as a photoanode for water oxidation. The photoelectrochemical properties of  $\text{Cu}_{11}\text{V}_6\text{O}_{26}$  and the effect of nanostructures on the photoelectrochemical properties and stability of CuO will be discussed in detail.

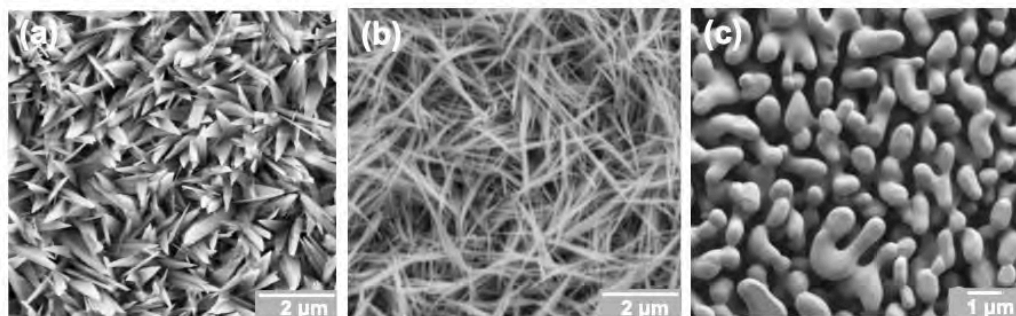


**Figure 1.** (a) SEM image of electrochemically grown Cu-HDS film ( $\text{Cu}_4\text{SO}_4(\text{OH})_6$ ); SEM images of (b) CuO electrode and (c)  $\text{Cu}_{11}\text{V}_6\text{O}_{26}$  electrode obtained from Cu-HDS precursor films.

## Fast single-site molecular water oxidation catalysts: one site is still enough

David W. Shaffer, Yan Xie, Gerald F. Manbeck, David J. Szalda, Javier J. Concepcion  
Chemistry Division  
Brookhaven National Laboratory  
Upton, NY 11973

The generation of solar fuels *via* artificial photosynthesis is a sustainable approach to address many of the challenges of our energy present and future. It requires the development of integrated systems that combine many features including light absorption, charge separation,

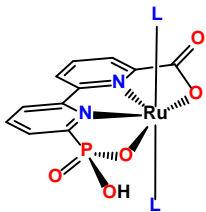


Figure 1. "Hybrid" bpcH catalysts.

water oxidation and water/CO<sub>2</sub> reduction catalysis. Local and bulk proton management, in combination with product separation, are also key requirements for efficient and safe operation. In this poster, we present our progress towards these efforts with a major focus on water oxidation. This reaction has received considerable attention in the last decade due to its relevance in energy conversion and storage and as a way to gain insight into water oxidation in natural photosynthesis. We will present a new family of single-site water oxidation catalysts that outperforms all previously reported molecular catalysts. This is the result of careful catalyst design to enhance fundamental aspects in the water oxidation mechanism from catalyst activation to the key O-O bond formation and O<sub>2</sub> evolution steps. Our catalysts are "hybrid" systems that combine important features from bda-based catalysts<sup>1-3</sup> and multifunctional bpa-catalysts,<sup>4</sup> Figure 1. The carboxylate group from the bda systems is the "gatekeeper" and allows water coordination at the Ru(III) state, Figure 2. This provides access to proton-coupled electron transfer (PCET) processes in the following catalyst activation steps resulting in lower overpotentials and faster rates for these steps. The multifunctional phosphonate group from the bpa systems is the "enforcer" and facilitates O-O bond formation by significantly lowering the activation energy for this step *via* intramolecular atom-proton transfer (IM-APT). In addition, the phosphonate group also provides low energy pathways for oxidative activation steps and oxidation steps preceding O<sub>2</sub> evolution *via* intramolecular PCET (IM-PCET). The results presented in this poster demonstrate that single-site water oxidation catalysis is a viable approach for reaching the required rates for practical applications in solar energy conversion. It also provides support for the potential role of this pathway in the oxygen evolving complex in photosystem II.

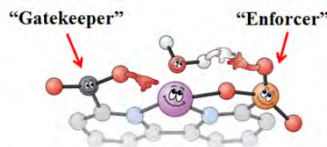


Figure 2. bda side allows IM-PCET; bpa side allows IM-APT.

(1) Mechanism of water oxidation by [Ru(bda)(L)<sub>2</sub>]: the return of the "blue dimer", Concepcion, J. J.; Zhong, D. K.; Szalda, D. J.; Muckerman, J. T.; Fujita, E. *Chem. Commun.* **2015**, 51, 4105.

(2) A molecular ruthenium catalyst with water-oxidation activity comparable to that of photosystem II, Duan, L.; Bozoglian, F.; Mandal, S.; Stewart, B.; Privalov, T.; Llobet, A.; Sun, L. *Nat. Chem.* **2012**, 4, 418.

(3) Manipulating the Rate-Limiting Step in Water Oxidation Catalysis by Ruthenium Bipyridine-Dicarboxylate Complexes, Shaffer, D. W.; Xie, Y.; Szalda, D. J.; Concepcion, J. J. *Inorg. Chem.* **2016**, 55, 12024.

(4) Water Oxidation by Ruthenium Complexes Incorporating Multifunctional Bipyridyl Diphosphonate Ligands, Xie, Y.; Shaffer, D. W.; Lewandowska-Andralojc, A.; Szalda, D. J.; Concepcion, J. J. *Angew. Chem., Int. Ed.* **2016**, 55, 8067.

## Time-Resolved Study of Luminescent Molecular Crystals with Anomalously Short Br...Br Contacts

*Philip Coppens, Krishnayan Basuroy, Sounak Sarkar, Gage Bateman, and Jason Benedict  
Chemistry Department, University at Buffalo, SUNY  
Buffalo, New York 14260-3000.*

The benefit of using organic phosphorescent materials have been limited by their extreme sensitivity towards the surrounding environment (humidity and temperature) and fast non-radiative quenching. Nonetheless, a recent study on purely organic phosphorescent molecules with unusually short Br...Br intermolecular contact distances has been reported.<sup>(1)</sup>

We have recently published the excited state geometry of a Br containing purely organic phosphorescent molecule, studied by means of In-House Time Resolved X-Ray Diffraction<sup>(2)</sup> The crystals contain infinite chains of Br..Br connected molecule and show strong luminescence only in solid state when excited at 355nm. There are no emissions on exposure of dilute dichloromethane solutions. Contrary to a published hypothesis<sup>(1)</sup> we observe in crystals upon light-induced excitation at 90K an increment in the Br...Br intermolecular contact distance from 3.29Å (GS) to 3.38Å (ES) (Fig. 1). The results are qualitatively supported by a DFT calculation.

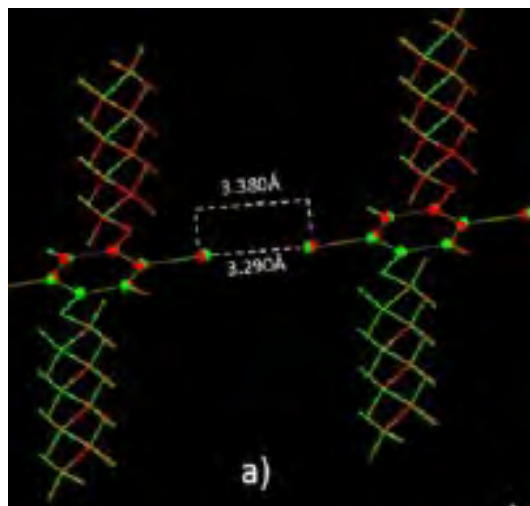


Fig. 1 Atomic shifts in crystals of  $\text{PhBr}_2(\text{O}(\text{CH}_2)_7(\text{CH}_3))_2$  on exposure: Green before exposure; distance=3.290Å, Red after exposure; d= 3.380Å

Recently additional crystals with short Br...Br intermolecular contacts have been reported, but studies are essentially limited to the crystal structure determination. We have synthesized a number of these and are exploring the spectroscopic and structural dynamic properties to explore if the feature is a general property of crystals with short Br...Br contacts, and whether the existence of an infinite chain of connected molecule is an essential feature for luminescence to occur. Results will be reported.

(1) Shi, H. F.; An, Z. F.; Li, P. Z.; Yin, J.; Xing, G. C.; He, T. C.; Chen, H. Z.; Wang, J. G.; Sun, H. D.; Huang, W.; Zhao, Y. L., *Cryst. Growth Des.* **2016**, *16*, 808.

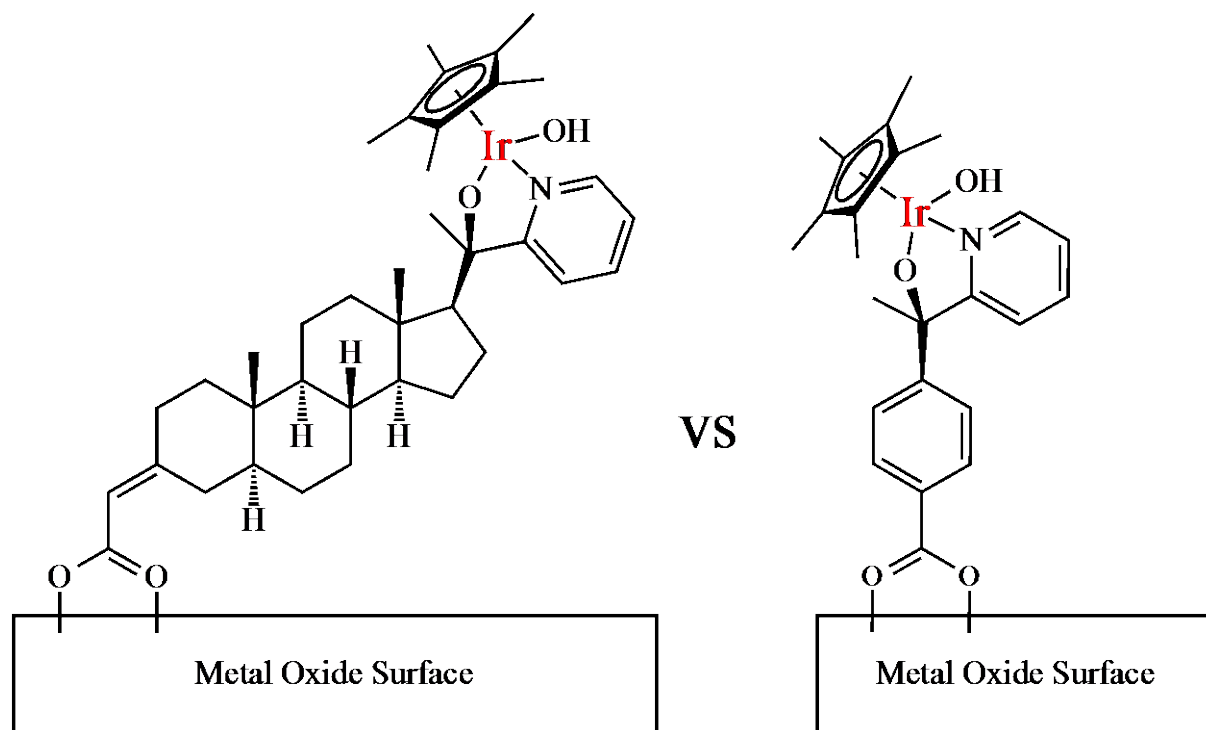
(2) Basuroy, K., Chen, Y., Sarkar, S., Benedict, J. and Coppens, P., *Structural Dynamics* **2017**, *4*, 024501.

## Iridium on Steroids: Covalently Binding Catalytic Centers to Metal-Oxide Surfaces with Rigid, Polycyclic, Aliphatic Molecular Linkers

Aaron J. Bloomfield, Subhajyoti Chaudhuri, Svante Hedström, Victor S. Batista and Robert H. Crabtree

Department of Chemistry  
Yale University  
New Haven, CT 06520

Water-splitting photoelectrochemical cells suffer from very low efficiencies, in large part due to charge-recombination processes, which outcompete the desired catalytic redox reactions. In this study, we set out to retard the rate of charge transfer from an oxidized catalytic metal center to the anode surface that the catalyst is covalently attached to. To this end, a rigid, polycyclic, aliphatic linker molecule was synthesized from a commercially available pregnenolone steroid molecule in five steps. The linker was then used to covalently attach a previously developed catalytically active iridium catalyst species<sup>1,2</sup> to the surface of a mesoporous metal oxide semiconductor film. *Ab-initio* quantum chemistry calculations were used to predict the rates of recombination for this species, as well as multiple synthetically viable alternatives.



1. Schley, N. D.; Blakemore, J. D.; Subbaiyan, N. K.; Incarvito, C. D.; D'Souza, F.; Crabtree, R. H.; Brudvig, G. W.; *J. Am. Chem. Soc.* 2011, *133*, 10473–10481.
2. Materna, K. L.; Rudshiteyn, B.; Brennan, B. J.; Kane, M. H.; Bloomfield, A. J.; Huang, D. L.; Shopov, D. Y.; Batista, V. S.; Crabtree, R. H.; Brudvig, G. W. *ACS Catalysis* 2016, *6*, 5371–5377.

## Multimetallic Systems for the Photocatalytic Production of Fuels from Abundant Sources

Claudia Turro<sup>1</sup> and Kim R. Dunbar<sup>2</sup>

<sup>1</sup>Department of Chemistry and Biochemistry

The Ohio State University

Columbus, OH 43210

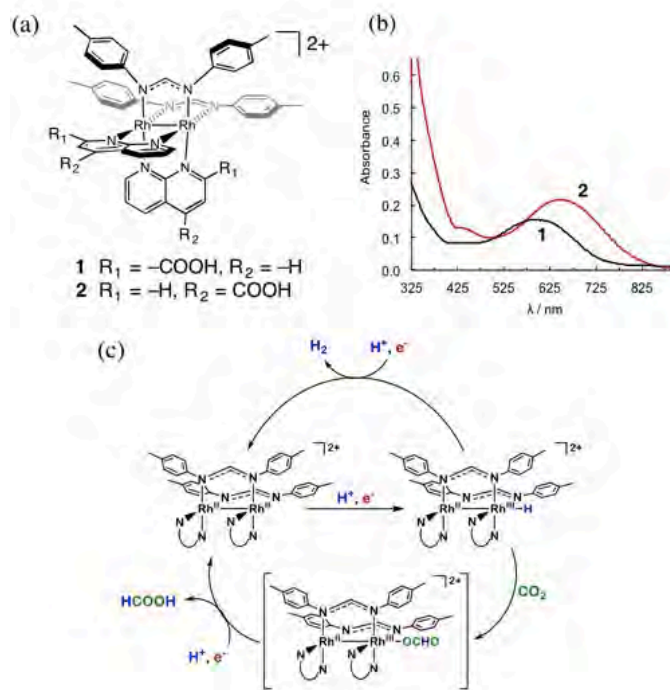
<sup>2</sup>Department of Chemistry

Texas A&M University

College Station, TX 77843

The search for renewable, clean sources of energy is critical for the future of the planet. The use of abundant sunlight to generate electricity or to efficiently and catalytically transform inexpensive simple molecules into clean fuels, such as H<sub>2</sub> from H<sub>2</sub>O and HCOOH from and CO<sub>2</sub>, remains a challenge. Systems for efficient conversion of sunlight into chemical fuels requires strong light absorption that is well-matched to the solar spectrum, catalysts that effect the desired transformation, followed by combining the light absorber (LA) with the catalyst (CAT) into functional LA-CAT architectures. Current LAs used in these applications typically do not absorb the entire solar spectrum efficiently from the ultraviolet, UV, to the near-IR (infrared) range, such that some fraction of photons that make up the solar spectrum are not utilized. We have developed new Rh<sub>2</sub>(II,II) complexes that serve as dyes that absorb light strongly throughout the visible region and into the near-IR. Two examples are shown in the figure (a and b). These compounds are capable of undergoing excited state redox processes, such as the photoinduced reduction of methyl viologen (MV<sup>2+</sup>) and known cobalt electrocatalysts that produce H<sub>2</sub> from protons, as measured using steady-state photolysis in the presence of a sacrificial donor and using transient absorption. In addition, new Rh<sub>2</sub>(II,II) complexes that act as catalysts (CATs) for the reduction of H<sup>+</sup> to H<sub>2</sub> and CO<sub>2</sub> to HCOOH will be presented. The variation of the bridging ligand from formamidinate to acetamide and acetate in these Rh<sub>2</sub>(II,II) catalysts results in increased selectivity toward CO<sub>2</sub> reduction instead of H<sub>2</sub> formation.

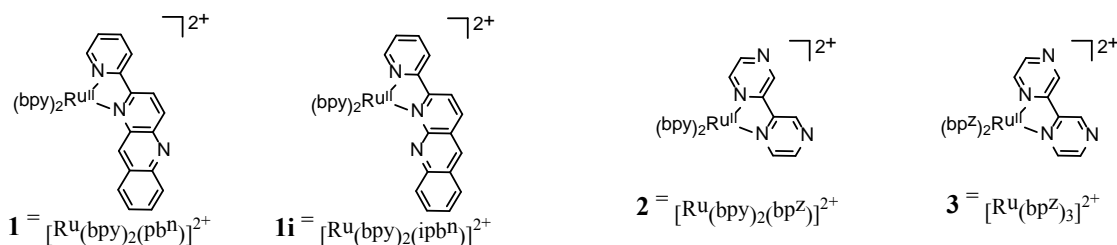
A schematic representation of the proposed mechanism is shown in panel (c) of the figure, where both H<sup>+</sup> and CO<sub>2</sub> reduction proceed via the formation of a Rh<sub>2</sub>(II,III)-H hydride intermediate. The characterization and reactivity of the Rh<sub>2</sub>(II,III)-H intermediate will be presented.



## Computational Investigation of Photoinduced Proton Coupled Electron Transfer from Phenols to Polypyridine Ruthenium Complexes

Mehmed Z. Ertem, Dmitry E. Polyansky, Sergei V. Lyamar  
Chemistry Division  
Energy & Photon Sciences, Brookhaven National Laboratory  
Upton, NY 11973-5000

Proton coupled electron transfer (PCET) plays an important role in natural and artificial photosynthetic transformations, frequently providing low energy pathways in charge separation, charge transport and redox catalysis. PCET reactions involving excited states, especially those of transition metal complexes, are of particular interest due to their relevance to the photoinduced charge transfer in photosynthetic reaction centers and artificial light harvesting systems. In the present work, we employ a combination of kinetic photochemical and computational techniques to investigate the PCET reactivity of Ru polypyridine complexes (Scheme 1) in their MLCT triplet states toward a series of *para*-substituted ( $-\text{NO}_2$ ,  $-\text{Cl}$ ,  $-\text{OCH}_3$ ) phenols covering a large range of Hammett substituent constants.



**Scheme 1.** Ruthenium complexes studied in this work; bpy = 2, 2'-bipyridine, bpz = 2, 2'-bipyrazine.

Density functional theory (DFT) calculations in conjunction with continuum solvation methods for dichloromethane and acetonitrile solvents were performed to map the energetics associated with the stepwise PT-ET, ET-PT and concerted electron proton transfer (EPT) pathways. In addition, constrained DFT (CDFT) calculations were utilized to generate diabatic energy surfaces to compute the rates of nonadiabatic transitions for EPT reactions, which were used to compute kinetic isotope effects associated with deuteration of the phenolic OH group (Figure 1). The computational results, together with the experimental data, provide new insights into PCET reactivity of Ru polypyridine complexes, such as the effect of modification of the PCET mechanism with the change of (i) the solvent polarity and hydrogen-bonding ability, and (ii) the driving force for the stepwise and concerted pathways.

**Acknowledgments:** We thank Prof. Hammes-Schiffer and Dr. Soudackov (U. Illinois, Urbana-Champaign) for insightful discussions, and Prof. Thummel (U. Houston) and Prof. Tanaka (U. Kyoto) for providing samples used in this study.

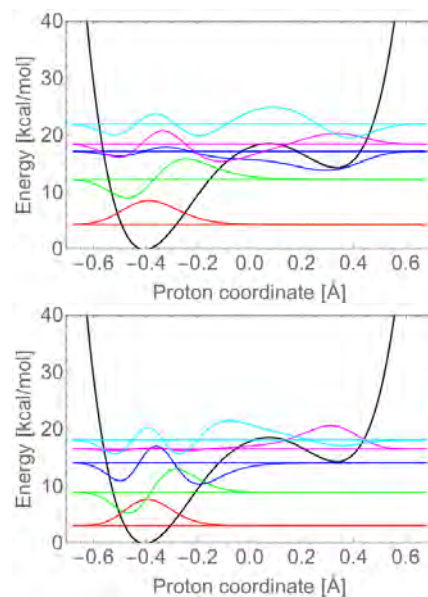


**Figure 1.** Computed diabatic surfaces and vibrational wavefunctions for proton (top) and deuterium (bottom) in reactant state of  $[\text{Ru}(\text{bpy})_2(\text{pbn})]^{2+}$  and *p*-methoxyphenol hydrogen bonded complex.

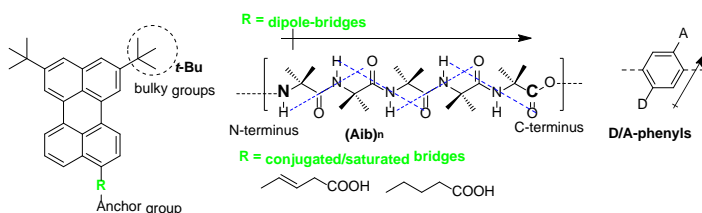
## Bridge Design for Photoactive Molecules at Semiconductor Interfaces

Hao Fan,<sup>1</sup> Ryan Harmer,<sup>1</sup> Sylvie Rangan,<sup>2</sup> Baxter Abraham,<sup>3</sup> Jesus Nieto-Pescador,<sup>4</sup>  
Lars Gundlach<sup>3,4</sup> Robert A. Bartynski<sup>2</sup> and Elena Galoppini<sup>1</sup>

<sup>1</sup>Department of Chemistry, Rutgers University-Newark, Newark, NJ; <sup>2</sup>Department of Physics and Astronomy, Rutgers University-New Brunswick, Piscataway, NJ; Department of <sup>3</sup>Chemistry and <sup>4</sup>Physics Department, University of Delaware, Newark, DE.

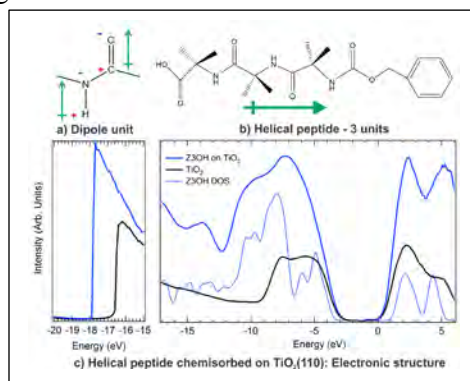
Electron transfer at the interface between a photoactive molecule and large bandgap nanostructured metal oxide semiconductors remains at the center of intense research in numerous areas of solar energy conversion. Such areas encompass photocatalysis and solar fuels, photovoltaics, energy storage, and artificial photosynthesis. An enduring challenge is the ability to achieve control of the chromophore/semiconductor interface at the molecular level. The goal of our DOE-supported research is to address it by a combination of synthetic design and surface studies. The poster will describe the development of “functional” linkers for chromophore-linker model compounds that are able to tune and control the energy level alignment of molecules on nanostructured or single crystal inorganic semiconductors:

**Synthesis.** We synthesized Perylene (Pe) substituted with “functional” linkers compounds. Pe is an important target for heterogeneous charge transfer studies because there is no spectral overlap of the absorption spectra of the ground, excited, and charge separated states of Pe. This



makes the combination perylenes-metal oxide interfaces ideal substrates for pump-probe spectroscopic investigations of the electron transfer processes. The linkers have a dipole, are insulating or conjugated. Syntheses of photo-switchable bridges will also be outlined.

**Surface Studies.** We will describe spectroscopic studies of helical peptides, short-chain dipole molecules and mixed monolayers comprised of chromophore-containing molecules in a matrix of nearly-identical molecules incorporating dipole linkers. Spectroscopic results are compared to first principles calculations assessing the state of the molecules at the surface, the influence of the substrate, and spectroscopic shifts associated with the formation of a dipole layer associated with the active linker portion of the molecule.

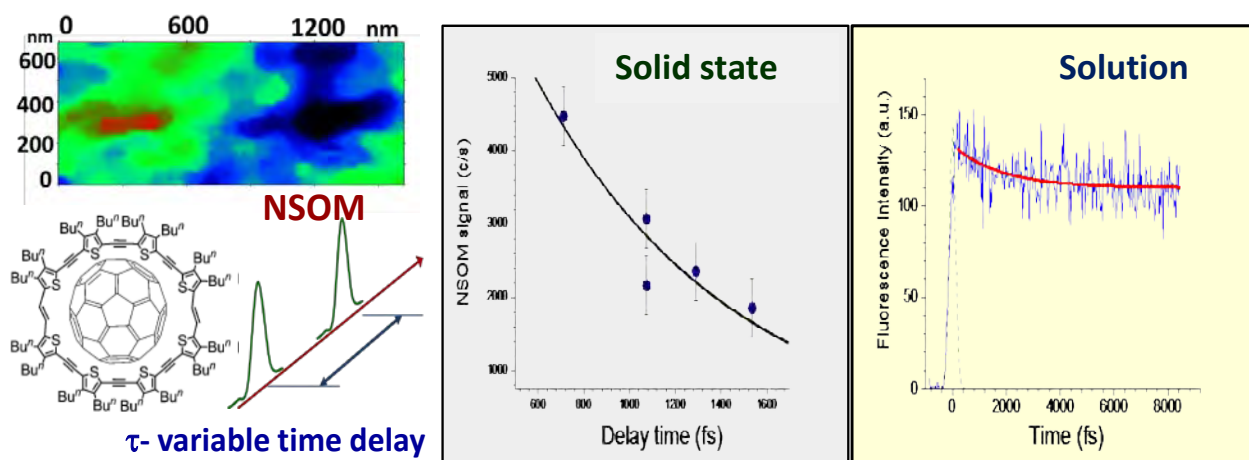


**Heterogenous Charge Transfer studies.** Electronic and vibrational excitation of the chromophore-bridge-anchor molecules are measured before, during and after heterogeneous electron transfer on nanostructured metal oxides by the Gundlach group by ultrafast techniques (white-light pump-probe (WPP), transient absorption (TA), pump-degenerate four-wave mixing (pump-DFWM), and pump-2D electronic spectroscopy (pump-2DES)]. The poster will report the most recent developments in this area.

# Femtosecond Energy Transport Properties with Spatial Resolution Measured in an Organic Solar Cell Film

Oleg Varnavski and Theodore Goodson III  
Department of Chemistry, University of Michigan,  
Ann Arbor, MI, 48109

The solid state organic light conversion devices are known to intrinsically possess substantial structural and electronic inhomogeneity. In order to better understand the local transport dynamics in these systems there is a great need to probe transport processes in the condensed phase and to follow the energy transport dynamics with fast time resolution and high spatial resolution. Here we demonstrate a femtosecond pulse-sequence near field optical microscopy which allows monitoring of the energy migration process in a single light conversion unit. We have investigated the local dynamics of optical excitations in small arrays of cyclic oligothiophene-C<sub>60</sub> complexes which form fiber-like structures. The pulse-pair near-field excitation followed by the fluorescence monitoring provides the information on the local population dynamics with time resolution  $\sim 100$ fs. For isolated oligothiophene-C<sub>60</sub> complexes with no or weak inter-complex interactions we found dynamics related to the intramolecular energy redistribution processes including coupling to the C<sub>60</sub> inside the macrocycle. However, for the case of the strongly coupled macrocycle aggregates the inter-pulse decay time dependence showed a different profile related to the subpicosecond energy transport between complexes.<sup>1</sup>



1. Varnavski, O.; Iyoda, M.; Goodson III, T. Ultrafast Spatially Resolved Dynamics within Ensembles of Cyclic Oligothiophene-C<sub>60</sub> Complexes Studied by Near-field Microscopy *J. Phys. Chem* **2017**, submitted for publication .

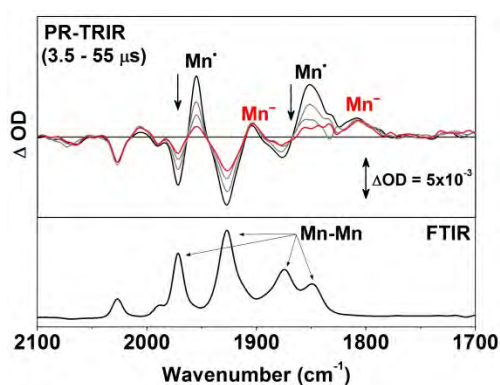
## Kinetic and Mechanistic Investigations of CO<sub>2</sub> Reduction Catalysts

David C. Grills, Mehmed Z. Ertem, Etsuko Fujita, James T. Muckerman, Dmitry E. Polyansky  
Chemistry Division, Brookhaven National Laboratory, Upton, NY 11973-5000

We perform coordinated laser flash photolysis (LFP) and pulse radiolysis (PR) investigations on new and established CO<sub>2</sub> reduction catalysts in order to identify key reaction intermediates and unravel mechanistic pathways. The primary tool we use for the identification of transient species is nanosecond time-resolved infrared (TRIR) spectroscopy, supported by UV/VIS transient absorption spectroscopy, density functional theory (DFT) calculations, and infrared spectroelectrochemical (IR-SEC) measurements. The advanced mechanistic knowledge gained from this work allows us to manipulate these species under non-equilibrium conditions, and ultimately leads to the development of new and more efficient catalytic systems.<sup>1</sup>

One class of CO<sub>2</sub> reduction catalysts that we are currently investigating are the cobalt macrocycles, such as Co<sup>II</sup>(HMD)<sup>2+</sup> (HMD = 5,7,7,12,14,14-hexamethyl-1,4,8,11-tetraazacyclotetradeca-4,11-diene). Chemical reduction of Co<sup>II</sup>(HMD)<sup>2+</sup> by Na/Hg in acetonitrile (CH<sub>3</sub>CN) followed by addition of CO<sub>2</sub>, provides the stable Co(HMD)(CO<sub>2</sub>)<sup>+</sup> intermediate, which is then used as a starting material for LFP/PR experiments. This has allowed us to directly probe the formation of the Co<sup>I</sup>(HMD)(CO)<sup>+</sup> product following the one-electron reduction of Co(HMD)(CO<sub>2</sub>)<sup>+</sup>, and to identify a previously unknown reaction pathway in the catalytic cycle.

Another class of CO<sub>2</sub> reduction catalysts that are of great interest to us are the MnL(bpy')(CO)<sub>3</sub><sup>n+</sup> complexes (L = Br<sup>-</sup>, OTf<sup>-</sup>, or CH<sub>3</sub>CN; bpy' = substituted 2,2'-bipyridine; n = 0 or 1). For example, we recently showed that the previously elusive “protonation-first” CO<sub>2</sub> reduction pathway can be turned on at reduced overpotential by incorporation of Brønsted-basic methoxy groups into the second coordination sphere of a new Mn catalyst, [*fac*-Mn({(MeO)<sub>2</sub>Ph}<sub>2</sub>bpy)(CO)<sub>3</sub>(CH<sub>3</sub>CN)](OTf).<sup>1</sup> The extremely bulky (MeO)<sub>2</sub>Ph groups at the 6,6'



positions of the bpy ligand prevent dimerization of the Mn radicals that result from one-electron reduction. In related work, we have also shown that one-electron reduction by PR of a chemically-synthesized Mn-Mn dimer, [Mn(Me<sub>2</sub>-bpy)(CO)<sub>3</sub>]<sub>2</sub>, produces one equivalent of the Mn-based radical (Mn•) and one equivalent of the desired two-electron reduced active catalytic species (Mn<sup>-</sup>) [see Figure]. We are probing the reactivity of Mn<sup>-</sup> with CO<sub>2</sub> and proton sources to directly observe the formation of the proposed metalcarboxylic acid catalytic intermediate (Mn-CO<sub>2</sub>H).

1. Ngo, K. T.; McKinnon, M.; Mahanti, B.; Narayanan, R.; Grills, D. C.; Ertem, M. Z.; Rochford, J. *J. Am. Chem. Soc.* **2017**, *139*, 2604-2618.

**Acknowledgments:** We thank our collaborators, Prof. Jonathan Rochford and Mr. Ken T. Ngo (U. Mass, Boston), for the synthesis of Mn catalysts and their electrochemical data. KTN is grateful to the DOE for an Office of Science Graduate Student Research (SCGSR) award.

# Integrated Synthetic, Computational, Spectroelectrochemical Study of Polyoxometalate Water Oxidation Catalyst-Based Photoanodes

Craig L. Hill, Tianquan Lian, Djameladdin G. Musaev

Department of Chemistry, Emory University, Atlanta, GA 30322

Our integrated experimental and theoretical team has obtained significant results in 3 interlinked areas:

**I. Polyoxometalate (POM) Water Oxidation Catalyst (WOC) Systems.** The complex,  $K_{12}Na_4[H_{23}NaO_8Cu_{24}(Nb_7O_{22})_8] \cdot 106H_2O$  (X-ray structure formula) is the first, molecular POM WOC that is very stable in strong base. Remarkably it forms a dynamic system that keeps an internal Cu oxide cluster intact and in solution for many hours of bulk electrolytic water oxidation. In order to provide additional compelling evidence that our fast and earth abundant-element-containing, molecular WOC,  $[Co_4(VW_9O_{34})_2]^{10-}$  is the real catalytically active species rather than a precursor of Co(II) and, consequently,  $CoO_x$  particles, we performed extensive stopped-flow kinetics,  $^{51}V$  NMR measurements, solution equilibration and other studies. These studies confirm our original assignment and allowed us to discover additional features of this catalyst. These and other recent studies extend this class of WOCs.

## II. Interfacial structure and charge transfer dynamics of ALD protected photoelectrodes.

We have examined how an ALD protection layer affects interfacial molecular structure and/or charge transfer dynamics on hybrid photoelectrodes. For GaP electrodes protected by ALD  $TiO_2$  layer, using time-resolved reflection spectroscopy, we showed that the presence of a p-n junction at the (p-)GaP/(n-)TiO<sub>2</sub> interface leads to efficient charge separation and the photo-generated transient surface charge carrier density correlates well with steady state IPCE measurement. This opens up the possibility of follow carrier dynamics under catalytic turnover conditions and studying the factors limiting the photocurrent on these electrodes. We have also studied, via vibrational sum-frequency generation spectroscopy and time-resolved IR spectroscopy, how ALD protection affects the structure of interfacial model sensitizer and catalysts and their interfacial charge-transfer kinetics on TiO<sub>2</sub> surfaces.

**III. Computational/Theoretical studies.** We continue development of a novel computational approach to study interfacial electron transfer (IET) between WOCs and sensitizers, as well as between quantum dots (QDs) and electron scavengers. Recently, we validated the newly developed hybrid DFT/FraMM method to study interfacial electron transfer (IET) from the multiply oxidized form of the  $[Ru_4W_{20}Si_2O_{82}H_{10}]^{n-}$  water oxidation catalyst to the photo oxidized  $[Ru(bpy)_3]^{3+}$  sensitizer (Figure 1). We found that electron transfer rate from WOC to sensitizer decreases with increasing oxidation state of the catalyst. Further analysis of the electronic coupling strength between catalyst and sensitizer requires large-scale MD simulations, which are currently in progress.

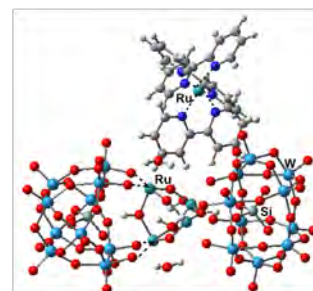


Figure 1

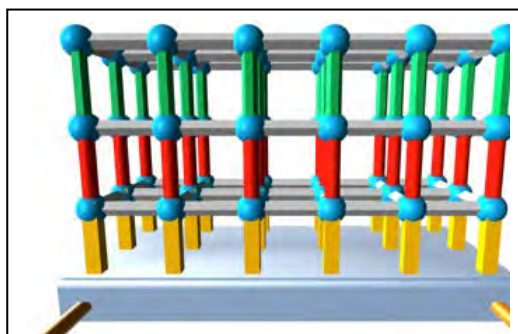
In parallel, we are developing a tight-binding-like TB-LCAO model to study QD-to-molecule electron/hole transfer. We completed parameterization of Cd-Se/Cd-Cd/Se-Se sets and calculated the orbitals and band-gap structures of  $Cd_{111}Se_{111}$ ,  $Cd_{201}Se_{201}$  and a few larger QDs.

## Light Harvesting, Antenna Behavior, and Directional Charge Transport in Metal-Organic Frameworks

Subhadip Goswami, Aaron Peters, Omar K. Farha, Joseph T. Hupp  
Department of Chemistry  
Northwestern University  
Evanston, IL 60208

Metal-organic framework (MOF) chemistry offers a precise way of organizing, spacing, and orienting molecular chromophores – important considerations for engendering antenna-type behavior in light-harvesting assemblies. This poster describes some of our recent work on supported, light-absorbing, thin-film MOFs.[1, 2] Automated layer-by-layer assembly permits the films to be reproducibly constructed with close to single-molecule control over average film thickness, a feature that greatly facilitates the experimental investigation of molecular-exciton transport distances and the systematic manipulation of light-harvesting efficiencies.

Using functionalized porphyrins, tetraphenylpyrenes, and related species as chromophoric components of thin-film MOFs, we find that: a) exciton transport distances can be substantially varied by paying close attention to the composition and geometry of non-chromophoric molecular components, b) related considerations for light-absorbing components can likewise be exploited to control exciton transport, c) antenna behavior, including highly directional energy transport, can be engendered, and d) hopping-based charge transport can be made fairly anisotropic, with rates of charge propagation in desired directions exceeding by about 100-fold, those in undesired directions. From these and related studies, hypothesis-tested and transferrable design rules for effective light harvesting, energy transport, and charge transport by MOF-organized arrays of chromophores are beginning to emerge.



Simplified schematic representation of an electrode-supported MOF film capable of panchromatic light-harvesting.

[1] “Toward Metal–Organic Framework-Based Solar Cells: Enhancing Directional Exciton Transport by Collapsing Three-Dimensional Film Structures” Subhadip Goswami, Lin Ma, Alex B. F. Martinson, Michael R. Wasielewski, Omar K. Farha, and Joseph T. Hupp *ACS Appl. Mater. Interfaces*, **2016**, *8*, 30863–30870. DOI: 10.1021/acsami.6b08552

[2] “Modulating the Rate of Charge Transport in a Metal–Organic Framework Thin Film Using Host:Guest Chemistry,” I. Hod, O. K. Farha and J. T. Hupp, *Chem. Commun.*, **2016**, *52*, 1705–1708. DOI: 10.1039/C5CC09695B

# Transient Grating Spectroscopy for Measuring Transport of Charges and Excitons in Polycrystalline Thin Films

Justin C. Johnson, Dylan H. Arias, David T. Moore, Jao van de Lagemaat  
Chemistry and Nanoscience Center  
National Renewable Energy Laboratory  
Golden, CO 80401

The transport of energy and charge after photoexcitation in nano- to microcrystalline thin films typically involves diffusion through crystalline regions, which is hindered at grain boundaries. The degree to which charges or excitons can circumvent barriers to efficient transport on the nanoscale will often determine whether or not a particular thin film is useful in an optoelectronic or photochemical context. We have adapted a form of transient grating spectroscopy (TGS) to effectively image the motion of charges in a series of methylammonium lead iodide perovskite (MAPbI<sub>3</sub>) thin films and single crystals. The TGS technique takes advantage of phase-matching between femtosecond laser beams that impinge on the sample at variable angles, which results in a fringe pattern of populated excited states. The relief of the “grating” is read out in a background-free direction as a function of delay time. Excited state motion and population dynamics are separated by the independence of the latter on fringe spacing. Diffusion coefficients can be derived from the dependence of the spacing-dependent decay kinetics, Fig 1A. We have found that charge carrier diffusion in the MAPbI<sub>3</sub> films is limited by grain boundaries that carriers do not traverse effectively, Fig 1B. Electromagnetic field simulations further bear out this result, which is demonstrated by comparing TGS decay kinetics as a function of grain size.

We are also expanding the technique to measure anisotropic transport in poled MAPbI<sub>3</sub> films and to monitor both exciton and charge motion in perovskite films of different compositions. A steady-state version of the technique is being constructed that will enable us to track the transport regime for films with especially long-lived species. For example, triplet excitons in tetracene are formed quickly via singlet fission and move concomitant with singlet excitons for several ns via triplet-triplet fusion and Forster energy transfer. On longer timescales, triplet exciton motion proceeds via a Dexter process and extends to  $\mu$ s. In some cases, charges or polarons are produced from these excitons, and their unique spectroscopic signatures can be independently probed using multi-color TGS. A complete picture of both population and transport dynamics of excited species can be obtained with this relatively simple yet highly sensitive technique.

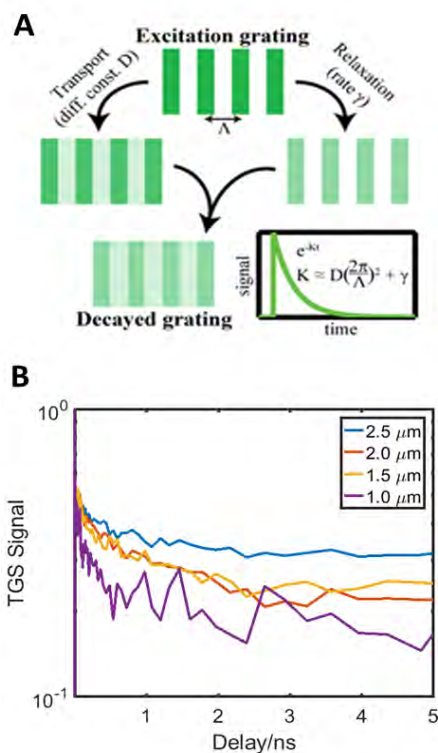


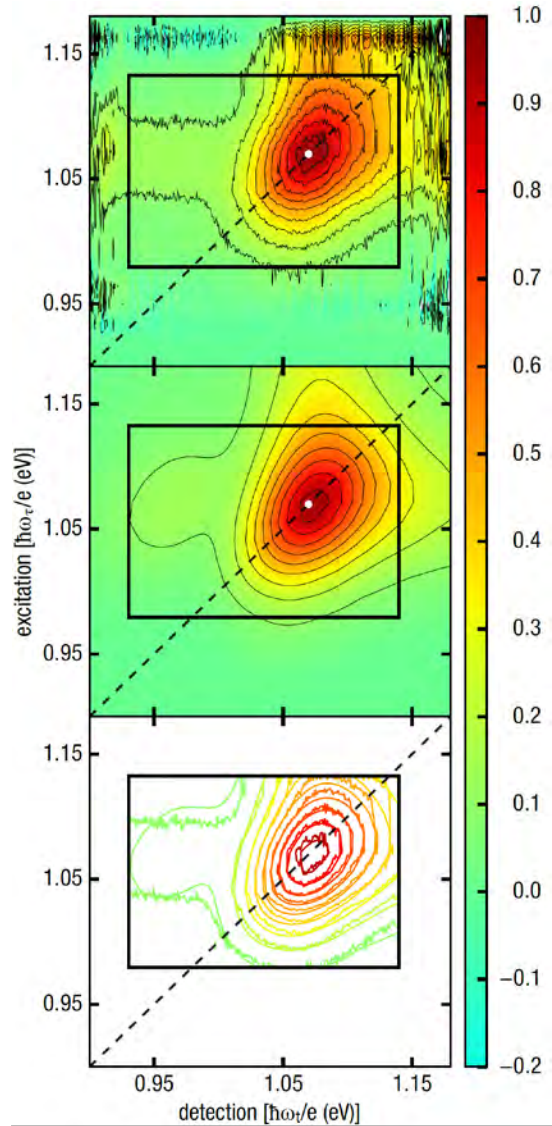
**Figure 1.** A, experimental schematic. B, TGS decay profiles vs. grating spacing, showing reduced decay when spacing is larger than average grain size.

## Weak carrier interactions in lead-sulfide quantum dots

Dmitry Baranov, Jisu Ryu, Samuel D. Park, and David M. Jonas  
Department of Chemistry and Biochemistry  
University of Colorado  
Boulder, CO 80309-0215

Carrier interactions in quantum dots have been intensely studied because Auger recombination is a detrimental loss process in photovoltaic, lighting, and display applications while its inverse, multiple exciton generation, is potentially beneficial in next generation photovoltaics. Transient spectroscopy of lead sulfide quantum dots has provided mixed results on both processes and on the bi-exciton binding energy, which also reflects carrier interactions. For PbS quantum dots, concerns have been raised about whether the strengths of the various signal contributions match theory and it has been remarked that the sub-100 fs dephasing “defies explanation”. To measure these interactions, we have used fully characterized 15 fs pulses to record 2D spectra of high quality colloidal PbS quantum dots with oleate ligands in tetrachloroethylene (PbCl<sub>2</sub> synthesis, 1.1 eV bandgap, 65% photo-luminescence quantum yield) in a UHV compatible spinning sample cell that eliminates oxygen and moisture and completely exchanges the sample between laser shots. Similar results were found for samples made by Jon Owen.

The figure at right shows a real-valued 2D spectrum, which is fully relaxed so that the ellipticity of the 1S-1S peak provides a precise measure of absorption bandgap inhomogeneity. It is striking that there is no negative region from excited state absorption (esa) to the bi-exciton state. In contrast to CdE dots with signal only from holes, there is a strong stimulated emission feature detected near 0.97 eV, indicating signal from electrons. The white dot marks the peak of the absorption lineshape, indicating a very small bi-exciton shift. So far, all of our transient data (2D correlation and relaxation spectra plus the near-zero polarization anisotropy) are consistent with strong (bulk-like) spin-orbit coupling for each carrier and extremely weak interactions between carriers.



Top) 2D relaxation spectrum of PbS dots at 1 ps waiting time after division to correct for pulse spectra and propagation effects (2.4% noise diverges outside the box). Middle) Fit using absorption, stimulated emission, and broadened excited state absorption (2.7% rms error). Bottom) Experiment & fit at 10% contours.

## Establishing the Role of the Electrode Surface in Solar-Driven Pyridine-Catalyzed CO<sub>2</sub> Reduction

Zhu Chen, Coleman X. Kronawitter and Bruce E. Koel  
Department of Chemical and Biological Engineering  
Princeton University  
Princeton, NJ 08540

An objective of this research is to provide new insights into the role of the semiconductor electrode surface in the mechanism of pyridine(C<sub>5</sub>H<sub>5</sub>N; Py)-catalyzed CO<sub>2</sub> reduction. Atypical high selectivity for the conversion of CO<sub>2</sub> to methanol has been reported when pyridine is dissolved in the electrolyte of a photoelectrochemical cell employing a p-type gallium phosphide (GaP) photocathode. Despite considerable electrochemical characterization and theoretical consideration, there is no consensus on the mechanism by which pyridine catalyzes CO<sub>2</sub>-to-methanol conversion. Our research includes a surface science approach to investigate surface chemistry and determine the role of heterogeneous processes in this catalysis. Gaining this fundamental understanding of the origin of high efficiency in this system is essential to the continued optimization of solar-driven CO<sub>2</sub> reduction.

Recent work has investigated the bonding of methanol (CH<sub>3</sub>OH) on GaP(111) and (110) surfaces using ambient-pressure X-ray photoelectron spectroscopy (APPEs) at the National Synchrotron Light Source II. Dissociative adsorption of methanol on GaP(111) leads to the formation of surface-bound methoxy (CH<sub>3</sub>O) species, while simultaneous formation of formate (HCOO) and methoxy occurs on the more reactive GaP(110) surface, as shown in Fig. 1. Other APPEs studies of the adsorption, bonding and thermal stability of pyridine on GaP(110) under high pressures of CO<sub>2</sub> and H<sub>2</sub> (1 torr) found weak adsorption of pyridine via dative bonding on clean GaP(110) and a stronger bonding mode, via a di-σ-cycloadduct, on hydrided GaP(110).

In a first experiment using a new *operando* FTIR setup, we observed that pyridinium is hydrogenated at Pt electrodes in electrochemical conditions consistent with those previously shown to yield selective reduction of carbon dioxide to methanol and formic acid.[1] Formation of a hydrogenated piperidinium (PyH<sub>7</sub><sup>+</sup>) near-surface species implies that dihydropyridinium (PyH<sub>3</sub><sup>+</sup>), the protonated form of a previously proposed hydride-shuttling reduction catalyst, must exist transiently during CO<sub>2</sub> reduction.

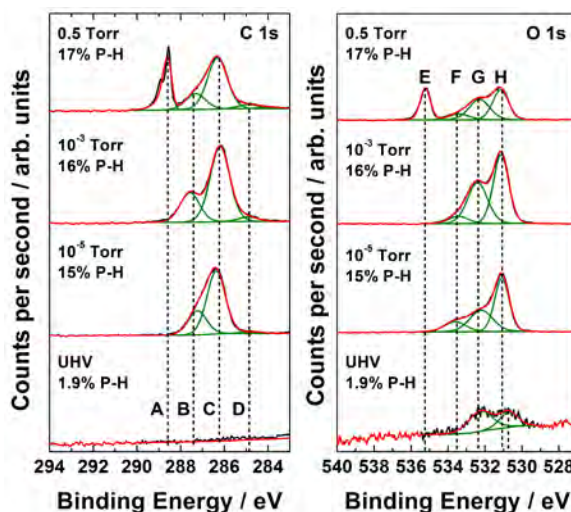


Figure 1. APPEs spectra of the C 1s (left) and O 1s (right) core levels of the GaP(110) surface exposed to different pressures of methanol. Peaks A and E are from gas phase methanol, peaks B and H are from formate, peaks C and G are from methoxy, peak D is from CH<sub>x</sub>, and peak F is from H<sub>2</sub>O. The surface concentration of P-H species is given in the upper left corner of the panels.

[1] C.X. Kronawitter, Z. Chen, P. Zhao, X. Yang, B.E. Koel, *Catal. Sci. Tech.* **2017**, 7, 831.

## Photophysics of Charged Excitons in Single-Walled Carbon Nanotubes

Zhentao Hou, Amanda R. Amori, Nicole M. B. Cogan, and Todd D. Krauss  
Department of Chemistry  
University of Rochester  
Rochester, New York 14627-0216

Single-walled carbon nanotubes (SWNTs) are fundamentally interesting and technologically relevant materials with size-tunable absorption and emission across visible and near infrared wavelengths. However, several important aspects of SWNT photophysical properties are not known well enough to predict how SWNTs will behave as part of a larger integrated solar photochemical system. Since SWNTs are comprised of all “surface” atoms, simple concepts such as the intrinsic photoluminescence efficiency (PL QY) are not understood for SWNTs, as they are strong functions of the local environment.

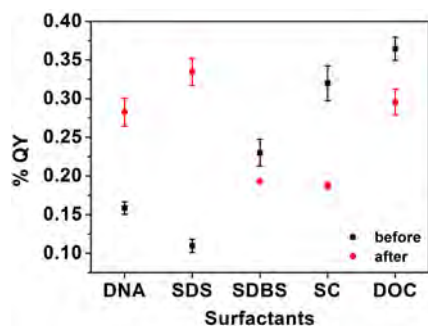


**Figure 1:** PL QY for SWNTs wrapped in various surfactants before and after addition of DTT.

We have found that addition of dithiothreitol (DTT) to DNA or sodium dodecyl sulfate (SDS) wrapped SWNTs causes PL brightening by several fold. In contrast, SWNTs dispersed in sodium dodecylbenzene sulfonate (SDBS), sodium cholate (SC) and sodium deoxycholate (DOC) solutions display fluorescence quenching upon addition of DTT. Time-resolved PL studies show that addition of DTT mitigates non-radiative decay processes, and also surprisingly increases the radiative decay rate for DNA and SDS-SWNTs (Figure 1). This combination leads to the increase of the PL QY. The opposite influences are found for the other SWNTs. The PL brightening (or quenching)

is consistent with surfactant reorganization upon addition of DTT, which changes the local dielectric environment and the relative surfactant coverage on the SWNT.

Recently, charge carrier doping of SWNTs has also garnered interest as a means of modifying SWNT optical properties. Specifically, chemically doping SWNTs with extra holes has been shown to quench the bright singlet exciton feature while causing a red-shifted, weaker feature to appear, attributed to a positively charged “trion.” However, several characteristics of the “trion” PL contradict such an interpretation. Using confocal microscopy of individual doped SWNTs at 10 and 295 K (Figure 2), we measured PL spectra and correlated photon statistics for trions versus excitons, and found that unlike the exciton, the trion PL did not narrow with decreasing temperature. Measurements were also made on SWNTs with various levels of chemical processing, with the interesting finding that the trion PL feature exists on more “defective” NTs. Altogether, our data suggests the trion PL feature is a consequence of recombination of an exciton at a charged defect site along the NT surface.

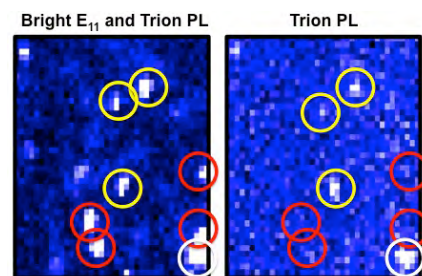


**Figure 2:** PL images of excitons and trions (left) and trions only (right) in SWNTs at 295 K. Some NTs have only exciton PL (red) while others also show trion PL (yellow), including a possible localized trion (white).

## Dynamics of the Injection and Transport of Holes and Electrons in DNA

Frederick D. Lewis  
Department of Chemistry  
Northwestern University  
Evanston, Illinois USA 60208

Charge transport in DNA can occur via the movement of either positive charge (holes) or negative charge (electrons) between bases, holes preferring to reside on bases of low electron affinity (purines and their derivatives) and electrons on bases of high electron affinity (pyrimidines and their derivatives). Hole and electron transport occur most efficiently in repeating homo(nucleotide) sequences (e.g. poly(adenine) or poly-(thymine)). We have recently investigated the efficiency and dynamics of hole transport in synthetic DNA hairpins having strand crossings or base mismatches.<sup>1</sup> TT or CC mismatches effectively block hole transport, while AA or GG mismatches slow but do not stop hole transport and promote strand crossings. With our collaborators at Delft and Northwestern we have found that the dynamics of hole transport in poly(adenine) sequences is strongly dependent upon the energetics of the hole injection step. Highly exergonic hole injection from naphthalenediimide (NDI) is proposed to populate high energy HOMO adenine orbitals which have much smaller barriers for hole transport than do lower energy HOMO orbitals populated upon hole injection from stilbenedicarboxamide (SA) (Figure 1).<sup>2</sup> We have also completed an investigation of charge separation dynamics in mini-hairpins possessing 1-3 A-T or G-C base pairs.<sup>3</sup>

As part of our continuing research on electron transport in DNA we have investigated the dynamics of electron injection and charge recombination into unusual cytosine base duplex structures known as i-motifs. Our synthetic i-motifs possess a stilbenediether (Sd) electron donor at one end an i-motif possessing 4- or 6-hemi-protonated C-C base pairs and a perylenediimide electron trap at the opposite end (Figure 2).<sup>4</sup> Electron injection and charge recombination are rapid, but there is no evidence for electron transport to the PDI trap. Molecular modeling of the parent i-motif lacking the pendant chromophores (Figure 2) shows that it possess stacked C-C base pairs which have short stacking distances but essentially zero  $\pi$ -orbital overlap between base pairs, consistent with the failure to observe e-transport.

(1) Thazhathveetil, A. K.; Harris, M. A.; Young, R. M.; Wasielewski, M. R.; Lewis, F. D. *J. Photochem. Photobiol., A* **2016**, *331*, 160. (2) Renaud, N.; Harris, M. A.; Singh, A. P. N.; Berlin, Y. A.; Ratner, M. A.; Wasielewski, M. R.; Lewis, F. D.; Grozema, F. C. *Nat. Chem.* **2016**, *8*, 1015. (3) Mishra, A. K.; Harris, M. A.; Young, R. M.; Wasielewski, M. R.; Lewis, F. D. **2017**, submitted. (4) Fujii, T.; Thazhathveetil, A. K.; Yildirim, I.; Young, R. M.; Wasielewski, M. R.; Schatz, G. C.; Lewis, F. D. **2017**, in preparation.

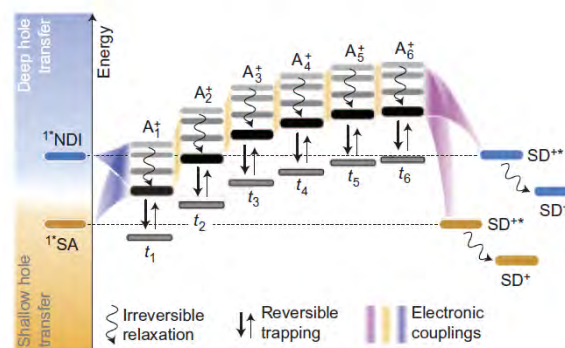


**Figure 1.** Model system for hole transfer simulations, where four propagating states and one trap state are considered for each adenine.

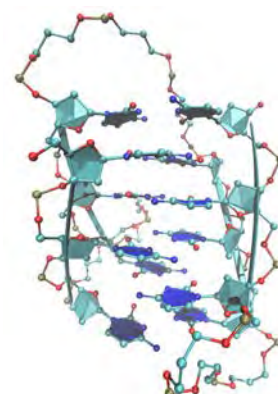


**Figure 2.** Minimized structure of a synthetic intramolecular i-motif

## Exploring the Synergy between Semiconductor Surfaces and Molecular Catalysts for Efficient Solar CO<sub>2</sub> Reduction

Sebastian Pantovich, Ethan Jarvis, Peipei Huang, Christine Caputo, and Gonghu Li  
Department of Chemistry  
University of New Hampshire  
Durham, NH 03824

Significant research progress has been made in solar fuel production using hybrid photocatalysts consisting of light-harvesting semiconductors and molecular catalysts. However, it remains unclear what governs interfacial electron transfer in such hybrid systems. In this project, we collaborate with Dr. Tijana Rajh of Argonne National Laboratory to investigate structural features of hybrid photocatalysts that are key to achieving efficient solar CO<sub>2</sub> reduction. We hypothesize that covalent linkages with appropriate *bend angles* and *flexibility* promote interfacial electron transfer from photoactivated semiconductors to surface molecular catalysts for fuel-producing reactions (**Figure 1**, right).

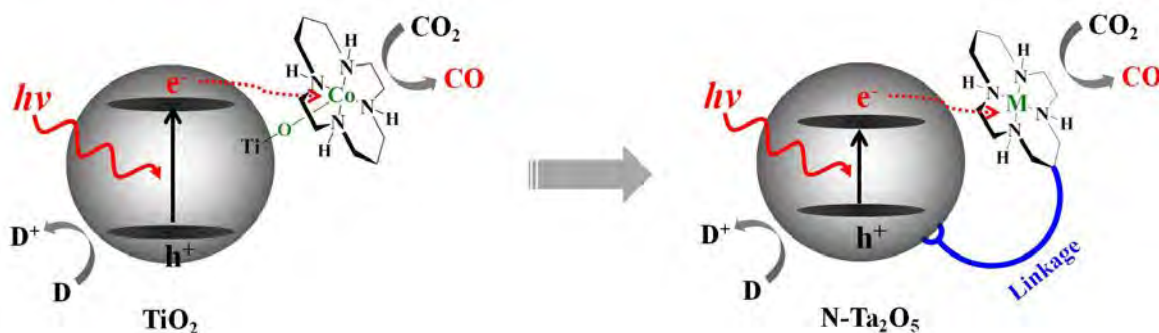


**Figure 1.** Design of hybrid photocatalysts based on prior work. M = Co(III), Cu(II).

In our prior work, CO<sub>2</sub>-to-CO conversion was achieved under UV irradiation using a macrocyclic Co(III) complex deposited on TiO<sub>2</sub> surfaces (**Figure 1**, left).<sup>1-2</sup> Our current work involves the use of nitrogen-doped tantalum oxide (N-Ta<sub>2</sub>O<sub>5</sub>, bandgap 2.4 eV) as the semiconductor support that can harvest visible light of the solar spectrum. We have synthesized mesoporous N-Ta<sub>2</sub>O<sub>5</sub> with high surface areas, and are currently developing a variety of covalent linkages for grafting macrocyclic Co(III) and Cu(II) complexes onto N-Ta<sub>2</sub>O<sub>5</sub>. Photochemical CO<sub>2</sub> reduction on the target hybrid photocatalysts will be studied using *in situ* FTIR spectroscopy. Light-induced interfacial electron transfer in the hybrid system will be investigated using the low-temperature EPR facility in Dr. Rajh's lab.

Results from this research will help understand synergistic interactions between semiconductor surfaces and molecular catalysts in hybrid systems. This project also enables us to establish research partnership between the state of New Hampshire and Argonne National Laboratory.

**Acknowledgements:** We thank Dr. Etsuko Fujita (Brookhaven National Laboratory) for helpful discussion. This project is co-sponsored by the DOE EPSCoR Program.

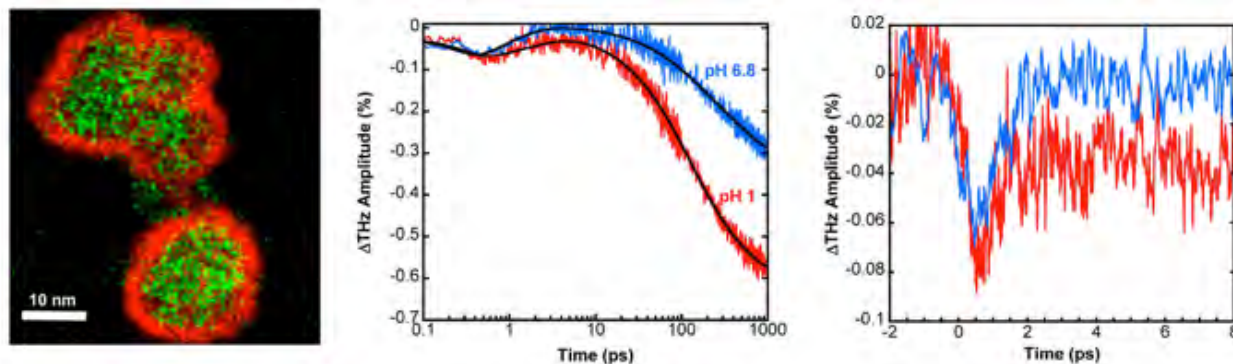
**References:** **1.** Jin, T.; Liu, C.; Li, G. *Chem. Commun.* **2014**, *50*, 6221-6224; **2.** Liu, C.; Jin, T.; Louis, M. E.; Pantovich, S. A.; Skraba-Joiner, S. L.; Rajh, T.; Li, G. *J. Mol. Catal. A* **2016**, *423*, 293-299.

## Nanostructured Solar Fuel Systems

Pengtao Xu, Nicholas S. McCool, Yuguang C. Li, Zhifei Yan, Christopher Gray, Yixin Hu, Sylvia Bintrim-Yang, Kamryn Curry, AJ Rothenberger, and Thomas E. Mallouk  
Department of Chemistry, The Pennsylvania State University, University Park, PA 16802  
John R. Swierk, Coleen T. Nemes, and Charles A. Schmuttenmaer  
Department of Chemistry, Yale University, New Haven, CT 06520  
Ian D. Sharp, Lawrence Berkeley National Laboratory, Berkeley, CA 94720

Our DOE-supported research investigates problems associated with overall water splitting and CO<sub>2</sub> electrolysis in molecule-based photoelectrochemical systems. We are studying dye-sensitized oxide semiconductors and core-shell structures as photoanodes and photocathodes, as well as composite membranes that manage the flow of protons in the cell and mitigate the crossover of fuel from the cathode to the anode.

A key problem in these systems is to control the relative rates of charge injection, transport, and recombination, especially at the anode where catalysis of the water oxidation reaction is slow. To do this we are studying core-shell electrode structures made by atomic layer deposition (ALD). By combining ultrafast time-resolved terahertz spectroscopy (TRTS) with other steady-



state and time resolved techniques, we are able to develop a detailed kinetic picture of electron injection, trapping, tunneling, and delocalization, as shown in the figure above for sensitized TiO<sub>2</sub>/SnO<sub>2</sub> shell-core electrode structures. In related experiments, we have studied “mummy” type core-shell electrodes in which a catalytic cobalt oxide layer deposited by ALD covers the dye layer. These electrodes show a dramatic improvement in stability as well as higher photoanodic current.

Proton transport from the anode to the cathode is also a significant system-level problem in both water splitting and CO<sub>2</sub> electrolysis cells. We and other groups have recently found that bipolar membranes, operated in reverse bias, can maintain stable photocurrent and solution pH in water electrolysis cells operated for many hours under direct current conditions. We have recently extended these studies to CO<sub>2</sub> electrolysis cells and have shown that current densities up to 200 mA/cm<sup>2</sup> can be stably maintained in bipolar membrane cells using a gas-diffusion cathode. We are using electrochemical impedance spectroscopy to understand water dissociation catalysis and other losses in bipolar membrane cells, and are studying cation and support effects on the selectivity and activity of heterogeneous catalysts for electrochemical CO<sub>2</sub> reduction.

## Singlet Fission: Optimization of Chromophore Packing

Eric Buchanan,<sup>1</sup> Zdenek Havlas,<sup>2</sup> and Josef Michl<sup>1,2</sup>

<sup>1</sup>Department of Chemistry and Biochemistry

University of Colorado

Boulder, CO 80309-0215

<sup>2</sup>Institute of Organic Chemistry and Biochemistry

AS CR

Prague, Czech Republic

We describe a new tool for guiding covalent dimer synthesis and crystal engineering of materials for efficient singlet fission. The procedure is based on an approximate version of the HOMO/LUMO model for the evaluation of intermolecular interaction contributions to the quantities needed for the Marcus theory expression for the rate of singlet fission in a pair of pi-electron chromophores as a function of dimer geometry. The quantities are the electronic matrix element, exoergicity, relative population of the two excitonic levels, and biexciton binding energy. Reorganization energy only needs to be computed once and the expressions for the other required quantities are simple enough to permit an identification of all local maxima of the desired quantities and thus optimal dimer geometries in the complete six-dimensional space available to a pair of rigid molecules. The search involves the evaluation of these quantities at tens or hundreds of millions of dimer geometries. The results agree well with the exact solution of the HOMO/LUMO model, and a comparison with higher-level ab initio models is currently underway. The procedure has been applied to a pair of ethylenes, the simplest pi-electron system, where the computation took only a few hours of CPU time and produced important fundamental insights. It has also been applied to an indigo-related heterocycle with 24 non-hydrogen atoms, where the computation took a few days of CPU time. In both cases, the dimer geometries with the largest electronic matrix elements are of the slip-stack type, and in both cases, they suffer from a large Davydov splitting, which involves a considerable energy penalty, making singlet fission less exoergic or less endothermic. As a result, the dimer geometry that is predicted as optimal for singlet fission is one in which the electronic matrix element is still large but the HOMO-LUMO transition moments of the two chromophores are exactly or nearly mutually orthogonal. Such geometries produce somewhat smaller electronic matrix elements but avoid the energy penalty associated with a large Davydov splitting. Extension of the procedure to dimers of other chromophores is underway, and the computer program developed is being prepared for public release.

## Controlling the Energetics and Stability of Metallic 2D MoS<sub>2</sub> with Surface Modifiers

Eric E. Benson, Samuel A. Schuman, Sanjini U. Nanayakkara, Suzanne Ferrere, Jeffery L. Blackburn and Elisa M. Miller  
Chemistry and Nanoscience Center  
National Renewable Energy Laboratory  
Golden, CO 80401

By varying the organic substituents on two-dimensional transition metal dichalcogenides (2D TMDCs), we can alter the fundamental electronic properties of 2D TMDCs, such as molybdenum disulfide (MoS<sub>2</sub>). We show that the 2D-MoS<sub>2</sub> surface energetics and stability can be controlled by chemical modification of the surface via organic molecules with varying electronics. Chemically-exfoliated, metallic MoS<sub>2</sub> is modified with substituted aryl rings containing substituents with various electron withdrawing/donating groups (*p*-NO<sub>2</sub>, 3,5-Cl<sub>2</sub>, *p*-Br, *p*-OCH<sub>3</sub>, and *p*-Et<sub>2</sub>N). This functionalization results in different electrochemical properties, specifically activity towards the hydrogen evolution reaction (HER). As the Hammett parameter is changed, different exchange currents as well as Tafel slopes are observed for the modified surfaces. In addition, the workfunction of the metallic MoS<sub>2</sub> surface depends on the functional group. There is a correlation between the electron withdrawing/donating character (Hammett parameter) of the functional group and the workfunction, which is measured *via* X-ray photoelectron spectroscopy (Fig. 1). Furthermore, the metallic nature of the MoS<sub>2</sub> films are preserved by the functional group and do not undergo conversion to the semiconducting state when annealed at 150 °C for 24 h. This result is critical to maintaining the catalytically active metallic state of 2D MoS<sub>2</sub>, which is verified via extended electrochemistry experiments. Functionalizing 2D TMDCs gives an extra handle on electronic properties and stability within the typically unstable metallic state.

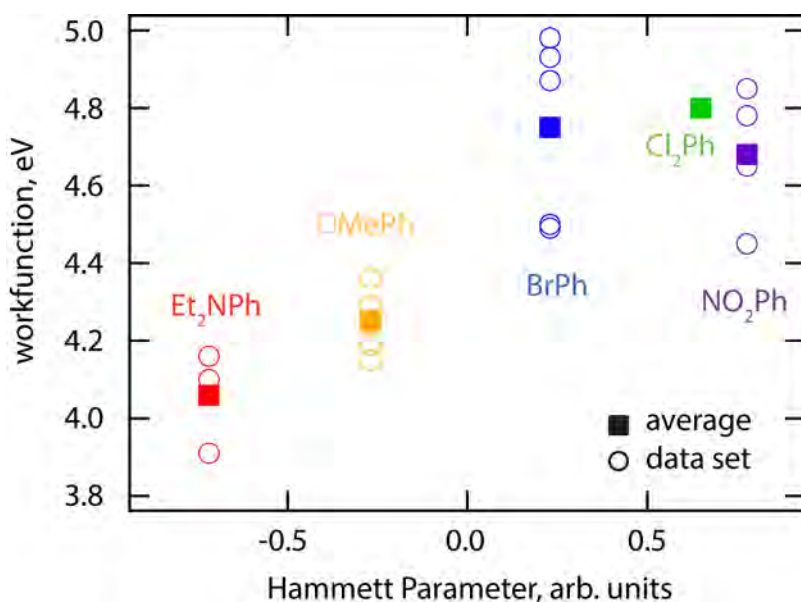


**Figure 1.** Workfunction as a function of Hammett Parameter for functionalized MoS<sub>2</sub>. The solid squares are averages of multiple measurements.

## Redox Potentials Without Electrolyte and Ion Pairing

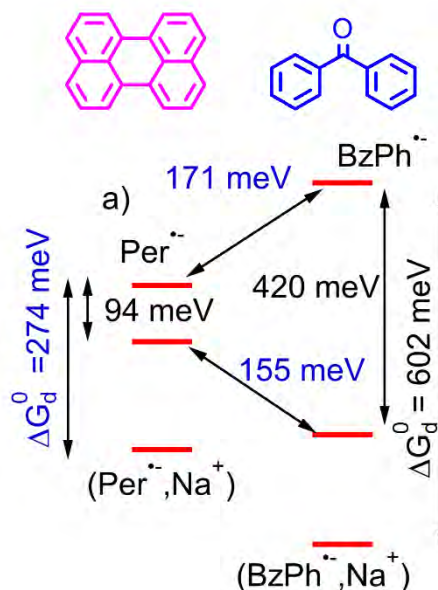
Matthew J. Bird, Tomokazu Iyoda, Nicholas Bonura,  
Jin Bakalis, Abram Ledbetter and John R. Miller  
Chemistry Department  
Brookhaven National Laboratory  
Upton, NY 11973

Many of us in the Solar Photochemistry Program use redox potentials to estimate energetics, but we rarely need energetics in high concentrations of electrolyte. How different are these potentials when we remove the electrolyte? In this poster we report experiments that determine reduction potentials for two molecules, benzophenone (BzPh) and perylene (Per), in the complete absence of electrolyte as well as in the presence of three different supporting electrolytes in the moderately polar solvent THF. Without electrolyte the redox potentials were 100-451 mV more negative than those with 100 mM electrolyte. These changes depended both on the molecule and the electrolyte. The dominant contributor to stabilization of radical anions by the electrolytes was ion pairing. Definite values were determined for energetics,  $\Delta G_d^\circ$ , of ion pairing. Values of  $\Delta G_d^\circ$  for ion pairing of some radical anions to alkali metals such as  $\text{Na}^+$  were previously known, but the present measurements include pairing of radical anions to tetrabutylammonium,  $\text{TBA}^+$ , usually used in electrochemistry, which were previously unknown. An equation was derived to give changes in redox potentials when electrolyte is added in terms of ion pair dissociation constants and activity coefficients.

$\text{TBA}^+$  was found to give  $\Delta G_d^\circ$  for binding to radical anions that can be similar to smaller, strongly-coordinating cations, but  $\Delta G_d^\circ$  often varies strongly with individual natures of both partners in ion pair. The status of  $\text{TBA}^+$  as a “weakly-coordinating cation” is thus in some doubt. The determinations described here arise from experiments not previously utilized for ion pairing including equilibria for electron transfer reactions, measured by pulse radiolysis with and without electrolytes. These methods establish a way to determine ion pairing energies for  $\text{TBA}^+$  and other ions. Computations with DFT methods were moderately successful at describing the results.

The determination of redox potentials in the absence of electrolyte has long been a goal in the electrochemical community, but electrochemical measurements with no electrolyte are difficult, even with ultramicroelectrodes. Here we combine electrochemical measurements with pulse radiolysis, which can inject charges into otherwise completely neutral solutions, allowing measurement of electron transfer equilibria without or with electrolyte, enabling construction of free energy cycles, such as the one to the right.

The poster will explain how this can be done without electrolyte and how pulse radiolysis is combined with chemical and electrochemical methods to determine free energy changes.

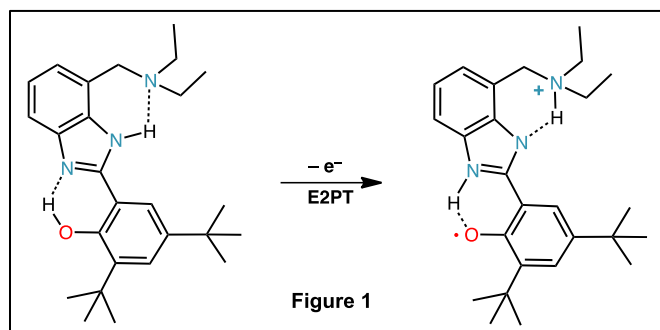


## Concerted One-Electron Two-Proton Transfer Processes in Models Inspired by the Tyr-His Couple of Photosystem II

Mioy T. Huynh<sup>†</sup>, S. Jimena Mora<sup>‡</sup>, Matias Villalba<sup>‡</sup>, Marely E. Tejada-Ferrari<sup>‡</sup>, Paul A. Liddell<sup>‡</sup>, Anne-Lucie Teillout<sup>§</sup>, Charles W. Machan<sup>‡</sup>, Clifford P. Kubiak<sup>‡</sup>, Devens Gust<sup>‡</sup>, Thomas A. Moore<sup>‡</sup>, Sharon Hammes-Schiffer<sup>†</sup> and Ana L. Moore<sup>‡</sup>

<sup>†</sup>Department of Chemistry, University of Illinois at Urbana-Champaign, Urbana, Illinois 61801. <sup>‡</sup>School of Molecular Sciences, Arizona State University, Tempe, Arizona 85287. <sup>§</sup>Laboratoire de Chimie Physique, Groupe d'Electrochimie et de Photoelectrochimie, UMR 8000 CNRS, Université Paris-Sud, 91405 Orsay Cedex, France. <sup>‡</sup>Department of Chemistry, University of Virginia, Charlottesville, Virginia 22904. <sup>‡</sup>Department of Chemistry and Biochemistry, University of California, San Diego, California 92093.

The design, synthesis, and study of simple systems where multiple proton transfers can be associated with the oxidation of a phenol in a concerted mechanism can provide a deeper understanding of the proton-coupled electron transfer (PCET) processes taking place in biology and can help to establish design principles for controlling proton activity at catalytic water oxidation sites in artificial photosynthesis, where managing proton activity is thought to be key to efficient catalysis. In this study, we provide theoretical and experimental evidence in biomimetic constructs consisting of benzimidazole phenols (BIPs) substituted with amino groups



for a concerted one-electron two-proton transfer process (E2PT) that takes place when the phenol is oxidized electrochemically (see Figure 1 for the example of BIP-CH<sub>2</sub>NEt<sub>2</sub>). Theory predicts that E2PT leads to a reduction in the oxidation potential of the phenol by ~300 mV and a small kinetic isotope effect (KIE). Electrochemical, spectroelectrochemical, and KIE experimental data are

consistent with these predictions. The E2PT process shown in Figure 1 results in the translocation of protons over a distance of ca. 7 Å and is a starting point for the design of bioinspired proton wires. Although oxidation of the phenol in the amino-BIPs reported here is electrochemically driven, the E2PT process could be light-powered by substituting the BIP of photochemically activated triad systems previously reported by amino-BIPs.<sup>1,2,3</sup>

1. Megiatto Jr., J. D.; Mendez-Hernandez, D. D.; Tejada-Ferrari, M. E.; Teillout, A.-L.; Llansola Portoles, M. J.; Kodis, G.; Poluektov, O. G.; Rajh, T.; Mujica, V.; Groy, T. L.; Gust, D.; Moore, T. A.; Moore, A. L., A bioinspired redox relay that mimics radical interactions of the Tyr-His pairs of photosystem II. *Nature Chem.* **2014**, *6*, 423–428.

2. Moore, G. F.; Hamburger, M.; Gervaldo, M.; Poluektov, O. G.; Rajh, T.; Gust, D.; Moore, T. A.; Moore, A. L., A bioinspired construct that mimics the proton coupled electron transfer between P680<sup>+</sup> and the Tyrz-His190 pair of photosystem II. *J. Am. Chem. Soc.* **2008**, *130*, 10466–10467.

3. Megiatto Jr., J. D.; Antoniuk-Pablant, A.; Sherman, B. D.; Kodis, G.; Gervaldo, M.; Moore, T. A.; Moore, A. L.; Gust, D., Mimicking the electron transfer chain in photosystem II with a molecular triad thermodynamically capable of water oxidation. *Proc. Natl. Acad. Sci. USA* **2012**, *39*, 15578–15583.

## Enhanced Catalysis through Metal Organic Framework Incorporation – MOFs for Water Oxidation and Carbon Dioxide Reduction

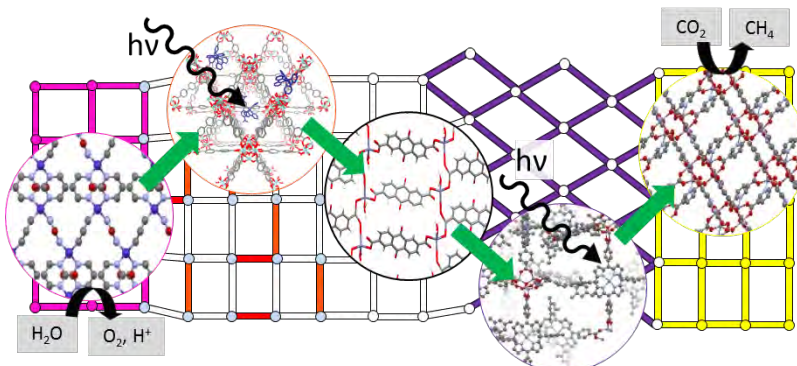
Lin, S.Y.; Zhu, J.; Usov, P.; Ahrenholtz, S.R.; Morris, A.J.

Department of Chemistry

Virginia Tech

Blacksburg, VA 24060

Work in the Morris laboratory is motivated by the study of energy transfer and photo-driven catalytic reactivity within well-defined, three-dimensional (3D) molecular, metal organic frameworks (MOFs) for ultimate applications in artificial photosynthesis. Herein, we will summarize our recent results on both water oxidation catalysis and a new venture, carbon dioxide activation and reduction.



**Water Oxidation.** We have recently reported the incorporation of known homogeneous, molecular water oxidation catalysts into stable zirconium-based metal organic framework backbones. Most important, both frameworks exhibit superior stability relative to previously employed MOF water oxidation catalysts. Indeed, we argue that these materials are the first molecular-MOFs to oxidize water. The two frameworks are PCN-224-Ni (porphyrin-based) and RuTERPY-doped UiO-67. *PCN-224-Ni*. In this work, we observed evidence of synergistic electron transfer/proton abstraction process occurring inside PCN-224-Ni between the linker and the inorganic node. The mechanism of water oxidation at PCN-224-Ni was found to proceed via the initial oxidation of the porphyrin linker followed by binding of water to the Ni(II) of Ni(II)TCPP. Subsequent proton transfer to the Zr nodes enabled the eventual release of O<sub>2</sub>. *RuTERPY-UiO-67*. Catalyst concentration dependent electrochemistry indicates a redox-hopping mechanism and *in*-MOF reactivity. At the highest achieved electroactive site coverage, the observed current is more than 120 times higher than a full packing monolayer of the homogenous analog on the same FTO electrode ( $\sim 1 \times 10^{-10}$  mol/cm<sup>2</sup>).

**Carbon Dioxide Reduction.** Herein, we will introduce a new class of MOFs we have developed for the simultaneous capture and conversion of CO<sub>2</sub>, VPI-100-M. The MOF framework is composed of Zr nodes and metallo-tetraazamacrocycles (in short cyclam). Cyclam has a rich history in the CO<sub>2</sub> reduction literature and we capitalize on this chemistry to produce an active MOF capable of redox-hopping catalysis. Interestingly, through simple metal substitution, the MOF platform is capable of tunable reactivity from the aforementioned synthesis fuels through CO<sub>2</sub> reduction to the synthesis of value-added chemicals through CO<sub>2</sub> activation.

Grant Period Manuscripts - J. Mater. Chem. A, 2016, 4, 16818-16823; ChemSusChem, 2017, 10, 514-522; J. Photochem. Photobiol. A: Chem., 2017, 337, 207-215; J. Photochem. Photobiol. A: Chem., *in review*; ACS Appl. Mater. Inter. 2017, accepted; Book Chapter - Sustainable Energy and Environment Remediation (1st Edition), Royal Society of Chemistry, 202-239.

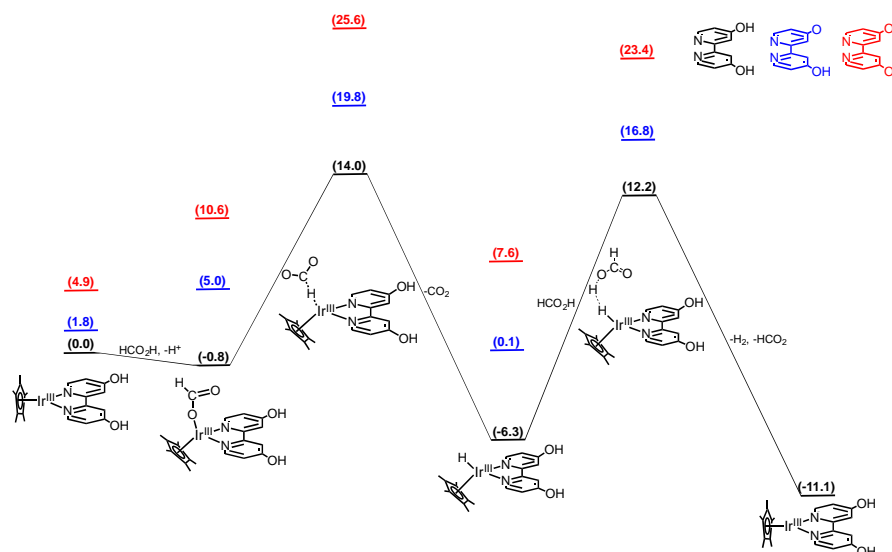
# Interconversion of Formic Acid and Carbon Dioxide by Proton-Responsive, Half-Sandwich Cp\*Ir(III) Complexes: A Computational Mechanistic Investigation

M. Z. Ertem,<sup>1</sup> Y. Himeda,<sup>2</sup> E. Fujita<sup>1</sup> and J. T. Muckerman<sup>1</sup>

<sup>1</sup> Chemistry Division  
Brookhaven National Laboratory  
Upton, NY 11973-5000

<sup>2</sup> National Institute of Advanced Industrial Science and Technology, Tsukuba Central 5,  
1-1-1 Higashi, Tsukuba, Ibaraki 305-8565, Japan

Dihydrogen (H<sub>2</sub>) has many desirable features as a fuel, but utilization of H<sub>2</sub> is limited due to storage and transportation problems. A promising solution to these issues is reversible storage of hydrogen in the form of liquid-phase chemicals such as formic acid (FA), which could be accomplished by the development of efficient and robust catalysts. Recently, proton-responsive, half-sandwich Cp\*Ir<sup>III</sup> (where Cp\* = pentamethylcyclopentadienyl anion) complexes capable of reversible hydrogen storage via interconversion between H<sub>2</sub>/CO<sub>2</sub> and formic acid/formate in water have been reported. This interconversion is performed via CO<sub>2</sub> hydrogenation and FA dehydrogenation reactions and modulated by the pH of the medium. We report the results of a computational investigation of the mechanistic aspects of reversible hydrogen storage via two of these catalysts: namely, [Cp\*Ir(4DHBP)]<sup>2+</sup> (4DHBP = 4,4'-dihydroxy-2,2'-bipyridine) and [Cp\*Ir(6DHBP)]<sup>2+</sup> (6DHBP = 6,6'-dihydroxy-2,2'-bipyridine). Distinct features of the catalytic cycles of [Cp\*Ir(4DHBP)]<sup>2+</sup> and [Cp\*Ir(6DHBP)]<sup>2+</sup> for CO<sub>2</sub> hydrogenation and FA dehydrogenation reactions are demonstrated using density functional theory (DFT) calculations employing a “speciation” approach and probing deuterium kinetic isotope effects (KIE). In addition to the mechanistic insights and principles for the design of improved next-generation catalysts, the validation of computational methods for the investigation of the hydrogenation and dehydrogenation reactions is addressed.



Proposed mechanism for formic acid dehydrogenation by the [Cp\*Ir(4DHBP)]<sup>2+</sup> complex at pH 1.8 and 333.15 K. The relative free energies are reported in units of kcal/mol. The speciation of the protonation states of each intermediate and transition state is indicated by the color code of the structures in the upper right of the scheme.

## Design of Molecular Modules for Artificial Photosynthesis

Karen L. Mulfort, Lars Kohler, Dugan Hayes, Lin X. Chen, Oleg G. Poluektov, David M. Tiede  
Division of Chemical Sciences and Engineering  
Argonne National Laboratory  
Argonne, IL 60439

This poster will describe our group's progress in the design and discovery of modular, molecular architectures for artificial photosynthesis. New synthesis and targeted, high-resolution physical characterization of photocatalyst modules will contribute to our understanding of how each module behaves individually before linking with complementary functionality. Here we will present recent work on 1) CuHETPHEN photosensitizer modules and 2) Co(III)poly(pyridyl) catalyst modules.

The visible-light accessible metal-to-ligand charge transfer (MLCT) states of Cu(I)diimine complexes suggest that they may be viable replacements for benchmark  $\text{Ru}(\text{bpy})_3^{2+}$ -type photosensitizers. The heteroleptic phenanthroline (HETPHEN) synthesis approach presents a means to enable synthetic diversity for linking electron donors, acceptors, and catalyst modules to Cu(I)diimine complexes. We have recently reported the synthesis of a new HETPHEN blocking ligand, 2,9-di(2,4,6-triisopropyl-phenyl)-1,10-phenanthroline (**bL2**), and its use in the preparation of CuHETPHEN complexes. Coordination of **bL2** enforces a distorted tetrahedral geometry around the Cu(I) center, but prevents inter-ligand interaction (Figure 1). The  $^3\text{MLCT}$  excited state lifetime of the CuHETPHEN complexes depends strongly on each ligand, and can be tuned from  $\sim 700$  ps to over 70 ns in  $\text{CH}_3\text{CN}$ . Interestingly, the isolation of  $[\text{Cu}(\text{bL2})(\text{L3})](\text{PF}_6)$  was not possible and suggests an upper limit for 2,9-phenanthroline substitution and CuHETPHEN stability. The CuHETPHEN model complexes shown here are currently being used to build bridged bimetallic complexes comprising both Cu(I) and Ru(II) centers as well as exploring the interplay of electron transfer and solvent stabilization in linked CuHETPHEN-naphthalene diimide complexes.

The development of aqueous stable, long-lived catalyst modules based on earth-abundant elements is vital for integration of molecular complexes into systems for solar energy conversion. Recent work has focused on the synthesis of a new Co(III)poly(pyridyl) complex (**5**, Figure 2) which is closely related to Co(II)tetra- and penta(pyridyl) complexes under study by a number of research groups. Preliminary results show that **5** is highly active for aqueous proton reduction at moderate pH levels for *days* when photo-driven by  $\text{Ru}(\text{bpy})_3^{2+}$  using ascorbate as a sacrificial electron donor. Current efforts are focused on using the amine positions to link **5** directly to photosensitizers.

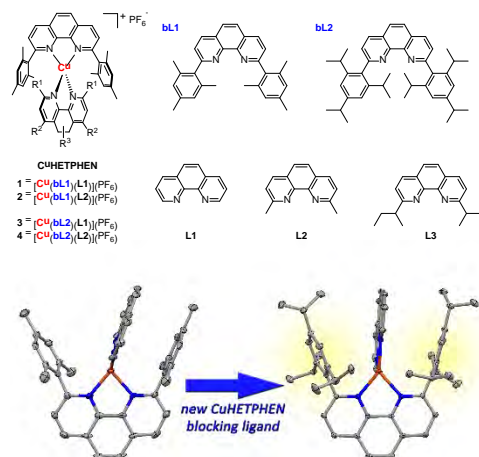


**Figure 1.** Top: chemical structures of model CuHETPHEN complexes. Bottom: comparison of crystal structures of **1** and **3** illustrating influence of blocking ligand on inter-ligand interaction.

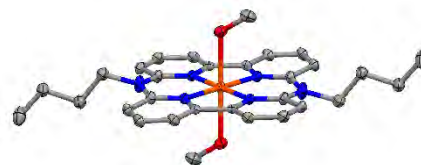


**Figure 2.** Crystal structure of molecular Co(III) proton reduction catalyst, **5**. Ellipsoids represent 50% probability. Hydrogen atoms, solvent molecules, and  $\text{BF}_4^-$  counterion are omitted for clarity. Carbon, gray; nitrogen, blue; oxygen, red; cobalt, orange.

## Tuning Semiconductor Photoelectrode Energetics by Molecular Surface Modification

Logan E. Garner,<sup>1</sup> K. Xerxes Steirer,<sup>1,2</sup> James L. Young,<sup>1</sup> Nicholas C. Anderson,<sup>1</sup> Elisa M. Miller,<sup>1</sup> Jonathan S. Tinkham,<sup>2</sup> Todd G. Deutsch,<sup>1</sup> Alan Sellinger,<sup>1,2</sup> John A. Turner,<sup>1</sup> and Nathan R. Neale

<sup>1</sup>Chemistry and Nanoscience Center, NREL, Golden, CO 80401

<sup>2</sup>Colorado School of Mines, Golden, CO 80401

Efficient water splitting using light as the only energy input requires stable semiconductor electrodes with favorable energetics for the water-oxidation and proton-reduction reactions. Strategies to tune electrode potentials using molecular dipoles adsorbed to the semiconductor surface have been pursued for decades but are often based on weak interactions and quickly react to desorb the molecule under conditions relevant to sustained photoelectrolysis.

In this presentation we show that covalent attachment of extreme dipoles based on fluorinated, aromatic molecules to *p*-GaAs(100) surfaces can be employed to tune the photocurrent onset potentials of *p*-GaAs(100) photocathodes and reduce the external energy required for hydrogen production. Results indicate that initial photocurrent onset potentials can be shifted by nearly 150 mV in pH -0.5 electrolyte under 1 sun illumination resulting from the covalently bound surface dipoles. X-ray photoelectron spectroscopy analysis reveals that the covalent molecular dipole attachment is not robust under extended 50 h photoelectrolysis. Instead, the surface modification chemistry seems to condition the surface and render it resistant to As<sub>2</sub>O<sub>3</sub> formation. Mitigating surface As<sub>2</sub>O<sub>3</sub> results in a *p*-GaAs(100) photoelectrode operating at a sustained photocurrent density of 20.5 mA cm<sup>2</sup> within 0.5 V of the reversible hydrogen electrode and more generally points a direction to stabilize III-V photoelectrodes through controlled surface oxidation.

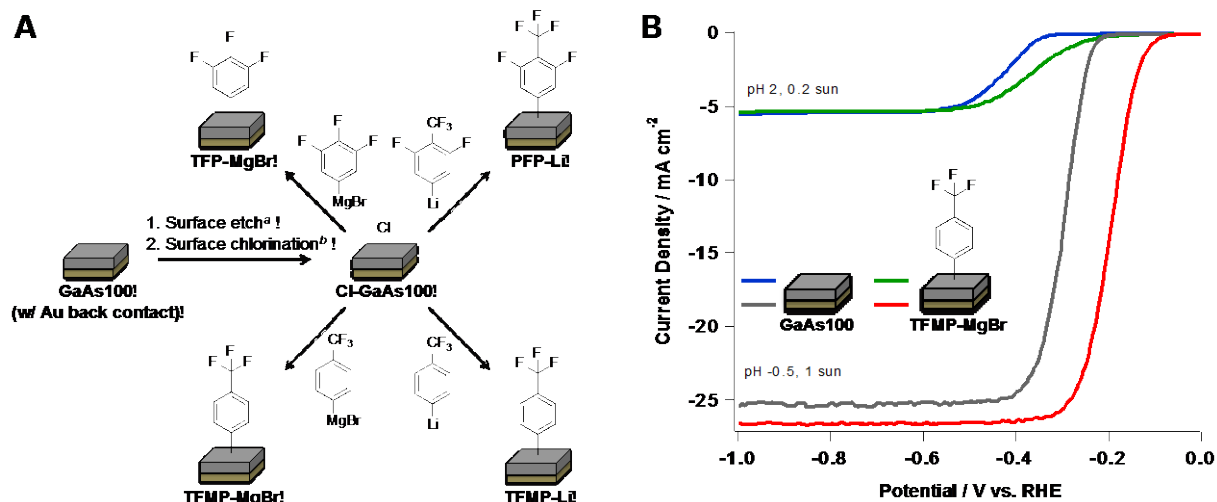


**Figure 1.** (A) Schematic of *p*-GaAs(100) modification with surface dipoles. Bare **GaAs100** electrodes are functionalized with chloride (**Cl-GaAs100**), and subsequently reacted with 3,4,5-trifluorophenyl (**TFP-MgBr**), 4-(trifluoromethyl)phenyl (**TFMP-MgBr** and **TFMP-Li**), and 3,5-difluoro-4-(trifluoromethyl)phenyl (**PFP-Li**). (B) Current density vs. potential traces of bare **GaAs100** and **TFMP-MgBr** photocathodes analyzed under pH 2/0.2 sun illumination (blue and green traces) and pH -0.5/1 sun illumination (dark grey and red traces).

## Enhanced Multiple Exciton Generation (MEG) in PbS/CdS Janus-like Heterostructure Nanocrystals

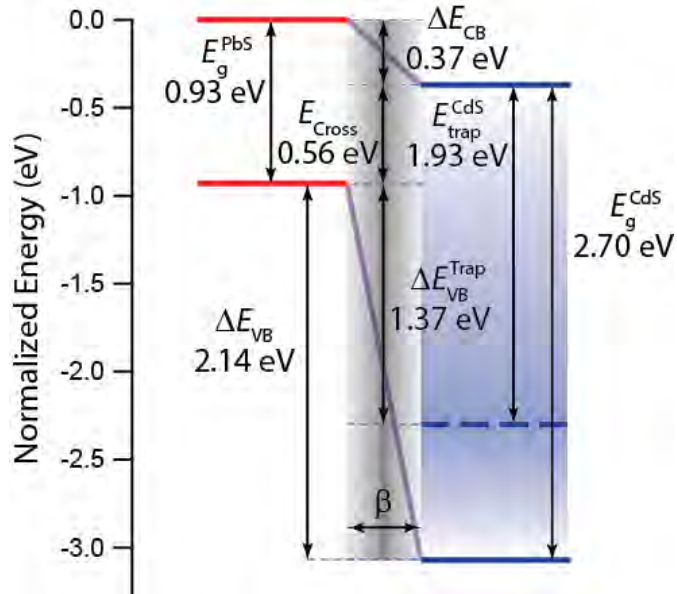
Daniel Kroupa<sup>\*,†</sup>, G. Pach<sup>\*</sup>, B. Chernomordik<sup>\*</sup>, A.J. Nozik<sup>\*,†</sup>, M.C. Beard<sup>\*</sup>

\* Chemistry and Nanoscience Center  
National Renewable Energy Laboratory  
Golden, CO 80401

and

<sup>\*,†</sup> Department of Chemistry  
University of Colorado  
Boulder, CO 80309

We use femtosecond transient absorption spectroscopy to study multiple exciton generation (MEG) in PbS/CdS Janus-like heterostructure nanocrystals. Our results show that these nanocrystals exhibit enhanced MEG over nanocrystals composed of only a single material, such as PbS and PbSe, as well as PbSe/CdSe core/shell quantum dots. We attribute this MEG enhancement to an increase in the MEG rate,  $k_{MEG}$ , arising from the built-in electric field across the PbS/CdS interface, as well as a slowing of the competing hot exciton cooling rate,  $k_{cool}$ , due to hot hole localization as it cools through the valence band manifold of hole states. Additionally, we show that PbS/CdS Janus-like heterostructure nanocrystals can be incorporated as the main absorber layer into functional solar cell device architectures.



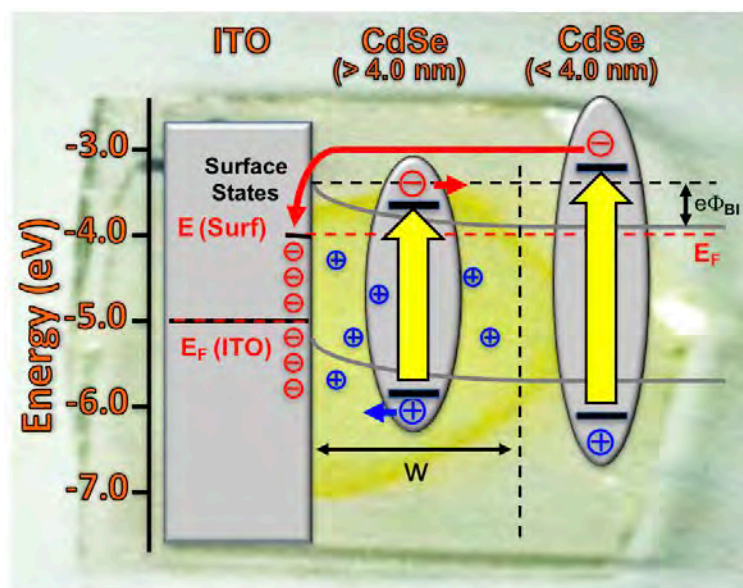
Energy level diagram for 50/50 PbS/CdS heterostructure NCs. A type-II band alignment exists between the PbS and CdS domains. Shaded blue area represents CdS related inter-gap hole states. Shaded black area represents the range of the electric field gradient across the PbS/CdS interface,  $\beta$ .

## Surface Photovoltage Spectroscopy Observes Built-in Voltage, Space Charge Layer Width and Effective Band Gap in CdSe Quantum Dot Films

Jing Zhao, Benjamin A. Nail, Michael A. Holmes, **Frank E. Osterloh**

Department of Chemistry  
University of California - Davis  
Davis, CA 95616

Here we use surface photovoltage spectroscopy (SPS) to study the photochemistry of mercaptoethanol-ligated CdSe quantum dot (2.0–4.2 nm diameter) films on indium doped tin oxide (ITO) in the absence of an external bias or electrolyte. The n-type films generate negative voltages under super band gap illumination ( $0.1\text{--}0.5\text{ mW cm}^{-2}$ ) by majority carrier injection into the ITO substrate. The photovoltage onset energies track the optical band gaps of the samples and are assigned as effective band gaps of the films. The photovoltage values ( $-125$  to  $-750$  mV) vary with quantum dot sizes and are modulated by the built-in potential of the CdSe–ITO Schottky type contacts. Deviations from the ideal Schottky junction model are attributed to Fermi level pinning in states approximately 1.1 V negative of the ITO conduction band edge. Positive photovoltage signals of  $+80$  to  $+125$  mV in films of  $>4.0$  nm nanocrystals and in thin (70 nm) nanocrystal films are attributed to electron–hole (polaron) pairs that are polarized by a space charge layer at the CdSe–ITO boundary. The space charge layer is 70–150 nm wide, based on thickness-dependent photovoltage measurements. The ability of SPS to directly measure built-in voltages, space charge layer thickness, sub-band gap states, and effective band gaps in drop-cast quantum dot films aids the understanding of photochemical charge transport in quantum dot solar cells.



Energy Scheme for CdSe quantum dot (QD) film on indium tin oxide (ITO) substrate. Arrows show direction of photochemical charge transfer and polarization. From Zhao, J.; Nail, B. A.; Holmes, M. A.; Osterloh, F. E. *J. Phys. Chem. Lett.* **2016**, 3335-3340. <https://doi.org/10.1021/acs.jpcllett.6b01569>

## Earth Abundant Transition Metal Catalysts for Photochemical Hydrogen Production: A Combined Study using Multi-Frequency EPR and DFT Calculations

Oleg G. Poluektov, Jens Niklas, Karen L. Mulfort, Lisa M. Utschig, David M. Tiede

Division of Chemical Sciences and Engineering

Argonne National Laboratory

Lemont, IL 60439

Kristy L. Mardis

Department of Chemistry & Physics, Chicago State University

Chicago, IL 60628

Current research in our group aims to mimic photosynthesis and reveal fundamental mechanisms for solar-to-chemical energy conversion which consists of capture, conversion, and storage of solar energy in high-energy molecular bonds, with the production of solar fuels. Molecular hydrogen stands out among the solar fuels, since it can be utilized essentially pollution-free. The development and improvement of solar energy conversion systems relies on understanding the inherent, fundamental mechanisms for coupling captured photons to fuel generation.

One key element of these systems is the catalyst. To achieve sustainable hydrogen generation, the catalysts should not be rare and expensive, but use earth abundant elements like first row transition metals. Both cobaloximes and Ni-bis(diphosphine) complexes are among the best molecular transition metal complexes for the reduction of protons to molecular hydrogen. The catalytic efficiency, which is the key issue for molecular catalysts, is determined to a large extent by its electronic structure. The electronic structure in turn is strongly influenced by its surroundings and in particular by the ligand(s) directly bound to the central metal ion, as well as hydrogen bonding with the ligand atoms and the dielectric properties of the medium might be important as well. To reveal electronic structure of these cobaloxime and Ni-bis(diphosphine) complexes and establish correlations between structure, surroundings and their catalytic activity we have used multi-frequency EPR/ENDOR spectroscopy at X-band (9 GHz), Q-band (34 GHz), and D-band (130 GHz) combined with X-ray crystallography and DFT calculations. Precise determination of the “key” magnetic parameters, such as  $g$ -tensors and hyperfine interaction with various magnetic nuclei like  $^{59}\text{Co}$ ,  $^{14}\text{N}$ ,  $^1\text{H}$  and  $^{31}\text{P}$ , in combination with comprehensive DFT analysis allows identification of the conformation states, the spin density distribution on the ligands, and interactions with coordination solvent molecules. The knowledge gained by these studies has been used to characterize the cobaloxime/Ni-bis(diphosphine) based complexes with light-harvesting and charge separation motifs in artificial and photosynthetic protein frameworks.

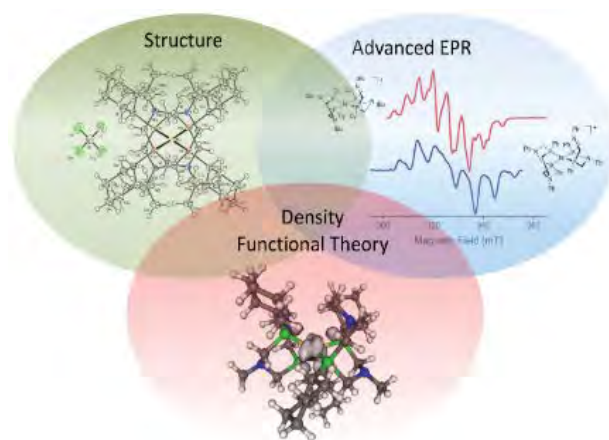


**Figure 1.** The molecular and electronic structures of the molecular catalysts have been revealed by a combination of EPR spectroscopy, X-ray crystallography, and DFT analysis.

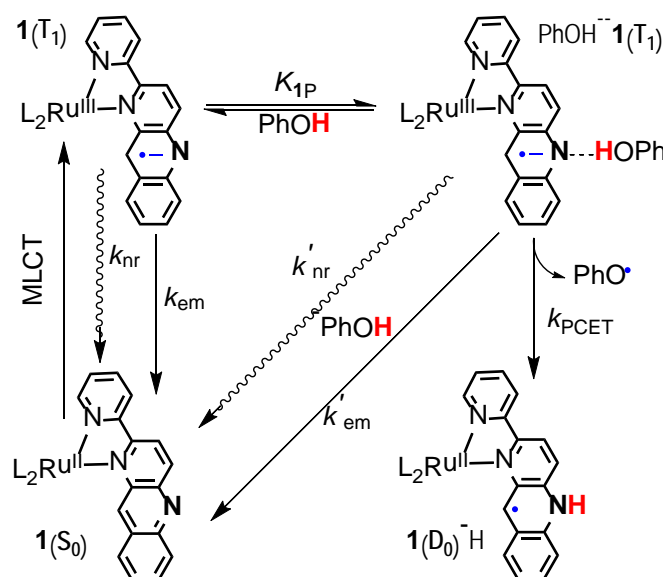
## The Role of Hydrogen Bonding in Proton-Coupled Electron Transfer: Reactions between Photoexcited Metal Complexes and Phenol Donors

Dmitry E. Polyansky, Mehmed Z. Ertem, Sergei V. Lymar

Chemistry Division, Energy & Photon Sciences Directorate, Brookhaven National Laboratory  
Upton, NY 11973-5000

Mechanistic studies of proton-coupled electron transfer (PCET) had received increased attention due to their relevance to natural and artificial photosynthetic transformations. It has been demonstrated that hydrogen-bonding (HB) between donor and acceptor molecules has a profound effect on the kinetics of a PCET process. However, when HB interactions involve transient species, such as transition metal complexes in their MLCT excited states, HB equilibrium cannot be measured directly and its value (e.g.,  $K_{1P}$  as shown in figure below) has to be extracted from excited state lifetime or luminescence measurements.

In this work we had examined PCET from *p*-substituted phenols to the MLCT-excited Ru polypyridine complexes containing an uncoordinated basic nitrogen site using comprehensive kinetic framework that takes into account the Ru complex-phenol, Ru complex-solvent, and phenol-solvent HB interactions. It was found that negative apparent activation enthalpies provide the only experimental evidence for the



formation of a precursor HB complex between the reactants, and several previously reported equilibrium constants for such precursors are shown to be in error caused by an inconsistent data analysis. The considerable strength of the phenol-solvent HB both prevents extracting the unimolecular PCET rate constant from the kinetic data and plays a major role in the observed kinetic solvent effect (KSE) between acetonitrile and dichloromethane. A thermochemical analysis of the alternative PCET pathways suggests that (i) the pathways initiated by electron transfer (ET) from phenols and those involving deprotonation of phenols by

solvent play no role; (ii) the most energetically favorable pathway provided by the concerted electron-proton transfer (EPT) operates for all phenols and both solvents, except for the most acidic phenols in acetonitrile, for which the energy gap favoring EPT over proton transfer (PT) virtually disappears; (iii) the Hammett  $\sigma_p$  constant provides a common descriptor linearly correlating all major thermochemical PCET parameters.

**Acknowledgments:** We thank Prof. R. Thummel (U. Houston) and Prof. K. Tanaka (U. Kyoto) for providing samples used in this work as well as Prof. S. Hammes-Schiffer and Dr. A. Soudackov (U. Illinois, Urbana-Champaign) for insightful discussions of quantum chemical calculations.

## Time-Domain Atomistic Modeling of Photo-Excitation Dynamics in Hybrid Nanoscale Systems for Solar Energy Harvesting

Oleg Prezhdo

Department of Chemistry  
University of Southern California  
Los Angeles, CA 90089

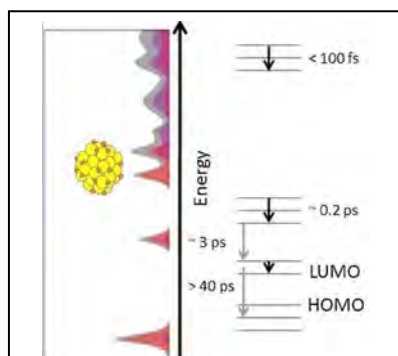


**Figure 1.** We investigated energy relaxation in gold nanoparticles and showed that molecular-like relaxation occurs only under special conditions. A long-lived intermediate in  $\text{Au}_{55}$  aligns with the conduction band edge of  $\text{TiO}_2$ , facilitating injection from  $\text{Au}_{55}$  into  $\text{TiO}_2$  and avoiding energy losses.

Photo-induced processes at interfaces form foundation of photovoltaic and photo-catalytic applications. They require understanding of dynamical response of novel systems on atomic and nanometer scales. Our non-adiabatic molecular dynamics techniques, implemented within time-dependent density functional theory, allow us to model such non-equilibrium response in real time. We focus on photo-initiated charge and energy transfer in several types of nanoscale systems. Recent examples include hybrid organic-inorganic perovskites, metallic and semiconducting nanoparticles, semiconductor surfaces sensitized with molecular chromophores, and interfaces of two-dimensional materials. These systems create many challenges due to stark differences between molecular and periodic, and organic and inorganic components. Our simulations provide a unifying description of quantum dynamics on nanoscale, characterize the rates and branching ratios of competing processes, resolve debated issues, and generate theoretical guidelines for development of novel systems for solar energy harvesting.

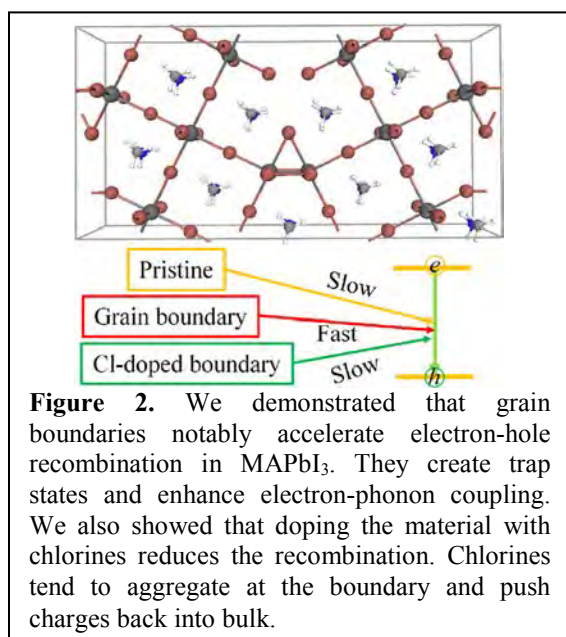


**Figure 2.** We demonstrated that grain boundaries notably accelerate electron-hole recombination in  $\text{MAPbI}_3$ . They create trap states and enhance electron-phonon coupling. We also showed that doping the material with chlorines reduces the recombination. Chlorines tend to aggregate at the boundary and push charges back into bulk.

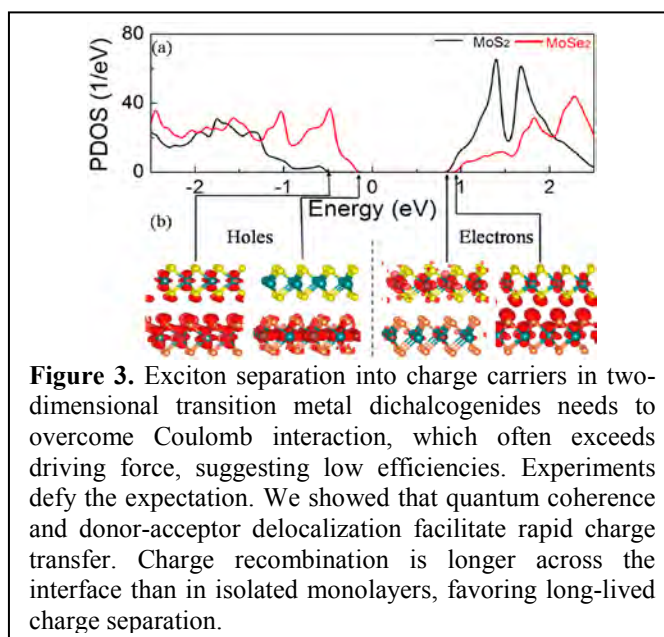


**Figure 3.** Exciton separation into charge carriers in two-dimensional transition metal dichalcogenides needs to overcome Coulomb interaction, which often exceeds driving force, suggesting low efficiencies. Experiments defy the expectation. We showed that quantum coherence and donor-acceptor delocalization facilitate rapid charge transfer. Charge recombination is longer across the interface than in isolated monolayers, favoring long-lived charge separation.

## Chemo-structural Composition and Photovoltaic Efficiency of $\text{CH}_3\text{NH}_3\text{PbI}_3$ Perovskite affected by external factors

Sylwia Ptasinska

Radiation Laboratory and Department of Physics  
University of Notre Dame  
Notre Dame, IN 46556

Interest in hybrid organic-inorganic lead halide perovskites has recently surged due to their potentially high impact for optical and photovoltaic applications. The high power conversion efficiency, simple fabrication techniques, low manufacturing cost, and relative insensitivity to defects make perovskite solar cells highly promising in photovoltaic technology. Despite the impressive achievements of perovskite materials in device efficiency, their operational instability must be overcome before they can be broadly applied. This concern has sparked a series of studies on the influence of external factors (e.g., humidity, air, UV light and polar molecules) on the transformation of perovskite.

To elucidate both the chemical changes and the influence of such factors on solar cell performance, we analyzed the results of X-ray photoelectron spectroscopy, scanning electron microscopy, and X-ray diffraction of perovskite films exposed to various conditions. Chemical analysis revealed the loss of  $\text{CH}_3\text{NH}_3^+$  and  $\text{I}^-$  species from  $\text{CH}_3\text{NH}_3\text{PbI}_3$  under ambient conditions and its subsequent decomposition into lead carbonate, lead hydroxide, and lead oxide (Fig. 1) [1]. After long-term storage, morphological analysis revealed that randomly distributed defects and cracks, initially present in the densely packed crystalline structure, had transformed into relatively small grains. Films stored under such conditions were incorporated into photovoltaic cells, and we observed a significant decrease in the photovoltaic efficiency of modified  $\text{CH}_3\text{NH}_3\text{PbI}_3$ . Moreover, low-energy electrons [2] and polar molecules [3] can also affect the structural and chemical properties of  $\text{CH}_3\text{NH}_3\text{PbI}_3$ , leading to transformations of the organic part of the material.

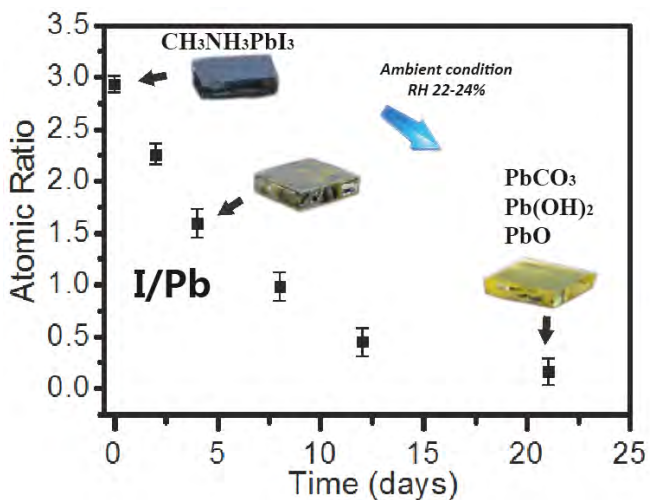


Fig. 1 Probing the transformations of  $\text{CH}_3\text{NH}_3\text{PbI}_3$  exposed to ambient conditions using in situ X-ray photoelectron spectroscopy and microscopy techniques.

1. W. Huang, J. Manser, P.V. Kamat, S. Ptasinska. *Chem. Mat.* 28 (2016) 303-3011
2. A.R. Milosavljević, W. Huang, S. Sadhu, S. Ptasinska. *Angew. Chem. Int. Ed.* 128 (2016) 10237-10241
3. W. Huang, J.S. Manser, S. Sadhu, P.V. Kamat, S. Ptasinska. *J. Phys. Chem. Lett.* 7 (2016) 7 5068-5073

## Transformations of Ru complexes under catalytic condition of water oxidation

Yulia Pushkar, Yuliana Smirnova, Darren Erdman  
Department of Physics  
Purdue University  
West Lafayette, Indiana 47907

Realization of artificial photosynthesis carries the promise of cheap and abundant energy. The water molecule is an ideal source of electrons and protons for fuel forming reactions, but the chemical complexity of water splitting makes practical realization challenging. To advance the catalyst's rational design, detailed information on the structure of the catalyst under reaction conditions and mechanisms of O-O bond formation are required.<sup>1-3</sup>

$[\text{Ru}^{\text{II}}(\text{NPM})(4\text{-pic})_2(\text{H}_2\text{O})]^{2+}$  (NPM = 4-*t*-butyl-2,6-di(1',8'-naphthyrid-2'-yl)pyridine, pic = 4-picoline) was the first reported Ru-based single site catalyst.<sup>4</sup> Here, we used a combination of EPR, freeze quench and stopped flow spectroscopy with ms-s time resolution, X-ray absorption spectroscopy (XAS), Resonance Raman (RR) and DFT to follow catalyst dynamics under conditions of water oxidation. We report a unique EPR signal with  $g$ -tensor,  $g_x = 2.30$ ,  $g_y = 2.18$  and  $g_z = 1.83$  which allowed us to observe fast dynamics (on few sec time scale) of oxygen atom transfer from the  $\text{Ru}^{\text{IV}}=\text{O}$  oxo species to uncoordinated nitrogen of the NPM ligand. NPM ligand modification occurs on the time scale of catalyst activation and results in  $[\text{Ru}^{\text{III}}(\text{NPM-NO})(4\text{-pic})_2(\text{H}_2\text{O})]^{3+}$  and  $[\text{Ru}^{\text{III}}(\text{NPM-NO,NO})(4\text{-pic})_2]^{3+}$  complexes. Combined spectroscopic results allowed us to re-assign the previously reported  $[\text{Ru}^{\text{IV}}(\text{NPM})(4\text{-pic})_2(\text{O}_2)]^{2+}$  peroxy intermediate<sup>5</sup> as a product of NPM ligand oxidation. Spectroscopic signatures of proposed  $[\text{Ru}^{\text{V}}(\text{NPM})(4\text{-pic})_2=\text{O}]^{3+}$  intermediate were not detected under the tested conditions. Reported results have implication for rational design of water oxidation catalysts. We demonstrated that proximal base might be beneficial in O-O bond formation via nucleophilic water attack on oxo species by DFT analysis of transition state. However, non-coordinating nitrogen cannot be used as a base in water oxidation catalysts due to its facile conversion to N-O group. The reported results open new horizons for understanding the real structure of Ru catalysts under water oxidation conditions and point towards the need to further investigate the role of N-O ligand in promoting water oxidation catalysis.

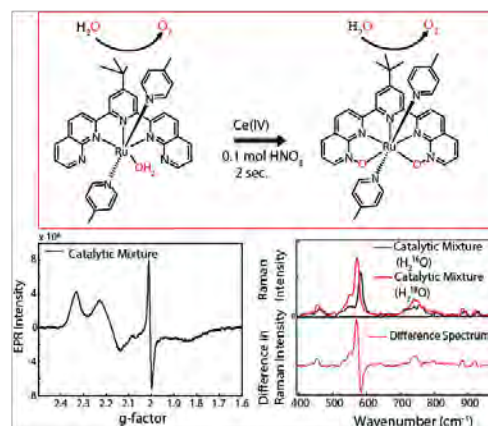


Figure 1. EPR, RR and XAS detected catalysts modification.

### References

1. Moonshiram, D.; Pineda-Galvan, Y.; Erdman, D.; Palenik, M.; Zong, R.; Thummel, R.; Pushkar Y. *J. Am. Chem. Soc.* 2016, *138* (48), 15605.
2. Lin, S.; Pineda-Galvan, Y.; Maza, W. A.; Epley, C. C.; Zhu, J.; Kessinger, M. C.; Pushkar, Y.; Morris, A. J. *ChemSusChem*, 2017, *10*, 3, 514-522.
3. Erdman, D.; Pineda-Galvan, Y.; Pushkar, Y. *Catalysts*, 2017, *v. 7* (2) article number 39.
4. Zong, R.; Thummel, R. P. *J. Am. Chem. Soc.* 2005, *127*, 12802.
5. Polyansky, D. E.; Muckerman, J. T.; Rochford, J.; Zong, R.; Thummel, R. P.; Fujita, E. *J. Am. Chem. Soc.* 2011, *133* (37), 14649.

## Carrier Dynamics in Metals Oxides for Water-Splitting Dye-Sensitized Photoelectrochemical Cells

John R. Swierk, Kevin P. Regan, Jens Neu, Jianbing Jiang, Gary W. Brudvig and Charles A. Schmuttenmaer  
Department of Chemistry  
Yale University  
New Haven CT 06511

In water-splitting dye-sensitized photoelectrochemical cells, a mesoporous, nanoparticulate metal oxide functions both as support for molecular components and electronic conductor. Many of the major challenges in the development of dye-sensitized water splitting are specific to the metal oxide: low injection yields, fast recombination, poor electron transport, etc. We have focused on the electron-transfer dynamics in these metal oxides, particularly ultrafast dynamics, as well as the development of new metal oxides for use in dye-sensitized water-splitting cells. Recently, we probed the transient photoconductivity of bare and sensitized  $\text{SnO}_2$  and found that the method of charge generation had a significant effect on both the overall charge injection and trapping dynamics.<sup>1</sup> In addition, because of a photoinduced change in permittivity, the transient photoconductivity deviates from the behavior described by the standard Drude-Smith model. We also proposed the use of rutile  $\text{TiO}_2$  (r- $\text{TiO}_2$ ) as a novel photoanode material.<sup>2</sup> Compared to the more commonly utilized anatase  $\text{TiO}_2$  (a- $\text{TiO}_2$ ), the conduction band of r- $\text{TiO}_2$  is  $\sim 200$  mV more positive allowing for injection yields that approach unity. Recombination in r- $\text{TiO}_2$  is slower by approximately one order of magnitude, leading to enhanced photoelectrochemical performance when compared to a- $\text{TiO}_2$ .

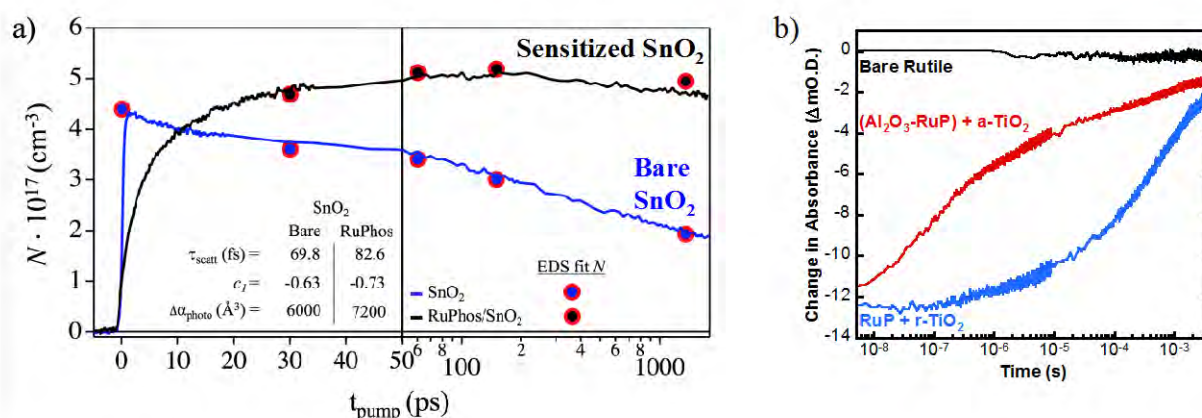


**Figure 1.** a) Optical pump-terahertz probe traces for sensitized and bare  $\text{SnO}_2$  overlaid with the carrier density,  $N$ , shown as blue and black symbols with red border, which was the only parameter varied at each pump-probe delay time. Samples are sealed with 0.1 M  $\text{HClO}_4$  (aq). b) Transient absorption monitored for sensitized r- $\text{TiO}_2$  and a- $\text{TiO}_2$  samples. The injection yield for a- $\text{TiO}_2$  is 0.2-0.3, while for r- $\text{TiO}_2$  the injection yield is  $0.74 \pm 0.13$ .

1. Regan, K.P.; Swierk, J.R.; Neu, J.; Schmuttenmaer, C.A., *submitted*.
2. Swierk, J.R.; Regan, K.P.; Jiang, J.; Brudvig, G.W.; Schmuttenmaer, C.A., *ACS Energy Lett.*, **2016**, *1*, 603.

## What does Coherence Mean in Electron Transfer Reactions? The betaine-30 Example.

Shahnawaz Rafiq and Gregory D. Scholes  
Frick Chemistry Laboratory  
Princeton University  
Princeton, NJ 08542

The possible role of coherent vibrational motion in ultrafast photo-induced electron transfer remains unclear despite considerable experimental and theoretical advances. What coherence means for electron transfer will be discussed. As one example, our work tracking the back-electron transfer reaction after ultrafast photoexcitation of Betaine-30 will be reported. Broad-band pump-probe spectroscopy allows us to follow the evolution of the vibrational spectrum in time with remarkable clarity, Fig 1. Dephasing time constant of certain high-frequency vibrations depend on solvent, following the trend measured for the electron transfer rate constants. In the purview of the Bixon-Jortner model, high-frequency quantum vibrations bridge the reactant-product energy gap by providing activationless vibronic channels. Such interaction reduces the effective coupling significantly. We find that the reaction does not show coherence effects because of the large driving force and rapid internal conversion.

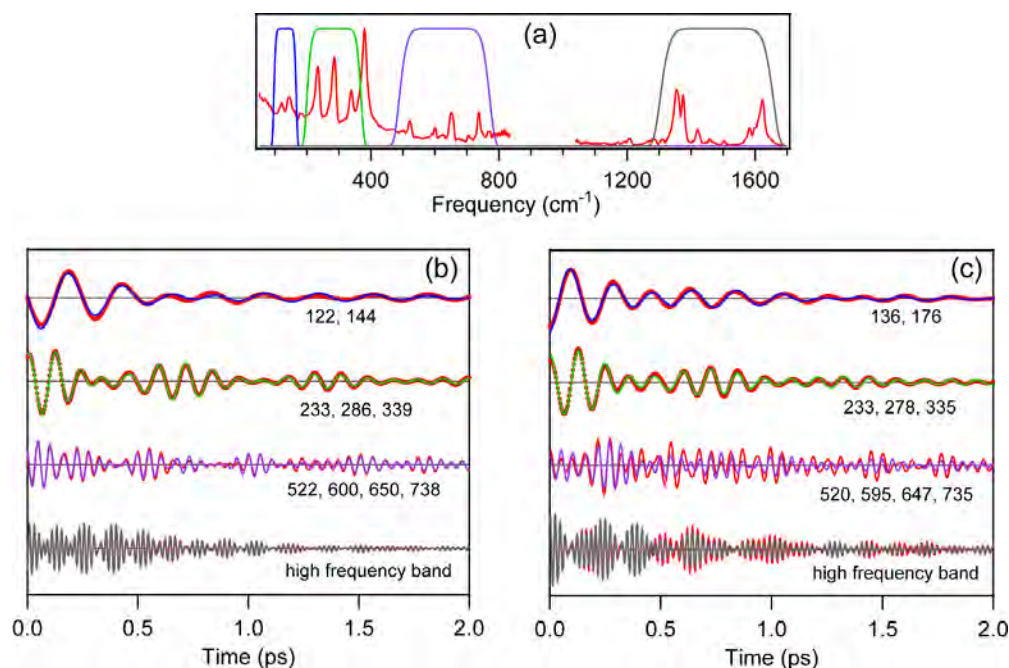


**Figure 1:** (a) Integrated Fourier transform of the broad-band pump-probe spectrum of Betaine-30 in acetonitrile. On top of the Fourier transform trace are super-Gaussian windows used in our filtering procedure. The solvent Raman peak at  $918\text{ cm}^{-1}$  is removed for clarity. Inverse Fourier transform of the filtered frequency bands brings the signal back into the time domain as shown in (b) and (c) for Betaine-30 in acetonitrile and methanol respectively.

## Interfacial Charge Transfer Pathways and Photocarrier Dynamics in Heterostructured Nanocomposite Photoanodes

Lucas H. Hess, Jason K. Cooper, and Ian D. Sharp  
Chemical Sciences Division  
Lawrence Berkeley National Laboratory  
Berkeley, CA 94720

Efficient capture and conversion of solar energy in photoelectrochemical systems requires that photogenerated charge carriers be separated and extracted across interfaces before they can recombine. While transition metal oxides offer considerable promise in terms of stability and scalability, they often suffer from poor charge transport properties and low charge extraction probabilities. Heterostructured nanocomposites, in which nanoscale compounds exhibiting complimentary optoelectronic properties are combined, offer promise for overcoming these issues by directing charge transfer along pathways that reduce recombination and promote efficient charge extraction. The result is systems that exhibit functional properties that exceed those of the isolated components. However, interfacial energetics and associated kinetic pathways often differ significantly from predictions derived from the characteristics of pure component materials, particularly at the nanoscale. Here, the emergent properties of  $\text{TiO}_2/\text{BiVO}_4$  nanocomposite photoanodes are explored using a combination of X-ray and optical spectroscopies, together with photoelectrochemical (PEC) characterization [1]. Application of these methods to both the pure components and the fully assembled nanocomposites reveals unpredicted interfacial energetic alignment, which promotes ultrafast injection of electrons from  $\text{BiVO}_4$  into  $\text{TiO}_2$ . Physical charge separation yields extremely long-lived photoexcited states and correspondingly enhanced photoelectrochemical functionality. This work highlights the importance of probing emergent interfacial energetic alignment and kinetic processes for understanding mechanisms of solar energy conversion in complex nanocomposites. These findings, combined with improved understanding of basic charge transport limitations in  $\text{BiVO}_4$  [2], provide guidance for the design of systems exhibiting improved energy conversion efficiency. Despite such advances, which yield improved photocurrent densities, photovoltage generation remains limited and future plans for understanding the primary factors that contribute to these deviations from ideality will be discussed.

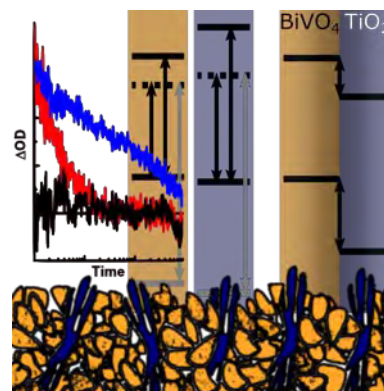


**Figure 1.** Heterostructured  $\text{BiVO}_4/\text{TiO}_2$  nanostructures exhibit unpredicted interfacial band alignment that promotes ultrafast electron injection from  $\text{BiVO}_4$  absorbers into  $\text{TiO}_2$  transport layers. The resulting long-lived charge separated states promote efficient photoanode function.

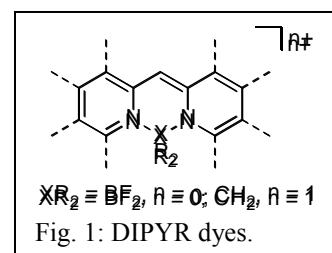
[1] L.H. Hess, J.K. Cooper, A. Loiudice, C.-M. Jiang, R. Buonsanti, & I.D. Sharp, *Nano Energy* **34**, 375 (2017).

[2] I.D. Sharp, J.K. Cooper, F.M. Toma, & R. Buonsanti, *ACS Energy Lett.* **2**, 139 (2017).

## Chromophores for Efficient Photoinduced Charge Generation

Stephen Bradforth, Mark Thompson, Jessica Golden, Laura Estergreen, Peter Djurovich  
Department of Chemistry  
University of Southern California  
Los Angeles, CA 90089

Taking a lead from the BODIPY family of dyes, we are investigating a new family of highly absorbing dyes, based on a dipyrrolyl-methene framework (DIPYR dyes, Figure 1). The goal is to use these dyes in solar photochemical systems, where both high molar absorptivity and high excited state electrochemical potential are needed to drive the reactions needed to produce solar fuels. Both BODIPY and DIPYR dyes have high molar absorptivity and can be assembled as electronically isolated dimer pairs that give efficient symmetry breaking charge transfer (SBCT). The SBCT process gives efficient charge separation, forming oxidized and reduced version of the same chromophore in a single moiety, generating the highest excited state redox potentials possible for a given chromophore. We have previously reported SBCT in meso-bridged BODIPYs and analogous Zn(dipyrrin)<sub>2</sub> complexes.<sup>1</sup> We will discuss the photophysical properties of several DIPYR dyes and our studies of the dynamical properties of dimer pairs of DIPYR and dipyrrin compounds, with an eye to better understand and enhance the SBCT process.



DIPYR dyes were prepared with pyridyl, quinolyl, and isoquinolyl groups. The three dyes absorb strongly in the blue-green part of the spectrum ( $\epsilon = 0.3\text{--}1 \times 10^5 \text{ M}^{-1}\text{cm}^{-1}$ ) and fluoresce with high quantum yields ( $\Phi_{\text{PL}} = 0.2, 0.8$  and  $0.8$ , respectively). The high  $\Phi_{\text{PL}}$  of the quinoline and isoquinoline derivatives result from a reordering of  $S_1$  and  $T_2$  state energies upon benzannulation. We will discuss our success in shifting the absorption spectra of DIPYR dyes into the red/NIR.

The kinetics of symmetry breaking charge transfer is dependent on the location of the SBCT state relative to the initial  $S_1$ , the solvent polarity and the degree of coupling. An example of the latter effect is shown for a DIPYR dimer in non-polar cyclohexane and weakly polar THF. The transient absorption data shows a dramatic difference (Figure 2). For the cyclohexane environment, the transient spectra show a long-lived  $S_1$  state characterized by well resolved vibronic structure in the excited state absorption below 450 nm and in the stimulated emission longer than 500 nm. However, in THF there is a fast evolution to a new excited state. A series of compounds where central coupling is either by a single bond linkage or a coordinating zinc center are explored to modulate the symmetry breaking and push the first absorption band further red. We will discuss our dynamical studies of the formation of the SBCT and triplet states.

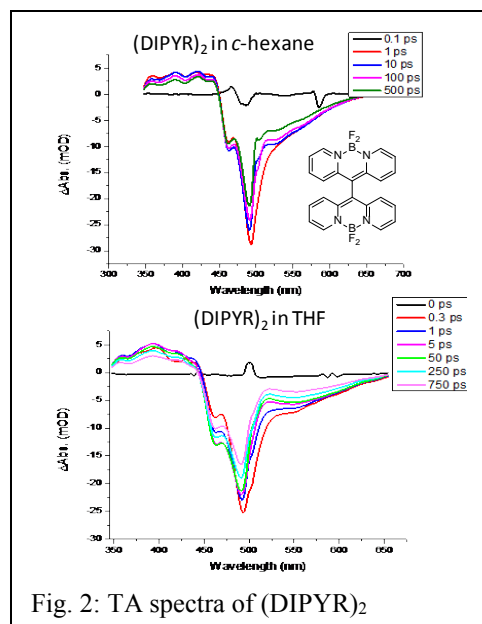


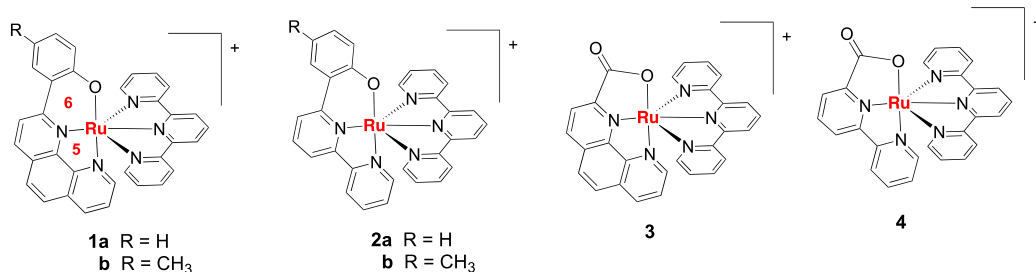
Fig. 2: TA spectra of (DIPYR)<sub>2</sub>

1. (a) Trinh, C., et al., *The Journal of Physical Chemistry C* **2014**; (b) Whited, M. T., et al., *Chem. Commun.* **2012**, 48, 284-286.

## Evidence for Oxidative Decay of a Ru-Bound Ligand During Catalyzed Water Oxidation

Husain Kagalwala, Lianpeng Tong, Lars Kohler, and Randolph P. Thummel  
Department of Chemistry  
University of Houston  
Houston, Texas 77204-5003

There are two fundamental features that are desirable in an effective water oxidation catalyst (WOC). Firstly, the catalyst should exhibit a high turnover frequency (TOF) meaning that it should facilitate water decomposition at a fast rate. Secondly, the catalyst should be very stable under the reaction conditions. Ideally, the catalyst will provide many millions of turnovers before becoming inactive. For a metal-polypyridine catalyst a likely decomposition pathway would involve oxidation of the polypyridine ligand, leading to fragmentation of the complex and ultimately release of the metal.



We were surprised to find that the catalytic activities towards water oxidation for complexes **1a** and **3** were almost identical (Figure 1) suggesting that perhaps a common intermediate might be involved. The incorporation of a 4-methyl substituent on **1a** inhibited the formation of the presumed quinone precursor to **3**. The corresponding bipyridine systems **2** and **4** were found to be less reactive.

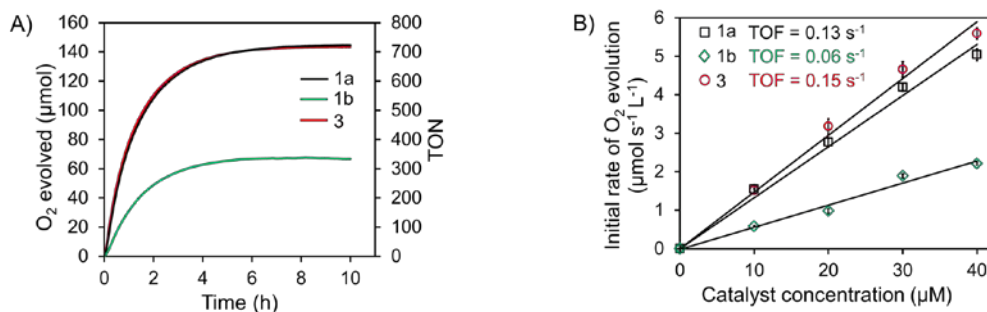


**Figure 1.** A: O<sub>2</sub> evolution versus time and corresponding TON plots for catalysts **3** (red line), **1a** (black line) and **1b** (green line). Conditions: 20 μM catalyst and 0.2 M CAN in 10 mL HNO<sub>3</sub> (pH = 1.0). B: Initial rate of O<sub>2</sub> evolution versus concentrations of catalysts.

Part of the problem may be due to the high oxidation potential of the sacrificial reagent, ceric ammonium nitrate ( $E_{\text{ox}} = +1.71$  V). Although this reagent may be useful for mechanistic evaluations of catalytic activity, adopting milder conditions may contribute to better stability.<sup>1</sup>

1. *ACS Catalysis* **2017**, *7*, 2607-2615.

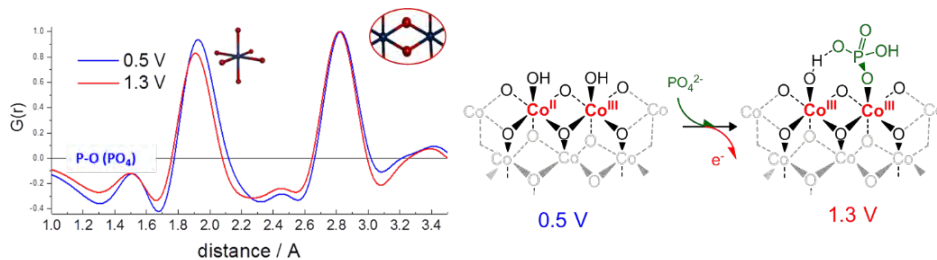
## Resolving Sites for Solar-Driven Catalysis in Amorphous Oxide and Molecular Water Oxidation Catalysts Using *In-situ* X-ray Techniques

David M. Tiede<sup>1</sup>, Gihan Kwon<sup>1</sup>, Alex B. F. Martinson<sup>2</sup>, Hoyoung Jang<sup>3</sup>, Jun-Sik Lee<sup>3</sup>, Karen L. Mulfort<sup>1</sup>, Lisa M. Utschig<sup>1</sup>, Oleg G. Poluektov<sup>1</sup>, Lin X. Chen<sup>1</sup>

<sup>1</sup>Chemical Sciences and Engineering and <sup>2</sup>Materials Sciences Divisions, Argonne National Laboratory, <sup>3</sup>SLAC National Accelerator Laboratory

Our program develops advanced synchrotron X-ray, electron paramagnetic resonance, and ultrafast transient optical approaches for investigating structures and mechanisms at the atomic scale, and that are applied for the analysis of solar energy conversion in natural and artificial photosynthesis. This presentation will discuss the resolution of sites for solar-driven catalysis in amorphous cobalt oxide and molecular water-oxidation catalysts using a combination of *in-situ* high energy X-ray (60 keV) scattering with atomic pair distribution function (PDF) analysis, cobalt L<sub>3</sub> edge X-ray absorption spectroscopy, and anomalous wide angle X-ray scattering (AWAXS), with a goal of resolving structure, "one electron at a time", following successive, single-electron, photo-initiated electron transfers.

The PDF technique allows resolution of atomic pair correlations across the full inner and outer shell coordination spheres for transition metal complexes with 0.2 Å spatial resolution. We have extended the *in-situ* PDF technique by developing 3-D porous electrode architectures that enable structural characterization of interfacial thin films during photo-electrochemistry. PDF-electrochemistry measurements for the cobalt borate OEC film, CoBi, poised across the potentials from 0.5 V and 1.4 V vs NHE show lattice contraction of the domains as a result of bond shortening by the accumulation of metal centers in high valence oxidation states. The structural change is associated with increased metal-oxo covalency and charge delocalization.



Comparable *in-situ* PDF measurements for the cobalt phosphate, CoPi, OEC show that charge accumulation leads to similar domain lattice contraction. In addition, for CoPi the Co<sup>II</sup>Co<sup>III</sup> to Co<sup>III</sup>Co<sup>III</sup> transition is found to be coupled to Co-O peak broadening and amplitude decreases for pairs involving edge O atoms, identifying these as the sites for redox activity. Corresponding changes are seen in the P-O peak. These results provide experimental evidence for a Pi edge-associated model (Nocera, 2015) with bond length disorder. The PDF data shows that Pi remains edge-bound at the onset of water oxidation, suggesting the possible positioning of Pi for function in proton-coupled electron transfer. The cobalt OEC are also distinguished by X-ray absorption at the L<sub>3</sub> edge, with CoPi showing both octahedral and tetrahedral Co(II) assigned to lattice and edge or extra-domain connecting sites, respectively. Finally, we demonstrate new AWAXS measurements for structure resolution in molecular and mixed metal OEC.

|                        | Co ions | Co <sub>3</sub> O <sub>4</sub> | CoBi | CoPi |
|------------------------|---------|--------------------------------|------|------|
| T <sub>d</sub> Co(II)  |         | 33.33                          | 0    | 25.8 |
| O <sub>h</sub> Co(III) |         | 66.67                          | 75.4 | 46.5 |
| O <sub>h</sub> Co(II)  |         | 0                              | 24.6 | 27.7 |

## Studies in Photoelectrochemical Processes in Interfacial Catalysis and MEG

Jing Gu, Yong Yan, Ryan W. Crisp, Jeffery A. Aguiar, Boris D. Chernomordik, Gregory Pach, Suzanne Ferrere, K. Xerxes Steirer, Chuanxiao Xiao, James L. Young, Andrew Norman, Mowafak Al-Jassim, Ashley R. Marshall, Nathan R. Neale, Matthew C. Beard & John A. Turner  
Chemical and Nanoscience Center  
National Renewable Energy Laboratory  
Golden, CO, 80401

Incorporation of proper electrocatalysts onto the illuminated SC surface can both stabilize the PEC interface and increase catalysis, thus enhancing the overall device performance. The branching ratio between catalysis and corrosion must be extremely high ( $>10^6$ ) in order for the system to have the necessary lifetime, thus the catalysts must have a very high turnover frequency (TOF) and turnover number (TON). Such materials for SC surface modification are particularly beneficial if they are potentially low-cost and scalable, transparent and conductive while also highly catalytically active and stable.

Two approaches to interfacial catalysis have been studied: i) the immobilization of a cobaltoxime hydrogen evolution catalyst on an ALD  $\text{TiO}_2$  modified p-GaInP<sub>2</sub> surface and its catalytic activity under illumination in pH 13 aqueous solution and ii) the use of a graded  $\text{MoS}_x/\text{MoO}_x/\text{TiO}_2$  layer that retains much of the high catalytic activity of amorphous  $\text{MoS}_x$  but with a stability similar to crystalline  $\text{MoS}_2$ .

Our work on the cobaltoxime system was the subject of a previous poster.

We present here a new strategy for stabilizing the GaInP<sub>2</sub> photocathode using a catalytically active interfacial layer based on  $\text{MoS}_2/\text{MoO}_x/\text{TiO}_2$ . Annealing a bilayer of amorphous titanium dioxide ( $\text{TiO}_x$ ) with a top layer of amorphous molybdenum sulfide ( $\text{MoS}_x$ ) deposited onto GaInP<sub>2</sub> results in a graded  $\text{MoS}_x/\text{MoO}_x/\text{TiO}_2$  coating. This coating provides the GaInP<sub>2</sub> photocathode with high catalytic activity (current density of 11 mA/cm<sup>2</sup> at a potential of 0 V vs. RHE under 1 sun illumination) and stability (retains 80% of its initial photocurrent density over a 20 h durability test) for the hydrogen evolution reaction in strong acid solution as compared with the traditional GaInP<sub>2</sub> surface-deposited platinum-ruthenium co-catalysts.

An area of significance for PEC is the confirmation of capturing MEG via hydrogen production. We have developed an approach that confirms an external quantum efficiency for hydrogen generation (EQE<sub>h</sub>) exceeding 100% using PbS QD photoelectrodes. The system consists of two separated electrodes and is constructed such that hydrogen generation is accomplished with no external voltage bias as depicted below. The energy necessary to split H<sub>2</sub>S is provided by a combination of the chemical bias (via pH difference) and the photovoltage of the QD PbS electrode.

## A Semiconductor-to-Metal Transition in Rutile TiO<sub>2</sub> is Induced by Tensile Strain and Improves Electrochemical Activity

Eric E. Benson, Elisa M. Miller, Sanjini U. Nanayakkara, Drazenka Svedruzic, Suzanne Ferrere, Nathan R. Neale, Jao van de Lagemaat, and Brian A. Gregg  
Chemistry and Nanoscience center  
National Renewable Energy Laboratory  
Golden, Colorado, 80401

This paper shows that it is possible to reversibly and degenerately dope titanium dioxide by strain, inducing a semiconductor-to-metal transition. This semiconductor-to-metal transition allows for the reversible on/off switching of electrochemical activity with simple redox couples but also strongly increases the activity of TiO<sub>2</sub> towards fuel forming reactions relevant to water splitting.

We applied tensile strain to thin films ( $\approx 50$  nm) of rutile TiO<sub>2</sub> that were thermally grown on superelastic nitinol (NiTi intermetallic) substrates. As shown by electrochemistry (Fig. 1), the application of tensile strain, while not cracking or otherwise irreversibly damaging the thin film, causes the film to behave metallic like instead of n-type semiconductor like. X-ray photoelectron spectroscopy confirmed the presence of filled electronic states at the Fermi energy and conducting atomic force microscopy showed a reversible change to a metallic surface under strain. Electrochemical impedance measurements indicate that under strain, the doping density in the near-surface region increases tenfold and the distribution of surface and near surface bandgap states shifts to higher energy. The surface states and increased doping can be attributed to the increased presence of oxygen vacancies under strain. As the carrier concentration is increased, the width of the depletion region is reduced, which then permits electron tunneling through the space charge barrier to the surface states, resulting in the observed metallic behavior. In addition to simple redox systems, we studied the effect of strain-induced metallic behavior on fuel-forming reactions and observed strongly increased activity towards hydrogen and oxygen evolution.

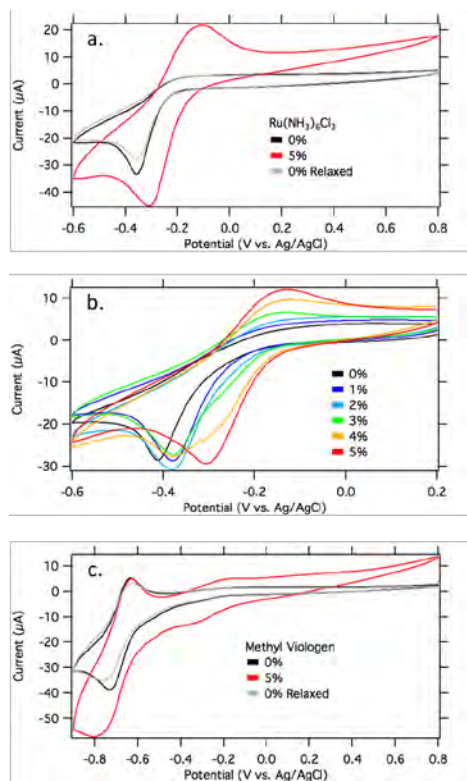


Fig. 1 The effect of applying tensile strain to thin films of TiO<sub>2</sub> on electrochemical activity shown for three different redox couples all at 1mM concentration in 0.1 M phosphate buffer (pH 7). All scans were taken on a 50 nm TiO<sub>2</sub> film at 50 mV/s with Ag/AgCl reference and Pt counter electrodes.

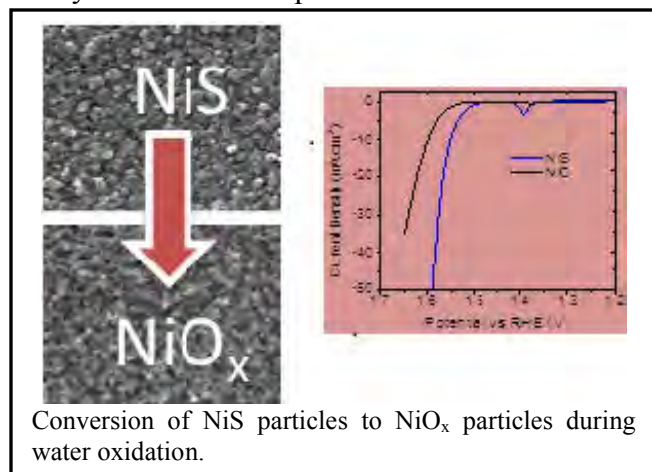
(1) Benson, E. E.; Miller, E. M.; Nanayakkara, S. U.; Svedruzic, D.; Ferrere, S.; Neale, N. R.; van de Lagemaat, J.; Gregg, B. A. Semiconductor-to-Metal Transition in Rutile TiO<sub>2</sub> Induced by Tensile Strain. *Chem Mater* **2017**, *29*, 2173–2179.



## Studies of Electrocatalysts for Water Oxidation

Bryan R. Wygant,\* Oluwaniyi Mabayoje,\* C. Buddie Mullins\*<sup>#</sup> and Allen J. Bard\*  
Departments of Chemistry\* and Chemical Engineering<sup>#</sup>  
University of Texas at Austin  
Austin, TX 78712

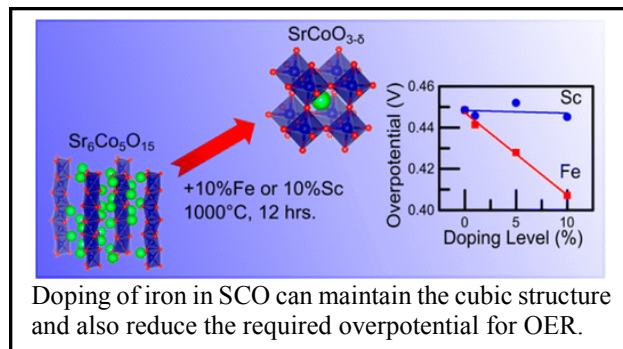
Oxygen evolution catalysts composed of a metal (Ni, Co, or Fe) and a pnictide or chalcogenide counterion are a promising class of electrocatalysts for the oxygen evolution reaction (OER), an important reaction in the photoelectrochemical splitting of water. We synthesized a nickel-based oxygen evolution catalyst derived from pulse-electrodeposited nickel sulfide. This catalyst was found to produce current densities of 10 mA/cm<sup>2</sup> at the relatively low overpotential of 320 mV in alkaline electrolyte (1 M KOH).



Importantly, we found that the sulfur anion in the nickel sulfide is depleted in the active form of the electrocatalyst and that the NiS is converted into an amorphous nickel oxide in the potential range where water is oxidized to oxygen. The superior catalytic activity of this nickel sulfide is thus unrelated to the sulfur anions in the active catalyst but is instead related to the metal sulfide's ability to act as a precursor to a highly active nickel oxide OER electrocatalyst. The nickel oxide derived from nickel sulfide was found to be

amorphous with a relatively high surface area, two factors that have been previously shown to be important in oxygen evolution electrocatalysis. *ACS Energy Lett.* **1**, 195-201 (2016).

Previous work regarding DFT calculations of the perovskite SrCoO<sub>3-δ</sub> (SCO) predict a surface binding energy ideal for OER catalysis but could not be compared to experimental results due to the material's propensity to form the incorrect trigonal crystal structure. By doping with iron and scandium, X-ray diffraction confirms that we have been able to synthesize a series of SCO catalysts of various crystal structures, culminating in cubic SCO. In doing so, we show that there is a limited correlation between the crystal structure and OER performance in alkaline media. Instead, the use of iron as a dopant is found to decrease the OER overpotential of the SCO by 40 mV in 0.1 M KOH and yield catalysts capable of performing water oxidation at an overpotential of 410 mV at 10 mA/cm<sup>2</sup>. The doped, cubic SCO catalysts are found to be more stable than the undoped material when tested for extended periods, showing only an approximate 3 mV increase in overpotential over a 2 h period at 10 mA/cm<sup>2</sup>. Our results show that proper doping of the B-site cation in SCO allows for tuning the structure, performance, and stability of the oxide as an OER electrocatalyst. *ACS Catalysis* **6**, 1122-1133 (2016).



## Metal-Tipped and Electrochemically Wired Semiconductor Nanocrystals: Modular Constructs for Directed Charge Transfer

Neal R. Armstrong, Jeffrey Pyun, S. Scott Saavedra  
Department of Chemistry/Biochemistry  
University of Arizona  
Tucson, Arizona 85721

DOE supported research efforts have focused on: i) CdSe semiconductor quantum dots, electrochemically “wired” to hole-harvesting contacts in photoelectrochemical platforms; ii) development of new synthetic routes to symmetrically and asymmetrically metal- and metal-oxide tipped CdSe and CdS nanorods (NRs); iii) development of new measurement science approaches to characterization of band edge energies ( $E_{CB}/E_{VB}$ ) which control energy conversion efficiencies (including spectroelectrochemical approaches to estimation of  $E_{CB}$ , and UV-photoemission approaches to estimation of  $E_{VB}$ ) – both approaches allow unique quantification of mid-gap state densities, especially following addition of metal (catalyst) tips; iv) development of new routes to monodisperse CdSe@CdS tetrapods (TPs), providing precise control over energetics (Type I versus quasi-Type II heterojunctions) via control of CdSe seed size (Fig. 1). Creation of these new nanostructured materials has enabled experiments which probe dynamics of charge formation, charge harvesting and recombination (collaborations with Lian group, Emory) all of which point to the important role that defect sites along the NR or TP arm play in limiting energy conversion efficiencies. New routes for passivation of these states have been developed, and we now return to “wiring” of these TP constructs to (oxide) hole-harvesting/electron-blocking contacts.

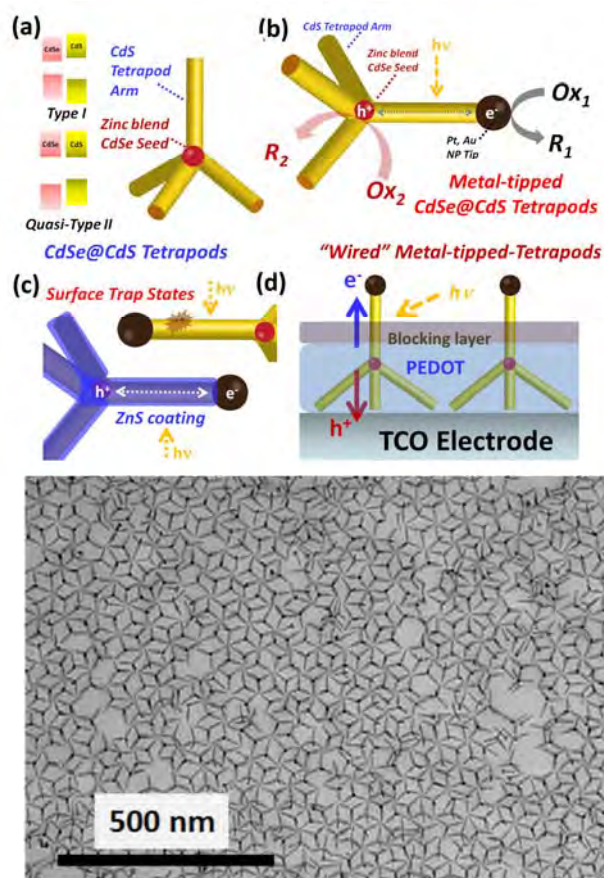


Fig. 1 -- (upper panel) – (a) new approaches to formation of II-VI semiconductor tetrapods – the variable size of the CdSe seed provides for either Type I or quasi-Type II heterojunctions; (b) these resultant constructs provide a platform to test whether hole-harvesting can be selectively located at the CdSe seed; (c) new approaches to passivation of hole-traps along the CdS arm, including monolayer ZnS coatings; (d) vision for “wiring” of the CdSe@CdS TP to hole-harvesting contacts; (lower panel) – a near-monolayer array of CdSe@CdS TPs, drop-cast onto a carbon coated copper grid from chlorobenzene, demonstrating the monodispersity of these nanomaterials, at scale.

## Coherent Coupling of Electronic and Phononic Resonances

M. Kirschner,<sup>1</sup> C. M. LeThiec,<sup>1</sup> C. Chapman,<sup>1</sup> X.M. Lin,<sup>2</sup> G. C. Schatz,<sup>1</sup> L.X. Chen,<sup>1,3</sup> R. D. Schaller<sup>1,2</sup>

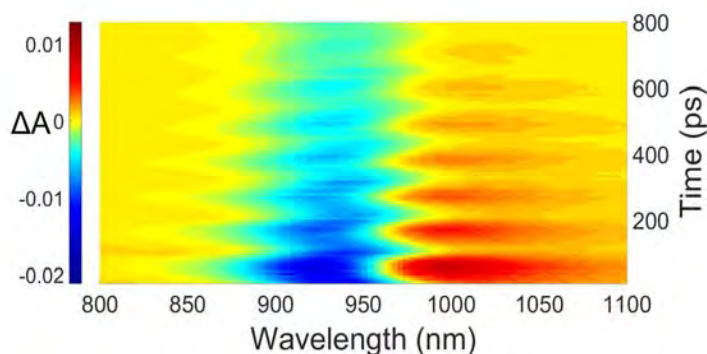
<sup>1</sup>Department of Chemistry

Northwestern University, Evanston, IL 60208

<sup>2</sup>Nanoscience and Technology, <sup>3</sup>Chemical Science and Technology

Argonne National Laboratory, Lemont, IL 60439

Light absorption can induce mechanical motions in molecules and particles that subsequently mediate electronic phenomena such as charge transfer and energy migration. Indeed, for organic donor-acceptor systems, recent reports have indicated that vibrational excitation of a bond within a chromophore can alter or gate electron transfer rates and, as a result, offer a route to control electron transfer efficiencies.<sup>1</sup> In the studied organic systems, the molecular vibrational state has been an *intrinsic*, localized bond within the chromophore and altered rates of electron transfer have largely been attributed to vibrational influences on donor-acceptor coupling. Can oscillations in energy, such as induced by a coherent acoustic phonon involving a metal or semiconductor nanoparticle, impact charge transfer rates appreciably? We are working to demonstrate and understand charge transfer processes involving the *externally* applied coherent acoustic phonon of related Fano resonance plasmon-exciton coupled systems as well as the compression/expansion in semiconductor compositions. Impulsive excitation can reveal some of these coherences in ensemble measurements under particular circumstances, which we measure and evaluate. We build upon prior characterizations we've performed of coherent acoustic phonons that drive electronic resonance changes in inorganic, plasmonic systems<sup>2</sup> and move to understand hybridized systems.<sup>3</sup>



The figure to the left shows ensemble transient absorption measurements of plasmonic bipyramidal structures that oscillate in a pronounced manner owing to coherent acoustic phonon-driven elongation and compression. The center wavelength, modulation strength, and period of oscillation can be separately controlled and utilized to investigate related influences on proximal species.

[1] M. Delor et al. *Science*, 2014, v.346, p.1492

[2] M. Kirschner et al. *ACS Photonics*, 2016, v.3, p.758

[3] M. Kirschner et al. *in preparation*



## *List of Participants*

Neal Armstrong  
Department of Chemistry  
University of Arizona  
Tucson, AZ 85721  
520-621-8242  
nra@email.arizona.edu

John Asbury  
Pennsylvania State University  
Department of Chemistry  
University Park, PA 16801  
814-863-6309  
jba11@psu.edu

Robert Bartynski  
Department of Chemistry  
Rutgers University  
136 Frelinghuysen Rd.  
Piscataway, NJ 08854  
732-445-5500  
bart@physics.rutgers.edu

Victor Batista  
Department of Chemistry  
Yale University  
P.O. Box 208107  
New Haven, CT 06477  
203-432-6672  
victor.batista@yale.edu

Matt Beard  
National Renewable Energy Laboratory  
15013 Denver West Pkwy.  
Golden, CO 80401  
303-384-6781  
Matt.beard@nrel.gov

Louise Berben  
Department of Chemistry  
University of California, Davis  
Davis, CA 95616  
530-752-8475  
laberben@ucdavis.edu

Jeff Blackburn  
National Renewable Energy Laboratory  
15013 Denver West Pkwy.  
Golden, CO  
80401303-384-6649  
jeffrey.blackburn@nrel.gov

David Bocian  
University of California, Riverside  
Department of Chemistry  
Riverside, CA 92521  
951-827-3660  
David.Bocian@ucr.edu

Stephen Bradforth  
Department of Chemistry  
University of Southern California  
Los Angeles, CA 90089-0482  
213 740 0461  
stephen.bradforth@usc.edu

Kara Bren  
Department of Chemistry  
University of Rochester  
120 Trustee Rd.  
Rochester, NY 14627-0216  
585-275-4335  
bren@chem.rochester.edu

Gary Brudvig  
Yale University  
P.O. Box 208107  
New Haven, CT 06477  
203-432-5202  
gary.brudvig@yale.edu

Ian Carmichael  
University of Notre Dame  
223 Radiation Laboratory  
Notre Dame, IN 46556  
574-631-4502  
carmichael.1@nd.edu

Felix N. Castellano  
Department of Chemistry  
North Carolina State University  
2620 Yarbrough Dr.  
Raleigh, NC 27695  
919-515-3021  
fncastel@ncsu.edu

Lin Chen  
Argonne National Lab/Northwestern Univ.  
9700 S. Cass Ave.  
Argonne, IL 60439  
630-252-3533  
lchen@anl.gov

Kyoung-Shin Choi  
Department of Chemistry  
University of Wisconsin, Madison  
1101 University Ave.  
Madison, WI 53706  
608-262-5859  
kschoi@chem.wisc.edu

Javier Concepcion  
Brookhaven National Laboratory  
Chemistry Department  
Upton, NY 11973-5000  
631-344-4369  
jconcepc@bnl.gov

Philip Coppens  
Department of Chemistry  
University at Buffalo SUNY Buffalo  
732 NSC Complex  
Buffalo, NY 14260-3000  
716-645-4273  
coppens@buffalo.edu

Robert Crabtree  
Department of Chemistry  
Yale University  
225 Prospect St.  
New Haven, CT 06520  
203-432-3925  
robert.crabtree@yale.edu

Jillian Dempsey  
University of North Carolina  
Department of Chemistry  
Chapel Hill, NC 27599-3290  
919-962-4617  
dempseyj@email.unc.edu

Kim Dunbar  
Texas A&M University  
Department of Chemistry  
College Station, TX 77843-3255  
979-845-5235  
dunbar@mail.chem.tamu.edu

Mehmed Ertem  
Brookhaven National Laboratory  
Chemistry Department  
Upton, NY 11973-5000  
631-344-7310  
mzertem@bnl.gov

Mohammed El Nagggar  
University of Southern California  
Los Angeles, CA 90089  
626-755-1489  
mnagggar@usc.edu

Graham Fleming  
Lawrence Berkeley National Laboratory  
One Cyclotron Rd.  
Berkeley, CA 94720  
510-643-2735  
grfleming@lbl.gov

Christopher Fecko  
U.S. Department of Energy  
1000 Independence Ave., SW  
Washington, DC 20585  
301-903-1303  
Christopher.Fecko@science.doe.gov

Heinz Frei  
Lawrence Berkeley National Laboratory  
One Cyclotron Rd.  
Berkeley, CA 94720  
510-486-4325  
HMFrei@lbl.gov

Etsuko Fujita  
Brookhaven National Laboratory  
Chemistry Department  
Upton, NY 11973-5000  
631-344-4356  
fujita@bnl.gov

Elena Galoppini  
Department of Chemistry  
Rutgers University  
73 Warren St.  
Newark, NJ 07041  
973-353-5317  
galoppin@rutgers.edu

Theodore Goodson III  
Department of Chemistry  
University of Michigan at Ann Arbor  
Ann Arbor, MI 48109-1055  
734-647-0274  
tgoodson@umich.edu

David Grills  
Brookhaven National Laboratory  
Chemistry Department  
Upton, NY 11973-5000  
631-344-4332  
dcgrills@bnl.gov

Erik Grumstrup  
Department of Chemistry  
Montana State University  
240 Gaines Hall  
Bozeman, MT 59717  
406-994-2988  
erik.grumstrup@montana.edu

Lars Gundlach  
Department of Physics & Astronomy  
University of Delaware  
Newark, DE 19716  
302- 831-2331  
larsg@udel.edu

Devens Gust  
Arizona State University  
Dept. Chemistry and Biochemistry  
Tempe, AZ 85287  
480-965-4547  
gust@asu.edu

Thomas Hamann  
Department of Chemistry  
Michigan State University  
578 S. Shaw Ln., RM 411  
East Lansing, MI 48824  
517-355-9715  
hamann@chemistry.msu.edu

Alexander Harris  
Brookhaven National Laboratory  
Chemistry Department  
Upton, NY 11973-5000  
631-344-4301  
alexh@bnl.gov

Craig Hill  
Department of Chemistry  
Emory University  
1515 Dickey Dr., NE  
Atlanta, GA 30322  
404-727-6611  
chill@emory.edu

Dewey Holten  
Washington University  
Chemistry Department  
St. Louis, MO 63130  
314-93 5-6502  
holten@wustl.edu

Libai Huang  
Purdue University  
West Lafayette, IN 47907  
765-494-7851  
Libai-huang@purdue.edu

Joseph Hupp  
Department of Chemistry  
Northwestern University  
2145 Sheridan Rd.  
Evanston, IL 60208  
847-441-0136  
j-hupp@northwestern.edu

Justin Johnson  
National Renewable Energy Laboratory  
15013 Denver West Pkwy.  
Golden, CO 80401  
303-384-6190  
justin.johnson@nrel.gov

David Jonas  
University of Colorado  
215 UCB  
Boulder, CO 80309-0215  
303-492-3818  
david.jonas@colorado.edu

Prashant Kamat  
University of Notre Dame  
223 Radiation Laboratory  
Notre Dame, IN 46556  
574-631-5411  
pkamat@nd.edu

Christine Kirmaier  
Department of Chemistry  
Washington University  
Dept. of Chemistry, Box 1134  
St. Louis, MO 63130  
314-725-6157  
kirmaier@wustl.edu

Bruce Koel  
Princeton University  
Dept. Chem. & Biol. Eng.  
Princeton, NJ 08544  
609-258-4524  
bkoel@princeton.edu

Todd Krauss  
University of Rochester  
120 Trustee Rd.  
Rochester, NY 14627-0216  
585-275-5093  
krauss@chem.rochester.edu

Frederick Lewis  
Department of Chemistry  
Northwestern University  
2145 Sheridan Rd.  
Evanston, IL 60208  
847-491-3441  
fdl@northwestern.edu

Nathan Lewis  
Department of Chemistry  
California Institute of Technology  
1200 E. California Blvd.  
Pasadena, CA 91125  
626-395-6335  
nslewis@caltech.edu

Gonghu Li  
Department of Chemistry  
University of New Hampshire  
Durham, NH 03824  
603-862-0607  
gonghu.li@unh.edu

Tianquan Lian  
Department of Chemistry  
Emory University  
Atlanta, GA 30322  
404-727-6649  
tlian@emory.edu

Jonathan Lindsey  
Department of Chemistry  
North Carolina State University  
CB8204, 2620 Yarbrough Dr.  
Raleigh, NC 27695-8204  
919-5 15-6406  
jlindsey@ncsu.edu

Elisa Miller Link  
National Renewable Energy Laboratory  
15013 Denver West Pkwy.  
Golden, CO 80401  
elisa.miller@nrel.gov

Mark Lonergan  
University of Oregon  
1253 Department of Chemistry  
Eugene, OR 97403  
541-346-4748  
lonergan@uoregon.edu

Stephen Maldonado  
Department of Chemistry  
University of Michigan at Ann Arbor  
930 N. University Ave.  
Ann Arbor, MI 48109-1055  
734-647-4750  
smald@umich.edu

Thomas Mallouk  
Pennsylvania State University  
Department of Chemistry  
University Park, P A 16801  
814-863-9637  
tom@chem.psu.edu

Diane Marceau  
U.S. Department of Energy  
1000 Independence Ave., SW  
Washington, DC 20585  
301-903-0235  
Diane.Marceau@science.doe.gov

James McCusker  
Department of Chemistry  
Michigan State University  
578 South Shaw Ln.  
East Lansing, MI 48824-1322  
517-355-9715  
jkm@chemistry.msu.edu

Gail McLean  
U.S. Department of Energy  
1000 Independence Ave., SW  
Washington, DC 20585  
301- 903-7807  
Gail.Mclean@science.doe.gov

Dmitry Matyushov  
Department of Physics  
Arizona State University  
Tempe, AZ 85287  
480-965-0057  
dmitrym@asu.edu

Gerald Meyer  
University of North Carolina  
Department of Chemistry  
Chapel Hill, NC 27599-3290  
919-962-6320  
gjmeier@email.unc.edu

Thomas Meyer  
University of North Carolina  
Department of Chemistry  
Chapel Hill, NC 27599-3290  
919-843-8313  
tjmeier@unc.edu

Josef Michl  
University of Colorado  
Dept. Chem. and Biochem., 215 UCB  
Boulder, CO 80309-0215  
303-492-6519  
michl@eefus.colorado.edu

Alexander Miller  
University of North Carolina  
Department of Chemistry  
Chapel Hill, NC 27599-3290  
919-962-4618  
ajmm@email.unc.edu

John Miller  
Brookhaven National Laboratory  
Chemistry Department  
Upton, NY 11973  
631-344-4354  
jrmiller@bnl.gov

Michael Mirkin  
Department of Chemistry  
CUNY Queens College  
New York, New York 10031  
718-997-4111  
mmirkin@qc.cuny.edu

Ana Moore  
Arizona State University  
Dept. Chemistry and Biochemistry  
Tempe, AZ 85287-1604  
480-965-2747  
amoore@asu.edu

Thomas Moore  
Arizona State University  
Dept. Chemistry and Biochemistry  
Tempe, AZ 85287-1604  
480-965-3308  
tmoore@asu.edu

Amanda Morris  
Virginia Polytechnic Institute  
Department of Chemistry  
Blacksburg, VA 24061-0212  
540-231-5585  
ajmorris@vt.edu

James Muckerman  
Brookhaven National Laboratory  
Chemistry Department  
Upton, NY 11973-5000  
631-344-4368  
muckerma@bnl.gov

Karen Mulfort  
Argonne National Laboratory  
9700 S. Cass Ave.  
Argonne, IL 60439  
630-252-3545  
mulfort@anl.gov

Charles Mullins  
University of Texas at Austin  
Dept. of Chemical Eng. C0400  
Austin, TX 78712  
512-471-5817  
mullins@che.utexas.edu

Djamaladdin Musaev  
Emory University  
1515 Dickey Dr.  
Atlanta, GA 30322  
404-727-2382  
dmusaev@emory.edu

Nathan Neale  
National Renewable Energy Laboratory  
15013 Denver West Pkwy.  
Golden, CO 8040 1  
303-384-6165  
nathan.neale@nrel.gov

Marshall Newton  
Brookhaven National Laboratory  
Chemistry Department  
Upton, NY 11973  
631-344-4366  
newton@bnl.gov

Daniel Nocera  
Department of Chemistry  
Harvard University  
12 Oxford St.  
Cambridge, MA 02138  
617-495-8904  
dnocera@fas.harvard.edu

Arthur Nozik  
Department of Chemistry  
University of Colorado  
215 UCB  
Boulder, CO 80309  
303-384-6603  
arthur.nozik@colorado.edu

Colin Nuckolls  
Department of Chemistry  
Columbia University  
New York, NY 10027  
212-854-6289  
cn37@columbia.edu

Frank Osterloh  
University of California, Davis  
Department of Chemistry  
Davis, CA 95616  
530-754-6242  
fosterloh@ucdavis.edu

Bruce Parkinson  
Department of Chemistry  
University of Wyoming  
1000 E. University Ave.  
Laramie, WY 82071  
303-766-9891  
bparkin1@uwyo.edu

Oleg Poluektov  
Argonne National Laboratory  
9700 S. Cass Ave.  
Argonne, IL 60439  
630-252-3546  
Oleg@anl.gov

Dmitry Polyansky  
Brookhaven National Laboratory  
Chemistry Department  
Upton, NY 11973-5000  
631-344-4315  
dmitriyp@bnl.gov

Oleg Prezhdo  
University of Southern California  
Department of Chemistry  
Los Angeles, CA 90089  
213-821-3116  
prezhdo@usc.edu

Sylwia Ptasinska  
University of Notre Dame  
223 Radiation Laboratory  
Notre Dame, IN 46556  
574-631-1846  
sptasins@nd.edu

Yulia Pushkar  
Department of Physics  
Purdue University  
525 Northwestern Ave.  
West Lafayette, IN 97407  
765-496-3279  
ypushkar@purdue.edu

Garry Rumbles  
National Renewable Energy Laboratory  
15013 Denver West Pkwy.  
Golden, CO 80401  
303-384-6502  
garry.rumbles@nrel.gov

Richard Schaller  
Argonne National Laboratory  
9700 S. Cass Ave.  
Argonne, IL 60439  
630-252- 1423  
schaller@anl.gov

Charles Schmuttenmaer  
Department of Chemistry  
Yale University  
225 Prospect St.  
New Haven, CT 06520-8107  
203-432-5049  
charles.schmuttenmaer@yale.edu

Gregory Scholes  
Princeton University  
Department of Chemistry  
Princeton, NJ 08544  
6092580729  
gscholes@princeton.edu

Richard Schrock  
Massachusetts Institute of Technology  
Department of Chemistry  
Cambridge, MA  
617-253-1596  
rrs@mit.edu

Ian Sharp  
Lawrence Berkeley Laboratory  
One Cyclotron Rd.  
Berkeley, CA 94720  
510-495-8715  
idsharp@lbl.gov

Mark Spitler  
U.S. Department of Energy  
1000 Independence Ave., SW  
Washington, DC 20585  
301-903-4568  
mark.spitler@science.doe.gov

Michael Therien  
Department of Chemistry  
Duke University  
124 Science Dr. 5330 FFSC  
Durham, NC 27708-0346  
919-660-1670  
michael.therien@duke.edu

Mark Thompson  
Department of Chemistry  
University of Southern California  
Los Angeles, CA 90089-0482  
213-740-6402  
met@usc.edu

Randolph Thummel  
University of Houston  
Chemistry Department  
Houston, TX 77204-5003  
713-743-2734  
thummel@uh.edu

David Tiede  
Argonne National Laboratory  
9700 S. Cass Ave.  
Argonne, IL 60439  
630-252-3539  
tiede@anl.gov

William Tumas  
National Renewable Energy Laboratory  
15013 Denver West Pkwy.  
Golden, CO 80401  
303-384-7955  
bill.tumas@nrel.gov

John Turner  
National Renewable Energy Laboratory  
15013 Denver West Pkwy.  
Golden, CO 80401-3393  
303-275-4270  
John.Turner@nrel.gov

Claudia Turro  
Department of Chemistry  
Ohio State University  
100 W. 18th Ave.  
Columbus, OH 43210  
614-292-6708  
turro@chemistry.ohio-state.edu

Jao van de Lagemaat  
National Renewable Energy Laboratory  
15013 Denver West Pkwy.  
Golden, CO 80401  
303-384-6143  
jao.vandelagemaat@nrel.gov

Michael Wasielewski  
Department of Chemistry  
Northwestern University  
2145 Sheridan Rd.  
Evanston, IL 60208  
847-467-1423  
m-wasielewski@northwestern.edu

Jenny Yang  
Department of Chemistry  
University of California, Irvine  
Irvine, CA 92697  
949-824-1533  
jyang@uci.edu

Xiaoyang Zhu  
Department of Chemistry  
Columbia University  
New York, NY 10027  
212-851-7768  
xyzhu@columbia.edu



# *Index*

## P.I. Author Index

|                    |               |                         |                    |
|--------------------|---------------|-------------------------|--------------------|
| Armstrong, N.....  | 186           | Lian, T.....            | 92, 152            |
| Asbury, J.....     | 135           | Lindsey, J.....         | 128                |
| Bard, A.....       | 185           | Lonergan, M.....        | 13                 |
| Bartynski, R.....  | 149           | Maldonado, S.....       | 113                |
| Batista, V.....    | 136, 146      | Mallouk, T.....         | 160                |
| Beard, M.....      | 137, 169, 182 | Matyushov, D.....       | 95                 |
| Berben, L.....     | 73            | McCusker, J.....        | 21                 |
| Blackburn, J.....  | 138, 162      | Meyer, G.....           | 116                |
| Bocian, D.....     | 128           | Meyer, T.....           | 10                 |
| Boettcher, S.....  | 139           | Michl, J.....           | 161                |
| Bradforth, S.....  | 179           | Miller, A.....          | 65                 |
| Bren, K.....       | 140           | Miller, E.....          | 137, 162, 168, 183 |
| Brudvig, G.....    | 141, 176      | Miller, J.....          | 164, 165           |
| Castellano, F..... | 39            | Moore, A.....           | 164                |
| Chen, L.....       | 142, 181      | Moore, T.....           | 164                |
| Choi, K.S.....     | 143           | Morris, A.....          | 165                |
| Concepcion, J..... | 75, 144       | Muckerman, J.....       | 75, 151, 166       |
| Coppens, P.....    | 145           | Mulfort, K.....         | 167, 171, 181      |
| Crabtree, R.....   | 141, 146      | Mullins, C.....         | 185                |
| Dempsey, J.....    | 89            | Musaev, J.....          | 152                |
| Dunbar, K.....     | 147           | Neale, N.....           | 168, 182, 183      |
| Eisenberg, R.....  | 140           | Newton, M.....          | 95                 |
| El Naggar, M.....  | 1             | Nocera, D.....          | 83                 |
| Ertem, M.....      | 75, 148, 151  | Nozik, A.....           | 169                |
| Fleming, G.....    | 125           | Nuckolls, C.....        | 184                |
| Frei, H.....       | 99            | Osterloh, F.....        | 170                |
| Fujita, E.....     | 75, 151       | Parkinson, B.....       | 27                 |
| Gaffney, K.....    | 19            | Poluektov, O.....       | 167, 171, 181      |
| Galoppini, E.....  | 120, 149      | Polyansky, D.....       | 75, 148, 151, 172  |
| Goodson, T.....    | 150           | Prezhdo, O.....         | 173                |
| Grills, D.....     | 39, 59, 127   | Ptasinska, S.....       | 174                |
| Grumstrup, E.....  | 108           | Pushkar, Y.....         | 175                |
| Gundlach, L.....   | 120, 149      | Rumbles, G.....         | 55                 |
| Gust, D.....       | 164           | Schaller, R.....        | 187                |
| Hamann, T.....     | 7             | Schmittenmaer, C.....   | 141, 176           |
| Hill, C.....       | 152           | Scholes, G.....         | 177                |
| Holten, D.....     | 128           | Schrock, R.....         | 63                 |
| Huang, L.....      | 31            | Sharp, I.....           | 178                |
| Hupp, J.....       | 153           | Therien, M.....         | 51                 |
| Johnson, J.....    | 138, 154      | Thompson, M.....        | 179                |
| Jonas, D.....      | 155           | Thummel, R.....         | 180                |
| Kamat, P.....      | 103           | Tiede, D.....           | 167, 171, 181      |
| Kirmaier, C.....   | 128           | Turner, J.....          | 182                |
| Koel, B.....       | 156           | Turro, C.....           | 147                |
| Krauss, T.....     | 140, 157      | Van de Lagemaat, J..... | 137, 154, 183      |
| Lewis, F.....      | 158           | Wasielewski, M.....     | 43                 |
| Lewis, N.....      | 34            | Yang, J.....            | 68                 |
| Li, G.....         | 159           | Zhu, X.....             | 184                |